

**IN VITRO EVALUATION OF  
BACTERIAL RNA POLYMERASE  
SIGMA: CORE INHIBITORS**

**DISSERTATION**

zur Erlangung des Grades  
des Doktors der Naturwissenschaften  
der Naturwissenschaftlich-Technischen Fakultät III  
Chemie, Pharmazie, Bio- und Werkstoffwissenschaften  
der Universität des Saarlandes

von

**Kristina Hüsecken**

Saarbrücken

2014

Tag des Kolloquiums: 14. November 2014

Dekan: Prof. Dirk Bähre

Berichterstatter: Prof. Rolf W. Hartmann

Prof. Alexandra K. Kiemer

Vorsitz: Prof. Claus-Michael Lehr

Akad. Mitarbeiter: Dr. André Schäftlein

Die vorliegende Arbeit wurde von Januar 2011 bis Juli 2014 unter Anleitung von Herrn Prof. Dr. Rolf W. Hartmann in der Fachrichtung 8.2 Pharmazeutische und Medizinische Chemie der Naturwissenschaftlich-Technischen Fakultät III der Universität des Saarlandes angefertigt.

**ICH BIN IMMER NOCH VERWIRRT,  
ABER AUF EINEM HÖHEREN NIVEAU.**

ENRICO FERMI

(italienischer Kernphysiker 1901-1954)

**EXPERIENCE IS WHAT YOU GET  
WHEN YOU DIDN'T GET WHAT YOU WANTED.**

RANDOLPH FREDERICK PAUSCH

(US-amerikanischer Informatiker 1960-2008)

## SUMMARY

In order to identify and characterize novel inhibitors of bacterial RNA polymerase, an *in vitro* test system was developed. Therefore, *Escherichia coli* was used as model organism. The inhibitors should prohibit the protein-protein interaction of the  $\beta'$  subunit of the core enzyme of RNA polymerase and the dissociable  $\sigma^{70}$  factor, and inhibit thereby transcription. This inhibition mechanism shall prevent cross-resistances with clinically used Rifamycins and fidaxomicin.

The test system consists of various binding and functional assays, of which most are based on the biophysical surface plasmon resonance technology. The variable assays allow on the one hand the determination of affinity and activity of the inhibitors, and on the other hand the determination of the mode of action. The binding mode was investigated by competition experiments with the  $\sigma^{70}$  factor and comparative binding studies to wild-type and point-mutated, truncated  $\beta'$  proteins.

Within the scope of this work, three inhibitor classes of small molecules and one peptide were identified that effectively inhibited the  $\sigma^{70}$  – core RNA polymerase interaction. By the generation of structure-activity relationships as well as elucidation of the binding mode, the developed test system contributed to the optimization of the compounds.

## ZUSAMMENFASSUNG

Zur Identifizierung und Charakterisierung neuer Hemmstoffe der bakteriellen RNA Polymerase als potentielle antibiotisch wirksame Arzneistoffe wurde ein *in vitro* Testsystem aufgebaut. Dabei wurde *Escherichia coli* als Modellorganismus verwendet. Die Hemmstoffe sollen die Protein-Protein Interaktion zwischen der  $\beta'$  Untereinheit des Core-Enzyms der RNA Polymerase und dem dissoziierbaren  $\sigma^{70}$  Faktor unterbinden und so die Transkription verhindern. Dadurch sollen Kreuzresistenzen mit den in der Klinik eingesetzten Rifamycinen und Fidaxomicin vermieden werden.

Das Testsystem besteht aus zahlreichen Bindungs- und funktionalen Assays, die größtenteils auf der biophysikalischen Oberflächenplasmonresonanz-Technologie basieren. Die unterschiedlichen Tests erlauben zum einen die Bestimmung von Affinität und Aktivität, zum anderen die Bestimmung des Bindungsmodus. Der Bindungsmodus wird mit Hilfe von Kompetitionsversuchen mit dem  $\sigma^{70}$  Faktor und vergleichenden Bindungsstudien an Wildtyp und punktmutierten, verkürzten  $\beta'$  Proteinen untersucht.

Im Rahmen dieser Arbeit konnten drei Wirkstoffklassen kleiner Moleküle und ein Peptid identifiziert werden, welche die  $\sigma^{70}$  – Core RNA Polymerase Interaktion effektiv hemmen. Durch die Generierung von Struktur-Wirkungsbeziehungen konnte das entwickelte Testsystem zur Optimierung der Verbindungen und zur Aufklärung von deren Bindungsmodi beitragen.

## PAPERS INCLUDED IN THIS THESIS

This thesis is divided into three/four publications, which are referred to in the text by their Roman numerals.

**I      Surface plasmon resonance – more than a screening technology: Insights in the binding mode of  $\sigma^{70}$ :core RNAP inhibitors**

Kristina Hüsecken, Stefan Hinsberger, Walid A. M. Elgaher, Jörg Haupenthal, and Rolf W. Hartmann

*Future Med. Chem.* 2014, **6**, 1551-1565.

**II     Peptide-based investigation of the *Escherichia coli* RNA polymerase  $\sigma^{70}$ :core interface as target site**

Kristina Hüsecken, Matthias Negri, Martina Fruth, Stefan Boettcher, Rolf W. Hartmann, and Jörg Haupenthal

*ACS Chem. Biol.* 2013, **8**, 758-766.

**III    Discovery of novel bacterial RNA polymerase inhibitors: pharmacophore-based virtual screening and hit optimization**

Stefan Hinsberger, Kristina Hüsecken, Matthias Groh, Matthias Negri, Jörg Haupenthal, and Rolf W. Hartmann

*J. Med. Chem.* 2013, **56**, 8332-8338.

**IV    Influence of DNA template choice on transcription and inhibition of *Escherichia coli* RNA polymerase**

Jörg Haupenthal, Kristina Hüsecken, Matthias Negri, Christine K. Maurer, and Rolf W. Hartmann

*Antimicrob. Agents Chemother.* 2012, **56**, 4536-4539.

## CONTRIBUTION REPORT

The author wishes to clarify her contributions to the publications I-IV in the thesis.

- I** The author significantly contributed to the concept of the study, wrote the manuscript and interpreted the results. All biosensor experiments were planned, executed and analyzed by the author. Additionally, the author performed the heterologous expression and purification of the truncated  $\beta'$  subunit as well as planned and generated the mutants. Furthermore, the author planned and analyzed the ELISA-based assembly inhibition experiments.
- II** The author significantly contributed writing the manuscript and interpreting the results. In addition the author established, planned, executed and analyzed all ELISA-based assembly inhibition and initiation inhibition assay (primed abortive transcription assay) experiments. The author also performed the heterologous expression and purification of the *Escherichia coli*  $\sigma^{70}$  factor.
- III** The author planned and analyzed the core/holo transcription as well as the ELISA-based assembly inhibition assay experiments. By interpretation of the results, the author significantly contributed to discover the mode of action for the described RNAP inhibitors. Additionally, the author performed the heterologous expression and purification of the *Escherichia coli*  $\sigma^{70}$  factor.
- IV** The author performed the heterologous expression and purification of the *Escherichia coli*  $\sigma^{70}$  factor. Furthermore, the author executed transcription experiments with different DNA templates in absence and presence of the  $\sigma^{70}$  factor and interpreted the results. The author also helped writing parts of the manuscript.



## ABBREVIATIONS

3D	Three dimensional
aa	Amino acid
ACN	Acetonitrile
ADME	Absorption, distribution, metabolism, excretion
AGP	$\alpha_1$ -acid glycoprotein
avg	Average
bp	Base pair
Cam	Chloramphenicol
CC	Column chromatography
Cer	Cerulein
CHAPS	3-[(3-cholamidopropyl)dimethylammonio]-1-propanesulfonate
Cipro	Ciprofloxacin
clogP	Calculated logP
CMD	Carboxymethyl dextran
compd	Compound
cpm	Counts per minute
ddH <sub>2</sub> O	Double-distilled water
DMSO	Dimethyl sulfoxide
dsDNA	Double stranded DNA
DTT	Dithiothreitol
<i>E. coli</i> / <i>Ec</i>	<i>Escherichia coli</i>
EDC	<i>N</i> -ethyl- <i>N'</i> -(dimethylaminopropyl)carbodiimide
ELISA	Enzyme-linked immunosorbent assay
ESI	Electrospray ionization
FDA	Food and drug administration
HBA	Hydrogen bond acceptor
HBD	Hydrogen bond donor
HHQ	Heptyl-4-hydroxyquinoline
HIV	Human immunodeficiency virus
HPLC	High-performance liquid chromatography
HSA	Human serum albumin
HTS	High throughput screening
IC <sub>50</sub>	Concentration at 50 % inhibition
ITC	Isothermal titration calorimetry
$k_a/k_{on}$	Association rate
$K_D$	Equilibrium dissociation constant
$k_d/k_{off}$	Dissociation rate
LB	Lysogeny broth
Lpm	Liparmycin
LRET	Luminescence resonance energy transfer
LRS	Lid-rudder-system
M	Molar [mol/l]
MALDI-TOF	Matrix-assisted laser desorption/ionization-time of flight
MD	Molecular dynamics
MIC	Minimal inhibitory concentration
MM-GBSA	Molecular mechanics-generalized born surface area
MS	Mass spectrometry
Myx	Myxopyronin
nd	Not determined

NHS	<i>N</i> -hydroxysuccinimide
ni	No inhibition
nt/NTP	Nucleotide
OD <sub>600</sub>	Optical density at 600 nm
PCR	Polymerase chain reaction
PDB	Protein data bank
Ph	Phenyl
PPB	Plasma protein binding
PPI	Protein-protein interaction
PQS	<i>Pseudomonas</i> quinolone signal
QSAR	Quantitative SAR
Rif	Rifampicin
RNAP	RNA polymerase
RPc	Closed RNAP-promoter complex
RPo	Open RNAP-promoter complex
RU	Resonance unit
SAR	Structure-activity relationship
SBBA	Structure-based biophysical analysis
SD/sd	Standard deviation
SPR	Surface plasmon resonance
ssDNA	Single stranded DNA
Taq	<i>Thermus aquaticus</i>
TCA	Trichloro acetic acid
TLC	Thin layer chromatography
TT	Transcription and translation
WHO	World health organization
β' CC	Coiled-coil in the β' subunit of RNAP

# TABLE OF CONTENTS

<b>1</b>	<b>Introduction.....</b>	<b>1</b>
1.1	Biomolecular interaction analysis by surface plasmon resonance spectroscopy .....	1
1.1.1	Surface plasmon resonance principle .....	1
1.1.2	SPR-based assays .....	2
1.1.3	Biosensors in drug discovery .....	6
1.2	RNA polymerase .....	9
1.2.1	Structure and function .....	9
1.2.2	RNAP as drug target .....	12
1.2.3	$\sigma^{70}$ :core RNAP inhibitors .....	15
<b>2</b>	<b>Aims of the thesis .....</b>	<b>17</b>
<b>3</b>	<b>Results .....</b>	<b>18</b>
3.1	Surface plasmon resonance – more than a screening technology: Insights in the binding mode of $\sigma^{70}$ :core RNAP inhibitors (Publication I).....	18
3.2	Peptide-based investigation of the <i>Escherichia coli</i> RNA polymerase $\sigma^{70}$ :core interface as target site (Publication II).....	19
3.3	Discovery of novel bacterial RNA polymerase inhibitors: pharmacophore-based virtual screening and hit optimization (Publication III) .....	36
3.4	Influence of DNA template choice on transcription and inhibition of <i>Escherichia coli</i> RNA polymerase (Publication IV) .....	51
<b>4</b>	<b>Final discussion .....</b>	<b>52</b>
4.1	Evaluation of $\sigma^{70}$ :core RNAP inhibitor test system.....	52
4.1.1	<i>In vitro</i> transcription assay and core/holo assay.....	52
4.1.2	$\sigma^{70}$ :core assembly inhibition assay .....	53
4.1.3	Initiation inhibition assay .....	55
4.1.4	SPR screening assay .....	55
4.1.5	SPR competition assay .....	57
4.1.6	Binding site identification using wild type and mutant proteins.....	57
4.1.7	Affinity ranking and kinetic profiling .....	58
4.2	Future of $\sigma^{70}$ :core RNAP inhibitors.....	59
<b>5</b>	<b>References .....</b>	<b>61</b>

<b>6</b>	<b>Supporting information .....</b>	<b>70</b>
6.1	Supporting information to Publication I .....	70
6.2	Supporting information to Publication II .....	74
6.3	Supporting information to Publication III .....	81
6.4	Supporting information to Publication IV .....	128
<b>7</b>	<b>Acknowledgments .....</b>	<b>135</b>
<b>8</b>	<b>Appendix .....</b>	<b>136</b>
8.1	Curriculum vitae .....	136
8.2	Publications .....	137
8.3	Oral presentations .....	138
8.4	Poster presentations .....	138

# 1 Introduction

## 1.1 Biomolecular interaction analysis by surface plasmon resonance spectroscopy

Surface plasmon resonance (SPR) spectroscopy is a biophysical method to analyze biomolecular interactions in real-time. Biomolecular interactions or adsorption are fundamental life processes as they are involved for example in intra-/extracellular trafficking [Johnson 2005, Mellmann and Warren 2000], cell signaling [Neiditch *et al.* 2006, Jones *et al.* 2005], DNA transcription and RNA translation [McGhee and von Hippel 1974], and many more. Therefore the study of biomolecular interactions is important in the development of new drugs. In the next sections, the SPR principle, the steps of an assay and the use of SPR in the drug discovery process are described.

### 1.1.1 Surface plasmon resonance principle

Surface plasmon resonance occurs when parallel or p-polarized light shines through a prism on a sensor chip, coated with a thin metal film on top, and the light is reflected. This phenomenon is called total internal reflection. By changing the angle of incidence, the intensity of the reflected light passes through a minimum, the SPR dip. When the light strikes the sensor chip, the photons interact with the free electrons of the metal layer, usually gold, and induce an evanescent wave which is the oscillation of the electrons. Thereby the intensity of the reflected light is reduced. The angle at which the maximum loss of reflected light is detected is called SPR angle [Schasfoort and Tudos 2008]. This angle depends on the refractive indices of the media on both sides of the gold film. When proteins or small molecules adsorb or the medium changes (e.g. buffer composition, concentration) on the chip surface, the refractive index on that side of the metal changes whereas the refractive index on the prism side remains constant. The change in refractive index then in turn shifts the SPR dip. SPR can measure this shift in time, converting the angle shift into a sensorgram (Figure 1). This response signal is usually expressed as resonance units (RU). If this shift is due to a biomolecular interaction, the kinetics of the interaction can be studied in real-time.

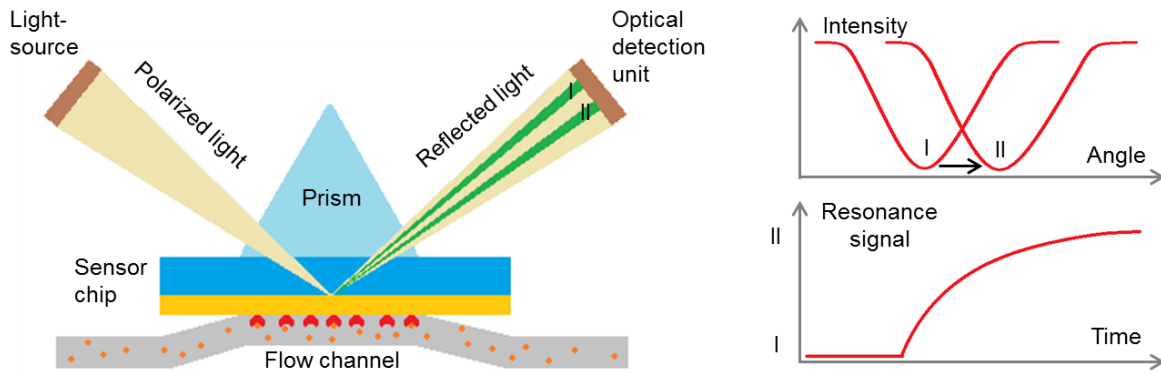


**Figure 1.** Schematic set-up of an SPR experiment (Kretschmann configuration; left side), modified from Löfås (2004). A laser creates p-polarized light that shines through a prism on a sensor chip coated with a gold film. At a certain angle of incidence the reflected light reaches a minimum (SPR dip; I in the upper right panel). In dependence of the mass on the chip the refractive index on the side of the flow channel changes. In turn the SPR dip shifts (II in the upper right panel). When this shift is monitored over time, the result is a sensorgram (lower right panel), from which the kinetic parameters of the biomolecular interaction can be derived.

The correlation of mass adsorption and response signal has been determined experimentally [Stenberg *et al.* 1991] to:

$$1 \text{ RU} = 1 \text{ pg/mm}^2$$

However, the penetration depth of the evanescent field on the sensor surface is limited to approximately 200 nm and fades with increasing distance [Schasfoort and Tudos 2008]. Thus, one of the interaction partners, e.i. the ligand, needs to be fixed relatively close to the surface. This process is called immobilization and will be described in the following section.

### 1.1.2 SPR-based assays

During an SPR experiment the first step is always to immobilize a target biomolecule, the so-called ligand, to the sensor surface. Next, the ligand has to be evaluated regarding its integrity, since only properly folded proteins bind analytes specifically. Then the biosensor is ready for various applications such as detection of binding, binding selectivity, binding affinity, binding kinetics, determination of active concentration, and thermodynamics [Biacore.com April 2014, Myszka and Rich 2000] providing a much greater information depth than traditional

end-point assays, which can give only limited ranges of affinity and only one binding characteristic per experiment [Löfås 2004].

### ***Immobilization***

The term immobilization of the protein ligand is often misunderstood as immobile fixation onto a surface. However, the ligand is more tethered than immobilized, since it is usually bound at only one point to the inert immobilization hydrogel. This 3D matrix improves the ligand's accessibility and can also protect it against denaturation [Schasfoort and Tudos 2008]. Therefore, the composition and choice of the biosensor chip is of importance for the assay set up. A sensor chip contains glass as a carrier which is covered with a thin gold film, enabling surface plasmons to be excited. On top of the metal is an adhesion linking layer, connecting the gold with the immobilization matrix. The matrix is the most critical element of the sensor chip, since it is in contact with both, the ligand and the analyte. The most common matrix polymers are polysaccharides, such as carboxymethyldextran (CMD). It can be used directly for amine coupling or can be modified with streptavidin in order to capture biotinylated ligands. A schematic representation of a biosensor chip with the above described coupling techniques is shown in Figure 2.

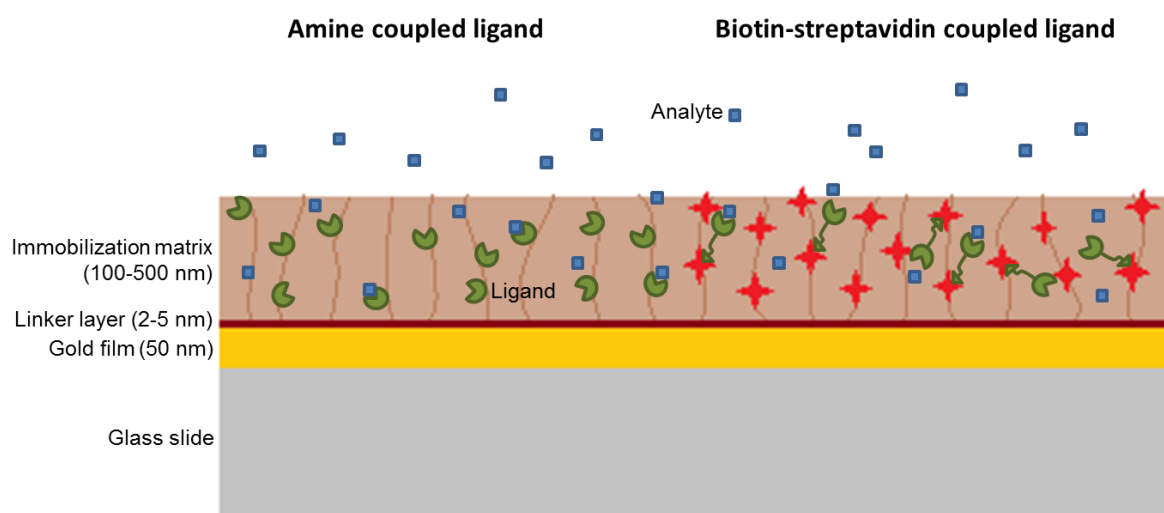


**Figure 2.** Biosensor chip composition. Protein-ligands (green) are directly covalently coupled to the CMD matrix (left side) or – in case of biotin-tagged ligands – captured by one of the four biotin-binding sites of streptavidin-modified (red) immobilization matrices (right side).

**Amine coupling.** The first choice coupling procedure is covalent amine coupling, since it usually gives high yields and stable bonds. Disadvantageous are the random orientation of the

protein ligands on the chip and the low pH used for coupling that may result in the inactivation of the protein, leaving a heterogeneous surface. In order to couple a protein to the biosensor by its surface exposed lysine residues, first the carboxylic acid functions of the CMD matrix have to be activated by *N*-ethyl-*N*'-(dimethylaminopropyl)carbodiimide (EDC). At pHs between 4.5-6.5 the *O*-acylisourea intermediate is formed before being replaced with the *N*-hydroxysuccinimide (NHS), which gives a more stable active ester intermediate. Upon injection of the ligand, aminolysis takes place, releasing the NHS and leaving the protein coupled to the CMD by an amide bond [Johnsson *et al.* 1991] (Figure 3).

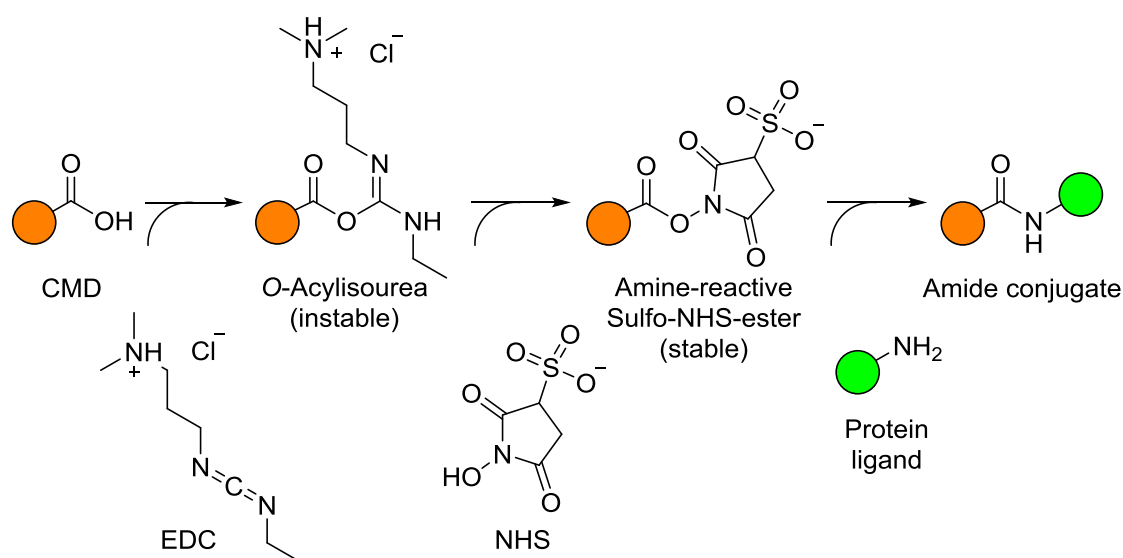


**Figure 3.** Amine coupling reaction, modified from Schasfoort and Tudos (2008) and piercenet.com (NHS and Sulfo-NHS, 05/05/2014).

**Biotin coupling.** An indirect immobilization technique can be achieved by capturing biotinylated ligands on streptavidin-coated sensor chips. This directed coupling method is milder than amine coupling and therefore usually better retains the ligand's integrity. Although this is a non-covalent attachment of the ligand, “chip bleeding” (loss of target protein from the biosensor over time) is minimal due to the strong complex formation ( $K_D \sim 10^{-15}$  M) [Schasfoort and Tudos 2008] which is stable over a wide pH and temperature range.

### ***Biomolecular interactions***

Once the ligand is tethered to the biosensor surface, the first step in an experiment is to condition it with a suitable buffer solution. A stable baseline is very important for high quality



interaction data, as drifts may alter the sensorgram shape. When injecting the analyte, which is captured by the target, the mass on the surface increases, allowing adsorption kinetics to be determined in real-time. This adsorption can also be non-specific to either the ligand or the linker layer, hence, a suitable reference flow cell is needed. The SPR response expresses the mass accumulated on the sensor surface. By a constant flow of running buffer dissociation is induced, flushing off non-specifically-bound compounds first and then also all other reversible bound analytes. In case of very tight interactions, where buffer flow alone is not sufficient to get back to baseline-level, a regeneration solution is injected, breaking the interactions between ligand and analyte. The choice of regeneration solution is vital, since it should leave the ligand intact for hundreds of analysis cycles but at the same time should remove the analyte quantitatively. Then the surface is again conditioned with running buffer for the next analysis cycle (Figure 5). Typical interactions that are analyzed by SPR include antibody-antigen, ligand-receptor, and protein-nucleic acid interactions [Rich and Myszka 2000].

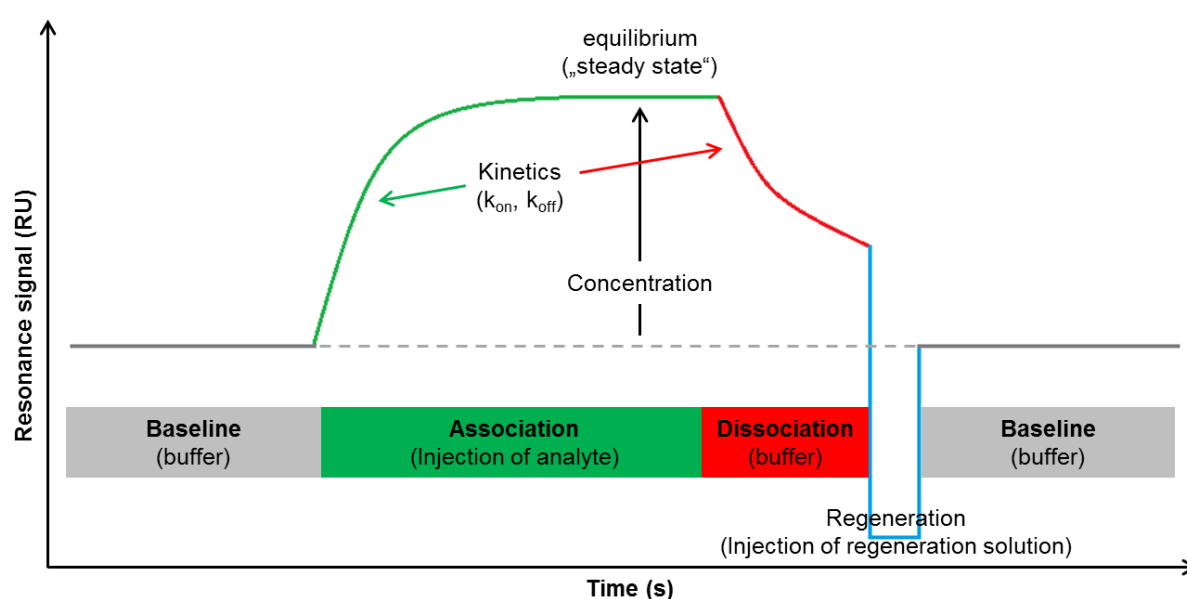


**Figure 5.** Steps of an analysis cycle, modified from Cooper (2002). First, the ligands are conditioned with buffer (baseline), then the analyte is injected and binds to the ligand (association), which can be observed by the increasing resonance signal. After a certain time the injection is stopped and buffer is flowed over the sensor surface, inducing dissociation. Finally, the left-over analytes (in case of strong ligand-analyte complexes) are cleared from the surface by injecting a regeneration solution, leaving the ligands intact for the next analysis cycle.

Although there are many possible applications for SPR, it is used predominately to determine the kinetics of a one-to-one binding process, in which the ligand (A) captures the analyte (B), forming the complex (AB). Global analysis of the shape of the sensorgram for multiple concentrations give the kinetic parameters listed in Table 1.

Parameter	Reaction	Unit
$k_a$ or $k_{on}$	$A + B \rightarrow AB$	$[M^{-1}*s^{-1}]$
$k_d$ or $k_{off}$	$AB \rightarrow A + B$	$[s^{-1}]$
$K_D$	$[A]*[B]/[AB] = k_d/k_a$	$[M]$

**Table 1.** Kinetic parameters obtained from the global analysis of multiple sensorgrams over a wide concentration range.

However, some binding events, especially weak ones (e.g. fragments binding to proteins), cannot be resolved into on- and off-rates by the instrument's sampling frequency (typically 10 Hz), since they equilibrate too quickly [Giannetti 2011].

### 1.1.3 Biosensors in drug discovery

Apart from simple drug target analysis, there are numerous other applications for SPR in the drug development pipeline, as summarized in Figure 6.

As matrix-assisted laser desorption/ionization-time of flight mass spectrometry (MALDI-TOF MS) and electrospray ionization-mass spectrometry (ESI-MS) are particularly powerful tools in protein analysis and thereby target identification, MS was fused with SPR for proteome analysis [Williams and Addona 2000]. In this setup SPR is used for affinity-purification of the protein sample. Additionally, SPR-MS is applicable for an approach called ligand fishing. Here, crude tissue extracts or cell homogenates are screened for possible ligands mostly of orphan receptors [Catimel *et al.* 2000].

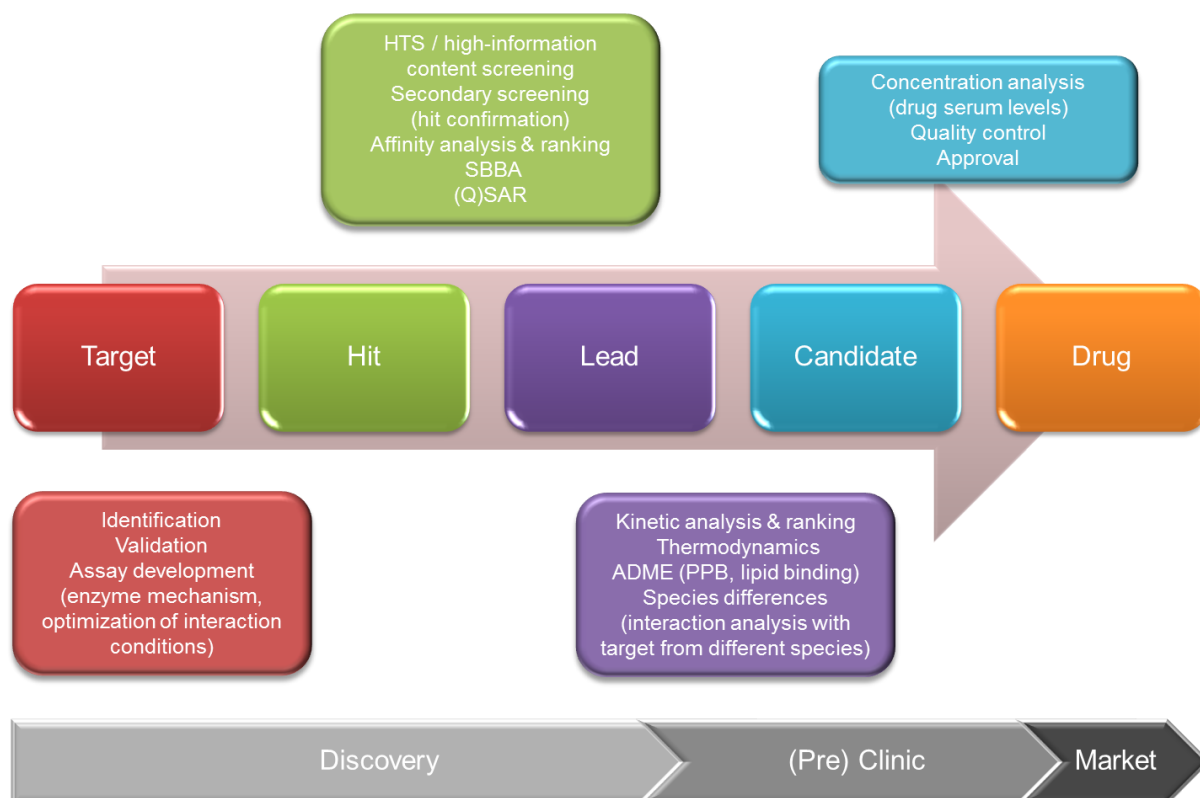


**Figure 6.** Applications of SPR in the drug development pipeline. HTS, high-throughput screening; SBBA, structure-based biophysical analysis; (Q)SAR, (quantitative) structure-activity relationship; ADME, absorption distribution metabolism excretion; PPB, plasma-protein binding.

Furthermore, SPR improves *in vitro* assay development by buffer screening and establishment of regeneration conditions that help elucidating the compound's mode of action. An optimized assay is suitable for direct screening of small molecules with high information content, such as kinetic rate constants and equilibrium response for affinity ranking. This concept was introduced in 2000 by Hämalainen *et al.* searching for HIV-1 protease inhibitors. However, the primary applications for SPR in the pharmaceutical industry are secondary screening to confirm hits and their kinetic characterization [Cooper 2002, Huber 2005]. In most cases – e.g. enzyme inhibitors – compounds with fast association and slow dissociation rate constants are preferred. Another application of SPR is the identification of compounds that truly bind to the target's active/binding site by using mutated target proteins as references in SPR studies. Huber termed the integration of bioinformatics approaches in SPR “structure-based biophysical analysis” (SBBA) [Huber 2005]. At Hoffman-La Roche, selective hydroxymethyl-pterin pyrophosphokinase inhibitors were identified by an SBBA attempt. Based on the crystal structure of the target protein in complex with a substrate-analog, a pharmacophore was generated and virtual screening hits selected. In order to identify substrat

pocket binders only, a mutant target protein was produced and served as reference in the SPR assay. Thus, only compounds with high affinity to the wildtype and impaired affinity to the mutant were selected for further development. [Huber 2005]. An example for an SPR-assisted QSAR study is given by Markgren *et al.* (2002). They demonstrated how structural changes of HIV-1 protease inhibitors affect not only the activity but also the kinetic parameters. Further applications of SPR during drug development are early ADME studies. Especially for larger numbers of compounds it is convenient to screen them for their affinity to the plasma proteins human serum albumin (HSA) and  $\alpha_1$ -acid glycoprotein (AGP). The equilibrium dissociation constant  $K_D$  can then be converted into “% bound” as carried out in Nyberg *et al.* (2002). Lipid interaction models to predict membrane permeability are reviewed in Heyse *et al.* (1998).

## 1.2 RNA polymerase

The first step of gene expression is called transcription. During transcription, which is divided in three steps – initiation, elongation, and termination – the RNA polymerase generates an RNA copy from a DNA template. The transcription process is highly conserved in all living cells [Artsimovitch and Vassyleyev 2006].

### 1.2.1 Structure and function

Bacterial RNA polymerase (RNAP) is a multi-subunit enzyme. Core RNAP is comprised of five subunits  $\alpha_2\beta\beta'\omega$  with a molecular weight of 378 kDa in *E. coli*. The two  $\alpha$  subunits are required for enzyme assembly. The big  $\beta$  and  $\beta'$  subunits – connected by the bridge helix – together form the active site, where  $\beta$  is involved in chain initiation and elongation and  $\beta'$  in binding of the DNA template [Chopra 2007, Mariani and Maffioli 2009]. The small  $\omega$  subunit supports assembly of core RNAP. This subunit composition makes it one of the most complex enzymes yet studied [Burgess 1971]. Together with a dissociable  $\sigma$ -factor ( $\sigma^{70}$  in *Escherichia coli*), which is responsible for promoter recognition and transcription initiation [Saecker *et al.* 2011], the holo enzyme is formed (458 kDa). The crystal structure of the *E. coli* holo enzyme was solved in 2013 by Murakami. Its overall shape resembles a crab claw (Figure 7).

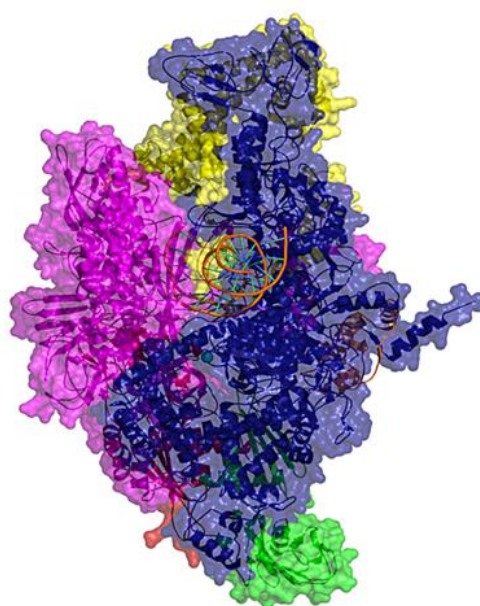


**Figure 7.** Composition of the *E. coli* RNA polymerase holo enzyme with bound DNA (homology model created by M. Negri, HIPS-DDOP).  $\alpha$  subunits in green and red,  $\beta$  subunit in magenta,  $\beta'$  subunit in blue,  $\omega$  subunit in orange, and  $\sigma^{70}$  in yellow.

Transcription initiation is a multi-step process during which RNAP and DNA undergo several conformational changes [Saecker *et al.* 2011]. After holo enzyme formation, RNAP binds specifically to the promoter duplex DNA region, forming the closed RNAP-promoter complex (RPc) [Artsimovitch and Vassilyev 2006]. Then the “transcription bubble” is formed by unwinding and actively opening 13-15 base pairs (bp) of DNA [Gruber and Gross 2003], including the start site. The DNA template strand is loaded into the active site, forming the stable open RNAP-promoter (RPo) complex [Saecker *et al.* 2011]. Then either productive or abortive transcription starts. Abortive RNA transcripts are usually 3-12 nucleotides (nt) in length [Hsu 2002] and have been detected also *in vivo* [Goldman *et al.* 2009]. These abortive products may rebind and function as primer for transcription [Goldman *et al.* 2009]. When the RNA transcript reaches 12 nt the promoter contacts are loosened and the  $\sigma$ -factor is released [Hsu 2002, Mooney *et al.* 2005], transcription moves on to the elongation phase. During elongation, several nucleotide (NTP) addition cycles are carried out by a two-metal mechanism [Steiz and Steiz 1993]. One  $Mg^{2+}$  ion remains tightly bound in the active center, coordinated by three aspartates, and a second  $Mg^{2+}$  ion is delivered with each incoming NTP substrate through the secondary channel. A schematic representation of the transcription elongation complex can be found in Figure 8.

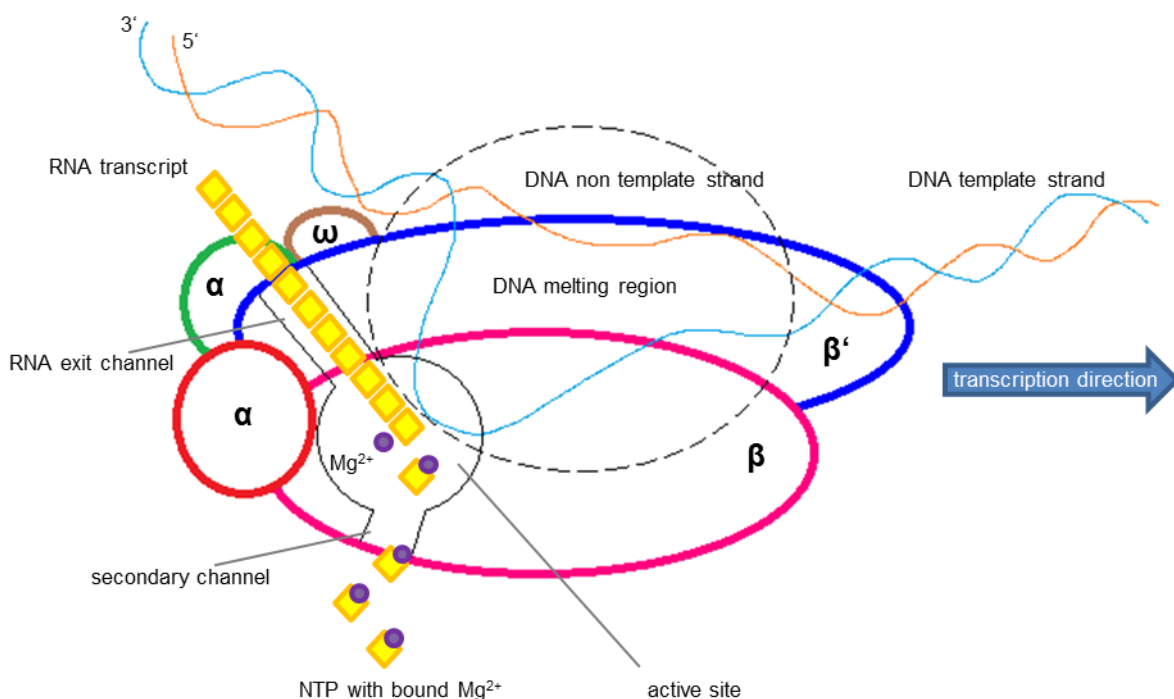


**Figure 8.** Transcription elongation complex modified from Mariani and Maffioli (2009).

When RNAP encounters a terminator sequence or the terminator factor Rho [Artsimovitch and Vassilyev 2006], transcription is stopped and RNAP released from the DNA.

### $\sigma$ -factors

Although core RNAP alone is capable to transcribe DNA from ends or nicks, it requires a  $\sigma$ -factor to specifically initiate transcription from a promoter [Burgess *et al.* 1969, Travers and Burgess 1969]. The primary  $\sigma$ -factor in *E. coli* is  $\sigma^{70}$ , an acidic protein with a size of 70 kDa. This “housekeeping”  $\sigma$ -factor is sufficient for growth under nutrient rich conditions [Saecker *et al.* 2011]. However, when the bacteria suffer from stress, alternative  $\sigma$ -factors such as  $\sigma^H$  (heat shock),  $\sigma^N$  (nitrogen assimilation) or  $\sigma^E$  (extracellular stress) take over [Gruber and Gross 2003, Paget and Helmann 2003, Gourse *et al.* 2006].

$\sigma^{70}$  consists of four independently folded domains (regions 1.1, 1.2, 2 and 4) that are connected by regions of variable length [Helmann and Chamberlin 1988, Lonetto *et al.* 1992]. Region 1.1 of free  $\sigma$  binds to region 4.2, forming a compact structure, and thereby also auto-inhibits region 4.2 from binding to DNA [Schwartz *et al.* 2008]. Regions 2.1 and 2.2 of  $\sigma^{70}$  (residues 361-390) [Lesley and Burgess 1989] are responsible for the tight binding to the  $\beta'$  coiled-coil (residues 260-309) [Arthur *et al.* 2000]. Regions 2.3 and 2.4 however recognize the -10 promoter element [Siegele *et al.* 1989, Waldburger *et al.* 1990, Saecker *et al.* 2011], whereas region 4.2 binds to the -35 consensus sequence [Gardella *et al.* 1989, Saecker *et al.* 2011]. Region 3 interacts with DNA upstream of the Pribnow box [Villain-Guillot *et al.* 2007a] and the residues 1060-1240 of the  $\beta$  subunit of core RNAP [Burgess and Anthony 2001]. Functions and interaction partners of  $\sigma^{70}$  are also illustrated in Figure 9.

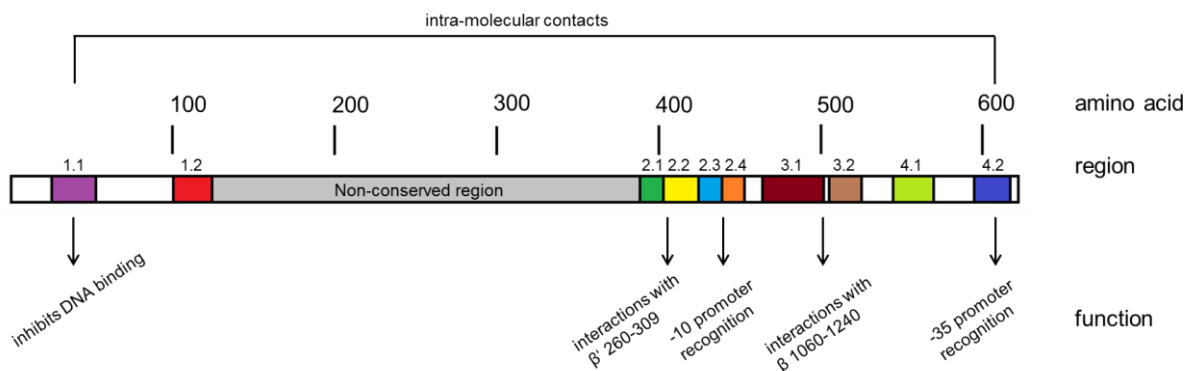


**Figure 9.** Schematic representation of *E. coli*  $\sigma^{70}$  modified from Burgess and Anthony (2001). Conserved regions are colored and their functions indicated as described in the text.

### 1.2.2 RNAP as drug target

According to the World Health Organization (WHO) and experts in the field of anti-infective research, resistance against antibacterial drugs is an increasing problem all over the world [WHO.int 05/15/2014, Chopra 2003, Thomson and Bonomo 2005, McGowan 2006, Rice 2006, Talbot *et al.* 2006]. Especially the so-called ESKAPE strains (*Enterococcus faecium*, *Staphylococcus aureus*, *Klebsiella* species, *Acinetobacter baumannii*, *Pseudomonas aeruginosa*, and *Enterobacter* species) are often multi-drug resistant [Boucher *et al.* 2009, Rice 2008]. For the drug discovery it is wise to inhibit established targets with existing proof-of-principle, but search for new modes of action [Chopra 2007, Payne *et al.* 2007]. RNAP is such a validated target protein, since the RNAP inhibitor rifampicin is approved in the clinical treatment of tuberculosis since many years. The effectivity is explained by the essentiality of RNAP for bacterial growth and survival [Ji *et al.* 2001, Xu *et al.* 2005, Artsimovitch and Vassylyev 2006]. Furthermore, RNAP is highly conserved among pathogenic bacteria, allowing the development of broad-spectrum antibiotics [Darst 2004, Ho *et al.* 2009]. Selectivity towards eukaryotic RNAPs – especially mammalian RNAP II – is possible due to only partially homologous sequences as well as different surface properties and shape [Cramer 2002, Artsimovitch and Vassylyev 2006]. The clinically used rifampicins and fidaxomicin are described in more detail in the following.

As stated in Ma *et al.* (2013), the majority of RNAP inhibitors bind to the active site, which is a large cleft offering multiple binding sites. The most important anti-transcription drugs that are used in the treatment of tuberculosis and leprosy are rifampicin, rifapentin and rifabutin [Villain-Guillot *et al.* 2007a]. The first of these rifamycins were discovered in 1959 as a fermentation product of actinomycetes and differ only in the C3 or C3/C4 substitutions [Artsimovitch and Vassylyev 2006]. They bind with high affinity to the  $\beta$  subunit in the DNA channel only 12 Å away from the active site. Thereby, the ansa-ring forms polar and van der Waals interactions with 12 amino acid residues of  $\beta$  [Campbell *et al.* 2001]. Rifamycins inhibit transcription initiation by inducing a steric clash with the nascent RNA/DNA-hybrid strand (3-4 bp) [Campbell *et al.* 2001, Feklistov *et al.* 2008, McClure and Cech 1978] and are active against Gram-positive and Gram-negative bacteria [Artsimovitch & Vassylyev 2006]. However, the resistance frequency – due to mutations in the *rpoB* gene, encoding for  $\beta$  – is relatively high [Villain-Guillot *et al.* 2007a]. The most frequent substitutions that account for more than 75 % of rifampicin-resistance in clinical isolates of *Mycobacterium tuberculosis* are  $\beta$ D441V,  $\beta$ H451D/Y, and  $\beta$ S456L (D516, H526, S531 in *E. coli*) [Ramaswamy and



Musser 1998]. Other transcription inhibitors that bind to one of the multiple sites within the active center cleft are sorangicin [Campbell *et al.* 2005], streptolydigin [Crum *et al.* 1955, Temiakov *et al.* 2005, Kyzer *et al.* 2005], microcin J25 [Salomón and Farías 1992, Blond *et al.* 2001, Villain-Guillot *et al.* 2007a], GE-23077 [Zhang *et al.* 2014], tagetitoxin [Artsimovitch *et al.* 2011], and  $\alpha$ -amanitin [Bushnell *et al.* 2002].

Further binding sites on the RNAP are the switch region [Srivastava *et al.* 2011], the  $\sigma^{70}$ :core interface (described in the next section) and allosteric sites, such as a cavity between the  $\beta'$  subunit and the bridge helix where the CBR-703 antimicrobials and salinamide A bind to [Artsimovitch *et al.* 2003, Malinen *et al.* 2014, Degen *et al.* 2014] or the interface of  $\beta'$  and  $\omega$  to which the alarmone ppGpp binds that regulates RNAP function under harsh environmental conditions [Ross *et al.* 2013, Zuo *et al.* 2013].

Switch region binders are reported to be the natural products myxopyronin [Mukhopadhyay *et al.* 2008, Belogurov *et al.* 2009, Ho *et al.* 2009], coralopyronin [Haebich and von Nussbaum 2009], ripostatin [Haebich and von Nussbaum 2009], and lipiarmycin/fidaxomicin (Figure 10) as well as the synthetic ureidothiophenes [Arhin *et al.* 2006, Sahner *et al.* 2013], pyridyl-benzamides [McPhillie *et al.* 2011], and squaramides [Buurman *et al.* 2012]. Lipiarmycin which is structurally very similar to fidaxomicin, is a macrocyclic antibiotic discovered in 1975 produced by a fermentation mix [Sergio *et al.* 1975, Arnone and Nasini 1987, Cavalleri *et al.* 1988]. They specifically inhibit the initiation step [Sonenshein *et al.* 1977] by binding to the  $\beta'$  subunit [Gualtieri *et al.* 2006] within the switch region. The switch region can be imagined as a hinge that connects the catalytic subunits ( $\beta$  and  $\beta'$ ) and interacts with the template DNA [Artsimovitch *et al.* 2012]. It is U-shaped and located between two hydrophobic pockets [McPhillie *et al.* 2011]. Fidaxomicin was found to be particularly active against *Clostridium difficile* RNAP *in vivo* [Swanson *et al.* 1991] and was therefore approved by the FDA in May 2011 for the treatment of *C. difficile* infections [FDA.gov 05/19/2014].

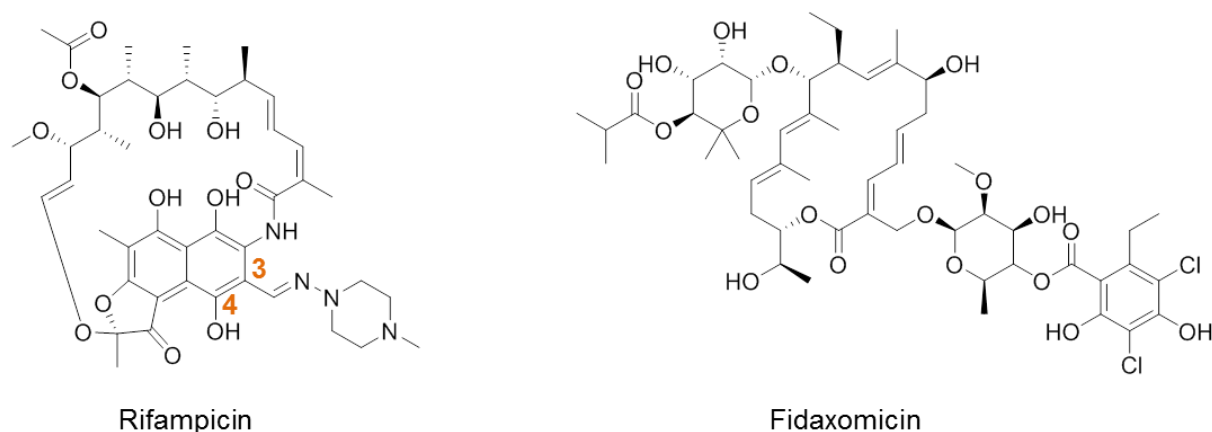


**Figure 10.** Clinically used RNAP inhibitors rifampicin (the common modification positions C3 and C4 are labeled in orange) and fidaxomicin.

### $\sigma^{70}$ :core interface as target site

Although the protein-protein interaction of core RNAP and the  $\sigma^{70}$  factor does not offer any clefts as binding sites for small molecules, the inhibition of this interaction is still very attractive for the antibiotics drug discovery [Bergendahl *et al.* 2003, André *et al.* 2004, Ma *et al.* 2013]. Firstly,  $\sigma$  factors are unique to bacteria and are indispensable to initiate transcription [Murakami and Darst 2003], that means bacterial growth is impossible upon complete disruption of this essential interaction. Secondly, the interface including the  $\beta'$  coiled-coil and region 2.1-2.2 of  $\sigma^{70}$  are highly conserved among bacteria (Figure 11) [Sharp *et al.* 1999, Vassylyev *et al.* 2002, Lesley and Burgess 1989, Owens *et al.* 1998]. Thirdly, eukaryotic transcription factors – except for  $\sigma$  factors in mitochondria [Tracy and Stern 1995] and chloroplasts [Allison 2000], which are more related to viral transcription systems [Glaser *et al.* 2007] – diverge from their prokaryotic counterparts. Hence, by targeting this protein-protein interaction not only broad-spectrum activity but also selectivity may be gained. Fourth and finally, the  $\sigma^{70}$  interaction site on  $\beta'$  is used by several other  $\sigma$  factors. Therefore, the development of drug resistance by point mutations is unlikely, since these mutations would affect the interaction with essential protein partners as well [Bergendahl *et al.* 2003, André *et al.* 2004].

**$\sigma^{70}$  region 2.1-2.2 homologs**

	375	416
	↓	↓
E. coli	AKKEMVEANLRLVISIAKKYTNRGLQFLDLIQEGNIGLMKAV	
M. xanthus	AKSELVEANLRLVVSI AKKYTNRGLQFLDLIQEGNIGLMKAV	
S. aureus	AKSRLAEANLRLVVSI AKRYVGRGMLFLDLIQEGNMGLIKAV	
B. subtilis	SKRRLAEANLRLVVSI AKRYVGRGMLFLDLIQEGNMGLMKAV	
T. aquaticus	ARQHLEANLRLVVSI AKKYTGRGLSFLDLIQEGNQGLIRAV	
H. influenza	AKKEMVEANLRLVISIAKKYTNRGLQFLDLIQEGNIGLMKAV	
P. aeruginosa	AKKEMVEANLRLVISIAKKYTNRGLQFLDLIQEGNIGLMKAV	
	* :*****:****:* ** ***** ** :**	
	region 2.1	region 2.2

 **$\beta'$  coiled-coil homologs**

	260	309
	↓	↓
E. coli	FATSDLNDLYRRVINRNNRLKRLDLAAPDIIVRNEKRMLQEAVDALLDN	
M. xanthus	FATSDLNDLYRRVINRNNRLKRLQELNAPDIIIRNEKRMLQEAVDALFDN	
S. aureus	FATSDLNDLYRRVINRNNRLKRLDLGAPGIIIVQNEKRMLQEAVDALIDN	
B. subtilis	FATSDLNDLYRRVINRNNRLKRLDLGAPSIIVQNEKRMLQEAVDALIDN	
T. aquaticus	FATSDLNDLYRRLINRNNRLKLLAQGAPEIIIRNEKRMLQEAVDAVIDN	
H. influenza	FATSDLNDLYRRVINRNNRLKRLDLIAPDIIVRNEKRMLQESVDALLDN	
P. aeruginosa	FATSDLNDLYRRVINRNNRLKRLDLAAPDIIVRNEKRMLQEAVDALLDN	
	*****:*****:* ** **: ***** **:***	

**Figure 11.** Conserved sequences of the  $\sigma^{70}$ : $\beta'$  interface (\* identical amino acids, : homolog amino acids).

**1.2.3  $\sigma^{70}$ :core RNAP inhibitors**

Since one decade researchers are developing assays [Bergendahl *et al.* 2003, André *et al.* 2004] in order to screen natural product and small molecule libraries for inhibitors targeting the interaction between  $\sigma^{70}$  and core RNAP. For example the group of Burgess developed a robust luminescence resonance energy transfer (LRET)-based high-throughput assay and screened a chemical library to interrupt the tight interaction between  $\beta'_{100-309}$  and  $\sigma^{70}$  ( $K_D$  10-50 nM) [Glaser *et al.* 2007]. They identified four hits that also inhibited transcription. However, they had serious problems with compound insolubility. Further  $\sigma^{70}$ :core inhibitors are described below.

**SB series.** The SB series of compounds are phenyl-furanyl-rhodanines. They have been discovered as  $\sigma^{70}$ :core RNAP assembly inhibitors in 2004 by the group of Leonetti [André *et al.* 2004] in an ELISA-based screening. One of the most potent compounds was SB2 (Figure

**Bis-indoles.** Recently, a structure-based approach was applied to identify new  $\sigma$ :core RNAP inhibitors. Ma et al. created a pharmacophore model based on the structural data of the protein-protein interface and screened a peptidomimetic library. Some bis-indoles reached the highest scores and were synthesized. Most effective disruption of transcription initiation complexes was reported for the 7,7'-linked amides and glyoxylamides (best GKL003, Figure 12) [Mielczarek *et al.* 2014]. By performing isothermal titration calorimetry (ITC) experiments with wildtype and mutant proteins, it was shown that GKL003 binds to the coiled-coil of the  $\beta'$  subunit [Ma *et al.* 2013]. Additionally, *in vivo* activity on both Gram-positive and Gram-negative bacteria was claimed [Ma *et al.* 2013, Mielczarek *et al.* 2014], however inhibitory concentrations were very high with around 1 mM.

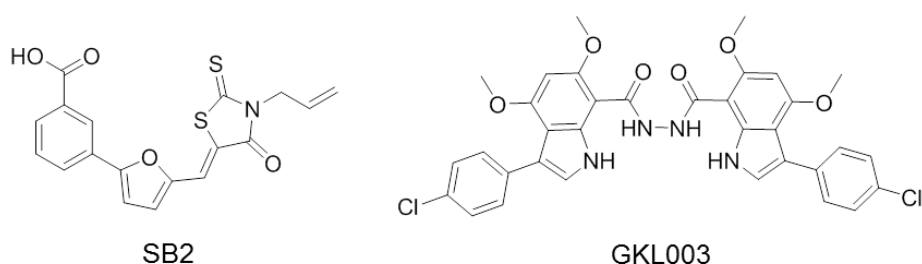


**Figure 12.** The  $\sigma$ :core assembly inhibitor SB2 [André *et al.* 2006] and the initiation complex formation inhibitor GKL003 [Ma *et al.* 2013].

## 2 Aims of the thesis

Infectious diseases are a constant threat for human and animal health, especially nowadays with multiple antibiotic drug resistances. Hence, new antibiotics with novel modes of action and target sites – in order to avoid cross-resistances with existing antimicrobial drugs – are urgently needed. We focus on bacterial RNA polymerase as a validated drug target. A promising target site within this enzyme is the essential protein-protein interaction between core and the  $\sigma^{70}$  factor, which is indispensable for specific initiation of transcription (see chapter 1.2 of the introduction). This interaction surface is highly conserved and has no overlaps with the binding sites of the clinically used rifamycins and fidaxomicin.

In order to identify, characterize, and classify such  $\sigma^{70}$ :core RNAP inhibitors, we need robust *in vitro* assays. They provide a solid basis for the hit selection and the rational design and optimization of new drugs. For the structure-based drug design and optimization, the exact binding site is of utmost importance. Therefore, the following binding and functional assays have been planned to be developed and evaluated in the course of this thesis:

- Transcription assay variations of the existing *in vitro* transcription assay with separate addition of  $\sigma^{70}$  to study the effect on diverse DNA templates as well as RNAP inhibitors. For this purpose recombinant production of the  $\sigma^{70}$  is required.
- ELISA-based  $\sigma^{70}$ :core assembly inhibition assay to identify and classify inhibitors of holo enzyme formation.
- HPLC-based initiation inhibition assay to verify the concept of  $\sigma^{70}$ :core inhibition leading to inhibition of transcription initiation and classify the protein-protein interaction inhibitors.
- SPR screening assay to identify small molecule compounds binding to the coiled-coil and/or lid-rudder-system of the  $\beta'$  subunit (amino acids 200-341, abbreviated  $\beta'$  CC-LRS) of RNAP which is mostly responsible for the interaction with  $\sigma^{70}$ . Therefore, cloning, expression, and purification of this truncated  $\beta'$  subunit is necessary.
- SPR competition assay to show the direct inhibition of the protein-protein interaction hot spot between  $\beta'$  and  $\sigma^{70}$  (not mediated through an allosteric effect).
- SPR-based binding site identification using wildtype  $\beta'$  CC-LRS and site-directed mutant proteins.
- SPR kinetic profiling: Determination of association and dissociation rates, as well as equilibrium dissociation constants to characterize and rank  $\beta'$  CC-LRS binders.

### 3 Results

#### 3.1 Surface plasmon resonance – more than a screening technology: Insights in the binding mode of $\sigma^{70}$ :core RNAP inhibitors

Kristina Hüsecken, Stefan Hinsberger, Walid A. M. Elgaher, Jörg Haupenthal, and Rolf W. Hartmann

Full text article in *Future Med. Chem.* 2014, **8**, 1551-65.

doi: 10.4155/fmc.14.105

#### Publication I

##### ABSTRACT:

**Background:** Antibiotic resistance has become a major health problem. The  $\sigma^{70}$ :core interface of bacterial RNA polymerase is a promising drug target. Recently, the coiled-coil and lid-rudder-system of the  $\beta'$  subunit has been identified as an inhibition hot spot. **Results/Methodology:** By using surface plasmon resonance-based assays, inhibitors of the protein-protein interaction were identified and competition with  $\sigma^{70}$  was shown. Effective inhibition was verified in an *in vitro* transcription and a  $\sigma^{70}$ :core assembly assay. For one hit series we found a correlation between activity and affinity. Mutant interaction studies suggest the inhibitors' binding site. **Conclusion:** Surface plasmon resonance is a valuable technology in drug design, that has been used in this study to identify and evaluate  $\sigma^{70}$ :core RNA polymerase inhibitors.

### 3.2 Peptide-based investigation of the *Escherichia coli* RNA polymerase $\sigma^{70}$ :core interface as target site

Kristina Hüsecken<sup>#</sup>, Matthias Negri<sup>#</sup>, Martina Fruth, Stefan Boettcher, Rolf W. Hartmann, and Jörg Haupenthal

<sup>#</sup> These authors contributed equally to this work.

Reprinted with permission from *ACS Chemical Biology* 2013, **8**: 758-766. Copyright © 2013 American Chemical Society.

#### Publication II

**ABSTRACT:** The number of bacterial strains that are resistant against antibiotics increased dramatically during the past decades. This fact stresses the urgent need for the development of new antibacterial agents with novel modes of action targeting essential enzymes such as RNA polymerase (RNAP). Bacterial RNAP is a large multi-subunit complex consisting of a core enzyme (subunits:  $\alpha_2\beta\beta'\omega$ ) and a dissociable sigma factor ( $\sigma^{70}$ ; holo enzyme:  $\alpha_2\beta\beta'\omega\sigma^{70}$ ) that is responsible for promoter recognition and transcription initiation. The interface between core RNAP and  $\sigma^{70}$  represents a promising binding site. Nevertheless, detailed studies investigating its druggability are rare. Compounds binding to this region could inhibit this protein–protein interaction and thus holo enzyme formation, resulting in inhibition of transcription initiation. Sixteen peptides covering different regions of the *Escherichia coli*  $\sigma^{70}$ :core interface were designed; some of them – all derived from  $\sigma^{70}$  2.2 region – led to a strong RNAP inhibition. Indeed, an ELISA-based experiment confirmed the most active peptide P07 to inhibit the  $\sigma^{70}$ :core interaction. Furthermore, an abortive transcription assay revealed that P07 impedes transcription initiation. In order to study the mechanism of action of P07 in more detail, molecular dynamics simulations and a rational amino acid replacement study were performed, leading to the conclusion that P07 binds to the coiled-coil region in  $\beta'$  and that its flexible N-terminus inhibits the enzyme by interaction with the  $\beta'$  lid-rudder-system (LRS). This work revisits the  $\beta'$  coiled-coil as a hot spot for the protein–protein interaction inhibition and expands it by introduction of the LRS as target site.

## Introduction

As bacterial RNA polymerase (RNAP) is essential for bacterial growth and survival, it is an attractive target for drug development.<sup>1,2</sup> RNAP is highly conserved among bacteria, enabling the development of broad spectrum antibiotics. Along with the recently (May 2011) FDA approved RNAP inhibitor Lipiarmycin (fidaxomicin/Dificid),<sup>3</sup> the Rifamycins are the only RNAP inhibitors that are in clinical use.<sup>2</sup> However, the use of the Rifamycins led to the occurrence of single point mutations in the *rpoB* gene (encoding for the beta subunit of the enzyme), resulting in strains that exhibit highly elevated MIC values.<sup>4,5</sup> Also resistance mechanisms other than target mutation have been reported for Rifampicin.<sup>6</sup> Besides the Rifamycin binding site, numerous other binding sites in RNAP for diverse inhibitors are known.<sup>7-11</sup> In this context several new inhibitors of RNAP have been discovered in *in vitro* tests, ranging from highly active natural products<sup>12-14</sup> to small organic molecules.<sup>7,8,15,16</sup> However, these compounds also bear several disadvantages, such as poor antibacterial activity,<sup>8</sup> insufficient specificity for RNAP,<sup>17</sup> minimal absorption into mammalian cells,<sup>18</sup> or inadequate physicochemical properties,<sup>19,20</sup> which impede their use in the clinic. A strategy to overcome these drawbacks is the development of new antibacterial agents with novel and defined modes of action. In this study we focus on the interface between the *Escherichia coli* (*E. coli* or *Ec*) RNAP core enzyme and  $\sigma^{70}$  as a potential binding site in order to inhibit their assembly, which is essential for transcription initiation. As no  $\sigma^{70}$  homologue has been found in mammalian cells except some specificity factors in mitochondria that seem to be more related to viral transcription systems,<sup>21</sup> we do not expect side effects of a drug targeting this assembly step. We applied a peptide approach to provide a basis for the generation of new classes of RNAP inhibitors that interfere with a defined binding site within this interface. The recent identification of a peptidic RNAP inhibitor<sup>22</sup> and the structural studies of Sharp and colleagues<sup>23</sup> motivated us to rationally design a set of peptides derived from different interface regions (taken from  $\beta$ ,  $\beta'$ , and  $\sigma^{70}$  subunits). The peptides were chosen on the basis of mutagenesis data<sup>23-27</sup> and 3D information of the enzyme (e.g., PDB 3IYD). In a transcription assay utilizing RNAP core and holo enzyme in parallel we identified two peptides with IC<sub>50</sub>'s in the low micromolar range, both of them derived from the  $\sigma^{70}$  2.2 region. They inhibited RNAP holo enzyme more strongly than the core enzyme, supporting our idea of their mode of action. ELISA-based binding experiments confirmed the most active peptide P07 to inhibit the interaction between  $\sigma^{70}$  and the core enzyme. Furthermore, an abortive transcription assay revealed that P07 impedes the initiation of transcription. Molecular dynamics (MD) simulations, which were accompanied by studies in which mutated



variants of P07 were examined, suggested P07 to target the  $\beta'$  coiled-coil and lid-rudder-system ( $\beta'$ CC-LRS) hot spot. In this work we revisited the  $\beta'$ CC, which was already proposed by the group of Burgess as a promising binding site,<sup>16,28</sup> and expanded it by introducing the LRS as target site, resulting in a hot spot for potent inhibition of the protein–protein interaction. Our data might lead to the generation of new antibacterial drugs targeting RNAP with a novel mode of action.

## Results and Discussion

**Design of Peptides.** In order to inhibit the  $\sigma^{70}$ :core protein–protein interaction, we designed 16 peptides derived from the most promising regions in the  $\sigma^{70}$ :core interface of *E. coli* RNAP. Their sequences span from 15 to 24 amino acids (aa) (Table 1). The bases for their selection were published mutagenesis data<sup>23–27</sup> and structural information. In detail, 12 peptides were selected from *Ec*  $\sigma^{70}$  (P01–12). We considered all aa that were reported to elicit at least 5-fold core binding defects, which were Leu384, Val387, Leu402, Asp403, Gln406, Glu407, Asn409, Met413, Pro453, Pro504, Glu555, Arg562, Ile565, and Leu598 (Table 1, aa highlighted in red).<sup>23</sup> Furthermore,  $\sigma^{70}$  residues 361–390 (P01–06) were reported to be important for efficient core-binding activity (Table 1, underlined aa).<sup>24</sup> Peptides P13–15 are derived from *Ec*  $\beta'$ 260–309, a coiled-coil region ( $\beta'$ CC) that is reported as binding hot spot for  $\sigma^{70}$ .<sup>22,25,26,29,30</sup> Amino acid mutations R275Q, E295K, and A302D led to inviable cells in an *in vivo* assay and prevented holo enzyme formation.<sup>25</sup> These relevant aa are present in P13–15 (Table 1, highlighted in red). P16 represents the *Ec*  $\beta$  flap-tip helix (underlined aa) and contains a hydrophobic patch described to interact with the  $\sigma^{70}$  region 4.<sup>27</sup> Four more peptides were chosen as control peptides that should not inhibit RNAP. The aa sequence of control peptide C01 was chosen randomly, whereas C02–04 are reported to have antimicrobial activity.<sup>31–36</sup>

**Table 1.** List of designed peptides; details concerning selected peptides are given

Peptide	Subunit <sup>a</sup>	Amino acid sequence <sup>b</sup>	Length (aa)
P01	$\sigma^{70}$ (375-390)	AKKEMVEAN <u>LRL</u> VISI	16
P02	$\sigma^{70}$ (380-395)	<u>VEAN</u> LRLVISIAKKYT	16
P03	$\sigma^{70}$ (385-402)	<u>RL</u> VISIAKKYTNRGLQFL	18
P04	$\sigma^{70}$ (385-408)	<u>RL</u> VISIAKKYTNRGLQFLDLIQEG	24
P05	$\sigma^{70}$ (387-404)	<u>VISIA</u> KKYTNRGLQFLDL	18

P06	$\sigma^{70}$ (390-407)	IAKKYTNRGLQF <u>LDLIQE</u>	18
P07	$\sigma^{70}$ (395-413)	TNRGLQF <u>LDLIQEGNIGLM</u>	19
P08	$\sigma^{70}$ (400-416)	QF <u>LDLIQEGNIGLM</u> KAV	17
P09	$\sigma^{70}$ (440-457)	TRSIADQARTIR <u>IPVHMI</u>	18
P10	$\sigma^{70}$ (492-507)	DKIRKVLKIAKE <u>PISM</u>	16
P11	$\sigma^{70}$ (552-568)	TAREAKVLRMR <u>FGIDMN</u>	17
P12	$\sigma^{70}$ (594-609)	ALRK <u>L</u> RHPSRSEVLRS	16
P13	$\beta'$ (265-280)	LNDLYRRVIN <u>RNNRLK</u>	16
P14	$\beta'$ (275-290)	<u>RNNRLK</u> RLLDLAAPDI	16
P15	$\beta'$ (291-306)	IVRNE <u>K</u> RMLQE <u>AVDAL</u>	16
P16	$\beta$ (893-907)	TQLT <u>PEEKLLRAIFG</u>	15
C01 <sup>c</sup>	-	LATKALYIERLASATA	16
C02 <sup>c</sup>	-	RQRVEELSKFSKKGAAARRRK	21
C03 <sup>c</sup>	-	SIGSALKKALPVAKKIGKIALPIAKAALP	29
C04 <sup>c</sup>	-	GWGSFFKKAHVGVGKAALTHYL	25

<sup>a</sup> $\sigma^{70}$ ,  $\beta$ , and  $\beta'$  subunits; in brackets: amino acid (aa) positions according to the *E. coli* RNAP subunit sequences. <sup>b</sup>Underlined and in red: aa that are most important for  $\sigma^{70}$ :core interaction, according to the literature.<sup>23–27</sup> P01–08 are shifted in their lines for comparability reasons. <sup>c</sup>Control peptides.

**Activity in Transcription Assay.** In order to investigate whether these peptides inhibit the  $\sigma^{70}$ :core interaction, transcription reactions with either core or holo RNAP were performed. We first tested the RNAP inhibitors Rifampicin, Coralopyronin, and CBR703,<sup>6,8,13</sup> which are described to inhibit the RNAP core enzyme, as well as Lipiarmycin (Lpm) and SB2, described to target the  $\sigma^{70}$ :core interaction.<sup>7,37–39</sup> As our results illustrate (Table 2), the IC<sub>50</sub> values of the core enzyme inhibitors were around 2-fold lower for the core enzyme (compared to holo), while SB2 and Lpm inhibited the holo enzyme to a higher extent. On the basis of the results of these reference compounds, we expected the peptides to show a stronger inhibition of the holo enzyme. Four out of the 16 interface-derived peptides showed >50% inhibition at 50  $\mu$ M (Table 2B). Surprisingly, also the control peptide C01 showed moderate activity. As a consequence, five mutant C01 peptides were designed indicating interactions with a (still unknown) target site (Supplementary Scheme SII). For the most active interface-derived peptides, IC<sub>50</sub> values were determined. All of them inhibited the holo enzyme more strongly than core RNAP. Interestingly, the most active peptides are all derived from  $\sigma^{70}$  2.1–2.2

regions (aa 375–416; P01–08) with P07 being the most potent one with an  $IC_{50}$  of 4.6  $\mu$ M in the holo enzyme assay.

**Table 2.** Transcription Assay with Reference Compounds and Peptides<sup>c</sup>

A.

Compound	Inhibition of RNAP core ( $IC_{50}$ )	Inhibition of RNAP holo ( $IC_{50}$ )	Ratio ( $IC_{50}$ core:holo <sub>compd</sub> / $IC_{50}$ core:holo <sub>rif</sub> )
Rifampicin	<b>15.7 nM</b>	27.4 nM	1.0
Corallopyronin	<b>408.0 nM</b>	649.8 nM	1.1
CBR703	<b>6.5 <math>\mu</math>M</b>	13.3 $\mu$ M	0.9
<u>SB2</u>	56.8 $\mu$ M	<b>37.9 <math>\mu</math>M</b>	2.6
<u>Liparmycin</u>	3.11 $\mu$ M	<b>0.90 <math>\mu</math>M</b>	6.1

B.

Peptide	Inhibition of RNAP core ( $IC_{50}$ in $\mu$ M) <sup>1</sup>	Inhibition of RNAP holo ( $IC_{50}$ in $\mu$ M) <sup>1</sup>	Ratio ( $IC_{50}$ core:holo <sub>peptide</sub> / $IC_{50}$ core:holo <sub>rif</sub> )
P01	45.3	<b>39.9</b>	2.0
P02	24.1	<b>22.9</b>	1.8
P03	15.5 % <sup>1</sup>	10.5 % <sup>1</sup>	<sup>a</sup>
P04	9.8	<b>5.8</b>	3.0
P05	21.0 % <sup>1</sup>	22.5 % <sup>1</sup>	<sup>a</sup>
P06	21.0 % <sup>1</sup>	11.0 % <sup>1</sup>	<sup>a</sup>
P07	5.5	<b>4.1</b>	2.4
P08	25.5 % <sup>1</sup>	18.0 % <sup>1</sup>	<sup>a</sup>
P09	n.i.	n.i.	<sup>a</sup>
P10	10.3 % <sup>1</sup>	n.i.	<sup>a</sup>
P11	31.4 % <sup>1</sup>	32.6 % <sup>1</sup>	<sup>a</sup>
P12	n.i.	n.i.	<sup>a</sup>
P13	n.i.	n.i.	<sup>a</sup>

P14	n.i.	n.i.	a
P15	n.i.	n.i.	a
P16	16.0 % <sup>1</sup>	n.i.	a
C1	42.2	<b>32.2</b>	2.3
C2	n.i.	n.i.	a
C3	n.i.	n.i.	a
C4	n.i.	n.i.	a

<sup>a</sup>Where a % inhibition value is given, the peptide was tested at 50  $\mu$ M. <sup>b</sup>Not determined; n.i., no inhibition (inhibition <10% at 50  $\mu$ M); bold designates the lower of the two compared IC<sub>50</sub> values (core vs holo). Given values are in round figures; ratios are based on exact values. <sup>c</sup>Comparison of *Ec* RNAP inhibition (RNAP core and holo) of selected reference compounds (A) and peptides (B). IC<sub>50</sub> values were determined. The core to holo IC<sub>50</sub> ratios were related to the Rifampicin core to holo IC<sub>50</sub> ratios.

Although some linear peptides are known to exhibit antibacterial activity,<sup>31–36</sup> our peptides P01–16 did not inhibit growth of *Ec* TolC.

**$\sigma^{70}$ :core Inhibition Leads to Inhibition of Transcription Initiation.** To validate P07 inhibiting the interaction between  $\sigma^{70}$  and RNAP core, we performed an ELISA-based RNAP assembly assay similar to the one published by André and colleagues.<sup>7</sup> In this binding experiment P07 prevented core enzyme from binding to  $\sigma^{70}$  in a concentration-dependent manner, whereas P14 displayed no significant inhibition of the protein–protein interaction (Figure 1).

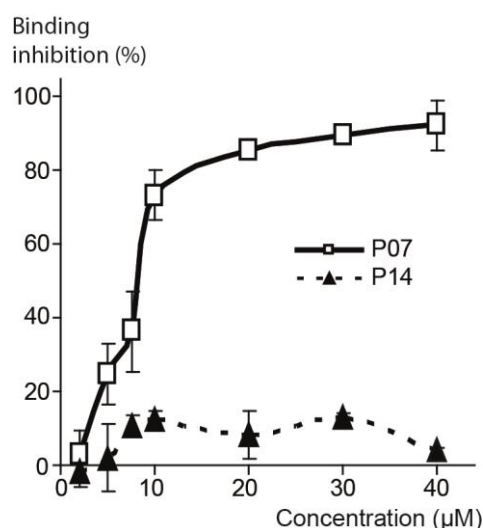


**Figure 1.** ELISA binding experiments. The binding inhibition of RNAP core to  $\sigma^{70}$  is shown in the presence of different concentrations of P07 and P14. Standard deviations from two independent experiments are given (black bars).

These results support our idea for the  $\sigma^{70}$ :core interface region as binding site for the peptide. Nevertheless we are aware that such an effect could be also observed in the case of a conformational change within the core enzyme induced by the peptide binding to an allosteric site. As the inhibition of  $\sigma^{70}$ :core interaction by P07 should inhibit promoter recognition and thus transcription initiation, an HPLC-based assay was performed aiming at the quantification of tritium-labeled abortive transcripts that are usually formed during the initiation process. As shown in Figure 2, in contrast to P14 and C03 that were inactive in the transcription assay, P07 led to a drastic reduction of abortive transcript formation, supporting again our proposed mode of action for P07.

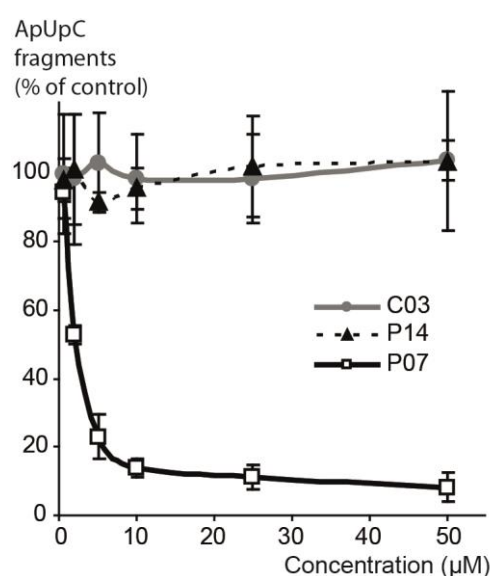


**Figure 2.** Primed abortive transcription assay. Inhibition of transcription initiation was measured by quantification of abortive transcripts (ApUpC\*) that have been formed using CTP\* and ApU as substrates. Asterisk (\*) designates  $^3\text{H}$  labeling. Standard deviations from three independent experiments are given (black bars).

**MD Simulations To Elucidate Mode of Action.** In the *Thermus thermophilus* holo RNAP structure (e.g., PDB 2BE5) and in our *Ec* RNAP homology model P07 is derived from a  $\sigma^{70}$  region that exhibits a helix-turn-helix motif (Figure 3A, “folding”). In order to elucidate the mechanism of action of P07 in more detail and to gain information about whether this peptide and the other peptides derived from this region (P01–08) maintain the secondary structure embodied in the holo RNAP structures, generalized Born implicit solvent simulations (100–250 ns) were carried out. The average secondary structure elements obtained are shown in Figure 3 and Supplementary Figure SI1. While P01 and P02 almost completely maintained their helical structure during these simulations, in P03–05 only a short segment of this N-terminal helix is preserved. An explanation for the good activity of P04 could be that its rigid N-terminus is stabilized by interactions with its own apparently helical C-terminus. This was

even more evident in the MD simulation of P04 in complex with a  $\beta'$  truncated construct.<sup>22</sup> In this MD simulation, amino acids Gln400–Glu407 of P04 moved slightly toward the  $\beta'$ -LRS, allowing interactions of the 2.1–2.2 turn residues (Tyr394–Gln400) with lid and rudder. Shortening of P04 at both ends (P05 and P06) led to a dramatic loss of activity, possibly by losing contacts to the core enzyme and/or the LRS. P06 is identical to a peptide that was described by Sharp *et al.*<sup>23</sup> to inhibit transcription initiation, if  $\sigma^{70}$  was present in unsaturated concentration. This effect was abolished if excess  $\sigma^{70}$  was added to the reaction. These results emphasize the competing behavior between such a peptide and  $\sigma^{70}$ . In contrast to the good results for P06 in the assay performed by Sharp *et al.*,<sup>23</sup> we found only a low inhibition, presumably due to sigma saturation in the holo enzyme assay. During the MD simulations, P07 and P08 preserved the long  $\alpha$ -helix seen in the holo RNAP structures for  $\sigma^{70}$  2.2.

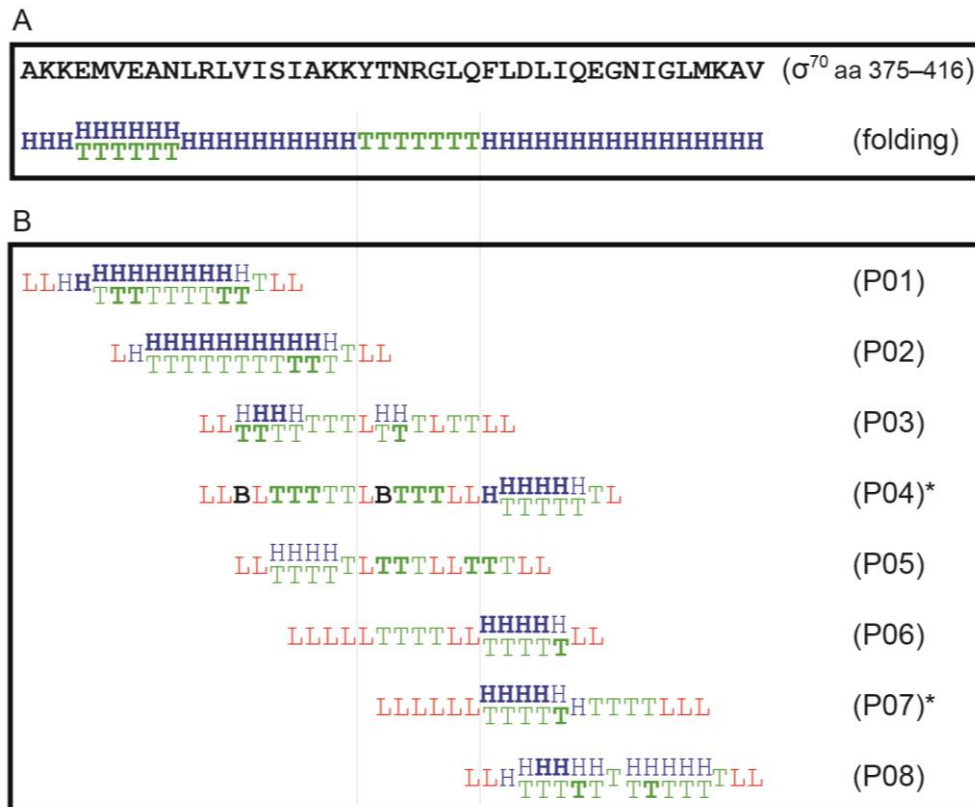


**Figure 3.** MD simulation results of P01–08. (A) The folding of the *E. coli*  $\sigma^{70}$  region 375–416 is illustrated according to our *Ec* RNAP homology model. (B) The folding of each aa in P01–08 is given as a result of our MD simulations. H, helix; T, turn; L, loop; B, beta-sheet. Bold: >40% occurrence of this folding in the MD simulations; nonbold: 18–40%. Asterisk (\*) designates most active peptides in the transcription assay.

Interestingly, P07 was much more potent than P08, although the  $\beta'$ CC binding affinity of the latter peptide should be more efficient. On the other hand P08 lacks the five N-terminal residues (compared to P07), hinting at the N-terminal loop to be responsible for the drastic

difference in activity. We speculate the LRS to be targeted by this flexible loop (instead of the rigid turn motif of P04) and decided to examine this hypothesis in more detail. To analyze whether specific interactions are formed, GPU accelerated MD simulations (30 ns) were performed for P07 in complex with a truncated version of  $\beta'$  (aa 94–346) containing the  $\beta'$ CC and LRS. The absence of  $\sigma^{70}$  allows an increased flexibility of the lid, which in the presence of P07 moves upward, tightening the fork formed with the rudder (distance between C $\alpha$  of Asp256 and Gly318 decreases from 23.7 to 13.8 Å) (Figure 4 and Supplementary Figure SI2). A polar network involves the C-term-core residues Gln400, Asp403, Gln406, and Glu407 and the cationic hot spot residues of  $\beta'$ CC Arg275, Arg278, and Arg281 (Supplementary Scheme SI2 and Supplementary Figures SI3 and SI5). In this simulation interactions can be observed between the C-terminal residues of P07 and the hydrophobic patch on the top of  $\beta'$ CC, which ensure an optimal placement of the peptide along the  $\beta'$ CC axis. As seen from the energy contribution data (Supplementary Figures SI1 and SI3), other residues strongly contributing to the binding affinity are located on the N-terminal loop of P07: Arg397 forms an ion-pair to Asp257 (lid), whereas Asn396 forms hydrogen bonds to Thr317 and Ser319 (rudder) (Figure 4). Consequently, the LRS is stabilized in a closed conformation, which is now unavailable for  $\sigma$  binding.

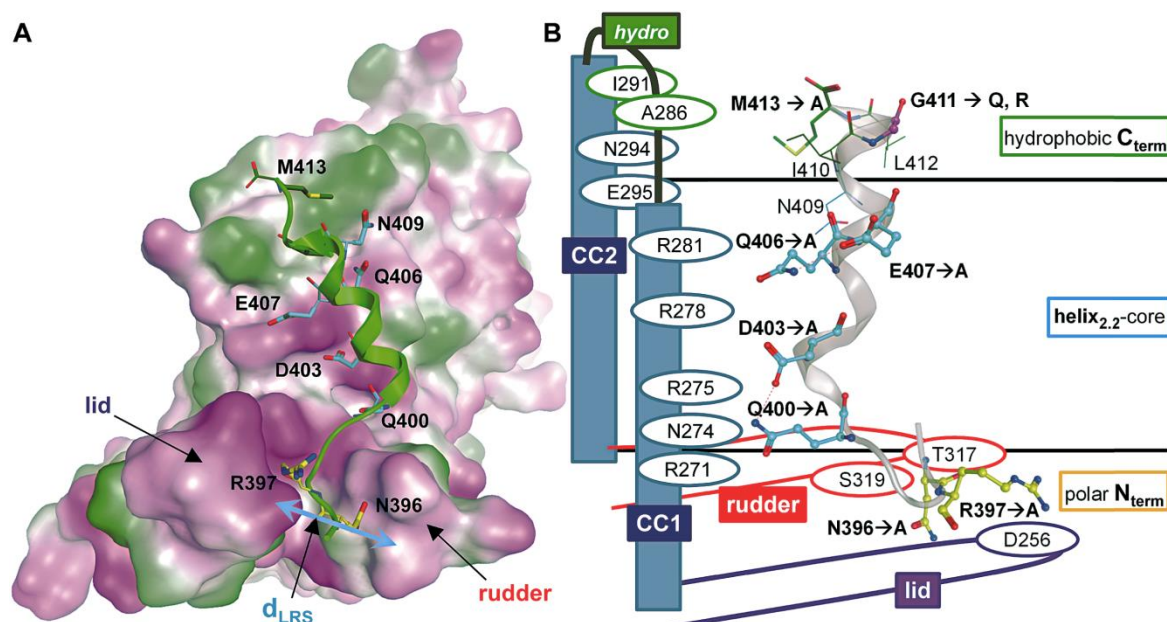


**Figure 4.** Binding of P07 to the  $\beta'$ <sub>trunc</sub> subunit. (A) The molecular surface representation of the  $\beta'$ <sub>trunc</sub> subunit (hydrophilic, magenta; neutral, white; lipophilic, dark green) is shown in complex with P07 (cartoon, green). Important residues of P07 are labeled. (B) Schematic representation of the interactions between P07 (gray cartoon) residues and the  $\beta'$  coiled-coil and LRS. Residues of P07 that were varied in this study are rendered as sticks, others as lines.



**Interaction Analysis by Peptide Mutants.** To confirm these hypothesized binding mechanisms and to establish a clear structure–function relationship, P07 was subjected to further *in vitro* experiments. In a first step, we designed eight mutant peptides with single-point mutations of the residues Asn396, Arg397, Gln400, Asp403, Gln406, Glu407 (all into Ala), and Gly411 (into Gln/Arg). Additionally, a truncated version of P07 lacking the six C-terminal residues was synthesized (Table 3). The P07 mutants N396A and R397A were generated in order to prove the interactions of the N-terminal part of P07 with the LRS. Interestingly, both of these mutants showed a significant loss of activity (Table 3A), confirming the MD predictions. The four mutated residues of the helix2.2-core (Gln400, Asp403, Gln406, Glu407) are regarded as key amino acids: they exhibited the highest binding energy contributions in the P07- $\beta'$ CC-LRS MD simulation due to interactions with Arg275, Arg278, Arg281, and Glu295 (Figure 4B, Supplementary Figure SI3 and Supplementary Scheme SI2). Indeed, our *in vitro* results show a significant increase of the  $IC_{50}$  values confirming the modeling results. Especially substitution D403A led to a more than 10-fold increase of the  $IC_{50}$  value compared to that of P07 (Table 3B). Finally, we examined the C-terminal part of P07 and its interactions with the hydrophobic patch at the tip of the  $\beta'$ CC by mutating Gly411 to Arg and Gln (Table 3C). In particular, we speculated that a neutral glutamine stabilizes the helical structure of the peptide, whereas for G411R a decreased helix stability and, notably, a repulsion with the  $\beta'$ CC cationic hot spot residues Arg278 and Arg281 was expected. Indeed, while the  $IC_{50}$  of G411Q was similar to that of P07, the  $IC_{50}$  of G411R increased around 7-fold (Table 3C). As expected a truncated version of P07 lacking the six C-terminal aa exhibits a reduced activity (26  $\mu$ M, Table 3C), suggesting that it might still target  $\beta'_{trunc}$ .

**Table 3.** Transcription Inhibition by P07 Mutants<sup>b</sup>

A.

Peptide	aa sequence	Inhibition of RNAP core ( $IC_{50}$ in $\mu$ M)	Inhibition of RNAP holo ( $IC_{50}$ in $\mu$ M)	Ratio ( $IC_{50}$ core:holo <sub>peptide</sub> / $IC_{50}$ core:holo <sub>ref</sub> )
P07	TNRGLQFLDLIQEGNIGLM	6.2	<b>4.6</b>	2.4
N396A <sup>1</sup>	T <b>A</b> RGLQFLDLIQEGNIGLM	35.3	<b>21.0</b>	2.9
R397A <sup>1</sup>	TN <b>A</b> GLQFLDLIQEGNIGLM	39.4	<b>18.8</b>	3.7

B.



Peptide	aa sequence	Inhibition of RNAP core (IC <sub>50</sub> in $\mu$ M)	Inhibition of RNAP holo (IC <sub>50</sub> in $\mu$ M)	Ratio (IC <sub>50</sub> core:holo <sub>peptide</sub> / IC <sub>50</sub> core:holo <sub>rif</sub> )
P07	TNRGLQFLDLIQEGNIGLM	6.2	<b>4.6</b>	2.4
Q400A	TNRGL <u>A</u> FLDLIQEGNIGLM	11.7	<b>8.0</b>	2.6
D403A	TNRGLQFL <u>A</u> LIQEGNIGLM	> 50	<b>&gt; 50</b>	n.d.
Q406A	TNRGLQFLDLI <u>A</u> EGNIGLM	18.6	<b>8.3</b>	3.9
E407A	TNRGLQFLDLIQ <u>A</u> GNIGLM	17.2	<b>16.3</b>	1.9

C.

Peptide	aa sequence	Inhibition of RNAP core (IC <sub>50</sub> in $\mu$ M)	Inhibition of RNAP holo (IC <sub>50</sub> in $\mu$ M)	Ratio (IC <sub>50</sub> core:holo <sub>peptide</sub> / IC <sub>50</sub> core:holo <sub>rif</sub> )
P07	TNRGLQFLDLIQEGNIGLM	6.2	<b>4.6</b>	2.4
G411Q	TNRGLQFLDLIQEGNI <u>Q</u> LM	9.3	<b>4.5</b>	3.6
G411R	TNRGLQFLDLIQEGNI <u>R</u> LM	44.1	<b>31.0</b>	2.5
395-407 <sup>a</sup>	TNRGLQFLDLIQE	31.9	<b>26.0</b>	2.2

<sup>a</sup>Short version of P07 (aa positions referring to *E. coli*  $\sigma^{70}$ ). n.d., not determined. <sup>b</sup>Selected aa of P07 were substituted (underlined). Modifications were performed in the (A) N<sub>term</sub> loop region, (B) helix<sub>2.2</sub> core, and (C) hydrophobic C<sub>term</sub>. IC<sub>50</sub> values (inhibition of core and holo RNAP) were determined for these peptides.

To further investigate the roles of the peptides D403A, G411Q, and G411R, they were simulated alone as well as in complex with the truncated  $\beta'$  construct. The helical structure of D403A was not altered compared to P07, but in contrast to P07, which is oriented parallel to the  $\beta'$ CC-axis with closed LRS, in the D403A- $\beta'$ <sub>trunc</sub> simulation D403A is rotated perpendicularly along the  $\beta'$ CC axis (Figure 5).

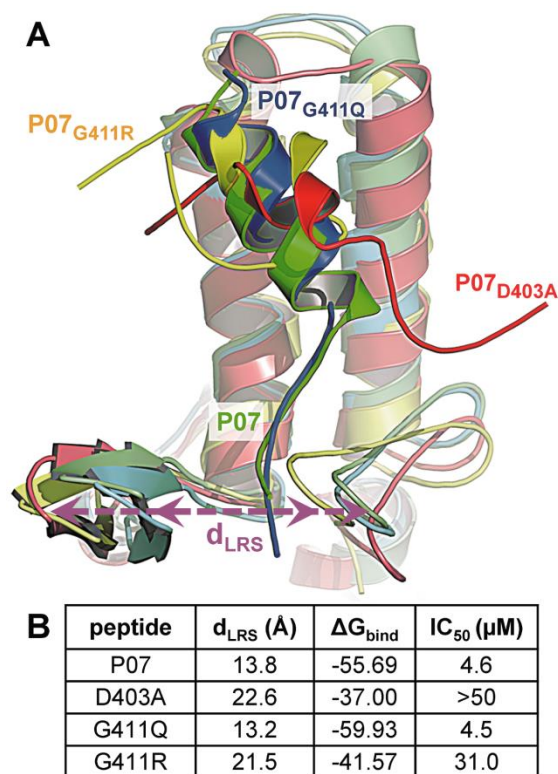


**Figure 5.** Binding of P07 and selected mutants to the  $\beta'_{trunc}$  subunit. (A) Superimposition of the simulated peptides- $\beta'_{trunc}$  complexes: P07 (green), D403A (red), G411Q (blue), G411R (yellow). (B) The shorter  $d_{LRS}$  values for P07 and G411Q correlate with more favorable  $\Delta G_{bind}$  and  $IC_{50}$  values.

The lack of interactions with lid or rudder leads to an opened LRS conformation ( $d_{LRS} = 22.6$  Å), which is likely accessible for  $\sigma$ . The decreased predicted binding energy is in agreement with the reduced inhibition, the energy contribution data (Supplementary Figure SI3), and the hydrogen bonds (Supplementary Scheme SI2). Notably, for the G411Q complex the peptide is oriented along the  $\beta'CC$  axis as seen for P07 with its N-terminal loop fitted in between a closed LRS ( $d_{LRS} = 13.2$  Å) (Figure 5B and Supplementary Figure SI2). Moreover, for this complex the binding energy was in agreement with the inhibitory potency. For the G411R- $\beta'_{trunc}$  simulation the ionpair network formed by Asp403 with Arg275 and Arg278 is maintained holding the helix2.2 core in place. However, it is rotated with respect to the  $\beta'CC$  axis (as seen for D403A). Arg411 is pulled away from the  $\beta'$  hydrophobic patch, leading to unfolding of the C-terminal helix. Along with the observation that the LRS is found in an opened conformation, these data explain the reduced RNAP inhibition by G411R. Accordingly, our MD-based hypothesis for the mechanism of action of P07 are consistent with our in vitro data.

## Conclusions.

In the present work we examined rationally designed peptides as inhibitors of  $\sigma^{70}$ :core interaction. We focused on peptide P07, which showed the best inhibitory activity. ELISA-based binding experiments as well as successful inhibition of transcription initiation by P07 strongly support the  $\sigma^{70}$ :core interface as a target site. After performing MD simulations and detailed mutagenesis studies, we conclude that P07 binds to the  $\beta'$ CC and to the LRS. Our results indicate that both interaction sites are essential for potent inhibition. Notably, P07 also led to a significant inhibition of the RNAP core enzyme. Although this result is at a first glance surprising, an explanation is found in the MD simulations and the mutagenesis results. In particular, interference of P07 with the conformational flexibility of the LRS might be the cause for the observed core RNAP inhibition. This hypothesis is supported by the fact that mutagenesis and deletion experiments of *lid*<sup>40</sup> and/or *rudder*<sup>41,42</sup> affected the initiation step (as expected for pure sigma-core inhibitors), but also other transcription events such as open promoter complex formation and RNA exit. These data might be used as a valuable starting point for the structure-based design of small organic molecules addressing this target site.

## Methods

**Transcription Assay.** Core and holo enzyme of *E. coli* RNA polymerase were purchased from Epicenter Biotechnologies. Final concentrations in a total volume of 30  $\mu$ L were 20 units of RNase inhibitor (RiboLock, Fermentas), 10 mM DTT, 40 mM Tris HCl (pH 7.5), 150 mM KCl, 10 mM MgCl<sub>2</sub>, 0.01% (v/v) Triton-X-100, 400  $\mu$ M ATP, CTP, and GTP, as well as 100  $\mu$ M UTP. As enzymes and for detection, 1 unit of RNAP holo enzyme was used along with 0.53  $\mu$ M <sup>3</sup>H-UTP and 1 unit of RNAP core enzyme was used along with 1.33  $\mu$ M <sup>3</sup>H-UTP. As template for the transcription reactions 425 ng of T7A1 (for holo) or T7 (for core) promoter containing PCR fragments served as templates, respectively. Prior to starting the experiment, the compounds were dissolved in DMSO, and the peptides were dissolved in a 1:1 mixture of acetonitrile (ACN) and ddH<sub>2</sub>O. The final DMSO concentration during the experiments was 2% (v/v) (1% (v/v) for ACN). Dilution series of compounds were prepared using a liquid handling system (Janus, Perkin-Elmer). Further steps including the preincubation, transcription reaction, purification, and quantification were performed as described previously.<sup>43</sup> To obtain inhibition values for each sample, their counts were related to DMSO or ACN/ddH<sub>2</sub>O controls, respectively.

**Preparation of DNA Templates.** To obtain the T7A1 template, a two-step PCR was performed using Taq DNA polymerase (New England Biolabs). First, a part of the neomycin

gene of pcDNA3.1 was amplified. The 3' primer (ttctcggcaggagcaaggtgag) was used along with a 5' oligo which was flanked by a T7A1 promoter (gactcagtgatatcaaaaagagtattgacttaaagtctaacctataggatacttacagccatcgagaggctgatcaagagacaggatgagg) resulting in a PCR product containing the 59-bp T7A1 promoter on the 5' end. The total size of the PCR product was 437 bp. To obtain the T7 promoter template the same procedure as above was followed with the difference that the T7A1 promoter sequence was substituted by the T7 promoter sequence. The PCR products were gel purified (kit from PEQLAB) and elongated in a second PCR using the same 3' oligos and a 5' oligo increasing the size by 13 bp (cagaccatgatcagactcagtgatc). The PCR products were purified (kit from Fermentas) and served as templates in our transcription assays.

**Determination of IC<sub>50</sub> Values.** Three different concentrations of a compound/peptide were chosen for the determination of an IC<sub>50</sub> value (two samples for each concentration). The calculation of the IC<sub>50</sub> value was performed by plotting the percent inhibition versus the concentration of inhibitor on a semilog plot. From this the molar concentration causing 50% inhibition was calculated. At least three independent determinations were performed for each compound.

**RNA Polymerase Inhibitors and Peptides That Were Used.** Rifamycin was purchased from Sigma-Aldrich. Coralopyronin was donated by K. Gerth (HZI). CBR703 (benzenecarboximidamide, N-hydroxy-N'-phenyl-3-(trifluoromethyl)) was synthesized according to a published procedure (WO 01/51456 A2). SB2 (benzoic acid, 3-[5-[[4-oxo-3-(2-propen-1-yl)-2-thioxo-5-thiazolidinylidene]methyl]-2-furanyl]) was synthesized as described in the literature.<sup>44</sup> Lipiarmycin was a generous gift from Novartis. Peptides were purchased from intavis, peptides&elephants, or were synthesized by our in house Platform Peptide Synthesis. Peptide sequences are given in Table 1.

**ELISA Experiments.** The procedure was performed as described in André *et al.*<sup>7</sup> with slight modifications regarding quantification. The cloning and purification of *Ec*  $\sigma^{70}$  was performed as described in Haupenthal *et al.*<sup>43</sup> As primary antibody for the detection of core enzyme binding, a monoclonal anti- $\alpha$  subunit antibody was purchased from NeoClone Biotechnology. This antibody was used in a 1:1000 dilution as recommended by the manufacturer. The secondary antibody, a goat anti-mouse IgG labeled with fluorescein (Santa Cruz Biotechnology) was used diluted 1:200. Fluorescein was excited at 485 nm, and fluorescence read out at 520 nm on a microplate reader (POLARstar Omega by BMG Labtech).

**HPLC-Based Abortive Transcription Assay.** *E. coli* RNA polymerase (RNAP) holoenzyme was purchased from Epicenter Biotechnologies. Final concentrations in a total

volume of 30  $\mu\text{L}$  were 1 unit of RNAP along with 20 units of RNase inhibitor (RiboLock, Fermentas), 10 mM DTT, 40 mM Tris-HCl (pH 7.5), 150 mM KCl, 10 mM  $\text{MgCl}_2$ , and 0.1% (w/v) CHAPS. The peptides were dissolved in a 1:1 mixture of acetonitrile (ACN) and water (final ACN concentration during experiments: 1% (v/v)). In the presence of the above-mentioned RNAP mixture they were incubated for 10 min at 25 °C prior to starting the experiment. Each transcription reaction was started by the addition of a mixture containing 1  $\mu\text{Ci}$  of [5- $^3\text{H}$ ]-CTP (Perkin-Elmer), 100  $\mu\text{M}$  of ApU dinucleotide (IBA), and 450 ng of the T7A1 promoter containing PCR product T7A1\_437 serving as the DNA template.<sup>43</sup> The transcription reactions were carried out at 37 °C for 60 min. The subsequent sample preparation and HPLC-based quantification of ApUpC formation were carried out as described in the Supporting Information.

**Molecular Dynamics (MD) Simulations, MM-GBSA Calculations, and Minimal Inhibitory Concentration (MIC) Determinations.** The description of these methods can be found in the Supporting Information.

### Supporting Information

This material is available free of charge via the Internet at <http://pubs.acs.org>.

### Acknowledgements

We thank E. Schmitt (Novartis) for providing Lipiarmycin and K. Gerth (HZI) for supplying us with Coralopyronin. Also we thank J. Jung for excellent technical support as well as J. C. de Jong for synthesizing CBR703 and SB2.

### References

- (1) Chopra, I. (2007) Bacterial RNA polymerase: a promising target for the discovery of new antimicrobial agents. *Curr. Opin. Invest. Drugs* 8, 600–607.
- (2) Mariani, R., and Maffioli, S.-I. (2009) Bacterial RNA polymerase inhibitors: an organized overview of their structure, derivatives, biological activity and current clinical development status. *Curr. Med. Chem.* 16, 430–454.
- (3) Talpaert, M., Campagnari, F., and Clerici, L. (1975) Lipiarmycin: an antibiotic inhibiting nucleic acid polymerases. *Biochem. Biophys. Res. Commun.* 63, 328–334.
- (4) Bryskier, A. (2005) Anti-MRSA agents: under investigation, in the exploratory phase and clinically available. *Expert Rev. Anti-Infect. Ther.* 3, 505–553.
- (5) Floss, H.-G., and Yu, T.-W. (2005) Rifamycin-mode of action, resistance, and biosynthesis. *Chem. Rev.* 105, 621–632.
- (6) Tupin, A., Gualtieri, M., Roquet-Banères, F., Morichaud, Z., Brodolin, K., and Leonetti, J.-P. (2010) Resistance to rifampicin: at the crossroads between ecological, genomic and medical concerns. *Int. J. Antimicrob. Agents* 35, 519–523.

- (7) André, E., Bastide, L., Villain-Guillot, P., Latouche, J., Rouby, J., and Leonetti, J.-P. (2004) A multiwell assay to isolate compounds inhibiting the assembly of the prokaryotic RNA polymerase. *Assay Drug Dev. Technol.* 2, 629–635.
- (8) Artsimovitch, I., Chu, C., Lynch, A.-S., and Landick, R. (2003) A new class of bacterial RNA polymerase inhibitor affects nucleotide addition. *Science* 302, 650–654.
- (9) Mukhopadhyay, J., Sineva, E., Knight, J., Levy, R.-M., and Ebright, R.-H. (2004) Antibacterial peptide microcin J25 inhibits transcription by binding within and obstructing the RNA polymerase secondary channel. *Mol. Cell* 14, 739–751.
- (10) Mukhopadhyay, J., Das, K., Ismail, S., Koppstein, D., Jang, M., Hudson, B., Sarafianos, S., Tuske, S., Patel, J., Jansen, R., Irschik, H., Arnold, E., and Ebright, R.-H. (2008) The RNA polymerase “switch region” is a target for inhibitors. *Cell* 135, 295–307.
- (11) Temiakov, D., Zenkin, N., Vassilyeva, M.-N., Perederina, A., Tahirov, T.-H., Kashkina, E., Savkina, M., Zorov, S., Nikiforov, V., Igarashi, N., Matsugaki, N., Wakatsuki, S., Severinov, K., and Vassilyev, D.-G. (2005) Structural basis of transcription inhibition by antibiotic streptolydigin. *Mol. Cell* 19, 655–666.
- (12) Irschik, H., Gerth, K., Höfle, G., Kohl, W., and Reichenbach, H. (1983) The myxopyronins, new inhibitors of bacterial RNA synthesis from *Myxococcus fulvus* (Myxobacterales). *J. Antibiot. (Tokyo)* 36, 1651–1658.
- (13) Irschik, H., Jansen, R., Höfle, G., Gerth, K., and Reichenbach, H. (1985) The coralopyronins, new inhibitors of bacterial RNA synthesis from *Myxobacteria*. *J. Antibiot. (Tokyo)* 38, 145–152.
- (14) Irschik, H., Jansen, R., Gerth, K., Höfle, G., and Reichenbach, H. (1987) The sorangicins, novel and powerful inhibitors of eubacterial RNA polymerase isolated from myxobacteria. *J. Antibiot. (Tokyo)* 40, 7–13.
- (15) Arhin, F., Bélanger, O., Ciblat, S., Dehbi, M., Delorme, D., Dietrich, E., Dixit, D., Lafontaine, Y., Lehoux, D., Liu, J., McKay, G.-A., Moeck, G., Reddy, R., Rose, Y., Srikumar, R., Tanaka, K.-S., Williams, D.-M., Gros, P., Pelletier, J., Parr, T.-R., Jr., and Far, A.-R. (2006) A new class of small molecule RNA polymerase inhibitors with activity against rifampicin-resistant *Staphylococcus aureus*. *Bioorg. Med. Chem.* 14, 5812–5832.
- (16) Glaser, B.-T., Bergendahl, V., Thompson, N.-E., Olson, B., and Burgess, R.-R. (2007) LRET-based HTS of a small-compound library for inhibitors of bacterial RNA polymerase. *Assay Drug Dev. Technol.* 5, 759–768.
- (17) Mariner, K.-R., Trowbridge, R., Agarwal, A.-K., Miller, K., O’Neill, A.-J., Fishwick, C.-W., and Chopra, I. (2010) Furanylrodanines are unattractive drug candidates for development as inhibitors of bacterial RNA polymerase. *Antimicrob. Agents Chemother.* 54, 4506–4509.
- (18) Louie, T., Miller, M., Donskey, C., Mullane, K., and Goldstein, E.-J. (2009) Clinical outcomes, safety, and pharmacokinetics of OPT-80 in a phase 2 trial with patients with *Clostridium difficile* infection. *Antimicrob. Agents Chemother.* 53, 223–228.
- (19) Haebich, D., and von Nussbaum, F. (2009) Lost in transcription–inhibition of RNA polymerase. *Angew. Chem., Int. Ed.* 48, 3397–3400.
- (20) O’Shea, R., and Moser, H.-E. (2008) Physicochemical properties of antibacterial compounds: implications for drug discovery. *J. Med. Chem.* 51, 2871–2878.
- (21) Tracy, R.-L., and Stern, D.-B. (1995) Mitochondrial transcription initiation: promoter structures and RNA polymerases. *Curr. Genet.* 28, 205–216.
- (22) Negri, M., Haupenthal, J., Hartmann, R.-W. “From-macro-to-micro”: dissecting bacterial RNA polymerase into druggable subdomains. (Helmholtz Institute for Pharmaceutical Research Saarland, Department of Drug Design and Optimization, Saarbrücken, Germany). Unpublished data.
- (23) Sharp, M.-M., Chan, C.-L., Lu, C.-Z., Marr, M.-T., Nechaev, S., Merritt, E.-W., Severinov, K., Roberts, J.-W., and Gross, C.-A. (1999) The interface of sigma with core RNA polymerase is extensive, conserved, and functionally specialized. *Genes Dev.* 13, 3015–3026.
- (24) Lesley, S.-A., and Burgess, R.-R. (1989) Characterization of the *Escherichia coli* transcription factor sigma 70: localization of a region involved in the interaction with core RNA polymerase. *Biochemistry* 28, 7728–7734.
- (25) Arthur, T.-M., Anthony, L.-C., and Burgess, R.-R. (2000) Mutational analysis of beta’260–309, a sigma 70 binding site located on *Escherichia coli* core RNA polymerase. *J. Biol. Chem.* 275, 23113–23119.
- (26) Zhang, G., Campbell, E.-A., Minakhin, L., Richter, C., Severinov, K., and Darst, S.-A. (1999) Crystal structure of *Thermus aquaticus* core RNA polymerase at 3.3 Å resolution. *Cell* 98, 811–824.
- (27) Geszvain, K., Gruber, T.-M., Mooney, R.-A., Gross, C.-A., and Landick, R. (2004) A hydrophobic patch on the flap-tip helix of *E. coli* RNA polymerase mediates sigma(70) region 4 function. *J. Mol. Biol.* 343, 569–587.

- (28) Bergendahl, V., Heyduk, T., and Burgess, R.-R. (2003) Luminescence resonance energy transfer-based high-throughput screening assay for inhibitors of essential protein-protein interactions in bacterial RNA polymerase. *Appl. Environ. Microbiol.* 69, 1492–1498.
- (29) Arthur, T.-M., and Burgess, R.-R. (1998) Localization of a sigma70 binding site on the N terminus of the Escherichia coli RNA polymerase beta' subunit. *J. Biol. Chem.* 273, 31381–31387.
- (30) Burgess, R.-R., and Anthony, L. (2001) How sigma docks to RNA polymerase and what sigma does. *Curr. Opin. Microbiol.* 4, 126–131.
- (31) Cole, A.-M., Weis, P., and Diamond, G. (1997) Isolation and characterization of pleurocidin, an antimicrobial peptide in the skin secretions of winter flounder. *J. Biol. Chem.* 272, 12008–12013.
- (32) Sung, W.-S., and Lee, D.-G. (2008) Pleurocidin-derived antifungal peptides with selective membrane-disruption effect. *Biochem. Biophys. Res. Commun.* 369, 858–861.
- (33) Park, C.-B., Lee, J.-H., Park, I.-Y., Kim, M.-S., and Kim, S.-C. (1997) A novel antimicrobial peptide from the loach Misgurnus anguillicaudatus. *FEBS Letters* 411, 173–178.
- (34) Cruciani, R.-A., Barker, J.-L., Durell, S.-R., Raghunathan, G., Guy, H.-R., Zasloff, M., and Stanley, E.-F. (1992) Magainin 2, a natural antibiotic from frog skin, forms ion channels in lipid bilayer membranes. *Eur. J. Pharmacol.* 226, 287–296.
- (35) Oren, Z., and Shai, Y. (1996) A class of highly potent antibacterial peptides derived from pardaxin, a pore-forming peptide isolated from Moses sole fish *Pardachirus marmoratus*. *Eur. J. Biochem.* 237, 303–310.
- (36) Marchini, D., Giordano, P.-C., Amons, R., Bernini, L.-F., and Dallai, R. (1993) Purification and primary structure of ceratotoxin A and B, two antibacterial peptides from the female reproductive accessory glands of the medfly *Ceratitis capitata* (Insecta: Diptera). *Insect Biochem. Mol. Biol.* 23, 591–598.
- (37) Tupin, A., Gualtieri, M., Leonetti, J.-P., and Brodolin, K. (2010) The transcription inhibitor lipiarmycin blocks DNA fitting into the RNA polymerase catalytic site. *EMBO J.* 29, 2527–2537.
- (38) Sonenshein, A.-L., Alexander, H.-B., Rothstein, D.-M., and Fisher, S.-H. (1977) Lipiarmycin-resistant ribonucleic acid polymerase mutants of *Bacillus subtilis*. *J. Bacteriol.* 132, 73–79.
- (39) André, E., Bastide, L., Michaux-Charachon, S., Gouby, A., Villain-Guillot, P., Latouche, J., Bouchet, A., Gualtieri, M., and Leonetti, J.-P. (2006) Novel synthetic molecules targeting the bacterial RNA polymerase assembly. *J. Antimicrob. Chemother.* 57, 245–251.
- (40) Naryshkina, T., Kuznedelov, K., and Severinov, K. (2006) The role of the largest RNA polymerase subunit lid element in preventing the formation of extended RNA-DNA hybrid. *J. Mol. Biol.* 361, 634–643.
- (41) Kuznedelov, K., Korzheva, N., Mustaev, A., and Severinov, K. (2002) Structure-based analysis of RNA polymerase function: the largest subunit's rudder contributes critically to elongation complex stability and is not involved in the maintenance of RNA-DNA hybrid length. *EMBO J.* 21, 1369–1378.
- (42) Touloukhonov, I., and Landick, R. (2006) The role of the lid element in transcription by *E. coli* RNA polymerase. *J. Mol. Biol.* 361, 644–658.
- (43) Haupenthal, J., Hüsecken, K., Negri, M., Maurer, C.-K., and Hartmann, R.-W. (2012) Influence of DNA template choice on transcription and inhibition of *E. coli* RNA polymerase. *Antimicrob. Agents Chemother.* 56, 4536–4539.
- (44) Villain-Guillot, P., Gualtieri, M., Bastide, L., Roquet, F., Martinez, J., Amblard, M., Pugniere, M., and Leonetti, J.-P. (2007) Structure-activity relationships of phenyl-furanyl-rhodanines as inhibitors of RNA polymerase with antibacterial activity on biofilms. *J. Med. Chem.* 50, 4195–4204.

### 3.3 Discovery of novel bacterial RNA polymerase inhibitors: pharmacophore-based virtual screening and hit optimization

Stefan Hinsberger, Kristina Hüsecken, Matthias Groh, Matthias Negri, Jörg Haupenthal, and Rolf W. Hartmann

Reprinted with permission from the *Journal of Medicinal Chemistry* 2013, **56**: 8332-8338. Copyright © 2013 American Chemical Society.

#### Publication III

**Abstract:** The bacterial RNA polymerase (RNAP) is a validated target for broad spectrum antibiotics. However, the efficiency of drugs is reduced by resistance. To discover novel RNAP inhibitors, a pharmacophore based on the alignment of described inhibitors was used for virtual screening. In an optimization process of hit compounds, novel derivatives with improved in vitro potency were discovered. Investigations concerning the molecular mechanism of RNAP inhibition reveal that they prevent the protein–protein interaction (PPI) between  $\sigma^{70}$  and the RNAP core enzyme. Besides of reducing RNA formation, the inhibitors were shown to interfere with bacterial lipid biosynthesis. The compounds were active against Gram positive pathogens and revealed significantly lower resistance frequencies compared to clinically used rifampicin.



## Introduction

The increasing resistance of bacteria against antibiotics has become a major public health problem.<sup>1</sup> Therefore, new potent antibacterial drugs are required.<sup>2</sup> RNA polymerase (RNAP) catalyzes the formation of RNA from a DNA template<sup>3</sup> and is essential for growth and survival of bacteria. It is highly conserved among various bacterial species but is different in eucaryotes.<sup>4</sup> Hence, inhibiting RNAP is an attractive strategy for the treatment of bacterial infections.<sup>4</sup> In spite of the fact that several inhibitors of bacterial RNA polymerase are known, only rifamycins and fidaxomicin (lipiarmycin) are currently approved for clinical use.<sup>3,5–7</sup> Because of an increasing amount of bacterial strains resistant to rifamycins, there is an urgent need to discover new RNAP inhibitors for clinical use which should not show cross-resistance to rifamycins, especially rifampicin (Rif). In this work, a flexible alignment of structurally similar selected synthetic molecules (**I–VII**) that are known to inhibit bacterial RNAP<sup>8–12</sup> was performed (Figure 1). The resulting pharmacophore model was subsequently used to virtually screen an in-house database. Thus, three hit compounds, containing an anthranilic acid core, were identified and experimentally validated. In the following, the compounds were optimized to improve the inhibitory profile and their mode of action was determined. Additionally, the compounds revealed good antibacterial activities.

## Pharmacophore-based virtual screening and hit compound discovery.

Seven synthetic bacterial RNAP inhibitors (**I–VII**) that exhibit similar structural features, although belonging to different classes and acting via different binding modes, were retrieved from literature (Figure S1, Supporting Information (SI)).<sup>8–12</sup> Compound **I** inhibits *Staphylococcus aureus* RNAP, but its binding site is not known.<sup>8</sup> **II** and **III** are described as inhibitors of *Escherichia coli* RNAP binding to a surface exposed groove at the junction of the  $\beta'$ -bridge helix and the  $\beta$ -subunit.<sup>9</sup> **IV–VI** are known to prevent the protein–protein interaction (PPI) between  $\sigma^{70}$  and the RNAP core enzyme.<sup>10,11</sup> **VII** shows structural similarity to known RNAP inhibitors but has only been described as an inhibitor of transcription and translation (TT) without any information about its mode of action.<sup>12</sup> We resynthesized **VII** and were able to demonstrate its inhibition of *E. coli* RNAP *in vitro* (SI). **I–VII** were employed in a flexible alignment with the aim to identify the common features of these molecules. The alignment with the best similarity score was used to generate an initial pharmacophore model, which was then manually refined. The resulting model derived from these differently acting compounds is not restricted to the identification of hits binding to one special site. It should rather support the discovery of an increased number of RNAP inhibitors

independent of their binding mode. The final model consisted of four core features (two aromatic, one HBD/HBA/aromatic and one O<sub>2</sub>/anion). Besides, one accessory feature (hydrophobic) and two aromatic projections were identified (Figure 1, Figure S2, SI). The fit of each inhibitor **I–VII** into the pharmacophore model is depicted in Figure S3, SI. The virtual screening of an in-house database comprising of approximately 2000 compounds using this pharmacophore model afforded 64 hits. A virtual hit had to match at least the core features and the aromatic projections, while the presence of the accessory feature was not mandatory.

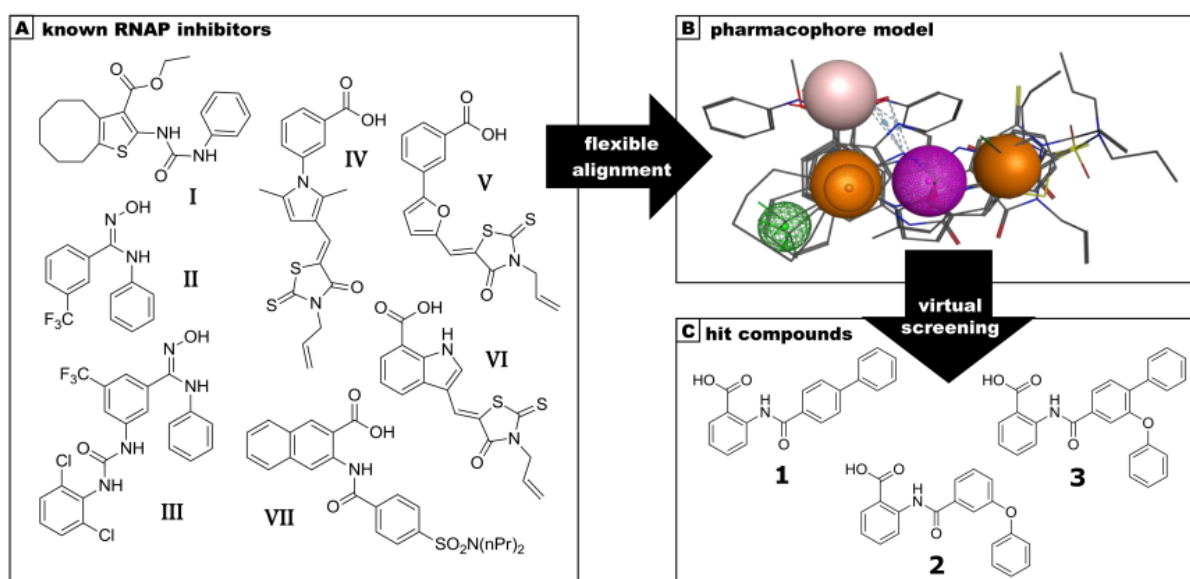


**Figure 1.** (A) Selected synthetic inhibitors of bacterial RNAP (**I–VII**) were used to perform a flexible alignment. (B) A pharmacophore model with four core features (aromatic, orange; HBD/HBA/aromatic, violet; O<sub>2</sub>/anion, rose), one accessory feature (hydrophobic, green), and two aromatic projections (one hatched orange, one hidden behind a core feature) was created and used for virtual screening. For an overlay of **I–VII** with the pharmacophore model, see Figure S3, SI. (C) Validated hit compounds **1–3** possessing an RNAP *in vitro* inhibition >20% at a concentration of 200  $\mu$ M.

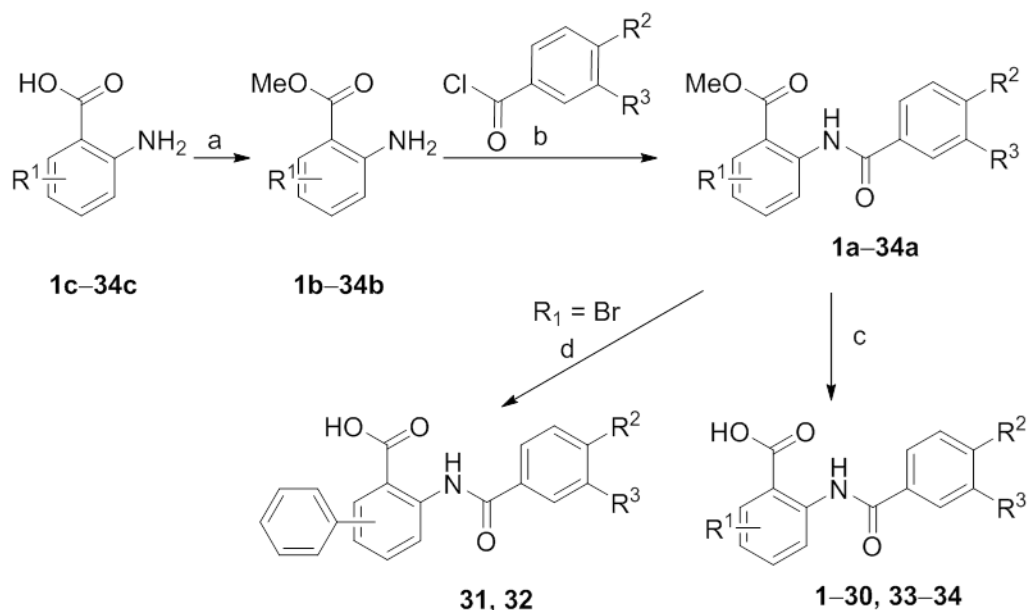
Eleven of these hit compounds originating from five different structural classes were experimentally confirmed to be active in our *in vitro* RNAP assay<sup>13</sup> (>20% inhibition at 200  $\mu$ M) (Figure S4, SI). Out of these, three promising compounds (**1–3**), containing an anthranilic acid core, were chosen for further optimization. They displayed 31% (**1**), 23% (**2**), and 100% (**3**, IC<sub>50</sub> 20  $\mu$ M) inhibition at 200  $\mu$ M, respectively.

## Chemistry

The synthesis of the target compounds was carried out starting from the appropriate anthranilic acids. The methyl 2-benzamidobenzoate intermediates **1a–34a** were synthesized

via coupling reaction with the benzoyl chloride derivatives (Scheme 1). The methyl esters were hydrolyzed to yield the target compounds. A Suzuki coupling with phenylboronic acid was performed with the appropriate brominated intermediates to obtain compounds **31** and **32**. The hydroxy substituted compound **24** was obtained from the methoxy intermediate **24a** by ether cleavage using boron tribromide.

**Scheme 1.** Synthetic Route to Compounds **1–34**<sup>a</sup>



<sup>a</sup>Reagents and conditions: (a) SOCl<sub>2</sub>, MeOH, reflux; (b) pyridine, DMAP, rt or TEA, CH<sub>2</sub>Cl<sub>2</sub>, rt or toluene, reflux; (c) NaOH, THF/MeOH/H<sub>2</sub>O, rt; (d) PhB(OH)<sub>2</sub>, Pd(PPh<sub>3</sub>)<sub>4</sub>, Cs<sub>2</sub>CO<sub>3</sub>, DME/H<sub>2</sub>O, reflux.

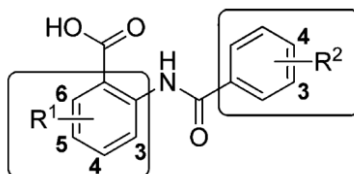
## Results and Discussion

Compounds **1–3** contain a 2-benzamidobenzoic acid partial structure which perfectly fits into the pharmacophore model. In addition, the structures contain a phenyl ring in para- and/or a phenoxy substituent in meta-position, respectively, which does not correspond to any feature of the pharmacophore model. Hence, the hit compounds were reduced in size to investigate whether these lipophilic residues are necessary for activity. Although the unsubstituted 2-benzamidobenzoic acid (**4**) fits the pharmacophore model, no activity was observed for this compound. This resulted in the conclusion that the features included in the first pharmacophore model are insufficient to differentiate between active and inactive substances. To provide a remedy, two new accessory hydrophobic/aromatic features were added on the eastern side of the pharmacophore model (representing the phenyl and the phenoxy substituents) (Figure S5, SI). Using this extended model, a compound will be defined as a hit if, beside the four core features, at least one of the new accessory features is present. As the

extended model is more limiting, its use should improve efficacy and reduce the occurrence of false positives in future screenings. An overlay of inhibitors with the extended pharmacophore model can be found in Figure S6, SI. To explore the structure–activity relationship (SAR) around the anthranilic acid core, substituents were introduced in 4- and 5-position where the pharmacophore model contains a lipophilic accessory feature. As the most potent hit compound **3** has a relatively high molecular weight, optimization efforts were started modifying the two smaller hits **1** and **2**. For each hit, a small series was synthesized introducing 4-Cl (**6** and **7**), 5-F (**11** and **12**), 5-Br (**16** and **17**), and 4,5-dimethoxy (**19** and **20**) substituents. The introduction of these substituents resulted in an increased *in vitro* activity, especially for the compounds with 4-Cl (**6** and **7**) and 5-Br (**16** and **17**) substituents. Aside from that, most 4-phenyl and 3-phenoxy compounds displayed very similar activities. To investigate whether the oxygen of the phenylether group has a beneficial effect as HBA, we synthesized compound **18** containing a 3-benzyl instead of the 3-phenoxy substituent. The removal of the oxygen did not affect the potency, indicating that a HBA is not necessary for *in vitro* activity. Therefore we regarded it as sufficient to continue the SAR studies introducing further substituents into the 4-phenyl series. To determine which kind of substituents could improve activity, substituents differing in electronic properties and lipophilicity were introduced in 5-position. The incorporation of the lipophilic, electron withdrawing chloro substituent resulted in the most potent compound **8** while a hydrophilic and electron donating hydroxy group (**24**) decreased activity in comparison to **1**. Introduction of a lipophilic and electron donating substituent (**30**, CH<sub>3</sub>) or a hydrophilic electron withdrawing substituent (**26**, CN) was tolerated and led to moderately active compounds. In a next step, the best position for a substitution at the anthranilic acid moiety was determined. Considering the good activity of chloro compound **8**, especially lipophilic, electron withdrawing substituents in different positions of the anthranilic acid moiety were introduced. A chloro substituent in 3-position (**5**) led to a total loss of activity. Similar results were found for the chloro, fluoro, and methoxy substituents in 6-position (**9**, **13**, **23**) (Table 1). As expected, the introduction of an electron donating methoxy substituent in 4- and 5-position afforded only a moderate improvement of activity. In contrast all the compounds bearing a lipophilic, electron withdrawing substituent in 4- or 5- position (**6**, **8**, **10**, **11**, **14**, **16**, **25**, **27–29**) possess a highly improved *in vitro* potency. Especially the introduction of a large lipophilic phenyl substituent in 4- or 5-position generated very potent inhibitors of RNAP (**31**, 14  $\mu$ M; **32**, 13  $\mu$ M). Interestingly, almost no difference in activity was observed between

compounds with a substituent in 4-position and compounds with the same substituent in 5-position (**6** and **8**, **10** and **11**, **14** and **16**, **27**, and **28**).

**Table 1.** Inhibitory activity against *E. coli* RNA polymerase *in vitro* and antibacterial activity



compd	R <sup>1</sup>	R <sup>2</sup>	IC <sub>50</sub> or % inhibition of <i>E. coli</i> RNAP <sup>a</sup>	MIC <i>E. coli</i> TolC (μg/ml) <sup>b</sup>
1	H	4-Ph	31%	13
2	H	3-OPh	23%	9
3	H	3-OPh, 4-PH	20 μM	13
4	H	H	ni	>100
5	3-Cl	4-Ph	ni	55
6	4-Cl	4-Ph	37 μM	3
7	4-Cl	3-OPh	44 μM	3
8	5-Cl	4-Ph	46 μM	2
9	6-Cl	4-Ph	ni	57
10	4-F	4-Ph	98 μM	4
11	5-F	4-Ph	138 μM	7
12	5-F	3-OPh	98 μM	5
13	6-F	4-Ph	14%	34
14	4-Br	4-Ph	28 μM	2
15	4-Br	3-OPh	34 μM	3
16	5-Br	4-Ph	31 μM	3
17	5-Br	3-OPh	34 μM	3
18	5-Br	3-CH <sub>2</sub> Ph	37 μM	2
19	4-,5-OMe	4-Ph	35%	19
20	4-,5-OMe	3-OPh	154 μM	6
21	4-OMe	4-Ph	162 μM	9
22	5-OMe	4-Ph	52%	8
23	6-OMe	4-Ph	ni	58
24	5-OH	4-Ph	17%	31
25	4-NO <sub>2</sub>	4-Ph	36 μM	>25
26	5-CN	4-Ph	23% @ 50 μM	7
27	4-CF <sub>3</sub>	4-Ph	27 μM	5
28	5-CF <sub>3</sub>	4-Ph	28 μM	2
29	5-OCF <sub>3</sub>	4-Ph	31 μM	4

<b>30</b>	5-Me	4-Ph	139 $\mu$ M	7
<b>31</b>	4-Ph	3-OPh	14 $\mu$ M	8
<b>32</b>	5-Ph	3-OPh	13 $\mu$ M	2
<b>33</b>	4-F	3-OPh, 4-Ph	13 $\mu$ M	>25
<b>34</b>	4-Cl	3-OPh, 4-Ph	9 $\mu$ M	>25
<b>Rif</b>			0.03 $\mu$ M	10
<b>Myx<sup>c</sup></b>			0.35 $\mu$ M	1

<sup>a</sup>IC<sub>50</sub> value (SD <20%) or percentage inhibition at 200  $\mu$ M (SD <40%); Data represent the mean values of at least three experiments. ni: no inhibition. <sup>b</sup>Minimum inhibitory concentration; data represent the mean values of at least two independent experiments (three for MIC <10  $\mu$ g/mL). <sup>c</sup>Myx: myxopyronin B.

From these results, it is obvious that especially lipophilic electron withdrawing substituents attached to the anthranilic acid core in 4- or 5-position are favorable, whereas substituents in 3- or 6-position strongly reduce the *in vitro* activity. After all, the acquired SAR information of the anthranilic acid core was used for the optimization of **3**. As it was not eligible to make the compounds too large and lipophilic, only F and Cl were introduced (**33** and **34**). As expected, these modifications had a beneficial effect on the activity and afforded the best *in vitro* compound of this series (**34**, 9  $\mu$ M). As the pharmacophore model is not restricted to one special binding site, it remains to be clarified where our compounds bind to RNAP. Comparing the structures of the optimized hit compounds and the inhibitors **I–VII**, used to create the pharmacophore model, it becomes apparent that the new compounds are very similar to **VII**. This suggests that **VII** and our compounds are likely to interact with the same RNAP site. However, the binding mechanism of **VII** is not known. One possible mechanism of action could be the inhibition of the PPI between  $\sigma^{70}$  and the RNAP core enzyme because this has been demonstrated to be the way compounds **IV–VI** function.<sup>10,11</sup> Hence, selected compounds (**3**, **9**, **14**, **28**, **32**, **34**) as well as TT inhibitor **VII** were tested in an ELISA-based RNAP assembly assay.<sup>14</sup> Rif and **V** were used as negative and positive controls, respectively. In contrast to Rif and inactive compound **9**, inhibitors **3**, **14**, **28**, **32**, **34**, and **VII**, which had been active in the transcription assay, inhibit PPI between  $\sigma^{70}$  and the RNAP core enzyme to a similar extent as positive control **V** (Table 2).

**Table 2.** Results of the ELISA-Based Assembly Inhibition Assay and the Core/Holo Transcription Assay

compd	assembly inhibition $\sigma^{70}$ /RNAP core (ELISA) (IC <sub>50</sub> ) <sup>a</sup>	inhibition of RNAP holo (IC <sub>50</sub> ) <sup>a</sup>	inhibition of RNAP core (IC <sub>50</sub> ) <sup>a</sup>	ratio <sup>b</sup>
<b>Rif</b> <sup>c</sup>	ni	27 nM	16 nM	1
<b>V</b> <sup>c</sup>	30 $\mu$ M	38 $\mu$ M	57 $\mu$ M	2.6
<b>VII</b>	97 $\mu$ M	52 $\mu$ M	81 $\mu$ M	2.6
<b>3</b>	41 $\mu$ M	20 $\mu$ M	36 $\mu$ M	3.0
<b>9</b>	ni	nd	nd	
<b>14</b>	68 $\mu$ M	27 $\mu$ M	39 $\mu$ M	3.0
<b>28</b>	60 $\mu$ M	28 $\mu$ M	67 $\mu$ M	4.0
<b>32</b>	47 $\mu$ M	16 $\mu$ M	27 $\mu$ M	2.8
<b>34</b>	33 $\mu$ M	7 $\mu$ M	12 $\mu$ M	2.9

<sup>a</sup>IC<sub>50</sub> value (SD <20%); Data represent the mean values of at least two experiments. ni: no inhibition; for **9** inhibition <10% at 50  $\mu$ M; for Rif inhibition <5% at 10  $\mu$ M. nd: not determined. <sup>b</sup>(IC<sub>50</sub> core:holocompd/IC<sub>50</sub> core:holoRif). The core:holo IC<sub>50</sub> ratios were related to the Rif core:holo ratio. <sup>c</sup>Inhibition values of core/holo transcription assay by Hüsecken *et al.*<sup>14</sup>

Inhibitors acting via such a mechanism would be expected to show a stronger effect in a  $\sigma^{70}$ -dependent transcription assay using holo enzyme than in a  $\sigma^{70}$ -independent transcription assay with core enzyme. To further confirm PPI interruption as RNAP inhibitory mechanism, we tested our compounds in both assays in parallel. Indeed, **3**, **14**, **28**, **32**, **34**, and **VII** were found to be more active in the assay using holo enzyme than in the core enzyme assay (Table 2). To normalize interassay conditions, ratios of IC<sub>50</sub> values (core:holo) were calculated in relation to IC<sub>50</sub> ratio (core:holo) of Rif, which was used as negative control not acting via PPI inhibition. The calculated IC<sub>50</sub> ratios (core:holo) of the tested compounds are within the range of **2–4**, comparable or even higher than the ratio of described PPI inhibitor **V** (Table 2). These results confirm the assumption that the mechanism of action of our compounds and TT inhibitor **VII** is the interference with the interaction between  $\sigma^{70}$  and RNAP core enzyme.

### Antibacterial activity

For investigation of antibacterial activity, minimum inhibitory concentration (MIC) values were determined for all compounds. Two described RNAP inhibitors were used as references: Rif, which reveals a good antibacterial activity against Gram-positive and negative strains,<sup>15–18</sup> and the natural product myxopyronin B, only active against Gram-positive

bacteria.<sup>19</sup> To evade effects associated with drug efflux, initial MIC tests were performed using *E. coli* TolC mutant, deficient in the AcrAB–TolC multidrug efflux system. There are several compounds possessing high antibacterial activity comparable to the reference compounds, especially **6–8**, **14–18**, **28**, and **32**, with MIC values in the range of 2–3 µg/mL. For most compounds, antibacterial activity roughly correlates with *in vitro* RNAP inhibition. However, for some highly potent inhibitors, compounds **25**, **33**, and **34**, bacterial growth inhibition was less than expected, a finding which possibly was caused by permeability problems. To further explore the antibacterial profile, MIC values for *E. coli* K12, *Pseudomonas aeruginosa*, *Bacillus subtilis*, and *Staphylococcus aureus* were determined for selected compounds (**6**, **7**, **12**, **15**, **28**, **32**, **33**; Table 3). None of the tested inhibitors reduced the growth of Gram-negative strains (*E. coli* K12 and *P. aeruginosa*). These results suggest that the compounds are either not able to penetrate the cell membranes of the Gram-negative bacteria or are discharged by efflux pumps. The latter mechanism is more probable considering the differences between the MIC values for *E. coli* K12 and *E. coli* TolC. On the other hand, the inhibitors were in general effective against Gram-positive bacteria; especially against *Bacillus subtilis* excellent MIC values were determined.

**Table 3.** Minimum Inhibitory Concentration (MIC) for Selected Compounds

compd	MIC (µg/ml) <sup>a</sup>			
	<i>E. coli</i> K12	<i>PAOI</i> <sup>b</sup>	<i>B. subtilis</i>	<i>S. aureus</i>
<b>Rif</b> <sup>c</sup>	7	13	5	0.02
<b>Myx</b> <sup>c</sup>	>25	>25	0.9	0.5
<b>6</b>	>50	>50	2	24
<b>7</b>	>50	>50	3	14
<b>12</b>	>100	>100	4	48
<b>15</b>	>25	>25	3	8
<b>28</b>	>50	>50	4	5
<b>32</b>	>25	>25	3	6
<b>33</b>	>25	>25	>25	17

<sup>a</sup>Minimum inhibitory concentration; Data represent the mean values of at least two independent experiments (three for MIC <10 µg/mL). <sup>b</sup>*P. aeruginosa*. <sup>c</sup>Rif, rifampicin; Myx, myxopyronin B.

It is striking that our compounds show very low MIC values comparable to the reference compounds although their RNAP inhibitory activities are less pronounced than those of the references. To confirm the mechanism of antibacterial activity, the impact on macromolecular



biosynthesis in *E. coli* TolC was examined. While exerting no appreciable effect on DNA and protein synthesis at  $4 \times \text{MIC}$ , **32** displayed an inhibition of RNA formation comparable to the clinically used RNAP inhibitor Rif (Figure 2). In addition, a strong decrease in lipid biosynthesis was observed (Figure 2). In this regard, it is also of interest that benzamidobenzoic acids, including compounds **2** and **3**, have been described in the context of anti-infective research. While compound **3** was shown to inhibit PqsD, an enzyme associated with the *Pseudomonas* quorum sensing system,<sup>20</sup> compounds **2** and **3** have been published as inhibitors of FabH, an enzyme involved in fatty acid synthesis.<sup>21</sup> Therefore, it can be supposed that the good antibacterial activity is due to an additional FabH inhibition.

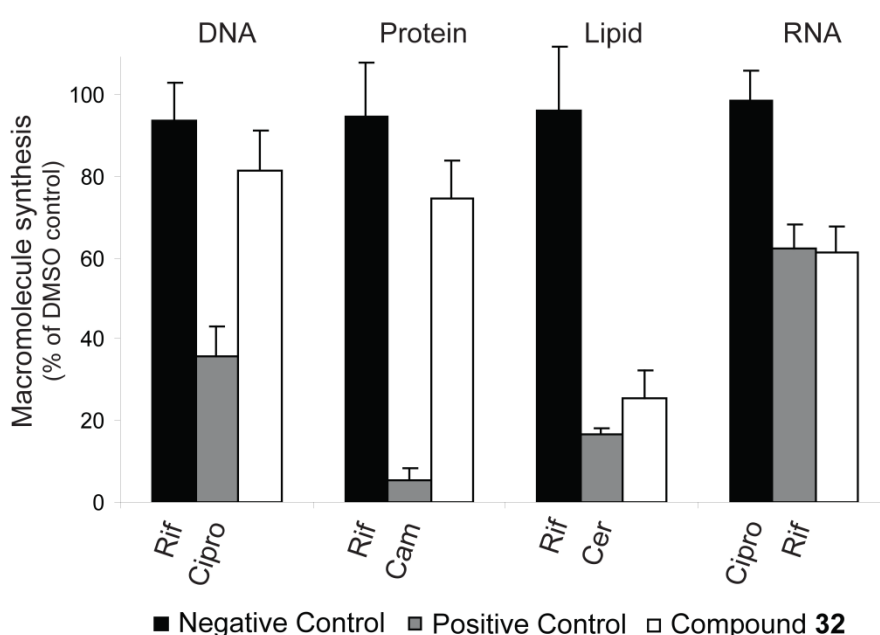


**Figure 2.** Effects of **32** at  $4 \times \text{MIC}$  on macromolecular synthesis in *E. coli* TolC. Controls: cerulenin (Cer), chloramphenicol (Cam), ciprofloxacin (Cipro), and rifampicin (Rif).

As it is our aim to develop compounds which are less susceptible to bacterial resistance development, the spontaneous resistance frequencies in *E. coli* TolC were determined *in vitro* for compounds **28** and **32** at  $2 \times \text{MIC}$ . Importantly, a lower resistance frequency ( $<4.5 \times 10^{-11}$ ) of both novel compounds compared to Rif ( $8.3 \times 10^{-8}$ ) was observed. One explanation for this remarkable observation could be the dual target effects of our compounds.

## Conclusion

RNAP is an attractive antibacterial target, but due to emerging resistance, new types of RNAP inhibitors are urgently needed. For the discovery of those, we performed a flexible alignment with a series of selected RNAP inhibitors<sup>8–12</sup> and developed a pharmacophore model which is

not focused on one particular binding site. Using this model, a virtual screening was performed, hit compounds were identified, and 11 of those subsequently experimentally validated. On the basis of three hits of one structural class, an optimization approach was performed, resulting in enhanced inhibitory potencies. Concerning the mechanism of RNAP inhibition, we could demonstrate that the new inhibitors prevent the PPI between  $\sigma^{70}$  and the RNAP core enzyme. Determination of MIC values revealed that the best compounds are highly active against *E. coli* TolC and the Gram-positive pathogens *B. subtilis* as well as the clinically relevant *S. aureus*. The wild-type Gram-negative strains *P. aeruginosa* and *E. coli* K12 were not affected, probably due to pharmacokinetic reasons. Regarding the effects of our compounds on macromolecule synthesis in *E. coli* TolC, an inhibition of bacterial lipid biosynthesis was observed beside the reduced RNA formation. This highly interesting dual target effect could explain the good MIC values and the significantly lower resistance rate compared to the clinically used inhibitor Rif. These findings are presently further elucidated. In conclusion, we consider the new compounds promising for further development.

## Experimental Section

**Chemistry.** All tested compounds have >95% chemical purity as measured by HPLC. Spectroscopic data for all compounds are provided in the SI.

### Procedure for the Synthesis of the Acyl Chlorides Used for Amide Coupling Reaction.

Benzoyl chlorides, if not commercially available, were obtained from the corresponding carboxylic acid via reaction with thionyl chloride (2.5 equiv) in  $\text{CH}_2\text{Cl}_2$  in the presence of catalytic amounts of dimethylformamide (4 h reflux).

**General Procedure for the Synthesis of Methyl 2-Aminobenzoates 5b, 21b–23b, 25b, 27b, 29b, and 30b. Method A.** A solution of the appropriate 2-aminobenzoic acid (1 equiv) in MeOH was cooled to 0 °C followed by a dropwise addition of thionyl chloride (2.5 equiv). The mixture was refluxed for 24 h. After evaporation of the solvent and neutralization by addition of a saturated aqueous  $\text{NaHCO}_3$  solution, the mixture was extracted with EtOAc and the combined organic layers were dried over  $\text{MgSO}_4$ . Purification by CC (n-hexane/EtOAc) provided the title compounds (yields, physical, and spectral data are reported in SI).

**General Procedure for the Synthesis of Methyl 2-Benzamidobenzoate Derivatives 1a–34a (Amide Coupling Reaction). Method B.** Three different procedures were used to obtain the title compounds: **BI**. The appropriate methyl 2-aminobenzoate (1 equiv) was added to a solution of the acyl chloride (1.2 equiv) in  $\text{CH}_2\text{Cl}_2$  under a  $\text{N}_2$  atmosphere. After the addition of TEA (2 equiv), the reaction mixture was stirred for 18 h at room temperature. **BII**.

The appropriate methyl 2-aminobenzoate (1 equiv) and a catalytic amount of DMAP were added to a suspension of the acyl chloride (1.5 equiv) in pyridine under a N<sub>2</sub> atmosphere. The reaction mixture was stirred for 18 h at room temperature, and 2 M HCl was added. The mixture was extracted with EtOAc, and the combined organic layers washed with saturated NaHCO<sub>3</sub> and dried over MgSO<sub>4</sub>. **BIII.** The appropriate methyl 2-aminobenzoate (1 equiv) and the acyl chloride (1.2 equiv) were dissolved in toluene and refluxed for 4 h (except for **5a** and **33a–34a**, which were refluxed for 18 or 72 h). For purification, the solvent was removed under reduced pressure and the remaining solid suspended in MeOH (except for **5a** and **31a–32a**). After filtration, the precipitate was washed with MeOH to yield the pure compound. For compounds **5a** and **31a–32a**, the purification step was performed by CC or preparative TLC.

**General Procedure for the Synthesis of 2-Benzamidobenzoate Derivatives 1–34. Method**

**C.** The methyl esters of the title compounds (**1a–34a**) were hydrolyzed with 5 M NaOH in THF/MeOH (2:1) at room temperature (18 h). The mixture was acidified by the addition of 1 M HCl and filtered, and the precipitate was washed with 1 M HCl to provide the title compounds. If the compound was not pure at this stage of the procedure, it was washed with MeOH and CH<sub>2</sub>Cl<sub>2</sub> or was purified by CC or preparative TLC.

**General Procedure for Suzuki Coupling. Method D.** A mixture of the appropriate methyl bromo-2-benzamidobenzoate (1 equiv), phenylboronic acid (1.5 equiv), Cs<sub>2</sub>CO<sub>3</sub> (3 equiv), and tetrakis-(triphenylphosphine)-palladium (0.01 equiv) in a degassed DME/water (1:1) solution was refluxed under a nitrogen atmosphere for 4 h. The reaction mixture was cooled to room temperature. The mixture was extracted with EtOAc. The combined organic layers were washed with 1 M HCl and dried over MgSO<sub>4</sub>. The product was purified by CC or preparative TLC.

**General Procedure for Ether Cleavage Using Boron Tribromide. Method E.** To a solution of the appropriate methoxy substituted methyl 2-benzamidobenzoate derivative (1 equiv) in anhydrous CH<sub>2</sub>Cl<sub>2</sub> at –78 °C (dry ice/acetone bath), boron tribromide (1 M in CH<sub>2</sub>Cl<sub>2</sub>, 6 equiv) was added dropwise. The reaction mixture was stirred for 18 h at room temperature under a nitrogen atmosphere. Water was added, and the aqueous layer was extracted with EtOAc. The combined organic layers were washed with brine and dried over MgSO<sub>4</sub>. The product was purified by CC followed by preparative TLC.

**Biology. Transcription Assay.** Transcription assay was performed as described previously.<sup>13,22</sup> During the transcription time of 10 min, the substrate concentration as well as

the enzyme activity were not limiting the transcription reaction. Consequently, the reaction process in our assay was linear.

**Determination of IC<sub>50</sub> Values.** For the determination of IC<sub>50</sub> values, three different concentrations of a compound were chosen (duplicate determination) in the linear range of the log dose response curve (20–80% inhibition) including concentrations above and below the IC<sub>50</sub> value. The calculation of the IC<sub>50</sub> value was performed by plotting the percent inhibition versus the concentration of inhibitor on a semilog plot. From this, the molar concentration causing 50% inhibition was calculated. At least three independent determinations were performed for each compound. Standard deviation was less than 20%.

**Minimal Inhibitory Concentration (MIC) Determinations.** These experiments were performed as described recently.<sup>22</sup> Given MIC values are means of two independent determinations (three if MIC <10 µg/mL) and are defined as the lowest concentration of compounds that reduced OD<sub>600</sub> by ≥95%.

**Determination of Resistance Frequencies.** Defined amounts of *E. coli* TolC cells were incubated in LB in presence of the 2 × MIC of compounds **28** and **32** in parallel (16 h, 37 °C, 50 rpm, 0.5% DMSO). On each of the three following days, a fraction of each of the samples was supplemented with fresh compound containing LB followed by recultivation (conditions as before). The final cultures were plated on LB agar to select spontaneous resistant mutants. The bacterial start concentration which was needed to yield at least one colony on the plates was determined. The reciprocal value of this threshold was defined to be the resistance frequency. For **28** and **32**, no colonies were detected at the highest possible bacterial start concentration, resulting in a resistance frequency <4.5 × 10<sup>-11</sup>.

**Macromolecular Biosynthesis Assay.** *E. coli* TolC was cultured in lysogeny broth (LB) medium. <sup>3</sup>H labeled precursors (1–1.25 µCi/mL) were added during the logarithmic growth phase and several min (3 min for uridine and thymidine, 5 min for acetic acid, 12 min for glutamine) before the addition of compound **32** and the controls chloramphenicol (Cam), cerulenin (Cer), ciprofloxacin (Cipro), and rifampicin (Rif) at four times their MICs. For DNA, RNA, and protein synthesis, 300 µL of the cultured bacteria were harvested 0 and 30 min after addition of the inhibitors and supplemented with 2 volumes of 10% TCA. After 45 min at 4 °C, the precipitates were collected and washed using 96-well glass fiber filter plates (Multiscreen GFB) (Millipore, Billerica, MA). After adding Optiphase Supermix (Perkin-Elmer, Waltham, MA), the quantification of radioactivity was performed using a Wallac MicroBeta TriLux system (Perkin-Elmer). For determination of lipid synthesis, cells were treated with CHCl<sub>3</sub>/MeOH (1:1) and water, subsequently. The organic phase was collected,

evaporated, redissolved in cyclohexane, and supplemented with Opti-Fluor O (Perkin-Elmer) before measuring the radioactivity in the MicroBeta TriLux.

**ELISA-Based RNAP Assembly Assay.** The procedure was performed as described by Hüsecken *et al.*<sup>14</sup>

**Core/Holo Transcription Assay.** The procedure was performed as described by Hüsecken *et al.*<sup>14</sup>

## Supporting Information

Synthesis, compound characterization, and computational chemistry. This material is available free of charge via the Internet at <http://pubs.acs.org>.

## Acknowledgements

We thank Jeannine Jung for determination of RNAP IC<sub>50</sub> values and Jannine Ludwig for determination of MIC values.

## References

- (1) Hooper, D. C.; DeMaria, A.; Limbago, B. M.; O'Brien, T. F.; McCaughey, B. Antibiotic resistance: how serious is the problem, and what can be done? *Clin. Chem.* **2012**, 58, 1182–1186.
- (2) Chopra, I. The 2012 Garrod Lecture: Discovery of Antibacterial Drugs in the 21st Century. *J. Antimicrob. Chemother.* **2013**, 68, 496–505.
- (3) Villain-Guillot, P.; Bastide, L.; Gualtieri, M.; Leonetti, J.-P. Progress in targeting bacterial transcription. *Drug Discovery Today* **2007**, 12, 200–208.
- (4) Ho, M. X.; Hudson, B. P.; Das, K.; Arnold, E.; Ebright, R. H. Structures of RNA polymerase–antibiotic complexes. *Curr. Opin. Struct. Biol.* **2009**, 19, 715–723.
- (5) Hardesty, J. S.; Juang, P. Fidaxomicin: a macrocyclic antibiotic for the treatment of *Clostridium difficile* infection. *Pharmacotherapy* **2011**, 31, 877–886.
- (6) Mariani, R.; Maffiolo, S. I. Bacterial RNA polymerase inhibitors: an organized overview of their structure, derivatives, biological activity and current clinical development status. *Curr. Med. Chem.* **2009**, 16, 430–454.
- (7) Chopra, I. Bacterial RNA polymerase: a promising target for the discovery of new antimicrobial agents. *Curr. Opin. Invest. Dr.* **2007**, 8, 600–607.
- (8) Arhin, F.; Bélanger, O.; Ciblat, S.; Dehbi, M.; Delorme, D.; Dietrich, E.; Dixit, D.; Lafontaine, Y.; Lehoux, D.; Liu, J.; McKay, G. A.; Moeck, G.; Reddy, R.; Rose, Y.; Srikumar, R.; Tanaka, K. S. E.; Williams, D. M.; Gros, P.; Pelletier, J.; Parr, T. R., Jr.; Far, A. R. A new class of small molecule RNA polymerase inhibitors with activity against rifampicin-resistant *Staphylococcus aureus*. *Bioorg. Med. Chem.* **2006**, 14, 5812–5832.
- (9) Artsimovitch, I.; Chu, C.; Lynch, A. S.; Landick, R. A new class of bacterial RNA polymerase inhibitor affects nucleotide addition. *Science* **2003**, 302, 650–654.
- (10) André, E.; Bastide, L.; Michaux-Charachon, S.; Gouby, A.; Villain-Guillot, P.; Latouche, J.; Bouchet, A.; Gualtieri, M.; Leonetti, J.-P. Novel synthetic molecules targeting the bacterial RNA polymerase assembly. *J. Antimicrob. Chemother.* **2006**, 57, 245–251.
- (11) Villain-Guillot, P.; Gualtieri, M.; Bastide, L.; Roquet, F. o.; Martinez, J.; Amblard, M.; Pugniere, M.; Leonetti, J.-P. Structure–Activity Relationships of phenyl-furanyl-rhodanines as inhibitors of RNA polymerase with antibacterial activity on biofilms. *J. Med. Chem.* **2007**, 50, 4195–4204.
- (12) Larsen, S. D.; Hester, M. R.; Craig Ruble, J.; Kamilar, G. M.; Romero, D. L.; Wakefield, B.; Melchior, E. P.; Sweeney, M. T.; Marotti, K. R. Discovery and initial development of a novel class of antibacterials: Inhibitors of *Staphylococcus aureus* transcription/translation. *Bioorg. Med. Chem. Lett.* **2006**, 16, 6173–6177.

- (13) Haupenthal, J.; Hüsecken, K.; Negri, M.; Maurer, C. K.; Hartmann, R. W. Influence of DNA template choice on transcription and inhibition of *Escherichia coli* RNA polymerase. *Antimicrob. Agents Chemother.* **2012**, 56, 4536–4539.
- (14) Hüsecken, K.; Negri, M.; Fruth, M.; Boettcher, S.; Hartmann, R. W.; Haupenthal, J. Peptide-based investigation of the *Escherichia coli* RNA polymerase  $\sigma 70$ : core interface as target site. *ACS Chem. Biol.* **2013**, 8, 758–766.
- (15) Thornsberry, C.; Hill, B. C.; Swenson, J. M.; McDougal, L. K. Rifampin: spectrum of antibacterial activity. *Rev. Infect. Dis.* **1983**, 5, 412–417.
- (16) Bandow, J. E.; Brötz, H.; Hecker, M. *Bacillus subtilis* tolerance of moderate concentrations of Rifampin involves the sigma(B)-dependent general and multiple stress response. *J. Bacteriol.* **2002**, 184, 459–467.
- (17) Fowler, C. E.; Soothill, J. S.; Oakes, L. MICs of rifampicin and chloramphenicol for mucoid *Pseudomonas aeruginosa* strains are lower when human lactoferrin is present. *J. Antimicrob. Chemother.* **1997**, 40, 877–879.
- (18) Williams, K. J.; Piddock, L. J. Accumulation of rifampicin by *Escherichia coli* and *Staphylococcus aureus*. *J. Antimicrob. Chemother.* **1998**, 42, 597–603.
- (19) Irschik, H.; Gerth, K.; Höfle, G.; Kohl, W.; Reichenbach, H. The myxopyronins, new inhibitors of bacterial RNA synthesis from *Myxococcus fulvus* (Myxobacterales). *J. Antibiot.* **1983**, 36, 1651–1658.
- (20) Pistorius, D.; Ullrich, A.; Lucas, S.; Hartmann, R. W.; Kzmaier, U.; Müller, R. Biosynthesis of 2-alkyl-4(1H)-quinolones in *Pseudomonas aeruginosa*: potential for therapeutic interference with pathogenicity. *ChemBioChem* **2011**, 12, 850–853.
- (21) Nie, Z.; Perretta, C.; Lu, J.; Su, Y.; Margosiak, S.; Gajiwala, K. S.; Cortez, J.; Nikulin, V.; Yager, K. M.; Appelt, K.; Chu, S. Structurebased design, synthesis, and study of potent inhibitors of  $\beta$ -ketoacyl carrier protein synthase III as potential antimicrobial agents. *J. Med. Chem.* **2005**, 48, 1596–1609.
- (22) Sahner, J. H.; Groh, M.; Negri, M.; Haupenthal, J.; Hartmann, R. W. Novel small molecule inhibitors targeting the “switch region” of bacterial RNAP: structure-based optimization of a virtual screening hit. *Eur. J. Med. Chem.* **2013**, 65, 223–231.

### 3.4 Influence of DNA template choice on transcription and inhibition of *Escherichia coli* RNA polymerase

Jörg Haupenthal, Kristina Hüsecken, Matthias Negri, Christine K. Maurer, and Rolf W. Hartmann

Full text article in *Antimicrob. Agents Chemother.* 2012, **56**: 4536-4539.

doi: 10.1128/AAC.00198-12

#### Publication IV

**Abstract:** In recent decades, quantitative transcription assays using bacterial RNA polymerase (RNAP) have been performed under widely diverse experimental conditions. We demonstrate that the template choice can influence the inhibitory potency of RNAP inhibitors. Furthermore, we illustrate that the sigma factor ( $\sigma^{70}$ ) surprisingly increases the transcription efficiency of templates with non-physiological non-prokaryotic promoters. Our results might be a useful guideline in the early stages of using RNAP for drug discovery.

## 4 Final discussion

The aim of this thesis was to generate a test system for the identification and characterization of  $\sigma^{70}$ :core RNAP inhibitors. The more information about the structure of the target, the binding site and mode of action of the inhibitor are available, the more likely rational drug design will be successful. To gain the information, reliable assays are essential. The assays developed in the course of this thesis are discussed and evaluated in the following section. Finally, the future perspectives of our in house  $\sigma^{70}$ :core RNAP inhibitors are discussed.

### 4.1 Evaluation of $\sigma^{70}$ :core RNAP inhibitor test system

#### 4.1.1 *In vitro* transcription assay and core/holo assay

For the evaluation of potential RNAP inhibitors regarding their inhibitory activity, an *in vitro* transcription assay using commercially available RNAP holo enzyme was developed [Haupenthal *et al.* 2012]. Inhibition in this functional assay is absolutely required for hit compounds that could be developed into future bactericidal drugs. The assay was modified to study the role of  $\sigma^{70}$  factor during the transcription of templates lacking prokaryotic promoter sequences. Therefore, the  $\sigma^{70}$  factor was recombinantly expressed and purified, allowing the separate addition to purchased RNAP core enzyme in various ratios as well as order of addition experiments. Although the purification procedure is tedious, since the protein is expressed in inclusion bodies, the obtained yield (~10 mg/L culture), purity (> 95 % with only one affinity purification step), and stability (at least 8 h at room temperature; over years at -80 °C) are satisfying. Using this  $\sigma^{70}$  factor in various ratios in the transcription assay, revealed that equal stoichiometric amounts of  $\sigma^{70}$  and RNAP core enzyme give the highest transcription rates. Further addition of  $\sigma^{70}$  factor leads to no more increase. Surprisingly, the addition of  $\sigma^{70}$  factor increased the transcription efficiency of different DNA templates with non-physiological and non-bacterial promoters. Thus, we reasoned that  $\sigma^{70}$  is needed for stabilization of the transcription bubble which is formed during initiation [Haupenthal *et al.* 2012]. Furthermore, we performed order-of-addition experiments. Usually, holo enzyme formation is allowed first, before adding the inhibitor and starting transcription. For the order-of-addition experiments we also tested preincubation of core RNAP with the inhibitor, before adding  $\sigma^{70}$ . Here, we expected equal inhibitory potencies for core RNAP inhibitors like rifampicin and higher potencies for  $\sigma^{70}$ :core inhibitors like SB2. We reasoned that small



organic compounds with weaker affinities than  $\sigma^{70}$  might have an advantage in binding to the core enzyme, when  $\sigma^{70}$  is not present. However, in both cases similar  $IC_{50}$  values were obtained when using the same DNA template (Figure 13). This fact could be due to low affinity (and/or a high dissociation rate) for SB2 to core RNAP compared to the high affinity binding of  $\sigma^{70}$ . Since this assay variant is not suitable to distinguish between the two inhibitor types, a new assay was needed.

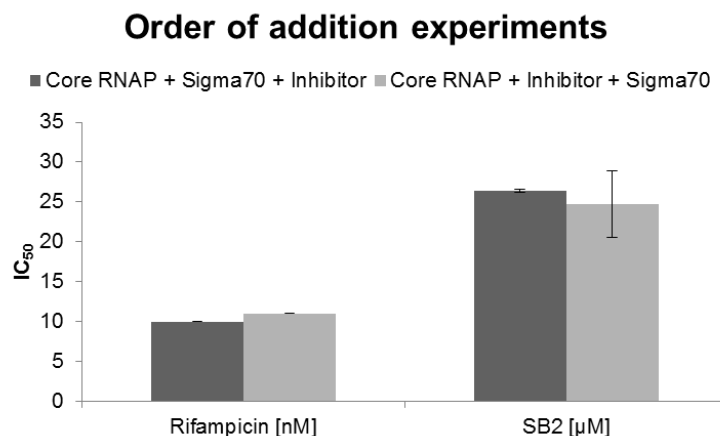


**Figure 13.** Order of addition experiments with the core RNAP inhibitor rifampicin and the  $\sigma^{70}$ :core inhibitor SB2.  $IC_{50}$  values for rifampicin are given in nM, whereas  $IC_{50}$ s of SB2 are in  $\mu$ M.

The core/holo assay uses core RNAP with T7 template which can be transcribed independently of promoter-specific recognition elements such as  $\sigma^{70}$  and holo RNAP with T7A1 promoter. For this template  $\sigma^{70}$  is required to initiate transcription. As shown in chapters 3.2 and 3.3, this assay provides a first hint in the direction of  $\sigma^{70}$ :core inhibitors. However, in some cases core RNAP can also be inhibited significantly by  $\sigma^{70}$ :core inhibitors, as observed for P07 (see chapter 3.2) due to interference with the lid-rudder system which is somehow involved in RPo formation [Kuznedelov *et al.* 2002, Touloukhonov and Landick 2006]. Hence, the results from the core/holo assay should always be confirmed in another assay such as the  $\sigma^{70}$ :core assembly inhibition assay.

#### 4.1.2 $\sigma^{70}$ :core assembly inhibition assay

The ELISA-based  $\sigma^{70}$ :core assembly inhibition assay is indispensable when it comes to identifying the mode of action of RNAP inhibitors. It uses the recombinant  $\sigma^{70}$  factor which is adsorbed to the bottom of a well-plate. Then the inhibitor and core enzyme are added simultaneously and after a few washing steps, bound core RNAP is detected. Thus, it directly

determines interference of a small molecule or peptide with the protein-protein interaction. But neither the ELISA nor the core/holo assay can tell if the protein-protein interface is really the target site, since positive results due to allosteric binding and induction of conformational changes in the core enzyme are also imaginable. However, such conformational changes need to be extensive in order to diminish core binding to  $\sigma^{70}$  since there are multiple contact sites (see also chapter 1.2). Thus, most likely disruption of the  $\sigma^{70}$ :core assembly means that the inhibitor binds in the interface between the  $\beta'$  coiled-coil and the  $\sigma^{70}$  factor region 2.1-2.2. Additionally, the allosteric inhibitor CBR-703 did not influence the  $\sigma^{70}$ :core assembly when tested in concentrations up to 200  $\mu\text{M}$ , underlining that the disruption of the holo enzyme formation due to conformational changes is only a theoretical possibility. When  $\text{IC}_{50}$  values of the transcription assay and the ELISA are plotted (Figure 14), a fairly good correlation is observed.

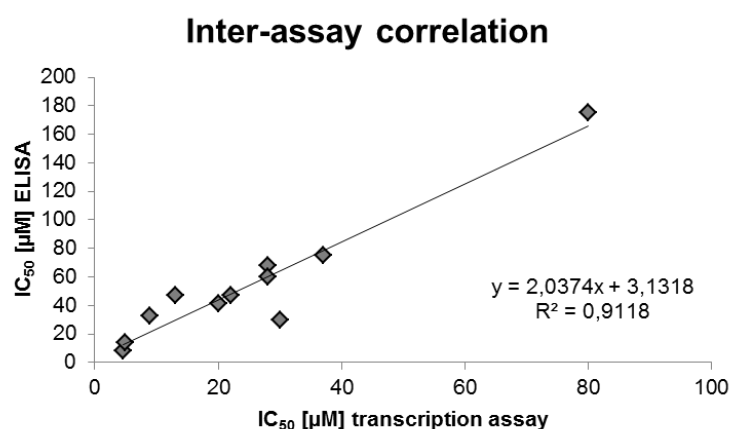


**Figure 14.** Inter-assay correlation of inhibitors from publications I-III between *in vitro* transcription and  $\sigma^{70}$ :core assembly inhibition assay.

Usually the  $\text{IC}_{50}$  values from the ELISA are twice as high as in the transcription assay. One explanation could be inter-assay differences such as the  $\sigma^{70}$ :core ratio (30:1 in the ELISA versus 1:1 in the transcription assay). Another explanation is the existence of a second target site within the RNAP. Since most of the plotted compounds belong to the benzamidobenzoic acid and the ureidothiophene carboxylic acids that target also the switch region [Sahner *et al.* 2013, Fruth *et al.* 2014], the steepness of the correlation might be erroneous, especially when considering that SB2 is the outlier underneath the curve, for which both  $\text{IC}_{50}$ s are equal. Further evidence that the switch region binding does not affect the protein-protein interaction is given by the negative performance of the specific switch region binders myxopyronin, coralopyronin and ripostatin in the ELISA.

### 4.1.3 Initiation inhibition assay

The initiation inhibition assay was developed in order to quantify inhibitory potencies regarding transcription initiation not only of  $\sigma^{70}$ :core inhibitors but also switch region binders. As described in chapter 1.2, in this first phase of transcription, promoter melting and synthesis of abortive products takes place [Hsu 2002]. For the assay, we modified an existing protocol [Smagowicz and Scheit 1978], but avoided the use of high energy radiolabels and simplified abortive transcript quantification by using reversed phase HPLC for separation combined with scintillation flow detection. Altogether this primed abortive initiation inhibition assay is favorable over existing methods, due to improved handling, quantification and safety. The exact quantification of the abortive products allows inhibitor ranking, which is needed for structure-activity-based inhibitor optimization. One major disadvantage of the assay is, that it does not really help to identify a compound's mode of action, since it works not exclusively for RNAP inhibitors that bind to the switch region or the  $\sigma^{70}$ :core interface, but also for nucleotide addition inhibitors, explaining almost identical inhibitory activities for the initiation and the transcription assay of all tested compounds. The only RNAP inhibitors that do not give positive results are streptolydigin and the rifamycins that inhibit elongation of transcripts longer than three nucleotides [Campbell *et al.* 2001]. Thus, this assay may support initiation inhibition but does not prove it as mode of action.

### 4.1.4 SPR screening assay

Since the aim of the thesis was not only to characterize existing RNAP inhibitors but also to identify new compounds in high-throughput that potentially inhibit the  $\sigma^{70}$ :core interaction by binding to the inhibition hot spot on the  $\beta'$  subunit, a suitable assay was needed. SPR was chosen as it offers several advantages. First, it directly measures binding – without binding, no inhibition is possible – in real-time, delivering the whole interaction and not only single point observations. Second, it does not require any labels. On the other side, the absence of labels means also the detection of non-specific binding to the sensor surface. Although this non-specific binding is usually referenced out by using a reference channel, it decreases data quality as the signal to noise ratio increases [Tudos and Schasfoort 2008].

As target protein for the screening, a truncated *E. coli*  $\beta'$  subunit (amino acids 200-341) including the coiled-coil and the lid-rudder system was cloned, expressed, and purified. This part of the  $\beta'$  subunit was chosen, since it is the major binding site of core RNAP for  $\sigma^{70}$

[Arthur and Burgess 1998, Arthur *et al.* 2000, chapter 3.2]. Furthermore, the whole core enzyme is not suitable for SPR-based small molecule screening, due to its large size and complex structure. It completely loses activity when immobilized by amine-coupling. Using only parts of a protein is always critical, since the structure determines its function. Thus, the  $\beta'$  CC-LRS expression conditions were optimized towards soluble protein, which are more likely folded correctly. Although the obtained yields were not as good as for the  $\sigma^{70}$  factor ( $\beta'$  CC-LRS: ~5 mg/l culture; >90 % pure; for  $\sigma^{70}$  see chapter 4.1.1), mostly due to the high isoelectric point (11.9, calculated with ExPASy ProtParam tool) that causes charge repulsion during  $\text{Ni}^{2+}$  affinity chromatography, they were still sufficient for the low amounts needed for SPR.

As  $\beta'$  CC-LRS contains many lysines, first amine-coupling was tried for immobilization. However, immobilization levels were not reproducible, possibly due to multiple coupling sites of some and only few coupling sites of other target proteins. Hence,  $\beta'$  CC-LRS was biotinylated and complexed on streptavidin sensor chips, giving very reproducible loading capacities. Next, the protein's integrity had to be verified. This was initially done by interaction with  $\sigma^{70}$  factor and then with SB2 during the screening (Publication I). Usually, the tethered protein was stable for 4-5 days at 18 °C. The concentration for the small molecule library compounds in the screening was set to 100  $\mu\text{M}$ . This is a good compromise, since high concentrations are needed to detect the usually low affinity binding of small molecules – corresponding to low signal intensities – and increased non-specific binding at very high concentrations [Giannetti 2011]. The screening of roughly 2,000 compounds with molecular weights smaller than 500 g/mol identified 59  $\beta'$  CC-LRS binders. Of these initial hits 5 compounds were active in the functional transcription assay and in the ELISA-binding assay. The other 54 compounds presumably did not bind the inhibition hot spot formed by the coiled-coil and lid-rudder system. More likely they bound to parts of the protein that are usually buried within the core RNAP or they form a sandwich complex together with the  $\sigma^{70}$  factor which did not impair holo enzyme function.

Surprisingly, P07 (Publication II) did not show an interaction with  $\beta'$  CC-LRS under all tested conditions despite the specific interactions in the molecular dynamics simulation with a very similar part of  $\beta'$  (amino acids 94-346) which was also supported by the decreased activities of the P07 mutants. So far, there is no satisfying explanation for this phenomenon. If the structure of the peptide was incorrect, it would not have inhibited the enzyme. The protein structure on the other hand can be assumed to be correct, since  $\sigma^{70}$  binds with reasonably high

affinity to it. Although it might be that the binding site of P07 was predicted wrong, the very supportive results from the mutagenesis study would be a too big coincidence. Possibly, the different assay conditions have a negative effect on the peptide folding. On the other hand this seems unlikely, since various conditions have been tested.

#### 4.1.5 SPR competition assay

The aim of this assay is to clearly identify inhibitors of the  $\beta'$  CC-LRS and the  $\sigma^{70}$  factor interaction. Since the  $\beta'$  CC-LRS is much smaller than the core RNAP, which is used in the ELISA-based protein-protein interaction inhibition assay, the chance of disruption of the interaction due to an allosteric effect in this SPR-based competition assay is very small. When saturating  $\beta'$  CC-LRS with either SB2, compound **1** (Publication I) or compound **4** (Publication I), the interaction with  $\sigma^{70}$  was significantly reduced. Although competition of the compounds and  $\sigma^{70}$  factor for their binding to the  $\beta'$  CC-LRS was shown this way, it would be more feasible to add  $\sigma^{70}$  to the running buffer and then inject the test compounds to reach a higher throughput. Additionally, this scenario would be closer to the *in vivo* situation, but would consume much higher amounts of  $\sigma^{70}$  factor.

#### 4.1.6 Binding site identification using wild type and mutant proteins

The knowledge of a hit compound's exact binding site is of utmost importance for the rational optimization of its affinity to the target protein. The gold standard for the identification of a compound's binding site is crystallography. An alternative approach is the generation of mutant target proteins. This can be either done by creating spontaneous mutants *in vitro* and sequencing of the genomic DNA or by introducing site-directed mutations at positions that are most likely important for the interaction. We chose to generate seven site-directed mutants of the  $\beta'$  CC-LRS. These amino acid residues have been predicted to be of high relevance for the interaction with the RNAP inhibiting P07 (Publication II). Six of them were obtained in sufficient amounts and used for SPR interaction studies. In order to compare the hit compounds' affinities towards wild type and mutant proteins, immobilization levels have to be nearly identical. Therefore, proteins were diluted to the same concentration and injected for identical time periods during immobilization. If then a hit compound exhibits lower affinity towards one of the mutant proteins, the amino acid that has been substituted by alanine is

important for binding of the hit compound. For each  $\sigma^{70}$ :core RNAP inhibitors class (SB, benzamidobenzoic acids, ureidothiophenes) binding to the  $\beta'$  coiled-coil arginine mutants R271A, R275A, and R278A was more or less decreased, as well binding to the  $\beta'$  rudder mutant T317A. Based on the results, probable binding modes were proposed. For SB2 and compound **1** (Publication I) it is likely that they bind parallel to the  $\beta'$  CC, whereas compound **4** (Publication I) seems to be oriented vertically to the  $\beta'$  CC. In all cases, the carboxylic acid moiety was predicted to interact with the before mentioned arginines.

One major point of discussion in this assay is the folding of the target protein. For the wild type  $\beta'$  CC-LRS we used  $\sigma^{70}$  factor and SB2 as positive control binders to control the integrity of the immobilized protein. However, for the mutant  $\beta'$  CC-LRS proteins, no such positive control exists. Hence, circular dichroism (CD) spectroscopy was applied. Although the obtained spectra are not identical, they have the same pattern with  $\alpha$ -helical and random coil portions. Based on the conformation in the RNAP crystal structure, this pattern was expected for this particular segment of the  $\beta'$  subunit. Quantitative secondary structure estimations were not carried out, since the storage buffer disturbs detection of the characteristic signal increase of the  $\alpha$ -helix between 190 and 195 nm [Greenfield 2006]. Thus, the absolute conformational integrity remains to be clarified, but there is evidence, that wild-type and mutant  $\beta'$  CC-LRS are folded alike.

A similar approach was followed to elucidate the binding site of P07 (Publication II). Here, the RNAP holo enzyme was left unchanged. Mutations – based on interactions predicted in a molecular dynamics simulation – were introduced on the peptide side. Decreased or lacking inhibitory potencies of the mutant peptides were in good accordance with the binding model but are no absolute proof. In future studies, further evidence could be obtained by site-directed mutations on the RNAP side. If however the  $\beta'$  CC-LRS is not the binding site of P07, this would probably explain the missing SPR-signal in interaction studies with this portion of core RNAP.

#### 4.1.7 Affinity ranking and kinetic profiling

As stated in Markgren *et al.* (2002) association and dissociation rates are important parameters for drug-target interactions. A desired inhibitor profile exhibits a fast association and slow dissociation rate. In the study, significant differences in the kinetic rates for HIV-1 protease inhibitors were found. Thus, despite similar inhibitory activities, structural changes

do alter drug-target interactions, underlining the relevance of SPR-based investigations. Hence, we aimed to characterize our  $\sigma^{70}$ :core RNAP inhibitors accordingly. We could determine  $k_{\text{off}}$  rates for the inhibitors and found a linear correlation between their inhibitory potency and their affinity ( $k_{\text{off}}$ ) as shown in Publication I. This finding confirms specific binding to the  $\beta'$  CC-LRS since slow dissociation rates can only be achieved by interactions with the target, whereas association rates can be influenced by the concentration at the target [Markgren *et al.* 2002]. Unfortunately, no reliable  $K_D$  values could be determined due to atypical association trends for some compounds. Moreover, solubility limitations in combination with low affinities impeded the intention (usually at least five different concentration duplicates below and above the equilibrium dissociation constant are required). In conclusion, kinetic analysis and affinity ranking are of high interest as they allow interaction-guided compound optimization and lead selection.

## 4.2 Future of $\sigma^{70}$ :core RNAP inhibitors

**P07.** The  $\sigma^{70}$ -derived peptidic inhibitor P07 (Publication II) was predicted to bind *in silico* to the  $\beta'$  CC-LRS. This model was supported by selected P07 mutants that exhibited significantly lower inhibitory potencies as the wild type P07. On the other hand, no binding in the SPR-based interaction study was detected. Additionally, macro-cyclization of the helical part – also based on the binding model – resulted in a loss of activity [Kamal 2013]. Now, further attempts to verify the binding site, such as an alanine scan of the peptide, mutations of key amino acid residues on the core site and ideally crystallization of the P07-core RNAP complex are necessary to follow a structure-based optimization strategy. These options are currently investigated by our group. If the binding mode is established, further improvements of the activity *in vitro* and *in vivo* are required. To this end, truncation, rigidization, side chain modifications, and addition of penetration enhancers may be successful. Even peptidomimetics should be considered, as they are usually more stable under physiological conditions.

**Benzamidobenzoic acids and ureidothiophene carboxylic acids.** These low molecular weight RNAP inhibitor classes are described to act not only on RNA polymerase but also on additional bacterial targets, such as FabH, an enzyme involved in fatty acid synthesis (Publication III) and PqsD, an enzyme in the production of *Pseudomonas aeruginosa* quorum sensing signal molecules HHQ and PQS [Sahner *et al.* 2014, Hinsberger *et al.* 2014]. This fact

brings up the question whether these compounds are promiscuous or can act selectively on multiple targets. Based on the molecular properties there are arguments pro and contra promiscuity. The high clogP values – most of the compounds have a clogP of around 5 – usually mark compounds that are more likely frequent hitters, whereas the carboxylic acid moiety in both classes stands in contrast to generally basic ( $\text{pK}_a [\text{base}] > 7$ ) promiscuous compounds [Peters 2013]. Moreover, the compounds do not only bind concentration dependent to  $\beta'$  CC-LRS in SPR-based assays but also to  $\sigma^{70}$  when immobilized by amine coupling. This might indicate unspecific binding due to high lipophilicity but may also indicate another specific binding site, since there seems to be a correlation between activity and affinity (Figure 16).

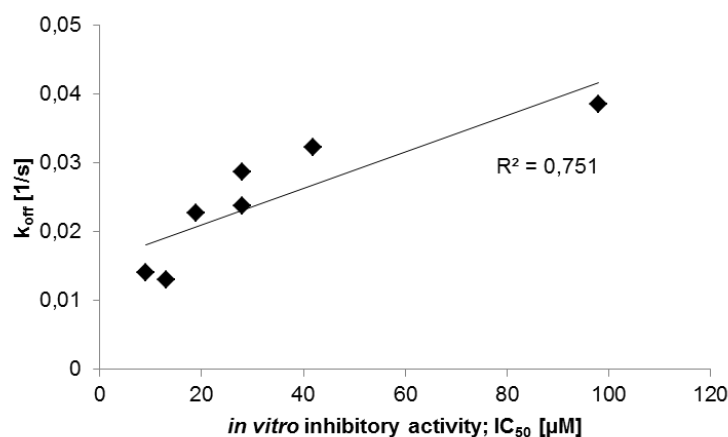


**Figure 16.** Linear correlation of *in vitro* transcription activity ( $\text{IC}_{50}$ ) and the dissociation rate constant ( $k_{\text{off}}$ ) from  $\sigma^{70}$  for the benzamidobenzoic acids.

If this second binding site would be opposite of the  $\beta'$  CC-LRS within the  $\sigma^{70}$ :core interface, this would actually be beneficial for the compound's inhibitory activity. However, given the current data this remains speculation. Further arguments against promiscuous behavior are different SAR for the different target proteins, no correlation of lipophilicity and activity, as well as activities in the nM range for the top PqsD inhibiting compounds [Sahner *et al.* 2014].



## 5 References

- Allison LA. (2000) The role of sigma factors in plastid transcription. *Biochimie* **82**, 537-548.
- André E, Bastide L, Villain-Guillot P, Latouche J, Rouby J, and Leonetti JP. (2004) A multiwall assay to isolate compounds inhibiting the assembly of the prokaryotic RNA polymerase. *Assay Drug Dev.* **2**, 629-635.
- André E, Bastide L, Michaux-Charachon S, Gouby A, Villain-Guillot P, Latouche J, Bouchet A, Gualtiéri M, and Leonetti JP. (2006) Novel synthetic molecules targeting the bacterial RNA polymerase assembly. *J. Antimicrob. Chemother.* **57**, 245-251.
- Arhin F, Bélanger O, Cilblat S, Deghbi M, Delorme D, Dietrich E, Dixit D, Lafontaine Y, Lehoux D, Liu J, McKay GA, Moeck G, Reddy R, Rose Y, Srikumar R, Tanaka KS, Williams DM, Gros P, Pelletier J, Parr TR Jr, and Far AR. (2006) A new class of small molecule RNA polymerase inhibitors with activity against rifampicin-resistant *Staphylococcus aureus*. *Bioorg. Med. Chem.* **14**, 5812-5832.
- Arnone A and Nasini G. (1987) Structure elucidation of the macrocyclic antibiotic lipiarmycin. *J. Chem. Soc. Perkin Trans. I* **6**, 1353-1359.
- Arthur TM and Burgess RR. (1998) Localization of a  $\sigma^{70}$  binding site on the N terminus of the Escherichia coli RNA polymerase  $\beta'$  subunit. *J. Biol. Chem.* **273**, 31381-31387.
- Arthur TM, Anthony LC, and Burgess RR. (2000) Mutational analysis of  $\beta'$  260-309, a  $\sigma^{70}$  binding site located on Escherichia coli core RNA polymerase. *J. Biol. Chem.* **275**, 23113-23119.
- Artsimovitch I, Chu C, Lynch AS, and Landick R. (2003) A new class of bacterial RNA polymerase inhibitor affects nucleotide addition. *Science* **302**, 650-654.
- Artsimovitch I and Vassylyev DG. (2006) Is it easy to stop RNA polymerase? *Cell Cycle* **5**, 399-404.
- Artsimovitch I, Svetlov V, Nemetski SM, Epshtein V, Cardozo T, and Nudler E. (2011) Tagetitoxin inhibits RNA polymerase through trapping of the trigger loop. *J. Biol. Chem.* **286**, 40395-40400.
- Artsimovitch I, Seddon J, and Sears P. (2012) Fidaxomicin is an inhibitor of the initiation of bacterial RNA synthesis. *Clin. Infect. Dis.* **55**(Suppl. 2), 127-131.
- Belogurov GA, Vassylyeva MN, Sevostyanova A, Appleman JR, Xiang AX, Lira R, Webber SE, Klyuyev S, Nudler E, Artsimovitch I, and Vassylyev DG. (2009) Transcription inactivation through local refolding of the RNA polymerase structure. *Nature* **457**, 332-335.
- Bergendahl V, Heyduk T, and Burgess RR. (2003) Luminescence resonance energy transfer-based high-throughput screening assay for inhibitors of essential protein-protein interactions in bacterial RNA polymerase. *Appl. Environ. Microbiol.* **69**, 1492-1498.

Biacore.com, April 2014.

Blond A, Cheminant M, Ségalas-Milazzo I, Péduzzi J, Barthélémy M, Goulard C, Salomón R, Moreno F, Farías R, Rebuffat S. (2001) Solution structure of microcin J25, the single macrocyclic antimicrobial peptide from *Escherichia coli*. *Eur. J. Biochem.* **268**, 2124-2133.

Boucher TW, Talbot GH, Bradley JS, Edwards JE, Gilbert D, Rice LB, Scheld M, Spellberg B, and Bartlett J. (2009) Bad bugs, no drugs: no ESKAPE! An update from the Infectious Diseases Society of America. *Clin. Infect. Dis.* **48**, 1-12.

Burgess RR, Travers AA, Dunn JJ, and Bautz EK. (1969) Factor stimulating transcription by RNA polymerase. *Nature* **221**, 43-46.

Burgess RR. (1971) RNA polymerase. *Annu. Rev. Biochem.* **40**, 711-740.

Burgess RR and Anthony L. (2001) How sigma docks to RNA polymerase and what sigma does. *Curr. Opin. Microbiol.* **4**, 126-131.

Bushnell DA, Cramer R, and Kornberg RD. (2002) Structural basis of transcription: alpha-amanitin-RNA polymerase II cocrystal at 2.8 Å resolution. *Proc. Natl. Acad. Sci. USA* **99**, 1218-1222.

Buurman ET, Foulk MA, Gao N, Laganas VA, McKinney DC, Moustakas DT, Rose JA, Shapiro AB, and Fleming PR. (2012) Novel rapidly diversifiable antimicrobial RNA polymerase switch region inhibitors with confirmed mode of action in *Haemophilus influenza*. *J. Bacteriol.* **194**, 5504-5512.

Campbell EA, Korzheva N, Mustaev A, Murakami K, Nair S, Goldfarb A, and Darst SA. (2001) Structural mechanism for rifampicin inhibition of bacterial RNA polymerase. *Cell* **104**, 901-912.

Campbell EA, Pavlova O, Zenkin N, Leon F, Irschik H, Jansen R, Severinov K, and Darst SA. (2005) Structural, functional, and genetic analysis of sorangicin inhibition of bacterial RNA polymerase. *EMBO J.* **24**, 674-682.

Catimel B, Weinstock J, Nerrie M, Domagala T, and Nice EC. (2000) Micropreparative ligand fishing with a cuvette-based optical mirror resonance biosensor. *J. Chromatogr. A* **869**, 261-273.

Cavalleri B, Arnone A, Di Modugno E, Nasini G, and Goldstein BP. (1988) Structure and biological activity of lipiarmycin B. *J. Antibiot.* **41**, 308-315.

Chopra I. (2003) Antibiotic resistance in *Staphylococcus aureus*: Concerns, causes and cures. *Expert Rev. Anti Infect. Ther.* **1**, 45-55.

Chopra I. (2007) Bacterial RNA polymerase: A promising target for the discovery of new antimicrobial agents. *Curr. Opin. Invest. Drugs* **8**, 600-607.

Cooper MA. (2002) Optical biosensors in drug discovery. *Nat. Rev. Drug Discov.* **1**, 515-528.

- Cramer P. (2002) Multisubunit RNA polymerases. *Curr. Opin. Struct. Biol.* **12**, 89-97.
- Crum GF, Devries WH, Eble TE, Large CM, and Shell JW. (1955) Streptolydigin, a new antimicrobial antibiotic. II. Isolation and characterization. *Antibiot. Annu.* **3**, 893-896.
- Darst SA. (2004) New inhibitors targeting bacterial RNA polymerase. *Trends Biochem. Sci.* **29**, 159-160.
- Degen D, Feng Y, Zhang Y, Ebright KY, Ebright YW, Gigliotti M, Vahedian-Movahed H, Mandal S, Talaue M, Connell N, Arnold E, Fenical W, and Ebright RH. (2014) Transcription inhibition by the depsipeptide antibiotic salinamide A. *eLife* **3**:e02451.
- FDA.gov (888-INFO-FDA) May 2011
- Feklistov A, Mekler V, Jiang Q, Westblade LF, Irschik H, Jansen R, Mustaev A, Darst SA, and Ebright RH. (2008) Rifamycins do not function by allosteric modulation of binding of  $Mg^{2+}$  to the RNA polymerase active center. *Proc. Natl. Acad. Sci. USA* **105**, 14820-14825.
- Fruth M, Plaza A, Hinsberger S, Sahner JH, Haupenthal J, Bischoff M, Jansen R, Müller R, and Hartmann RW. (2014) Binding mode characterization of novel RNA polymerase inhibitors using a combined biochemical and NMR approach. Submitted.
- Gardella T, Moyle T, and Susskind MM. (1989) A mutant Escherichia coli sigma 70 subunit of RNA polymerase with altered promoter specificity. *J. Mol. Biol.* **206**, 579-590.
- Giannetti AM. (2011) From experimental design to validated hits: A comprehensive walk-through of fragment lead identification using surface plasmon resonance. *Meth. Enzymology* **493**, 169-218.
- Glaser BT, Bergendahl V, Thompson NE, Olson B, and Burgess RR. (2007) LRET-based HTS of a small-compound library for inhibitors of bacterial RNA polymerase. *Assay Drug Dev.* **5**, 759-768.
- Goldman SR, Ebright RH, and Nickels BE. (2009) Direct detection of abortive RNA transcripts in vivo. *Science* **324**, 927-928.
- Gourse RL, Ross W, and Rutherford ST. (2006) General pathway for turning on promoters transcribed by RNA polymerases containing alternative  $\sigma$  factors. *J. Bacteriol.* **188**, 4589-4591.
- Grant EB, Guiadeen D, Baum EZ, Foleno BD, Jin H, Montenegro DA, Nelson EA, Bush K, and Hlasta DJ. (2000) The synthesis and SAR of rhodanines as novel class C  $\beta$ -lactamase inhibitors. *Bioorg. Med. Chem. Lett.* **10**, 2179-2182.
- Greenfield NJ. (2006) Using circular dichroism spectra to estimate protein secondary structure. *Nat. Protoc.* **1**, 2876-2890.
- Gruber TM and Gross CA. (2003) Multiple sigma subunits and the partitioning of bacterial transcription space. *Annu. Rev. Microbiol.* **57**, 441-466.

- Gualtieri M, Villain-Guillot P, Latouche J, Leonetti JP, and Bastide L. (2006) Mutation in the *Bacillus subtilis* RNA polymerase  $\beta'$  subunit confers resistance to lipiarmycin. *Antimicrob. Agents Chemother.* **50**, 401-402.
- Hämäläinen MD, Markgren PO, Schaal W, Karlén A, Classon B, Vrang L, Samuelsson B, Hallberg A, and Danielson UH. (2000) Characterization of a set of HIV-1 protease inhibitors using binding kinetics data from a biosensor screen. *J. Biomol. Screen.* **5**, 353-360.
- Haebich D and von Nussbaum F. (2009) Lost in transcription – inhibition of RNA polymerase. *Angew. Chem. Int. Ed.* **48**, 3397-3400.
- Hauptenthal J, Hüsecken K, Negri M, Maurer CK, and Hartmann RW. (2012) Influence of DNA template choice on transcription and inhibition of *Escherichia coli* RNA polymerase. *Antimicrob. Agents Chemother.* **56**, 4536-4539.
- Helmann JD and Chamberlin MJ. (1988) Structure and function of bacterial sigma factors. *Annu. Rev. Biochem.* **57**, 839-872.
- Heyse S, Stora T, Schmid E, Lakey JH, and Vogel H. (1998) Emerging techniques for investigating molecular interactions at lipid membranes. *Biochim. Biophys. Acta* **1376**, 319-338.
- Hinsberger S, de Jong JC, Groh M, Hauptenthal J, and Hartmann RW. (2014) Benzamidobenzoic acids as potent PqsD inhibitors for the treatment of *Pseudomonas aeruginosa* infections. *Eur. J. Med. Chem.* **76**, 343-351.
- Ho MX, Hudson BP, Das K, Arnold E, and Ebright RH. (2009) Structures of RNA polymerase-antibiotic complexes. *Curr. Opin. Struct. Biol.* **19**, 715-723.
- Hsu LM. (2002) Promoter clearance and escape in prokaryotes. *Biochim. Biophys. Acta* **1577**, 191-207.
- Huber W. (2005) A new strategy for improved secondary screening and lead optimization using high-resolution SPR characterization of compound-target interactions. *J. Mol. Recognit.* **18**, 273-281.
- Ji Y, Zhang B, Van Horn SF, Warren P, Woodnutt G, Burnham MKR, and Rosenberg M. (2001) Identification of critical staphylococcal genes using conditional phenotypes generated by antisense RNA. *Science* **293**, 2266-2269.
- Johnson AE. (2005) Fluorescence approaches for determining protein conformations, interactions and mechanisms at membranes. *Traffic* **6**, 1078-1092.
- Johnsson B, Löfås S, Lindquist G. (1991) Immobilization of proteins to a carboxymethyl-dextran-modified gold surface for biospecific interaction analysis in surface plasmon resonance sensors. *Anal. Biochem.* **198**, 268-277.

- Jones KA, Albeck JG, Gaudet S, Sorger PK, Lauffenburger DA, and Yaffe MB. (2005) A systems model of signaling identifies a molecular basis set for cytokine-induced apoptosis. *Science* **310**, 1646-1653.
- Kamal AAM. (2013) Synthesis and structural optimization of peptides inhibiting E. coli RNA polymerase. *Diploma thesis*. Saarland University.
- Kuznedelov K, Korzheva N, Mustaev A, and Severinov K. (2002) Structure-based analysis of RNA polymerase function: the largest subunit's rudder contributes critically to elongation complex stability and is not involved in the maintenance of RNA-DNA hybrid length. *EMBO J.* **21**, 1369-1378.
- Kyzer S, Zhang J, and Landick R. (2005) Inhibition of RNA polymerase by streptolydigin: No cycling allowed. *Cell* **122**, 494-496.
- Lesley SA and Burgess RR. (1989) Characterization of the Escherichia coli transcription factor 70: localization of a region involved in the interaction with core RNA polymerase. *Biochemistry* **28**, 7728-7734.
- Löfås S. (2004) Optimizing the hit to lead process using SPR analysis. *Assay Drug Dev. Technol.* **2**, 407-415.
- Lonetto M, Gribskov M, and Gross CA. (1992) The sigma 70 family: sequence conservation and evolutionary relationships. *J. Bacteriol.* **174**, 3843-3849.
- Ma C, Yang X, Kandemir H, Mielczarek M, Johnston EB, Griffith R, Kumar N, and Lewis PJ. (2013) Inhibitors of bacterial transcription initiation complex formation. *ACS Chem. Biol.* **8**, 1972-1980.
- Malinen AM, Mazumdar MN, Turtola M, Malmi H, Grocholski T, Artsimovitch I, and Belogurov GA. (2014) CBR antimicrobials alter coupling between the bridge helix and the  $\beta$  subunit in RNA polymerase. *Nat. Commun.* **5**:3408.
- Mariani R and Maffioli SI. (2009) Bacterial RNA polymerase inhibitors: An organized overview of their structure, derivatives, biological activity and current clinical development status. *Curr. Med. Chem.* **16**, 430-454.
- Mariner KR, Trowbridge R, Agarwal AK, Miller K, O'Neill AJ, Fishwick CWG, and Chopra I. (2010) Furanyl-rhodanines are unattractive drug candidates for development as inhibitors of bacterial RNA polymerase. *Antimicrob. Agents Chemother.* **54**, 4506-4509.
- Markgren PO, Schaal W, Hämäläinen M, Karlén A, Hallberg A, Samuelsson B, Danielson UH. (2002) Relationships between structure and interaction kinetics for HIV-1 protease inhibitors. *J Med Chem.* **45**, 5430-5439.
- McClure WR and Cech CL. (1978) On the mechanism of rifampicin inhibition of RNA synthesis. *J. Biol. Chem.* **253**, 8949-8956.

- McGhee JD and von Hippel PH. (1974) Theoretical aspects of DNA-protein interactions: co-operative and non-co-operative binding of large ligands to a one-dimensional homogeneous lattice. *J. Mol. Biol.* **86**, 469-489.
- McGowan JE. (2006) Resistance in nonfermenting Gram-negative bacteria: Multidrug resistance to the maximum. *Am. J. Med.* **119** (6 Suppl. 1), S29-S36.
- McPhillie MJ, Trowbridge R, Mariner KR, O'Neill AJ, Johnson AP, Chopra I, and Fishwick CWG. (2011) Structure-based ligand design of novel bacterial RNA polymerase inhibitors. *ACS Med. Chem. Lett.* **2**, 729-734.
- Mellmann I and Warren G. (2000) The road taken: past and future foundations of membrane traffic. *Cell* **100**, 99-112.
- Mielczarek M, Devakaram RV, Ma C, Yang X, Kandemir H, Purwono B, Black D StC, Griffith R, Lewis PJ, and Kumar N. (2014) Synthesis and biological activity of novel bis-indole inhibitors of bacterial transcription initiation complex formation. *Org. Biomol. Chem.* **12**, 2882-2894.
- Mooney RA, Darst SA, and Landick R. (2005) Sigma and RNA polymerase: An on-again, off-again relationship? *Mol. Cell* **20**, 335-345.
- Mukhopadhyay J, Das K, Ismail S, Koppstein D, Jang M, Hudson B, Sarafianos S, Tuske S, Patel J, Jansen R, Irschik H, Arnold E, and Ebright RH. (2008) The RNA polymerase "switch region" is a target for inhibitors. *Cell* **135**, 295-307.
- Murakami KS and Darst SA. (2003) Bacterial RNA polymerases: the whole story. *Curr. Opin. Struct. Biol.* **13**, 31-39.
- Murakami KS. (2013) The x-ray crystal structure of Escherichia coli RNA polymerase  $\sigma^{70}$  holoenzyme. *J. Biol. Chem.* **288**, 9126-9134.
- Myszka DG and Rich RL. (2000) Implementing surface plasmon resonance biosensors in drug discovery. *Pharm. Sci. Technol. Today* **3**, 310-317.
- Neiditch MB, Federle MJ, Pompeani AJ, Kelly RC, Swem DL, Jeffrey PD, Bassler BL, and Hughson FM. (2006) Ligand-induced asymmetry in histidine sensor kinase complex regulates quorum sensing. *Cell* **126**, 1095-1108.
- Nyberg S, Nordin H, Karlsson R, and Hämäläinen MD. (2002) Characterization of drug-plasma protein interactions using surface plasmon resonance. *Biacore publications*, Biacore Application Note 30, BR-9002-99.
- Owens JT, Miyake R, Murakami KS, Chmura AJ, Fujita N, Ishihama A, and Meares CF. (1998) Mapping the sigma70 subunit contact sites on Escherichia coli RNA polymerase with a sigma70-conjugated chemical protease. *Proc. Natl. Acad. Sci. USA* **95**, 6021-6026.
- Paget MS and Helmann JD. (2003) The  $\sigma^{70}$  family of sigma factors. *Genome Biol.* **4**, 203.

- Payne DJ, Gwynn MN, Holmes DJ, and Pompliano DL. (2007) Drugs for bad bugs: Confronting the challenges of antibacterial discovery. *Nat. Rev. Drug Discov.* **6**, 29-40.
- Peters JU. (2013) Polypharmacology – foe or friend? *J. Med. Chem.* **56**, 8955-8971.
- Piercenet.com (NHS and Sulfo-NHS), May 2014.
- Ramaswamy S and Musser J. (1998) Molecular genetic basis of antimicrobial agent resistance in *Mycobacterium tuberculosis*: 1998 update. *Tuberc. Lung Disease* **79**, 3-29.
- Rice LB. (2006) Antimicrobial resistance in Gram-positive bacteria. *Am. J. Med.* **119** (6 Suppl. 1), S11-S19.
- Rice LB. (2008) Federal funding for the study of antimicrobial resistance in nosocomial pathogens: no ESKAPE. *J. Infect. Dis.* **197**, 1079-1081.
- Rich RL and Myszka DG. (2000) Survey of the 1999 surface plasmon resonance biosensor literature. *J. Mol. Recognit.* **13**, 388-407.
- Ross W, Vrentas CE, Sanchez-Vazquez P, Gaal T, and Gourse RL. (2013) The magic spot: a ppGpp binding site on *E. coli* RNA polymerase responsible for regulation of transcription initiation. *Mol. Cell* **50**, 420-429.
- Saecker RM, Record Jr. MT, and deHaseth PL. (2011) Mechanism of bacterial transcription initiation: RNA polymerase – promoter binding, isomerization to initiation-competent open complexes, and initiation of RNA synthesis. *J. Mol. Biol.* **412**, 754-771.
- Sahner JH, Groh M, Negri M, Haupenthal J, and Hartmann RW. (2013) Novel small molecule inhibitors targeting the “switch region” bacterial RNAP: Structure-based optimization of a virtual screening hit. *Eur. J. Med. Chem.* **65**, 223-231.
- Sahner JH, Brengel C, Storz MP, Groh M, Plaza A, Müller R, and Hartmann RW. (2014) Combining in silico and biophysical methods for the development of *Pseudomonas aeruginosa* quorum sensing inhibitors: An alternative approach for structure-based drug design. *J. Med. Chem.* **56**, 8656-8664.
- Salomón RA and Farías RN. (1992) Microcin J25, a novel antimicrobial peptide produced by *Escherichia coli*. *J. Bacteriol.* **174**, 7428-7435.
- Schasfoort RBM and Tudos AJ. (2008) Handbook of Surface Plasmon Resonance. RCS Publishing. ISBN: 978-0-85404-267-8.
- Schwartz EC, Shekhtman A, Dutta K, Pratt MR, Cowburn D, Darst SA, and Muir TW. (2008) A full-length group 1 bacterial sigma factor adopts a compact structure incompatible with DNA binding. *Chem. Biol.* **15**, 1091-1103.
- Sergio S, Pirali G, White R, and Parenti F. (1975) Lipiarmycin, a new antibiotic from *Actinoplanes*. III. Mechanism of action. *J. Antibiot.* **7**, 543-549.

Sharp MM, Chan CL, Lu CZ, Marr MT, Nechaev S, Merritt EW, Severinov K, Roberts JW, and Gross CA. (1999) The interface of  $\sigma$  with core RNA polymerase is extensive, conserved, and functionally specialized. *Genes Dev.* **13**, 3015-3026.

Siegele DA, Hu JC, Walter WA, and Gross CA. (1989) Altered promoter recognition by mutant forms of the sigma 70 subunit of Escherichia coli RNA polymerase. *J. Mol. Biol.* **206**, 591-603.

Smagowicz WJ and Scheit KH. (1978) Primed abortive initiation of RNA synthesis by E. coli RNA polymerase on T7 DNA. Steady state kinetic studies. *Nucleic Acids Res.* **5**, 1919-1932.

Sonenshein AL, Alexander HB, Rothstein DM, and Fisher SH. (1977) Lipiarmycin-resistant ribonucleic acid polymerase mutants of Bacillus subtilis. *J. Bacteriol.* **132**, 73-79.

Srivastava A, Talaue M, Liu S, Degen D, Ebright RY, Sineva E, Chakraborty A, Druzhinin SY, Chatterjee S, Mukhopadhyay J, Ebright YW, Zozula A, Shen J, Sengupta S, Niedfeldt RR, Xin C, Kaneko T, Irschik H, Jansen R, Donadio S, Connell N, and Ebright RH. (2011) New target for inhibition of bacterial RNA polymerase: 'switch region'. *Curr. Opin. Microbiol.* **14**, 1-12.

Steiz TA and Steiz JA. (1993) A general two-metal-ion mechanism for catalytic RNA. *Proc. Natl. Acad. Sci. USA* **90**, 6498-6502.

Stenberg E, Persson BR, Roos HK, and Urbaniczky C. (1991) Quantitative determination of surface concentration of protein with surface plasmon resonance using radiolabeled proteins. *J. Colloid Interface Sci.* **143**, 513-526.

Swanson RN, Hardy DJ, Shipkowitz NL, Hanson CW, Ramer NC, Fernandes PB, and Clement JJ. (1991) In vitro and in vivo evaluation of tiamcemicins B and C against Clostridium difficile. *Antimicrob. Agents Chemother.* **35**, 1108-1111.

Talbot GH, Bradley J, Edwards JE, Gilbert D, Scheld M, and Bartlett JG. (2006) Bad bugs need drugs: An update on the development pipeline from the antimicrobial availability task force of the infectious diseases society of America. *Clin. Infect. Dis.* **42**, 657-668.

Temiaikov D, Zenkin N, Vassilyeva MN, Perederina A, Tahirov TH, Kashkina E, Savkina M, Zorov S, Nikiforov V, Igarashi N, Matsugaki N, Wakatsuki S, Severinov K, and Vassilyev DG. (2005) Structural basis of transcription inhibition by antibiotic streptolydigin. *Mol. Cell.* **19**, 655-666.

Thomson JD and Bonomo RA. (2005) The threat of antibiotic resistance in Gram-negative pathogenic bacteria:  $\beta$ -lactams in peril! *Curr. Opin. Microbiol.* **8**, 518-524.

Touloukhonov I and Landick R. (2006) The role of the lid element in transcription by E. coli RNA polymerase. *J. Mol. Biol.* **361**, 644-658.

Tracy RL and Stern DB. (1995) Mitochondrial transcription initiation: promoter structures and RNA polymerases. *Curr. Genet.* **28**, 205-216.

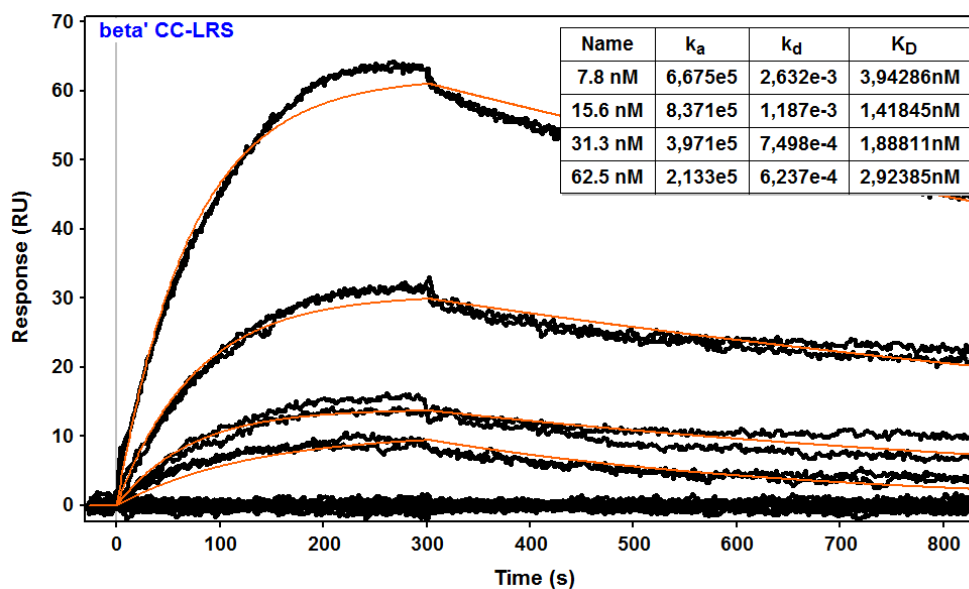


- Travers AA and Burgess RR. (1969) Cyclic re-use of the RNA polymerase sigma factor. *Nature* **222**, 537-540.
- Vassilyev DG, Sekine S, Laptenko O, Lee J, Vassilyeva MN, Borukhov S, and Yokoyama S. (2002) Crystal structure of a bacterial RNA polymerase holoenzyme at 2.6 Å resolution. *Nature* **417**, 712-719.
- Villain-Guillot P, Bastide L, Gualtieri M, and Leonetti JP. (2007a) Progress in targeting bacterial transcription. *Drug Discov. Today* **12**, 200-208.
- Villain-Guillot P, Gualtieri M, Bastide L, Roquet F, Martinez J, Amblard M, Pugniere M, and Leonetti JP. (2007b) Structure-activity relationships of phenyl-furanyl-rhodanines as inhibitors of RNA polymerase with antibacterial activity on biofilms. *J. Med. Chem.* **50**, 4195-4204.
- Waldburger C, Gardella T, Wong R, and Susskind MM. (1990) Changes in conserved region 2 of Escherichia coli sigma 70 affecting promoter recognition. *J. Mol. Biol.* **215**, 267-276.
- WHO.int (Antimicrobial resistance; Fact sheet N° 194) May 2014
- Williams C and Addona TA. (2000) The integration of SPR biosensors with mass spectrometry: possible applications for proteome analysis. *Trends Biotechnol.* **18**, 45-48.
- Xu M, Zhou YN, Goldstein BP, and Jin DJ. (2005) Cross-resistance of Escherichia coli RNA polymerases conferring rifampin resistance to different antibiotics. *J. Bacteriol.* **187**, 2783-2792.
- Zervosen A, Wei-Ping L, Chen Z, White RE, Demuth TM, and Frere JM. (2004) Interactions between penicillin-binding proteins (PBPs) and two novel classes of PBP inhibitors, arylalkylidene rhodanines and arylalkylidene iminothiazolidin-4-ones. *Antimicrob. Agents Chemother.* **48**, 961-969.
- Zhang Y, Degen D, Ho MX, Sineva E, Ebright KY, Ebright YW, Mekler V, Vahedian-Movahed H, Feng Y, Yin R, Tuske S, Irschik H, Jansen R, Maffioli S, Donadio S, Arnold E, and Ebright RH. (2014) GE23077 binds to the RNA polymerase 'i' and 'i+1' sites and prevents the binding of initiating nucleotides. *eLife* 3:e02450.
- Zuo Y, Wang Y, and Steitz TA. (2013) The mechanism of E. coli RNA polymerase regulation by ppGpp is suggested by the structure of their complex. *Mol. Cell* **50**, 430-436.

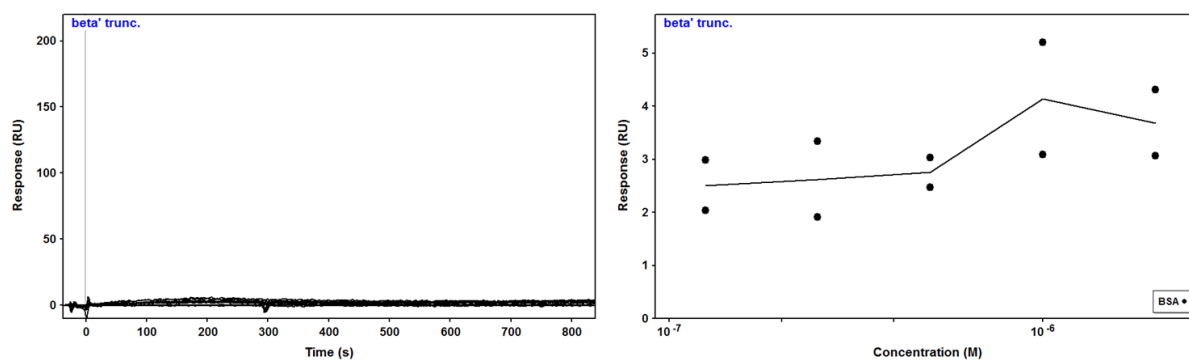
## 6 Supporting information

### 6.1 Supporting information to Publication I

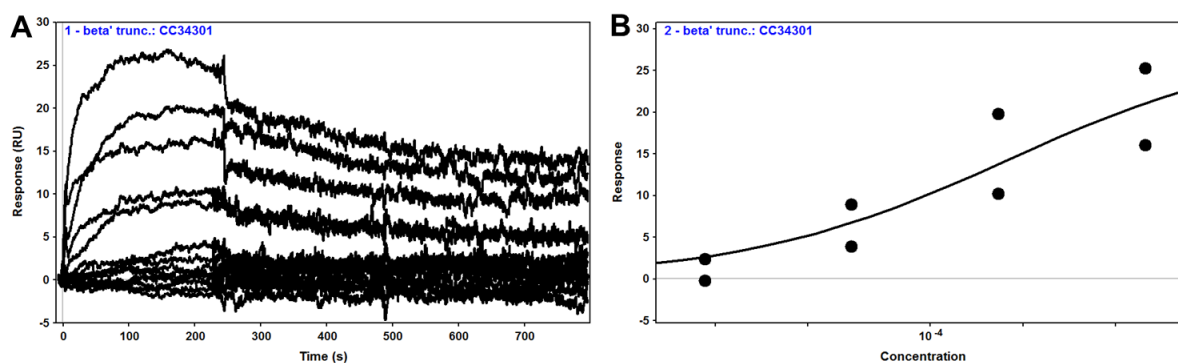
#### Supporting figures



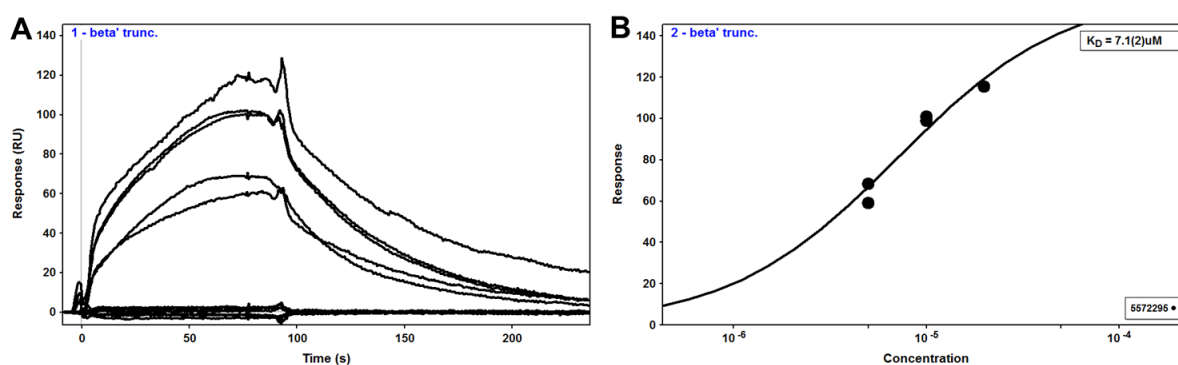
**Figure S1.** Kinetic evaluation of  $\sigma^{70}$  binding to  $\beta'$  CC-LRS. Curves were fitted individually to a 1:1 binding model. Higher concentrations were excluded since  $\sigma^{70}$  tends to aggregate. Kinetic rate constants are given in the box.



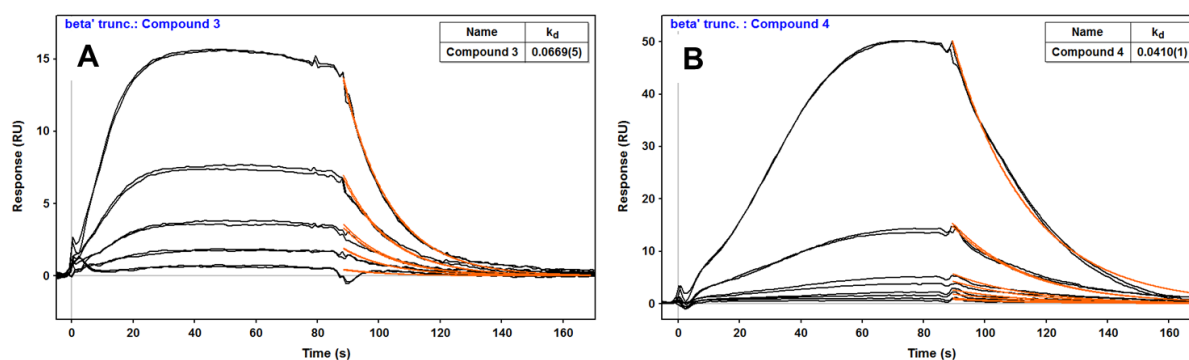
**Figure S2.** BSA (125-1,000 nM) was flowed over the  $\beta'$  CC-LRS sensor surface. No binding detectable.



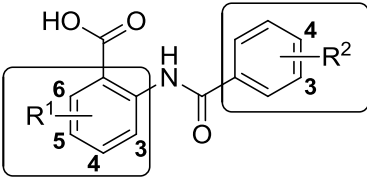
**Figure S3.** Maybridge fragment CC34301 binds dose-dependently to  $\beta'$  CC-LRS. However, double values are bad due to unsuitable regeneration with 5 mM hydrochloric acid. **A** Dose-response curves. **B** Equilibrium response.



**Figure S4.** Interchim compound 5572295 binds dose-dependently to  $\beta'$  CC-LRS. Atypical association phase for the highest concentration (20  $\mu\text{M}$ ) due to precipitation. Hence,  $K_D$  is not reliable. **A** Dose-response curves. **B** Equilibrium response.



**Figure S5.** Compounds **3** (A) and **4** (B) binding to the  $\beta'$  CC-LRS subunit. Analytes were injected to sensor surface in 6.25-100  $\mu\text{M}$ .

		
Compound	R <sup>1</sup>	R <sup>2</sup>
<b>1</b>	4-Cl	4-Ph
<b>2</b>	5-Ph	3-OPh
<b>5</b>	4-F	4-Ph
<b>6</b>	H	3-OPh, 4-Ph
<b>7</b>	4-Br	4-Ph
<b>8</b>	5-CF <sub>3</sub>	4-Ph
<b>9</b>	5-Me	4-Ph
<b>10</b>	4-Cl	3-OPh, 4-Ph
<b>11</b>	6-OH	4-Ph

**Figure S6.** Structures of the 2-benzamidobenzoic acid compounds, re-numbered from [35].

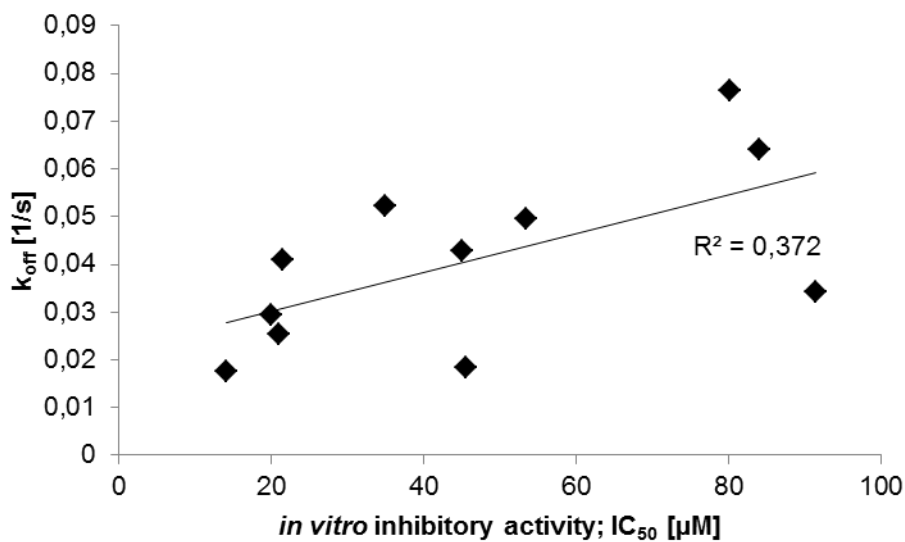


**Figure S7.** No linear correlation of *in vitro* transcription activity (IC<sub>50</sub>) and the dissociation rate constant (k<sub>off</sub>) for ureidothiophene carboxylic acid compounds.

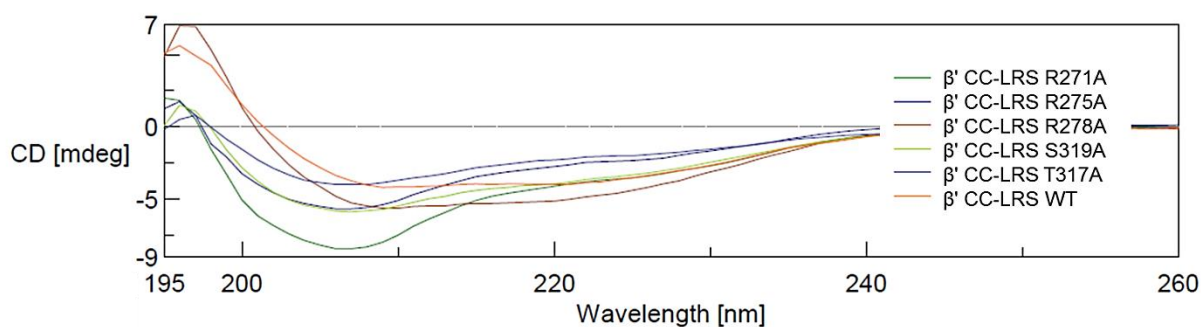


**Figure S8.** CD spectra of  $\beta'$  CC-LRS wild-type and mutants show similar patterns with  $\alpha$ -helical and random coil portions.

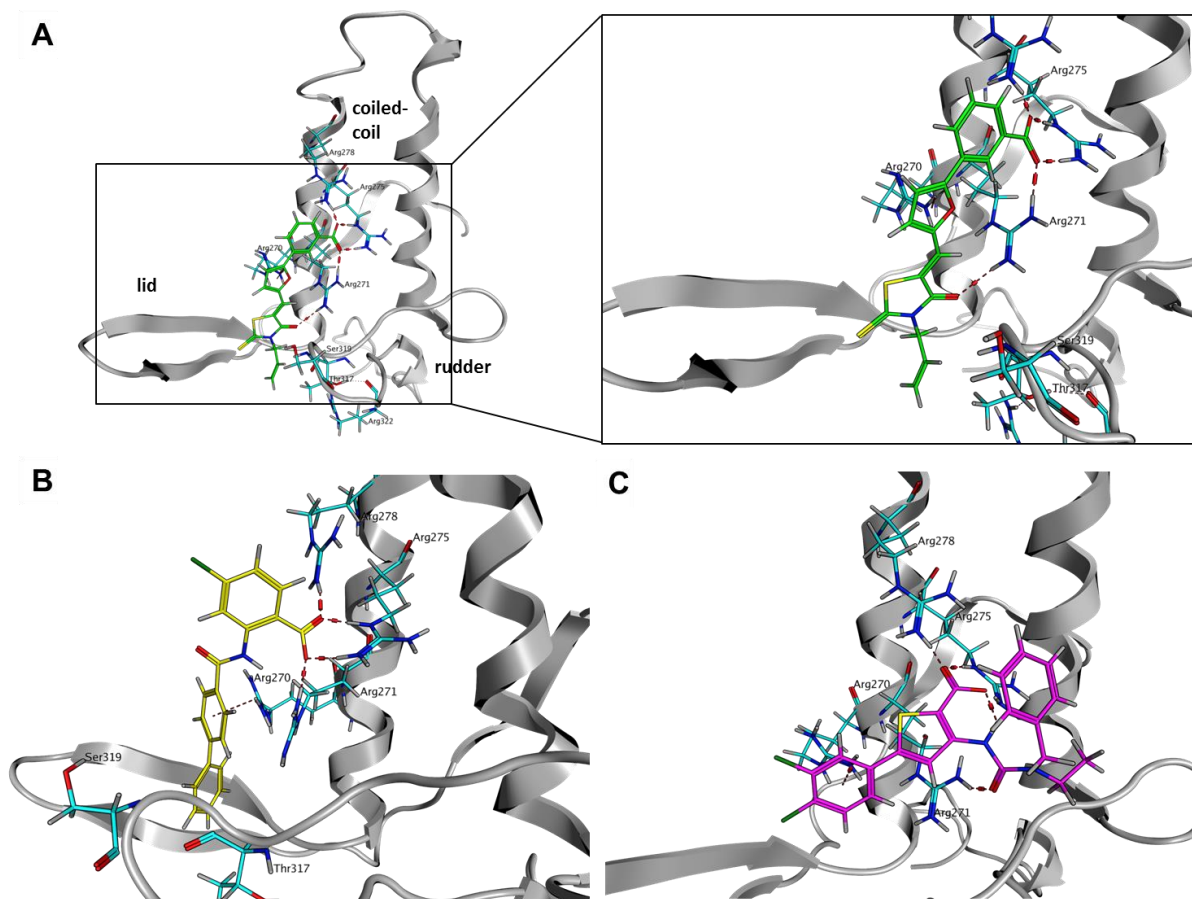


**Figure S9.** Visualization of possible binding poses for SB2 (A), Compound 1 (B), and Compound 4 (C) binding to the  $\beta'$  CC-LRS of *T. thermophilus* (e.g. PDB 3EQL). For comparison with the mutant studies, *E. coli* numbering was used.

## 6.2 Supporting information to Publication II

### Supplemental methods

**Molecular dynamics (MD) simulations.** All atomic coordinates were taken from our *E. coli* holo RNAP homology model (*Ec*RNAP) (1). Peptides P01–P16 as well as the P07 mutant derivatives D403A, G411Q, and G411R were extracted from the holo complex preserving their secondary structure. For C01 a linear unfolded structure was used as starting point. The four complexes with P07 (and with the three P07 mutants) and the  $\beta'$  truncated segment ( $\beta'_{\text{trunc}}$ ; Gln94–Arg346) (P07- $\beta'_{\text{trunc}}$ ) were extracted as well from *Ec*RNAP. The protonation states were determined at pH 7.4 with the Protonate3D module of MOE. The solvated systems were set up using the AMBER11 suite program xLeap (2) with AMBER99SB force field (3). For the four P07- $\beta'_{\text{trunc}}$  constructs a 10 Å pad of TIP3P waters was added to solvate each system as octahedral box. Neutralizing counter ions were added to each system. Simulations: For the peptides P01–16, C01 and their mutants generalized Born implicit solvent simulations of 100-250 ns were performed using the parallelized sander module of AMBER 11 on a 32 CPU opteron linux\_x86\_64 system. Minimization and equilibration phases were performed. The systems were heated to 325 K increasing the temperature of 50 K after 20, 40, 60, 80, 100, 120 and 200 ps. Production runs were made in the NPT ensemble at 325 K. All MD simulations were carried out using the pmemd.cuda module of AMBER11 using a GeForce GTX 280 NVIDIA graphic card. Minimization and equilibration phases were performed with backbone atoms restricted by harmonic restraints, which were progressively reduced (from 5 kcal mol<sup>-1</sup> Å<sup>-2</sup> to 4, 3, 2 1, and 0 kcal mol<sup>-1</sup>). The systems were heated to 300 K in the canonical NVT ensemble using a Langevin thermostat, with collision frequency of 3.0 ps<sup>-1</sup> Å<sup>-2</sup>, and increasing temperature of 50 K after 60, 120, 180, 240, and 300 ps. Production runs were made in the NPT ensemble at 300 K (temperature was controlled with Langevin thermostat with a 1.0 ps<sup>-1</sup> collision frequency). The time step used for all stages was 2 fs and with hydrogen atoms constrained using the SHAKE algorithm (4). Long-range electrostatics were included on every step using the Particle Mesh Ewald algorithm with a 4th order B-spline interpolation (5). Trajectory analysis and secondary structure determination were performed using the ptraj tool of AmberTools 1.5 (2) and VMD 1.9.1 (6).

**MM-GBSA calculations.** Binding energies  $\Delta G$  for P07 and the three mutants were estimated using MM-GBSA methods (Molecular Mechanic – General Born Surface Area) (7) using snapshots of the simulations sampled every 20 ps.

**HPLC-based abortive transcription assay.** All chemicals were purchased from Sigma Aldrich or from other suppliers as stated in the sample preparation section. All HPLC solvents were of chromatographic grade, Quickszint Flow 302 LSC Cocktail was used for scintillation. Prior to every experimental sequence the solvent channels of the HPLC were extensively flushed with RNase free solvents and the injection needle and the injection port were treated with RNase inhibitor (RNase AWAY wipes, MBP). The experiment was performed using an Agilent 1200 HPLC system consisting of a binary pump, an autosampler, a multi-wavelength detector (MWD; **Agilent Technologies, Inc.**) and a RAMONA® scintillation radio detector (Raytest GmbH). ChemStation® software was used for control and report. The injection volume was 25  $\mu\text{l}$ . A RP C18 NUCLEODUR® 100-3 (125  $\times$  30 mm) column (Macherey-Nagel GmbH) was used as stationary phase. The solvent system consisted of 100 mM ammonium acetate buffer, containing 0.1 % (v/v) trifluoroacetic acid (A) and 0.1 % (v/v) formic acid in acetonitrile (B). HPLC-Method: Flow rate 1.2 ml min<sup>-1</sup>; gradient run of initial 0 % (v/v) of B in A. In 3.5 min the ratio was changed to 50 % (v/v) of B followed by a rapid increase of 100 % (v/v) of B at 3.51 min, keeping B at 100 % (v/v) for 0.5 min. The scintillation pump was set to a flow of 2.0 ml min<sup>-1</sup>. The MWD was used for method development with the unlabeled substrate at higher concentration. Quantification was performed by automatic integration of the peaks in the radioactive count chromatogram.

### Supplemental figures

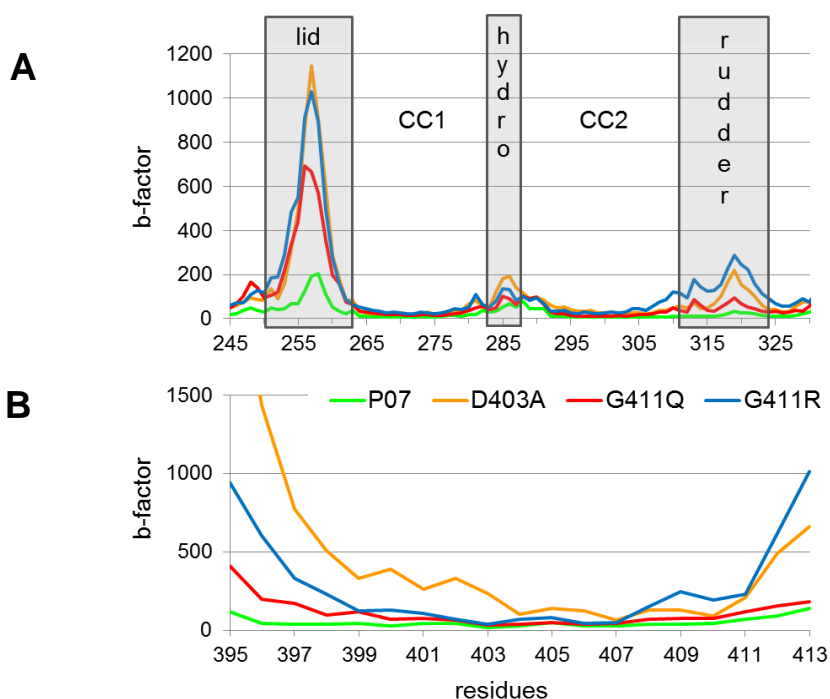


**Figure SI1.** Fluctuations per residue for the MD simulations P07- $\beta'$ <sub>trunc</sub> (green), D403A- $\beta'$ <sub>trunc</sub> (yellow), G411Q- $\beta'$ <sub>trunc</sub> (red), and G411R- $\beta'$ <sub>trunc</sub> (blue). In (A) the b-factor for the  $\beta'$ CC-LRS region of the  $\beta'$ <sub>trunc</sub> segment is shown, while in (B) the b-factors for the peptide amino acids are shown.

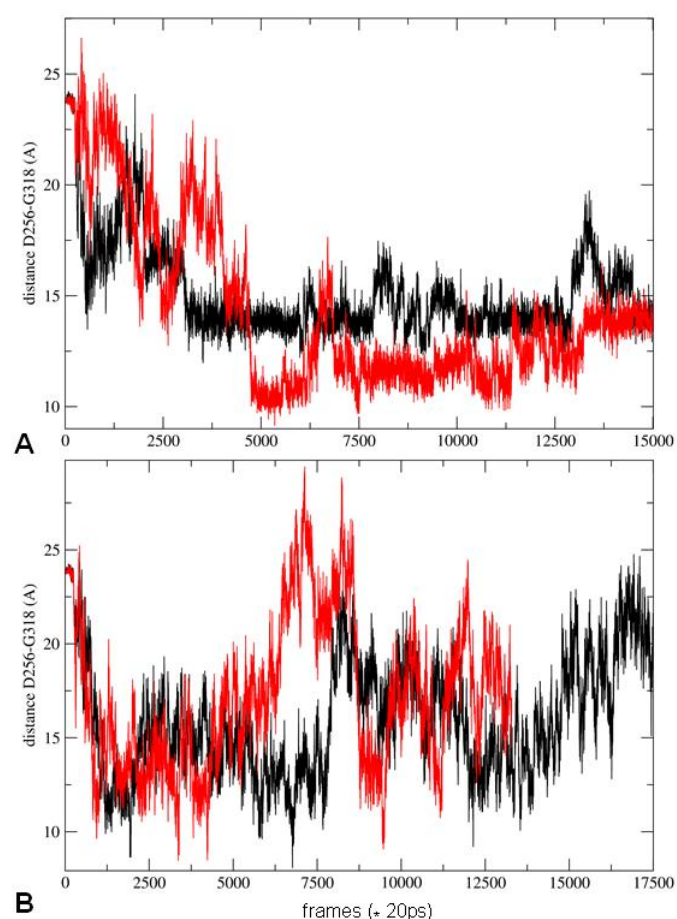


**Figure SI2.** Flexibility of the LRS depends on the interactions with the N-terminal loop of peptides P07, D403A, G411Q, and G411R. The distance between the C $\alpha$  of Asp256 (lid) and of Gly318 (rudder) is used as a measure of the open/closed state of the “lid-rudder-system”: (A) it closes in the P07- $\beta'$ <sub>trunc</sub> (black) and in the G411Q-  $\beta'$ <sub>trunc</sub> (red) MD simulations; (B) it fluctuates massively from open-to-closed-to-open in the D403A- $\beta'$ <sub>trunc</sub> (black) and in the G411R-  $\beta'$ <sub>trunc</sub> (red) MD simulations, where no interactions with the LRS take place.



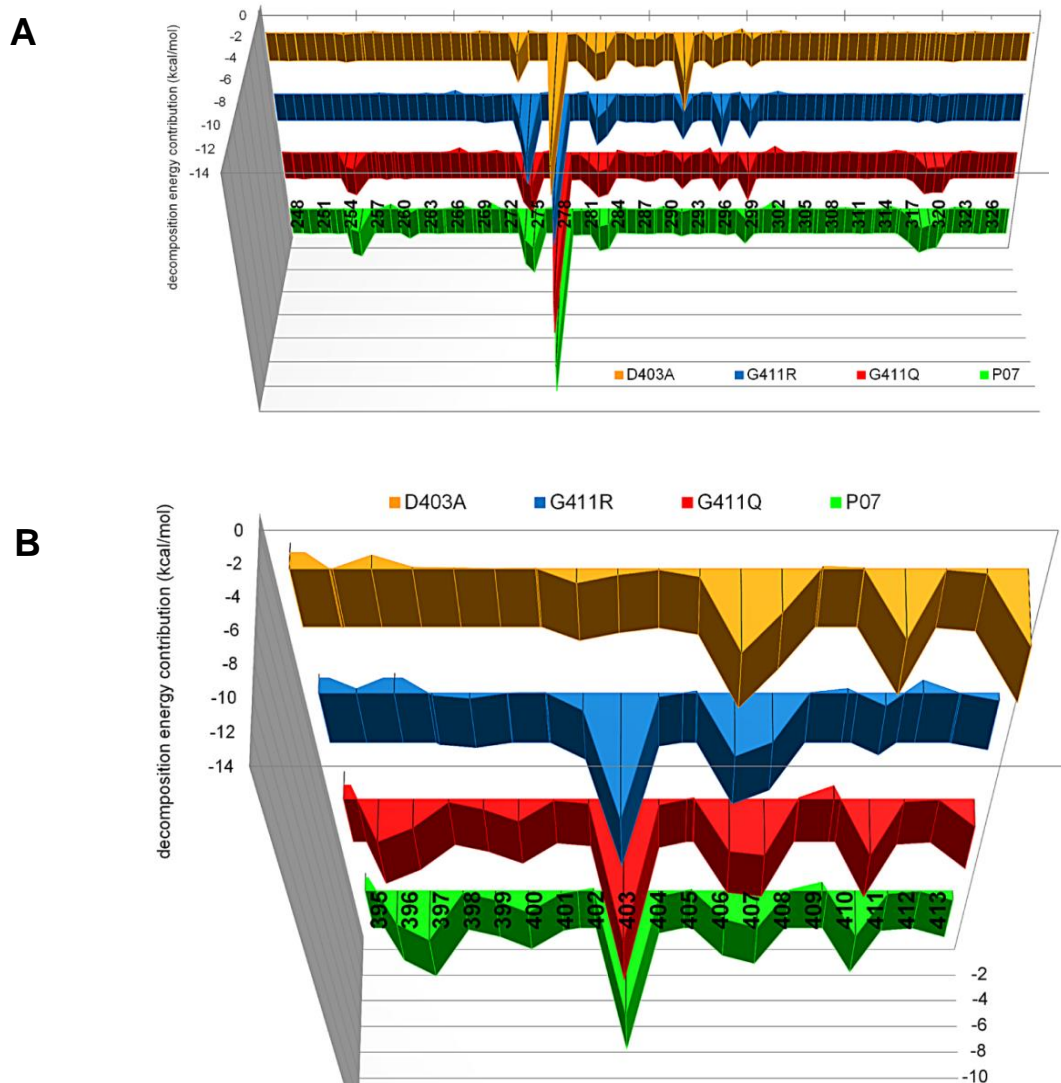


**Figure SI3.** Binding energy contributions per residue estimated by MM-GBSA methods for the MD simulations of the four P07- $\beta'$ <sub>trunc</sub> complexes (P07, D403A, G411Q, and G411R). In (A) the energy contributions per residue for the lid (250-263)- $\beta'$  coiled-coil (CC1: 264-281; hydrophobic turn: 282-287; CC2: 288-309)-rudder (310-326) segment are reported, whereas in (B) the energy contributions (kcal mol<sup>-1</sup>) for the peptide amino acids of the four complexes D403A (orange), G411R (blue), G411Q (red), and P07 (green) are compared.

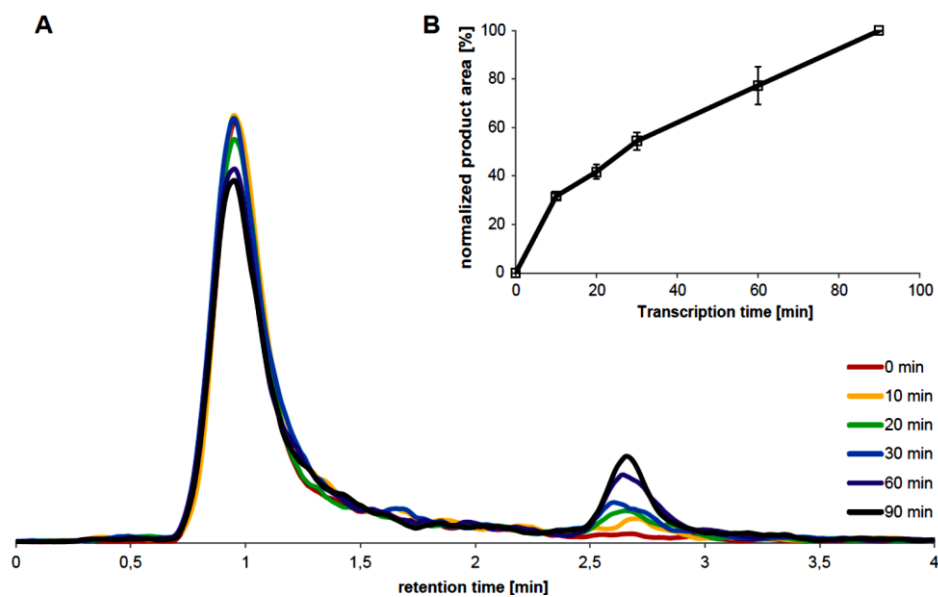


**Figure S14.** (A) Overlay of chromatograms displaying separated peaks of substrate  $^3\text{H}$ -CTP and product  $\text{ApUp}^3\text{H-C}$  for method validation; (B) Time-dependent product formation, amount of 90 min transcription sample was set to 100 % and other transcription sample yields were calculated accordingly. Standard deviations from three independent experiments are indicated by black bars.

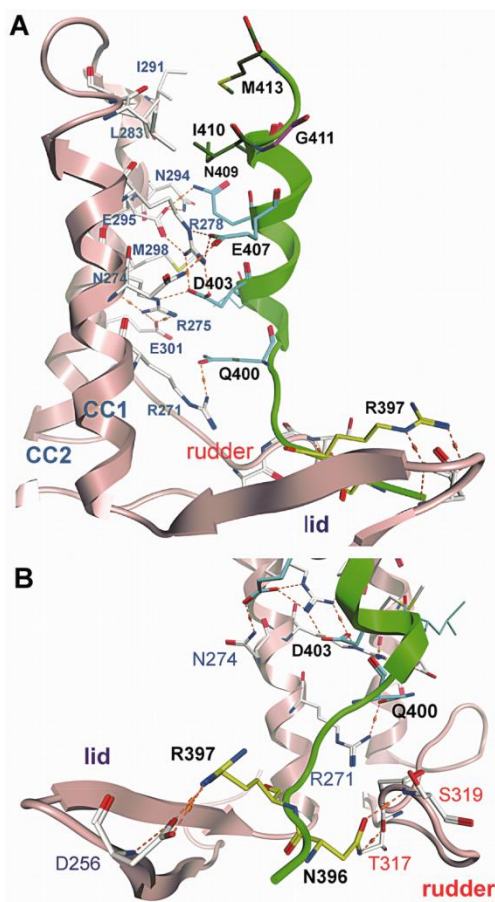


**Figure S15.** Binding of peptide P07 to the  $\beta'_{\text{trunc}}$  subunit. (A) Detailed side-view of the interface residues of P07 (green cartoon) and  $\beta'_{\text{CC}}$  (pink cartoon, residues as white sticks). Residues of P07 that have been varied are rendered as sticks and color-coded according to their position in P07: -T<sub>395</sub>NRG<sub>399</sub>- loop – yellow, helix<sub>2,2</sub>-core – cyan, hydrophobic C<sub>term</sub> – green). Hydrogen bonds are shown by orange dotted lines. (B) Zoomed-view of the lid-rudder-system with the N-terminal residues of P07.

### Supplemental schemes

	aa sequence	Inhibition of RNAP holo (IC <sub>50</sub> in $\mu\text{M}$ )
C01	LATKALYIERLASATA	32.2
C01-K4A	LATAALYIERLASATA	12.5
C01-Y7A	LATKALAIERLASATA	16.1
C01-E9A	LATKALYIARLASATA	>50
C01-E9P	LATKALYIPRLASATA	>50
C01-R10A	LATKALYIEALASATA	14.6

**Scheme S11.** Modifications of control peptide C01. List and sequences of peptides that were modified based on peptide C01. IC<sub>50</sub> values are given. In black: unpolar/hydrophobic aa; in green: polar/neutral aa; in blue: basic aa; in red: acidic aa; underlined: substituted aa. The mutants K4A, Y7A and R10A led to increased activity suggesting that making C01 more hydrophobic leads to favourable interactions with the enzyme. On the other hand the substitution of E9 to A or P led to a drastic reduction of activity. Thus we assume that this glutamic acid is important for the RNAP inhibitory activity of C01.

pept	$\beta'_{\text{trunc}}$		P07	D403A	G411Q	G411R
T395	D256	lid	39.71%		18.22%	
R397	D256	lid	62.06%		31.71%	
Q400	R271	CC1	15.88%			
Q400	R275	CC1			11.34%	
D403	R275	CC1	53.91%		53.53%	85.29%
D403	R278	CC1	92.78%		72.28%	61.69%
E407	N274	CC1	65.84%		56.30%	44.09%
E407	R278	CC1	57.93%	64.16%	63.50%	60.96%
Q411	R281	CC1			15%	
M413	N274	CC1		47.05%		
M413	R278	CC1		35.77%		
Q406	I291	hydro		67.77%		29.17%
N409	A286	hydro		16.49%		
Q406	N294	CC2		30.80%	12.17%	19.47%
Q406	E295	CC2	52.82%	75.91%	67.46%	81.05%
Q400	E301	CC2			15.18%	

Q400	I316	rudder	16.26%			
N396	T317	rudder	59.24%		54.52%	
N396	S319	rudder	64.57%		56.01%	

**Scheme SI2.** Hydrogen bonds formed between the peptides P07, D403A, G411Q, and G411R and the truncated  $\beta'$  segment ( $\beta'_{\text{trunc}}$ ). Their occurrence along the trajectory of the P07- $\beta'_{\text{trunc}}$  complexes is calculated with the plugin of VMD (6) and expressed in % (given if >10 %; max distance 3.5 Å, max angle difference from optimum 25 degrees). The order of the peptide residues reflects their interactions with lid, CC1 (first helix of the  $\beta'$ CC), hydro (hydrophobic patch at the tip of  $\beta'$ CC), CC2 (second helix of the  $\beta'$ CC), and rudder of the  $\beta'_{\text{trunc}}$ .

## Supplemental references

1. Negri, M., Hauptenthal, J., and Hartmann, R.-W. "From-macro-to-micro": dissecting bacterial RNA polymerase into druggable sub-domains. (Helmholtz Institute for Pharmaceutical Research Saarland, Department of Drug Design and Optimization, Saarbrücken, Germany). Unpublished data.
2. Case, D.-A., Darden, T.-A., Cheatham, T.-E. III., Simmerling, C.-L., Wang, J., Duke, R.-E., Luo, R., Walker, R.-C., Zhang, W., Merz, K.-M., Roberts, B.-P., Wang, B., Hayik, S., Roitberg, A., Seabra, G., Kolossváry, I., Wong, K.-F., Paesani, F., Vanicek, J., Liu, J., Wu, X., Brozell, S.-R., Steinbrecher, T., Gohlke, H., Cai, Q., Ye, X., Wang, J., Hsieh, M.-J., Cui, G., Roe, D.-R., Mathews, D.-H., Seetin, M.-G., Sagui, C., Babin, V., Luchko, T., Gusarov, S., Kovalenko, A., and Kollman, P.-A. (2010) AMBER 11, University of California, San Francisco.
3. Hornak, V., Abel, R., Okur, A., Strockbine, B., Roitberg, A., and Simmerling, C.-L. (2006) Comparison of multiple Amber force fields and development of improved protein backbone parameters. *Proteins* 65, 712–725.
4. Andersen, H.-C. (1983) Rattle: a 'velocity' version of the Shake algorithm for molecular dynamics calculations. *J. Comput. Phys.* 52, 24–34.
5. Darden, T., York, D., and Pedersen, L. (1993) Particle mesh ewald: an N-log(N) method for Ewald sums in large systems. *J. Chem. Phys.* 98, 10089–10092.
6. Humphrey, W., Dalke, A., and Schulten, K. (1996) "VMD - Visual Molecular Dynamics", *J. Molec. Graphics* 14, 33–38.
7. Kollman, P.-A., Massova, I., Reyes, C., Kuhn, B., Huo, S., Chong, L., Lee, M., Lee, T., Duan, Y., Wang, W., Donini, O., Cieplak, P., Srinivasan, J., Case, D.-A., and Cheatham, T.-E. III. (2000) Calculating structures and free energies of complex molecules: combining molecular mechanics and continuum models. *Acc. Chem. Res.* 33, 889–897.

## 6.3 Supporting information to Publication III

### General directions

Chemical names follow IUPAC nomenclature. Starting materials were purchased from Sigma-Aldrich, Acros, Maybridge, Combi Blocks, Fluka, ABCR, Alfa Aesar, Apollo and were used without purification.

Column chromatography (CC) was performed on silica gel (70–200  $\mu\text{m}$ ), preparative thin layer chromatography (TLC) on 1 mm SIL G-100 UV<sub>254</sub> glass plates (Macherey-Nagel), and reaction progress was monitored by TLC on Alugram SIL G UV<sub>254</sub> (Macherey-Nagel).

$^1\text{H}$  NMR and  $^{13}\text{C}$  NMR spectra were recorded on a Bruker AM500 spectrometer (500 MHz and 125 MHz) at 300 K in  $\text{CDCl}_3$  or  $\text{CD}_3\text{SOCD}_3$ . Chemicals shifts are reported in  $\delta$  values (ppm), the hydrogenated residues of deuterated solvent were used as internal standard ( $\text{CDCl}_3$ :  $\delta = 7.27$  ppm in  $^1\text{H}$  NMR and  $\delta = 77.0$  ppm in  $^{13}\text{C}$  NMR,  $\text{DMSO}-d_6$ :  $\delta = 2.50$  ppm in  $^1\text{H}$  NMR and  $\delta = 39.5$  ppm in  $^{13}\text{C}$  NMR). Signals are described as s, d, t, dd, ddd, dt and m for singlet, doublet, triplet, doublet of doublet, doublet of doublet of doublet, doublet of triplet and multiplet, respectively. Coupling constants ( $J$ ) are given in Hertz (Hz).

The reported yields are the isolated yields of purified material and are not optimized.

Purity of compounds **1** to **34** was determined using LC/MS as follows:

The SpectraSystems®-LC-system consisted of a pump, an autosampler, and a UV detector. Mass spectrometry was performed on a MSQ® electro spray mass spectrometer (Thermo Fisher, Dreieich, Germany). The system was operated by the standard software Xcalibur®.

A RP C18 NUCLEODUR® 100-5 (125 x 3 mm) column (Macherey-Nagel GmbH, Dueren, Germany) was used as stationary phase. All solvents were HPLC grade.

Solvent system:

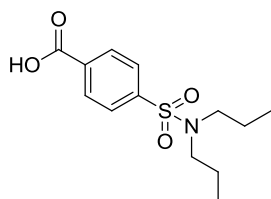
In a gradient run the percentage of acetonitrile (containing 0,1 % trifluoro-acetic acid) in 0,1 % trifluoro-acetic acid was increased from an initial concentration of 0 % at 0 min to 100 % at 15 min and kept at 100 % for 5 min.

The injection volume was 10  $\mu\text{L}$  and flow rate was set to 800  $\mu\text{L}/\text{min}$ . MS analysis was carried out at a spray voltage of 3800 V, a capillary temperature of 350  $^\circ\text{C}$  and a source CID

of 10 V. Spectra were acquired in positive mode from 100 to 1000 m/z and at 254 nm for the UV trace.

Melting points were determined on a Stuart Scientific melting point apparatus SMP3 and are uncorrected.

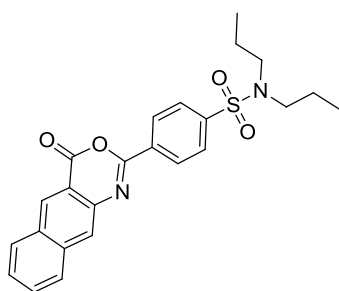
### Experimental and spectroscopic data of all compounds



**4-(N,N-dipropylsulfamoyl)benzoic acid (Vb).** To a solution of 4-(chlorosulfonyl)benzoic acid (1 equiv) in anhydrous  $\text{CH}_2\text{Cl}_2$  at  $0^\circ\text{C}$  dipropylamine (3 equiv) was added slowly by means of a syringe. The reaction mixture was stirred at room temperature for 18 h followed by extraction with 1N HCl. The organic layer was washed with  $\text{H}_2\text{O}$  and dried over  $\text{MgSO}_4$ . Evaporation of the solvent provided the title compound; yield: 99 %.  $^1\text{H}$  NMR (500 MHz,  $\text{CD}_3\text{COCD}_3$ )  $\delta$  = 8.24–8.19 (m, 2 H), 7.99–7.94 (m, 2 H), 3.17–3.12 (m, 4 H), 1.61–1.51 (m, 4 H), 0.86 (t,  $J$  = 7.4 Hz, 6 H) ppm.

$^{13}\text{C}$  NMR (125 MHz,  $\text{CD}_3\text{COCD}_3$ )  $\delta$  = 166.6, 145.3, 134.9, 131.3, 128.1, 50.9, 22.8, 11.4 ppm.

LC/MS:  $m/z$  = 286  $[\text{M} + \text{H}^+]$ ;  $t_{\text{R}}$  = 11.58 min; 94.8 % pure (UV).

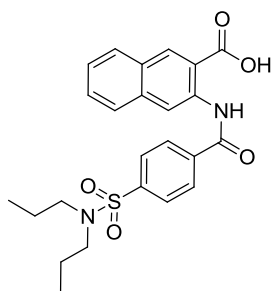


**4-(4-oxo-4H-naphtho[2,3-d][1,3]oxazin-2-yl)-N,N-dipropylbenzenesulfonamide (Va).** 4-(N,N-dipropylsulfamoyl)benzoic acid (**Vb**, 1.5 equiv) was converted to the corresponding

benzoyl chloride via reaction with thionyl chloride (3.75 equiv) in  $\text{CH}_2\text{Cl}_2$  in the presence of catalytic amounts of dimethylformamide (4 h reflux). After evaporation of the solvent the resulting benzoyl chloride and 3-amino-2-naphthoic acid (1 equiv) were suspended in toluene and the mixture was refluxed for 18 h. The product was purified by CC (*n*-hexane/EtOAc 8:2); yield: 28 %.  $^1\text{H}$  NMR (500 MHz,  $\text{CDCl}_3$ )  $\delta$  = 8.89 (s, 1 H), 8.49–8.44 (m, 2 H), 8.19 (s, 1 H), 8.09–8.00 (m, 2 H), 7.99–7.94 (m, 2 H), 7.74–7.69 (m, 1 H), 7.66–7.60 (m, 1 H), 3.19–3.12 (m, 4 H), 1.61–1.55 (m, 4 H), 0.90 (t,  $J$  = 7.4 Hz, 6 H,  $\text{CH}_3$ ) ppm.

$^{13}\text{C}$  NMR (125 MHz,  $\text{CDCl}_3$ )  $\delta$  = 159.4, 153.8, 143.6, 140.8, 137.6, 133.9, 132.4, 131.4, 129.9, 129.7, 128.7, 128.3, 127.5, 127.3, 125.8, 115.4, 49.9, 21.9, 11.2 ppm.

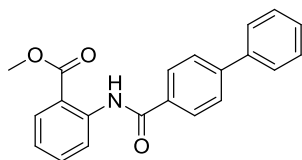
LC/MS:  $m/z$  = 437 [ $\text{M} + \text{H}^+$ ], 478 [ $\text{M}^+ + \text{CH}_3\text{CN}$ ];  $t_{\text{R}}$  = 17.57 min; 98.0 % pure (UV).



**3-(4-(N,N-dipropylsulfamoyl)benzamido)-2-naphthoic acid<sup>1</sup> (V).** 4-(4-oxo-4H-naphtho[2,3-d][1,3]oxazin-2-yl)-N,N-dipropylbenzenesulfonamide (**Va**) was dissolved in a mixture of THF/MeOH (2:1) and hydrolyzed by an aqueous solution containing 1 mol/L LiOH at room temperature (18 h). The mixture was acidified by the addition of 1 M HCl, filtered and the precipitate was successively washed with 1 M HCl. The product was purified by preparative TLC ( $\text{CH}_2\text{Cl}_2/\text{MeOH}$  9:1); yield: 24 %.  $^1\text{H}$  NMR (500 MHz,  $\text{CD}_3\text{SOCD}_3$ )  $\delta$  = 12.63 (br. s., 1 H, NH), 9.09 (s, 1 H), 8.76 (s, 1 H), 8.21–8.14 (m, 2 H), 8.06 (d,  $J$  = 8.2 Hz, 1 H), 8.04–7.99 (m, 2 H), 7.94 (d,  $J$  = 8.2 Hz, 1 H), 7.68–7.59 (m, 1 H), 7.56–7.47 (m, 1 H), 3.07 (t,  $J$  = 7.6 Hz, 4 H), 1.55–1.43 (m, 4 H), 0.82 (t,  $J$  = 7.4 Hz, 6 H,  $\text{CH}_3$ ) ppm.

$^{13}\text{C}$  NMR (125 MHz,  $\text{CD}_3\text{SOCD}_3$ )  $\delta$  = 169.9, 163.5, 142.4, 138.2, 136.1, 135.4, 133.2, 129.2, 129.1, 128.6, 128.1, 127.5, 127.3, 125.8, 118.7, 117.0, 49.7, 21.7, 11.0 ppm.

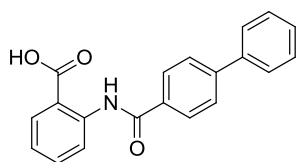
LC/MS:  $m/z$  = 455 [ $\text{M} + \text{H}^+$ ];  $t_{\text{R}}$  = 15.80 min; 99.0 % pure (UV).



**methyl 2-([1,1'-biphenyl]-4-ylcarboxamido)benzoate (1a)** was prepared according to method BIII. For purification the solvent was evaporated and the remaining solid was suspended in MeOH. After filtration the precipitate was washed with MeOH to provide the pure compound; yield: 58 %.  $^1\text{H}$  NMR (500 MHz,  $\text{CDCl}_3$ )  $\delta$  = 12.11 (br. s, 1 H, NH), 8.98 (dd,  $J$  = 8.5, 0.9 Hz, 1 H), 8.16–8.13 (m, 2 H), 8.11 (dd,  $J$  = 8.2, 1.6 Hz, 1 H), 7.78–7.75 (m, 2 H), 7.68–7.61 (m, 3 H), 7.51–7.47 (m, 2 H), 7.45–7.39 (m, 1 H), 7.18–7.12 (m, 1 H), 3.99 (s, 3 H,  $\text{OCH}_3$ ) ppm.

$^{13}\text{C}$  NMR (125 MHz,  $\text{CDCl}_3$ )  $\delta$  = 169.1, 165.4, 144.7, 141.9, 140.0, 134.9, 133.6, 131.0, 128.9, 128.0, 127.9, 127.5, 127.2, 122.6, 120.5, 115.1, 52.5 ( $\text{OCH}_3$ ) ppm.

LC/MS:  $m/z$  = 332 [ $\text{M} + \text{H}^+$ ], 373 [ $\text{M} + \text{H}^+ \text{CH}_3\text{CN}$ ], 663 [ $2\text{M} + \text{H}^+$ ];  $t_{\text{R}}$  = 14.92 min; 100.0 % pure (UV).

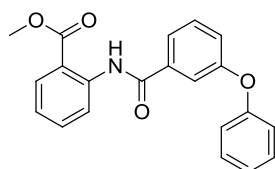


**2-([1,1'-biphenyl]-4-ylcarboxamido)benzoic acid<sup>2</sup> (1)** was prepared according to method C. Sufficient purity was achieved without further purification; yield: 74 %. Mp: 190 °C (decomposition).  $^1\text{H}$  NMR (500 MHz,  $\text{DMSO}-d_6$ )  $\delta$  = 12.26 (br. s, 1 H, NH), 8.74 (dd,  $J$  = 8.5, 0.9 Hz, 1 H), 8.07 (dd,  $J$  = 7.9, 1.5 Hz, 1 H), 8.06–8.02 (m, 2 H), 7.90–7.86 (m, 2 H), 7.77–7.74 (m, 2 H), 7.70–7.63 (m, 1 H), 7.53–7.49 (m, 2 H), 7.46–7.40 (m, 1 H), 7.27–7.17 (m, 1 H) ppm.

$^{13}\text{C}$  NMR (125 MHz,  $\text{DMSO}-d_6$ )  $\delta$  = 163.8, 163.7, 143.0, 143.0, 140.9, 140.7, 138.9, 133.9, 133.8, 131.5, 131.4, 130.9, 128.9, 128.0, 127.8, 126.8, 121.8, 121.7, 118.5, 118.4 ppm.

LC/MS:  $m/z$  = 318 [ $\text{M} + \text{H}^+$ ], 635 [ $2\text{M} + \text{H}^+$ ];  $t_{\text{R}}$  = 12.38 min; 99.4 % pure (UV).

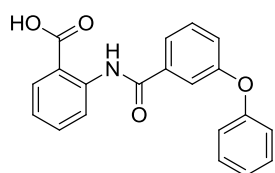




**methyl 2-(3-phenoxybenzamido)benzoate (2a)** was prepared according to method BI. For purification the solvent was evaporated and the remaining solid was suspended in MeOH. After filtration the precipitate was washed with MeOH to provide the pure compound; yield: 45 %.  $^1\text{H}$  NMR (500 MHz,  $\text{CDCl}_3$ )  $\delta$  = 12.02 (br. s, 1 H, NH), 8.91 (dd,  $J$  = 8.5, 1.3 Hz, 1 H), 8.09 (dd,  $J$  = 8.0, 1.7 Hz, 1 H), 7.77–7.74 (m, 1 H), 7.71–7.69 (m, 1 H), 7.61 (ddd,  $J$  = 8.6, 7.2, 1.9 Hz, 1 H), 7.49 (dd,  $J$  = 7.9, 7.9 Hz, 1 H), 7.42–7.36 (m, 2 H), 7.21 (ddd,  $J$  = 8.2, 2.5, 0.9 Hz, 1 H), 7.18–7.11 (m, 2 H), 7.11–7.07 (m, 2 H), 3.96 (s, 3 H,  $\text{OCH}_3$ ) ppm.

$^{13}\text{C}$  NMR (125 MHz,  $\text{CDCl}_3$ )  $\delta$  = 169.0, 165.1, 158.1, 156.5, 141.7, 136.9, 134.8, 130.9, 130.2, 129.9, 123.8, 122.7, 122.0, 121.5, 120.5, 119.5, 117.6, 115.2, 52.5 ( $\text{OCH}_3$ ) ppm.

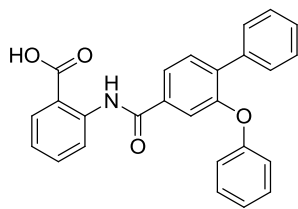
LC/MS:  $m/z$  = 348 [ $\text{M} + \text{H}^+$ ], 389 [ $\text{M} + \text{H}^+ \text{CH}_3\text{CN}$ ], 695 [ $2\text{M} + \text{H}^+$ ];  $t_R$  = 15.88 min; 96.9 % pure (UV).



**2-(3-phenoxybenzamido)benzoic acid<sup>3</sup> (2)** was prepared according to method C. Sufficient purity was achieved without further purification; yield: 85 %. Mp: 204–206 °C.  $^1\text{H}$  NMR (500 MHz,  $\text{DMSO}-d_6$ )  $\delta$  = 14.64 (br. s, 1H, NH), 8.70 (dd,  $J$  = 8.2 Hz, 0.9 Hz, 1H), 8.18 (dd,  $J$  = 7.9 Hz, 1.6 Hz, 1H), 7.84–7.82 (m, 1H), 7.63 (t,  $J$  = 1.9 Hz, 1H), 7.49 (t,  $J$  = 7.9 Hz, 1H), 7.43–7.39 (m, 3H), 7.19–7.15 (m, 2H), 7.07–7.03 (m, 3H) ppm.

$^{13}\text{C}$  NMR (125 MHz,  $\text{DMSO}-d_6$ )  $\delta$  = 171.7, 163.4, 157.2, 156.2, 140.8, 137.2, 131.6, 131.2, 130.4, 130.2, 123.9, 123.1, 122.0, 121.7, 121.5, 118.6, 119.0, 117.2 ppm.

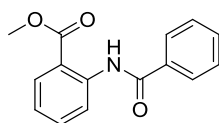
LC/MS:  $m/z$  = 334 [ $\text{M} + \text{H}^+$ ];  $t_R$  = 13.73 min; 96.9 % pure (UV).



**2-(2-phenoxy-[1,1'-biphenyl]-4-ylcarboxamido)benzoic acid<sup>3</sup> (3)** was prepared using the procedure described by *Nie et al.*<sup>3</sup> <sup>1</sup>H NMR (500 MHz, Acetone-*d*<sub>6</sub>)  $\delta$  = 12.32 (br. s, 1 H, NH), 7.89 (dd, *J* = 8.5, 1.9 Hz, 1 H), 8.18 (dd, *J* = 7.9, 1.6 Hz, 1 H), 7.89 (dd, *J* = 8.2, 1.9 Hz, 1 H), 7.71 (d, *J* = 7.9 Hz, 1 H), 7.65–7.63 (m, 4 H), 7.44–7.41 (m, 2 H), 7.37–7.34 (m, 3 H), 7.23–7.20 (m, 1 H), 7.11–7.08 (m, 1 H), 7.03–7.00 (m, 2 H) ppm.

<sup>13</sup>C NMR (125 MHz, CDCl<sub>3</sub>)  $\delta$  = 171.0, 164.9, 158.3, 155.0, 143.2, 138.1, 127.9, 136.7, 135.6, 132.8, 132.5, 131.0, 130.1, 129.2, 128.8, 124.3, 123.7, 123.3, 120.9, 120.8, 120.1, 119.2 ppm.

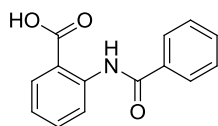
LC/MS: *m/z* = 410 [M + H<sup>+</sup>]; *t*<sub>R</sub> = 14.40 min; 95.2 % pure (UV).



**methyl 2-benzamidobenzoate (4a)** was prepared according to method BIII. For purification the solvent was evaporated and the remaining solid was resolved in a small amount of CH<sub>2</sub>Cl<sub>2</sub>. After addition of MeOH the CH<sub>2</sub>Cl<sub>2</sub> was evaporated. Crystals formed overnight in the remaining MeOH provided the pure compound; yield: 69 %. <sup>1</sup>H NMR (500 MHz, CDCl<sub>3</sub>)  $\delta$  = 12.05 (br. s, 1 H, NH), 8.95 (dd, *J* = 8.5, 1.3 Hz, 1 H), 8.10 (dd, *J* = 7.9, 1.6 Hz, 1 H), 8.08–8.04 (m, 2 H), 7.64–7.60 (m, 1 H), 7.60–7.50 (m, 3 H), 7.17–7.09 (m, 1 H), 3.98 (s, 3 H, OCH<sub>3</sub>) ppm.

<sup>13</sup>C NMR (125 MHz, CDCl<sub>3</sub>)  $\delta$  = 169.1, 165.7, 141.9, 134.9, 134.8, 131.9, 130.9, 128.8, 127.4, 122.6, 120.5, 115.2, 52.5 (OCH<sub>3</sub>) ppm.

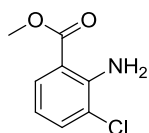
LC/MS: *m/z* = 256 [M + H<sup>+</sup>], 511 [2M + H<sup>+</sup>]; *t*<sub>R</sub> = 12.32 min; 100.0 % pure (UV).



**2-benzamidobenzoic acid<sup>4</sup> (4)** was prepared according to method C. Sufficient purity was achieved without further purification; yield: 94 %. Mp: 179–181 °C. <sup>1</sup>H NMR (500 MHz, DMSO-*d*<sub>6</sub>)  $\delta$  = 12.18 (br. s, 1 H, NH), 8.72 (dd, *J* = 8.2, 0.9 Hz, 1 H), 8.06 (dd, *J* = 7.9, 1.6 Hz, 1 H), 7.98–7.94 (m, 2 H), 7.69–7.63 (m, 2 H), 7.62–7.57 (m, 2 H), 7.23–7.19 (m, 1 H) ppm.

<sup>13</sup>C NMR (125 MHz, DMSO-*d*<sub>6</sub>)  $\delta$  = 170.0, 164.7, 141.1, 134.5, 134.3, 132.2, 131.3, 129.0, 127.0, 122.9, 119.9, 116.5 ppm.

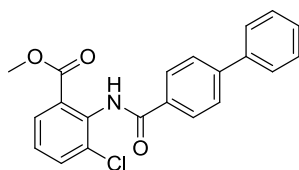
LC/MS: *m/z* = 242 [*M* + *H*<sup>+</sup>], 483 [2*M* + *H*<sup>+</sup>]; *t<sub>R</sub>* = 9.88 min; 100.0 % pure (UV).



**methyl 2-amino-3-chlorobenzoate (5b)** was prepared according to method A. The product was purified by CC (*n*-hexane/EtOAc 1:1); yield: 60 %. <sup>1</sup>H NMR (500 MHz, CDCl<sub>3</sub>)  $\delta$  = 7.82 (dd, *J* = 7.9, 1.6 Hz, 1 H), 7.41 (dd, *J* = 7.9, 1.6 Hz, 1 H), 6.59 (dd, *J* = 7.9, 7.9 Hz, 1 H), 6.28 (br. s, 2 H, NH<sub>2</sub>), 3.89 (s, 3 H, OCH<sub>3</sub>) ppm.

<sup>13</sup>C NMR (125 MHz, CDCl<sub>3</sub>)  $\delta$  = 168.1, 146.6, 133.78, 129.9, 120.2, 115.7, 111.8, 51.8 (OCH<sub>3</sub>) ppm.

LC/MS: *m/z* = 186 [*M* + *H*<sup>+</sup>], 227 [*M* + *H*<sup>+</sup> CH<sub>3</sub>CN]; *t<sub>R</sub>* = 11.68 min; 98.4 % pure (UV).

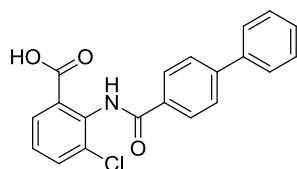


**methyl 2-([1,1'-biphenyl]-4-ylcarboxamido)-3-chlorobenzoate (5a)** was prepared according to method BIII. For purification the solvent was evaporated and the remaining solid was resolved in a small amount of CH<sub>2</sub>Cl<sub>2</sub>. After addition of MeOH the CH<sub>2</sub>Cl<sub>2</sub> was

evaporated. Crystals formed overnight in the remaining MeOH provided the pure compound; yield: 40 %.  $^1\text{H}$  NMR (500 MHz,  $\text{CDCl}_3$ )  $\delta$  = 9.51 (br. s, 1 H, NH), 8.12–8.06 (m, 2 H), 7.90 (dd,  $J$  = 7.9, 1.6 Hz, 1 H), 7.77–7.72 (m, 2 H), 7.68 (dd,  $J$  = 7.9, 1.6 Hz, 1 H), 7.67–7.63 (m, 2 H), 7.52–7.46 (m, 2 H), 7.44–7.39 (m, 1 H), 7.27 (dd,  $J$  = 7.9, 7.9 Hz, 1 H), 3.90 (s, 3 H,  $\text{OCH}_3$ ) ppm.

$^{13}\text{C}$  NMR (125 MHz,  $\text{CDCl}_3$ )  $\delta$  = 167.1, 165.0, 145.1, 140.0, 135.7, 134.3, 132.5, 131.2, 129.1, 128.9, 128.2, 128.1, 127.5, 127.3, 126.0, 126.0, 52.7 ( $\text{OCH}_3$ ) ppm.

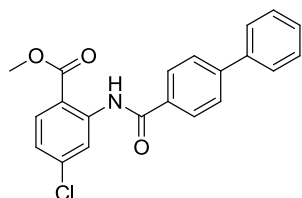
LC/MS:  $m/z$  = 365 and 367 [ $\text{M} + \text{H}^+$ ], 731 and 733 [ $2\text{M} + \text{H}^+$ ];  $t_R$  = 13.00 min; 93.8 % pure (UV).



**2-([1,1'-biphenyl]-4-ylcarboxamido)-3-chlorobenzoic acid (5)** was prepared according to method C. The product was purified by preparative TLC (*n*-hexane/EtOAc 1:1); yield: 93 %. Mp: 203–205 °C.  $^1\text{H}$  NMR (500 MHz,  $\text{DMSO}-d_6$ )  $\delta$  = 10.33 (br. s, 1 H, NH), 8.11–8.07 (m, 2 H), 7.86–7.75 (m, 6 H), 7.54–7.49 (m, 2 H), 7.47–7.40 (m, 2 H) ppm.

$^{13}\text{C}$  NMR (125 MHz,  $\text{DMSO}-d_6$ )  $\delta$  = 166.8, 165.1, 143.3, 139.2, 134.7, 132.8, 132.7, 131.9, 129.9, 129.0, 128.5, 128.2, 127.6, 127.0, 126.7 ppm.

LC/MS:  $m/z$  = 352 [ $2 + \text{H}^+$ ], 703 [ $2\text{M} + \text{H}^+$ ];  $t_R$  = 11.55 min; 99.2 % pure (UV).

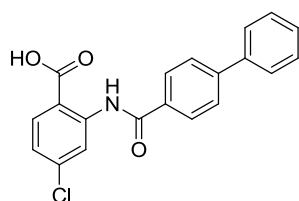


**methyl 2-([1,1'-biphenyl]-4-ylcarboxamido)-4-chlorobenzoate (6a)** was prepared according to method BI. For purification the solvent was evaporated and the remaining solid was suspended in MeOH. After filtration the precipitate was washed with MeOH to provide the pure compound; yield: 59 %.  $^1\text{H}$  NMR (500 MHz,  $\text{CDCl}_3$ )  $\delta$  = 12.13 (br. s, 1 H, NH), 9.08

(d,  $J = 2.1$  Hz, 1 H), 8.14–8.09 (m, 2 H), 8.01 (d,  $J = 8.8$  Hz, 1 H), 7.78–7.74 (m, 2 H), 7.69–7.61 (m, 2 H), 7.53–7.45 (m, 2 H), 7.44–7.38 (m, 1 H), 7.10 (dd,  $J = 8.8, 2.1$  Hz, 1 H), 3.98 (s, 3 H, OCH<sub>3</sub>) ppm.

<sup>13</sup>C NMR (125 MHz, CDCl<sub>3</sub>)  $\delta = 168.5, 165.4, 144.9, 142.7, 141.2, 139.9, 133.0, 132.0, 128.9, 128.1, 127.9, 127.5, 127.2, 122.8, 120.3, 113.3, 52.6$  (OCH<sub>3</sub>) ppm.

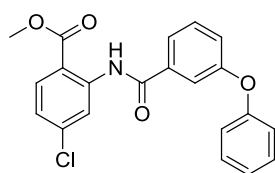
LC/MS:  $m/z = 367$  [M + H<sup>+</sup>], 733 [2M + H<sup>+</sup>];  $t_R = 16.36$  min; 98.2 % pure (UV).



**2-([1,1'-biphenyl]-4-ylcarboxamido)-4-chlorobenzoic acid (6)** was prepared according to method C. Sufficient purity was achieved without further purification; yield: 55 %. Mp: 323–324 °C. <sup>1</sup>H NMR (500 MHz, DMSO-*d*<sub>6</sub>)  $\delta = 15.29$  (br. s, 1 H, NH), 8.81 (d,  $J = 2.2$  Hz, 1 H), 8.15–8.08 (m, 3 H), 7.84–7.78 (m, 2 H), 7.74–7.68 (m, 2 H), 7.52–7.45 (m, 2 H), 7.44–7.38 (m, 1 H), 7.09 (dd,  $J = 8.2, 2.2$  Hz, 1 H) ppm.

<sup>13</sup>C NMR (125 MHz, DMSO-*d*<sub>6</sub>)  $\delta = 169.6, 164.2, 143.3, 142.0, 139.0, 134.8, 133.6, 133.1, 129.0, 128.2, 127.9, 126.9, 126.9, 122.8, 121.5, 117.9$  ppm.

LC/MS:  $m/z = 351$  and 353 [M + H<sup>+</sup>];  $t_R = 14.11$  min; 99.1 % pure (UV).

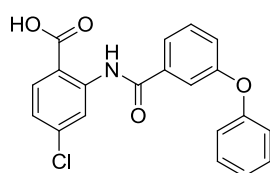


**methyl 4-chloro-2-(3-phenoxybenzamido)benzoate (7a)** was prepared according to method BI. For purification the solvent was evaporated and the remaining solid was suspended in MeOH. After filtration the precipitate was washed with MeOH to provide the pure compound; yield: 71 %. <sup>1</sup>H NMR (500 MHz, CDCl<sub>3</sub>)  $\delta = 12.07$  (br. s, 1 H, NH), 9.02 (d,  $J = 2.2$  Hz, 1 H), 8.00 (d,  $J = 8.8$  Hz, 1 H), 7.75–7.71 (m, 1 H), 7.70–7.65 (m, 1 H), 7.49 (dd,  $J = 8.2, 8.2$  Hz, 1

H), 7.41–7.37 (m, 2 H), 7.22 (ddd,  $J = 8.2, 2.2, 0.9$  Hz, 1 H), 7.19–7.15 (m, 1 H), 7.14–7.07 (m, 3 H), 3.96 (s, 3 H, OCH<sub>3</sub>) ppm.

<sup>13</sup>C NMR (125 MHz, CDCl<sub>3</sub>)  $\delta = 168.4, 165.1, 158.2, 156.4, 142.5, 141.2, 136.3, 133.0, 130.2, 130.0, 124.0, 123.0, 122.2, 121.4, 120.4, 119.5, 117.5, 113.4, 52.6$  (OCH<sub>3</sub>) ppm.

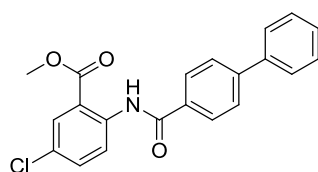
LC/MS:  $m/z = 382$  [M + H<sup>+</sup>];  $t_R = 15.99$  min; 95.5 % pure (UV).



**4-chloro-2-(3-phenoxybenzamido)benzoic acid (7)** was prepared according to method C. Sufficient purity was achieved without further purification; yield: 61 %. Mp: 205–206 °C. <sup>1</sup>H NMR (500 MHz, DMSO-*d*<sub>6</sub>)  $\delta = 12.26$  (br. s, 1 H, NH), 8.75 (d,  $J = 1.9$  Hz, 1 H), 8.03 (d,  $J = 8.5$  Hz, 1 H), 7.72–7.66 (m, 1 H), 7.61 (dd,  $J = 7.9, 7.9$  Hz, 1 H), 7.52 (s, 1 H), 7.47–7.41 (m, 2 H), 7.33–7.25 (m, 2 H), 7.23–7.17 (m, 1 H), 7.16–7.02 (m, 2 H) ppm.

<sup>13</sup>C NMR (125 MHz, DMSO-*d*<sub>6</sub>)  $\delta = 169.3, 164.2, 157.4, 155.9, 141.9, 138.7, 136.0, 132.9, 130.9, 130.3, 124.1, 123.0, 122.3, 121.6, 119.2, 119.1, 116.9, 115.4$  ppm.

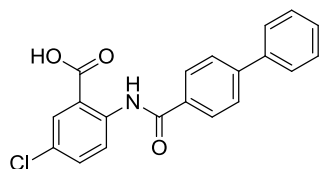
LC/MS:  $m/z = 368$  [M + H<sup>+</sup>], 409 [M + H<sup>+</sup> CH<sub>3</sub>CN];  $t_R = 13.98$  min; 100.0 % pure (UV).



**methyl 2-([1,1'-biphenyl]-4-ylcarboxamido)-5-chlorobenzoate (8a)** was prepared according to method BII. For purification the solvent was evaporated and the remaining solid was suspended in MeOH. After filtration the precipitate was washed with MeOH to provide the pure compound; yield: 86 %. <sup>1</sup>H NMR (500 MHz, CDCl<sub>3</sub>)  $\delta = 12.02$  (br. s, 1 H, NH), 8.97 (d,  $J = 9.1$  Hz, 1 H), 8.13–8.10 (m, 2 H), 8.07 (d,  $J = 2.5$  Hz, 1 H), 7.78–7.75 (m, 2 H), 7.67–7.64 (m, 2 H), 7.57 (dd,  $J = 9.1, 2.5$  Hz, 1 H), 7.52–7.47 (m, 2 H), 7.45–7.37 (m, 1 H), 4.00 (s, 3 H, OCH<sub>3</sub>) ppm.

$^{13}\text{C}$  NMR (125 MHz,  $\text{CDCl}_3$ )  $\delta$  = 168.1, 165.3, 144.9, 140.5, 139.9, 134.7, 133.2, 130.5, 128.9, 128.1, 127.9, 127.6, 127.5, 127.2, 121.9, 116.3, 52.8 ( $\text{OCH}_3$ ) ppm.

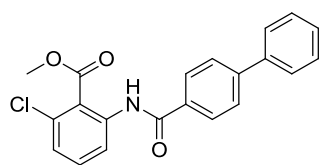
LC/MS:  $m/z$  = 366 [ $\text{M} + \text{H}^+$ ], 731 [ $2\text{M} + \text{H}^+$ ];  $t_{\text{R}}$  = 16.76 min; 97.0 % pure (UV).



**2-([1,1'-biphenyl]-4-ylcarboxamido)-5-chlorobenzoic acid (8)** was prepared according to method C. For purification the remaining solid was washed with MeOH and  $\text{CH}_2\text{Cl}_2$  to provide the pure compound; yield: 96 %. Mp: 274–276 °C.  $^1\text{H}$  NMR (500 MHz,  $\text{DMSO}-d_6$ )  $\delta$  = 12.14 (br. s, 1 H, NH), 8.74 (d,  $J$  = 9.1 Hz, 1 H), 8.05–8.02 (m, 2 H), 8.00 (d,  $J$  = 2.5 Hz, 1 H), 7.91–7.86 (m, 2 H), 7.79–7.75 (m, 2 H), 7.73 (dd,  $J$  = 9.1, 2.5 Hz, 1 H), 7.54–7.48 (m, 2 H), 7.47–7.41 (m, 1 H) ppm.

$^{13}\text{C}$  NMR (125 MHz,  $\text{DMSO}-d_6$ )  $\delta$  = 168.8, 164.4, 143.8, 139.9, 138.8, 133.9, 132.9, 130.4, 129.1, 128.3, 127.8, 127.2, 127.0, 126.5, 121.8, 118.6 ppm.

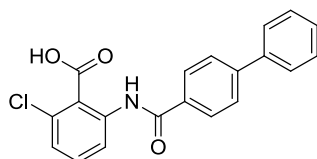
LC/MS:  $m/z$  = 352 and 354 [ $\text{M} + \text{H}^+$ ];  $t_{\text{R}}$  = 14.32 min; 99.3 % pure (UV).



**methyl 2-([1,1'-biphenyl]-4-ylcarboxamido)-6-chlorobenzoate (9a)** was prepared according to method BII. The product was purified by CC (*n*-hexane/EtOAc 8:2); yield: 76 %.  $^1\text{H}$  NMR (500 MHz,  $\text{CDCl}_3$ )  $\delta$  = 10.27 (br. s, 1 H, NH), 8.56 (dd,  $J$  = 8.2, 0.9 Hz, 1 H), 8.04–8.01 (m, 2 H), 7.77–7.74 (m, 2 H), 7.67–7.64 (m, 2 H), 7.52–7.41 (m, 4 H), 7.24 (dd,  $J$  = 8.2, 0.9 Hz, 1 H), 4.03 (s, 3 H,  $\text{OCH}_3$ ) ppm.

$^{13}\text{C}$  NMR (125 MHz,  $\text{CDCl}_3$ )  $\delta$  = 167.9, 165.0, 145.1, 139.8, 139.7, 133.6, 132.9, 132.6, 129.0, 128.2, 127.8, 127.6, 127.2, 125.9, 120.2, 119.9, 52.8 ( $\text{OCH}_3$ ) ppm.

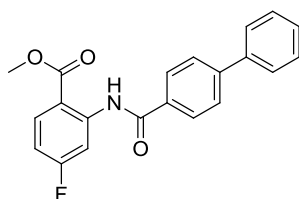
LC/MS:  $m/z$  = 366 [ $\text{M} + \text{H}^+$ ], 731 [ $2\text{M} + \text{H}^+$ ];  $t_{\text{R}}$  = 13.90 min; 98.2 % pure (UV).



**2-([1,1'-biphenyl]-4-ylcarboxamido)-6-chlorobenzoic acid (9)** was prepared according to method C. For purification the remaining solid was washed with  $\text{CH}_2\text{Cl}_2$  to provide the pure compound; yield: 79 %. Mp: 218–219 °C.  $^1\text{H}$  NMR (500 MHz,  $\text{DMSO}-d_6$ )  $\delta$  = 10.36 (br. s, 1 H, NH), 8.04–8.01 (m, 2 H), 7.86–7.83 (m, 2 H), 7.78–7.75 (m, 2 H), 7.61–7.58 (m, 1 H), 7.53–7.49 (m, 3 H), 7.46–7.40 (m, 2 H) ppm.

$^{13}\text{C}$  NMR (125 MHz,  $\text{DMSO}-d_6$ )  $\delta$  = 166.2, 165.2, 143.4, 139.0, 136.9, 132.7, 130.8, 130.5, 129.6, 129.1, 128.3, 128.2, 126.9, 126.8, 126.7, 125.1 ppm.

LC/MS:  $m/z$  = 352  $[\text{M} + \text{H}^+]$ , 705, 707  $[2\text{M} + \text{H}^+]$ ;  $t_R$  = 12.25 min; 100.0 % pure (UV).

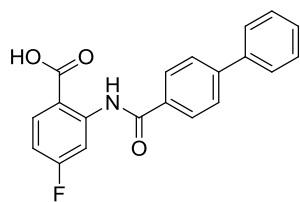


**methyl 2-([1,1'-biphenyl]-4-ylcarboxamido)-4-fluorobenzoate (10a)** was prepared according to method BI. For purification the solvent was evaporated and the remaining solid was suspended in MeOH. After filtration the precipitate was washed with MeOH to provide the pure compound; yield: 42 %.  $^1\text{H}$  NMR (500 MHz,  $\text{CDCl}_3$ )  $\delta$  = 12.25 (br. s, 1 H, NH), 8.80 (dd,  $J$  = 11.8, 2.4 Hz, 1 H), 8.21–8.03 (m, 3 H), 7.82–7.72 (m, 2 H), 7.72–7.61 (m, 2 H), 7.57–7.48 (m, 2 H), 7.48–7.39 (m, 1 H), 6.96–6.79 (m, 1 H), 3.99 (s, 3 H,  $\text{OCH}_3$ ) ppm.

$^{13}\text{C}$  NMR (125 MHz,  $\text{CDCl}_3$ )  $\delta$  = 168.5, 166.1 (d,  $J$  = 253.9 Hz), 165.6, 145.0, 144.1 (d,  $J_{CF}$  = 12.8 Hz), 139.9, 133.3 (d,  $J_{CF}$  = 11.0 Hz), 133.1, 128.9, 128.1, 127.9, 127.5, 127.2, 111.3 (d,  $J_{CF}$  = 2.7 Hz), 109.9 (d,  $J_{CF}$  = 22.9 Hz), 107.6 (d,  $J_{CF}$  = 28.4 Hz), 52.5 ppm ( $\text{OCH}_3$ ).

LC/MS:  $m/z$  = 350  $[\text{M} + \text{H}^+]$ , 391  $[\text{M} + \text{H}^+ \text{CH}_3\text{CN}]$ , 699  $[2\text{M} + \text{H}^+]$ ;  $t_R$  = 15.69 min; 96.4 % pure (UV).

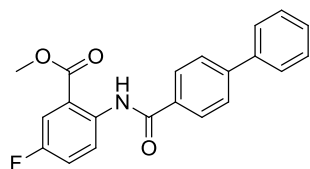




**2-([1,1'-biphenyl]-4-ylcarboxamido)-4-fluorobenzoic acid (10)** was prepared according to method C. For purification the compound was recrystallized from MeOH; yield: 24 %. Mp: 258–260 °C.  $^1\text{H}$  NMR (500 MHz, DMSO- $d_6$ )  $\delta$  = 12.47 (br. s, 1 H, NH), 8.59 (dd,  $J$  = 12.3, 2.5 Hz, 1 H), 8.14 (dd,  $J$  = 9.0, 6.8 Hz, 1 H), 8.07–8.00 (m, 2 H), 7.93–7.87 (m, 2 H), 7.81–7.72 (m, 2 H), 7.57–7.49 (m, 2 H), 7.49–7.41 (m, 1 H), 7.10–7.01 (m, 1 H) ppm.

$^{13}\text{C}$  NMR (125 MHz, DMSO- $d_6$ )  $\delta$  = 169.4, 165.1 (d,  $J_{\text{CF}}$  = 248.0 Hz), 164.6, 143.9, 143.3 (d,  $J_{\text{CF}}$  = 12.8 Hz), 138.8, 134.0 (d,  $J_{\text{CF}}$  = 11.0 Hz), 132.7, 129.1, 128.3, 127.7, 127.2, 127.0, 112.8 (d,  $J_{\text{CF}}$  = 2.7 Hz), 109.9 (d,  $J_{\text{CF}}$  = 22.0 Hz), 106.3 (d,  $J_{\text{CF}}$  = 28.4 Hz) ppm.

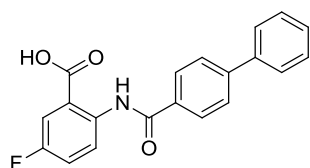
LC/MS:  $m/z$  = 336 [ $\text{M} + \text{H}^+$ ], 377 [ $\text{M} + \text{H}^+ \text{CH}_3\text{CN}$ ], 671 [ $2\text{M} + \text{H}^+$ ];  $t_{\text{R}}$  = 13.94 min; 100.0 % pure (UV).



**methyl 2-([1,1'-biphenyl]-4-ylcarboxamido)-5-fluorobenzoate (11a)** was prepared according to method BI. For purification the solvent was evaporated and the remaining solid was suspended in MeOH. After filtration the precipitate was washed with MeOH to provide the pure compound; yield: 64 %.  $^1\text{H}$  NMR (500 MHz,  $\text{CDCl}_3$ )  $\delta$  = 11.94 (br. s, 1 H, NH), 8.99 (dd,  $J$  = 9.1, 4.7 Hz, 1 H), 8.16–8.05 (m, 2 H), 7.81–7.71 (m, 3 H), 7.70–7.60 (m, 2 H), 7.54–7.45 (m, 2 H), 7.45–7.38 (m, 1 H), 7.38–7.30 (m, 1 H), 4.00 (s, 3 H,  $\text{OCH}_3$ ) ppm.

$^{13}\text{C}$  NMR (125 MHz,  $\text{CDCl}_3$ )  $\delta$  = 168.1, 165.3, 157.4 (d,  $J_{\text{CF}}$  = 244.0 Hz), 144.8, 140.0, 138.3 (d,  $J_{\text{CF}}$  = 2.7 Hz), 133.3, 128.9, 128.1, 127.9, 127.5, 127.2, 122.3 (d,  $J_{\text{CF}}$  = 6.4 Hz), 121.9 (d,  $J_{\text{CF}}$  = 22.0 Hz), 117.0, (d,  $J_{\text{CF}}$  = 23.8 Hz), 116.4 (d,  $J_{\text{CF}}$  = 7.3 Hz), 52.8 ppm ( $\text{OCH}_3$ ).

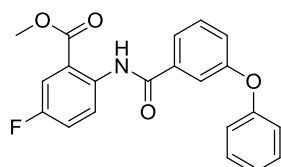
LC/MS:  $m/z$  = 350 [ $\text{M} + \text{H}^+$ ], 391 [ $\text{M} + \text{H}^+ \text{CH}_3\text{CN}$ ], 699 [ $2\text{M} + \text{H}^+$ ];  $t_{\text{R}}$  = 15.11 min; 96.7 % pure (UV).



**2-([1,1'-biphenyl]-4-ylcarboxamido)-5-fluorobenzoic acid (11)** was prepared according to method C. Sufficient purity was achieved without further purification; yield: 61 %. Mp: 259–263 °C.  $^1\text{H}$  NMR (500 MHz,  $\text{DMSO}-d_6$ )  $\delta$  = 14.97 (br. s, 1 H, NH), 8.75 (dd,  $J$  = 9.1, 5.4 Hz, 1 H), 8.15–8.07 (m, 2 H), 7.85 (dd,  $J$  = 9.9, 3.3 Hz, 1 H), 7.83–7.79 (m, 2 H), 7.75–7.70 (m, 2 H), 7.53–7.45 (m, 2 H), 7.44–7.37 (m, 1 H), 7.28–7.19 (m, 1 H) ppm.

$^{13}\text{C}$  NMR (125 MHz,  $\text{DMSO}-d_6$ )  $\delta$  = 168.9 (d,  $J_{\text{CF}}$  = 1.8 Hz), 163.7, 156.9 (d,  $J_{\text{CF}}$  = 239.2 Hz), 143.1, 139.1, 137.4 (d,  $J_{\text{CF}}$  = 1.8 Hz), 134.0, 129.1, 128.1, 127.8, 126.9, 126.6 (d,  $J_{\text{CF}}$  = 7.3 Hz), 120.1 (d,  $J_{\text{CF}}$  = 7.3 Hz), 117.3 (d,  $J_{\text{CF}}$  = 22.9 Hz), 117.2 (d,  $J_{\text{CF}}$  = 22.9 Hz), 117.0 ppm.

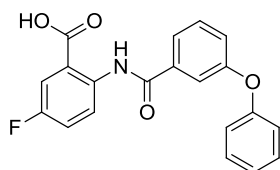
LC/MS:  $m/z$  = 334 [ $\text{M} - \text{H}^+$ ];  $t_{\text{R}}$  = 12.89 min; 96.8 % pure (UV).



**methyl 5-fluoro-2-(3-phenoxybenzamido)benzoate (12a)** was prepared according to method BI. For purification the solvent was evaporated and the remaining solid was suspended in MeOH. After filtration the precipitate was washed with MeOH to provide the pure compound; yield: 20 %.  $^1\text{H}$  NMR (500 MHz,  $\text{CDCl}_3$ )  $\delta$  = 11.86 (br. s, 1 H, NH), 8.92 (dd,  $J$  = 9.4, 5.0 Hz, 1 H), 7.77–7.71 (m, 2 H), 7.71–7.65 (m, 1 H), 7.49 (dd,  $J$  = 7.9, 7.9 Hz, 1 H), 7.42–7.35 (m, 2 H), 7.32 (ddd,  $J$  = 9.4, 7.5, 3.0 Hz, 1 H), 7.21 (ddd,  $J$  = 8.1, 2.4, 0.8 Hz, 1 H), 7.19–7.12 (m, 1 H), 7.12–7.07 (m, 2 H), 3.97 (s, 3 H,  $\text{OCH}_3$ ) ppm.

$^{13}\text{C}$  NMR (125 MHz,  $\text{CDCl}_3$ )  $\delta$  = 167.9 (d,  $J_{\text{CF}}$  = 2.7 Hz), 164.9, 158.1, 157.6 (d,  $J_{\text{CF}}$  = 242.9 Hz), 138.1 (d,  $J_{\text{CF}}$  = 1.8 Hz), 136.5, 130.2, 129.9, 123.9, 122.2 (d,  $J$  = 7.3 Hz), 122.0, 121.8 (d,  $J$  = 22.0 Hz), 121.4, 120.8, 119.4, 117.5, 117.0 (d,  $J_{\text{CF}}$  = 23.8 Hz), 116.4 (d,  $J_{\text{CF}}$  = 7.3 Hz), 52.8 ( $\text{OCH}_3$ ) ppm.

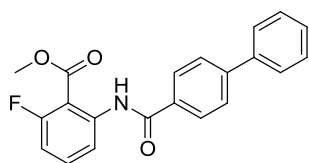
LC/MS:  $m/z = 366 [M + H^+]$ ;  $t_R = 14.93$  min; 93.7 % pure (UV).



**5-fluoro-2-(3-phenoxybenzamido)benzoic acid (12)** was prepared according to method C. Sufficient purity was achieved without further purification; yield: 87 %. Mp: 186–187 °C.  $^1\text{H}$  NMR (500 MHz,  $\text{DMSO-}d_6$ )  $\delta = 12.02$  (br. s, 1 H, NH), 8.62 (dd,  $J = 9.4, 5.2$  Hz, 1 H), 7.74 (dd,  $J = 9.4, 3.2$  Hz, 1 H), 7.72–7.68 (m, 1 H), 7.59 (dd,  $J = 7.9, 7.9$  Hz, 1 H), 7.56–7.50 (m, 2 H), 7.49–7.39 (m, 2 H), 7.27 (ddd,  $J = 7.9, 2.6, 0.9$  Hz, 1 H), 7.23–7.16 (m, 1 H), 7.14–7.04 (m, 2 H) ppm.

$^{13}\text{C}$  NMR (125 MHz,  $\text{DMSO-}d_6$ )  $\delta = 168.7$  (d,  $J_{CF} = 1.8$  Hz), 163.8, 157.3, 157.0 (d,  $J_{CF} = 242.0$  Hz), 156.0, 137.2 (d,  $J_{CF} = 1.8$  Hz), 136.3, 130.8, 130.2, 124.1, 122.3 (d,  $J_{CF} = 7.3$  Hz), 122.0, 121.6, 120.9 (d,  $J_{CF} = 22.0$  Hz), 119.4 (d,  $J_{CF} = 7.3$  Hz), 119.1, 117.0 (d,  $J_{CF} = 22.0$  Hz), 116.9 ppm.

LC/MS:  $m/z = 351 [M + H^+]$ , 392 [ $M + H^+ \text{CH}_3\text{CN}$ ];  $t_R = 12.87$  min; 96.2 % pure (UV).

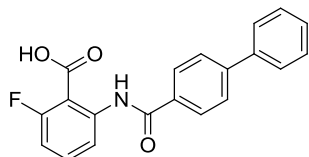


**methyl 2-([1,1'-biphenyl]-4-ylcarboxamido)-6-fluorobenzoate (13a)** was prepared according to method BII. For purification the solvent was evaporated and the remaining solid was suspended in MeOH. After filtration the precipitate was washed with MeOH to provide the pure compound; yield: 90 %.  $^1\text{H}$  NMR (500 MHz,  $\text{CDCl}_3$ )  $\delta = 11.68$  (br. s, 1 H, NH), 8.70 (d,  $J = 8.8$  Hz, 1 H), 8.12–8.07 (m, 2 H), 7.78–7.73 (m, 2 H), 7.68–7.64 (m, 2 H), 7.57–7.52 (m, 1 H), 7.51–7.47 (m, 2 H), 7.45–7.39 (m, 1 H), 6.89 (ddd,  $J = 11.0, 8.8, 0.9$  Hz, 1 H), 4.03 (s, 3 H,  $\text{OCH}_3$ ) ppm.

$^{13}\text{C}$  NMR (125 MHz,  $\text{CDCl}_3$ )  $\delta = 167.9$  (d,  $J_{CF} = 3.7$  Hz), 165.3, 162.4 (d,  $J_{CF} = 258.4$  Hz), 144.9, 142.1 (d,  $J_{CF} = 2.7$  Hz), 139.9, 134.8 (d,  $J_{CF} = 11.0$  Hz), 133.2, 128.9, 128.1, 127.9,

127.5, 127.2, 116.5 (d,  $J_{CF} = 3.7$  Hz), 111.1 (d,  $J_{CF} = 23.8$  Hz), 106.2 (d,  $J_{CF} = 12.8$  Hz), 52.9 (OCH<sub>3</sub>) ppm.

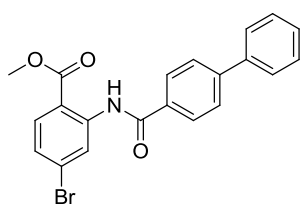
LC/MS:  $m/z = 350$  [M + H<sup>+</sup>], 699 [2M + H<sup>+</sup>];  $t_R = 15.22$  min; 97.5 % pure (UV).



**2-([1,1'-biphenyl]-4-ylcarboxamido)-6-fluorobenzoic acid (13)** was prepared according to method C. Sufficient purity was achieved without further purification; yield: 87 %. Mp: 232–233 °C. <sup>1</sup>H NMR (500 MHz, DMSO-*d*<sub>6</sub>)  $\delta = 11.23$  (br. s, 1 H, NH), 8.05–8.00 (m, 3 H), 7.90–7.84 (m, 2 H), 7.79–7.73 (m, 2 H), 7.61 (td,  $J = 8.3, 6.1$  Hz, 1 H), 7.53–7.49 (m, 2 H), 7.46–7.41 (m, 1 H), 7.11 (ddd,  $J = 10.6, 8.4, 0.9$  Hz, 1 H) ppm.

<sup>13</sup>C NMR (125 MHz, DMSO-*d*<sub>6</sub>)  $\delta = 166.5$  (d,  $J_{CF} = 1.8$  Hz), 164.7, 160.8 (d,  $J_{CF} = 254.0$  Hz), 143.6, 139.7 (d,  $J_{CF} = 4.6$  Hz), 138.9, 133.2 (d,  $J_{CF} = 11.0$  Hz), 132.9, 129.1, 128.3, 128.0, 126.9, 118.3 (d,  $J_{CF} = 3.7$  Hz), 112.0 (d,  $J_{CF} = 14.7$  Hz), 111.8 (d,  $J_{CF} = 22.9$  Hz) ppm.

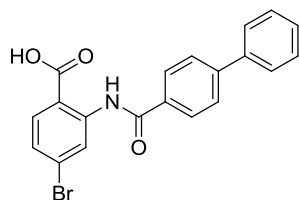
LC/MS:  $m/z = 336$  [M + H<sup>+</sup>], 671 [2M + H<sup>+</sup>];  $t_R = 12.85$  min; 100.0 % pure (UV).



**methyl 2-([1,1'-biphenyl]-4-ylcarboxamido)-4-bromobenzoate (14a)** was prepared according to method BII. For purification the solvent was evaporated and the remaining solid was suspended in MeOH. After filtration the precipitate was washed with MeOH to provide the pure compound; yield: 69 %. <sup>1</sup>H NMR (500 MHz, CDCl<sub>3</sub>)  $\delta = 12.12$  (br. s, 1 H, NH), 9.25 (d,  $J = 1.9$  Hz, 1 H), 8.14–8.09 (m, 2 H), 7.94 (d,  $J = 8.5$  Hz, 1 H), 7.79–7.74 (m, 2 H), 7.68–7.63 (m, 2 H), 7.52–7.47 (m, 2 H), 7.45–7.39 (m, 1 H), 7.27 (dd,  $J = 8.5, 1.9$  Hz, 1 H), 3.99 (s, 3 H, OCH<sub>3</sub>) ppm.

$^{13}\text{C}$  NMR (125 MHz,  $\text{CDCl}_3$ )  $\delta$  = 168.7, 165.4, 145.0, 142.7, 139.9, 133.0, 132.0, 129.9, 128.9, 128.1, 127.9, 127.5, 127.2, 125.8, 123.3, 113.7, 52.7 ( $\text{OCH}_3$ ) ppm.

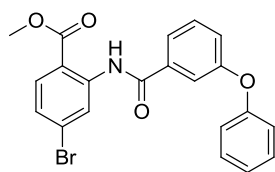
LC/MS:  $m/z$  = 409 and 411 [ $\text{M} + \text{H}^+$ ];  $t_{\text{R}}$  = 17.07 min; 100.0 % pure (UV).



**2-([1,1'-biphenyl]-4-ylcarboxamido)-4-bromobenzoic acid (14)** was prepared according to method C. For purification the remaining solid was washed with MeOH and  $\text{CH}_2\text{Cl}_2$  to provide the pure compound; yield: 81 %. Mp: 246–250 °C.  $^1\text{H}$  NMR (500 MHz,  $\text{DMSO}-d_6$ )  $\delta$  = 12.30 (br. s, 1 H, NH), 8.99 (d,  $J$  = 1.9 Hz, 1 H), 8.05–8.00 (m, 2 H), 7.97 (d,  $J$  = 8.5 Hz, 1 H), 7.93–7.87 (m, 2 H), 7.80–7.73 (m, 2 H), 7.55–7.48 (m, 2 H), 7.47–7.41 (m, 1 H), 7.41 (dd,  $J$  = 8.5, 1.9 Hz, 1 H) ppm.

$^{13}\text{C}$  NMR (125 MHz,  $\text{DMSO}-d_6$ )  $\delta$  = 169.5, 164.6, 143.9, 142.1, 138.8, 133.0, 132.7, 129.1, 128.3, 127.8, 127.8, 127.2, 127.0, 125.8, 122.1, 115.5 ppm.

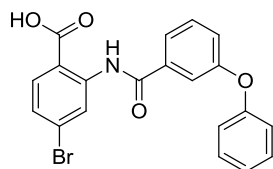
LC/MS:  $m/z$  = 793 [ $2\text{M} + \text{H}^+$ ];  $t_{\text{R}}$  = 14.71 min; 96.4 % pure (UV).



**methyl 4-bromo-2-(3-phenoxybenzamido)benzoate (15a)** was prepared according to method BII. For purification the solvent was evaporated and the remaining solid was suspended in MeOH. After filtration the precipitate was washed with MeOH to provide the pure compound; yield: 61 %.  $^1\text{H}$  NMR (500 MHz,  $\text{CDCl}_3$ )  $\delta$  = 12.04 (br. s, 1 H, NH), 9.18 (d,  $J$  = 2.2 Hz, 1 H), 7.92 (d,  $J$  = 8.5 Hz, 1 H), 7.73 (dd,  $J$  = 1.6, 0.9 Hz, 1 H), 7.69–7.65 (m, 1 H), 7.49 (dd,  $J$  = 7.9, 7.9 Hz, 1 H), 7.42–7.35 (m, 2 H), 7.26 (dd,  $J$  = 8.5, 2.2 Hz, 1 H), 7.22 (ddd,  $J$  = 8.2, 2.5, 0.9 Hz, 1 H), 7.19–7.14 (m, 1 H), 7.12–7.07 (m, 2 H), 3.96 (s, 3 H,  $\text{OCH}_3$ ) ppm.

$^{13}\text{C}$  NMR (125 MHz,  $\text{CDCl}_3$ )  $\delta$  = 168.5, 165.0, 158.2, 156.3, 142.5, 136.3, 132.0, 130.2, 130.0, 129.9, 126.0, 124.0, 123.3, 122.2, 121.4, 119.5, 117.4, 113.8, 52.7 ( $\text{OCH}_3$ ) ppm.

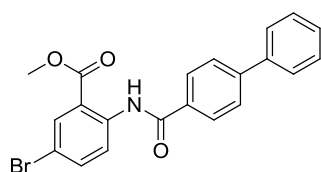
LC/MS:  $m/z$  = no ionization;  $t_R$  = 16.93 min; 99.8 % pure (UV).



**4-bromo-2-(3-phenoxybenzamido)benzoic acid (15)** was prepared according to method C. For purification the remaining solid was washed with MeOH and  $\text{CH}_2\text{Cl}_2$  to provide the pure compound; yield: 74 %. Mp: 194–195 °C.  $^1\text{H}$  NMR (500 MHz,  $\text{DMSO}-d_6$ )  $\delta$  = 12.22 (br. s, 1 H, NH), 8.90 (d,  $J$  = 2.2 Hz, 1 H), 7.95 (d,  $J$  = 8.5 Hz, 1 H), 7.70–7.68 (m, 1 H), 7.61 (dd,  $J$  = 7.9, 7.9 Hz, 1 H), 7.53–7.51 (m, 1 H), 7.46–7.40 (m, 3 H), 7.29 (ddd,  $J$  = 8.2, 2.5, 0.9 Hz, 1 H), 7.21 (tt,  $J$  = 7.4, 1.1 Hz, 1 H), 7.11–7.08 (m, 2 H) ppm.

$^{13}\text{C}$  NMR (125 MHz,  $\text{DMSO}-d_6$ )  $\delta$  = 169.4, 164.1, 157.4, 155.9, 141.8, 136.0, 132.9, 130.9, 130.3, 127.7, 125.9, 124.1, 122.3, 122.2, 121.6, 119.1, 116.8, 115.8 ppm.

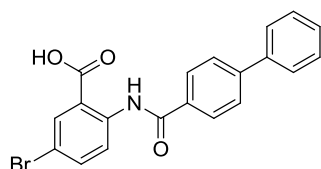
LC/MS:  $m/z$  = 823 and 825 and 827 [ $2\text{M} + \text{H}^+$ ];  $t_R$  = 14.65 min; 100.0 % pure (UV).



**methyl 2-([1,1'-biphenyl]-4-ylcarboxamido)-5-bromobenzoate (16a)** was prepared according to method BI. For purification the solvent was evaporated and the remaining solid was suspended in MeOH. After filtration the precipitate was washed with MeOH to provide the pure compound; yield: 26 %.  $^1\text{H}$  NMR (500 MHz,  $\text{CDCl}_3$ )  $\delta$  = 12.01 (br. s, 1 H, NH), 8.91 (d,  $J$  = 9.1 Hz, 1 H), 8.22 (d,  $J$  = 2.5 Hz, 1 H), 8.15–8.08 (m, 2 H), 7.79–7.74 (m, 2 H), 7.71 (dd,  $J$  = 9.1, 2.5 Hz, 1 H), 7.68–7.62 (m, 2 H), 7.54–7.46 (m, 2 H), 7.45–7.38 (m, 1 H), 4.00 (s, 3 H,  $\text{OCH}_3$ ) ppm.

$^{13}\text{C}$  NMR (125 MHz,  $\text{CDCl}_3$ )  $\delta$  = 168.0, 165.4, 144.9, 141.0, 139.9, 137.5, 133.5, 133.1, 128.9, 128.1, 127.9, 127.5, 127.2, 122.1, 116.6, 115.0, 52.8 ( $\text{OCH}_3$ ) ppm.

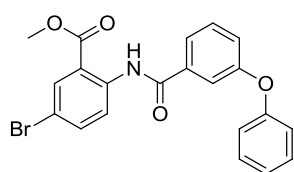
LC/MS:  $m/z$  = 409 and 411 [ $\text{M} + \text{H}^+$ ], 820 and 822 [ $2\text{M} + \text{H}^+$ ];  $t_R$  = 16.41 min; 98.4 % pure (UV).



**2-([1,1'-biphenyl]-4-ylcarboxamido)-5-bromobenzoic acid<sup>5</sup> (16)** was prepared according to method C. Sufficient purity was achieved without further purification; yield: 31 %. Mp: 289–293 °C.  $^1\text{H}$  NMR (500 MHz,  $\text{DMSO}-d_6$ )  $\delta$  = 15.22 (br. s, 1 H, NH), 8.68 (d,  $J$  = 8.8 Hz, 1 H), 8.23 (d,  $J$  = 2.5 Hz, 1 H), 8.15–8.06 (m, 2 H), 7.87–7.82 (m, 2 H), 7.79–7.70 (m, 2 H), 7.54 (dd,  $J$  = 8.8, 2.5 Hz, 1 H), 7.53–7.47 (m, 2 H), 7.45–7.39 (m, 1 H) ppm.

$^{13}\text{C}$  NMR (125 MHz,  $\text{DMSO}-d_6$ )  $\delta$  = 168.3, 163.9, 143.2, 140.2, 139.0, 133.8, 133.8, 132.9, 129.0, 128.2, 127.9, 126.9, 120.6, 117.4, 115.8, 113.5 ppm.

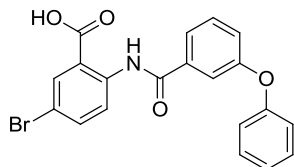
LC/MS:  $m/z$  = 395 [ $2\text{M} - \text{H}^+$ ];  $t_R$  = 13.90 min; 98.3 % pure (UV).



**methyl 5-bromo-2-(3-phenoxybenzamido)benzoate (17a)** was prepared according to method BI. For purification the solvent was evaporated and the remaining solid was suspended in MeOH. After filtration the precipitate was washed with MeOH to provide the pure compound; yield: 78 %.  $^1\text{H}$  NMR (500 MHz,  $\text{CDCl}_3$ )  $\delta$  = 11.94 (br. s, 1 H, NH), 8.83 (d,  $J$  = 9.1 Hz, 1 H), 8.19 (d,  $J$  = 2.5 Hz, 1 H), 7.74–7.71 (m, 1 H), 7.70–7.66 (m, 2 H), 7.48 (dd,  $J$  = 7.9, 7.9 Hz, 1 H), 7.42–7.36 (m, 2 H), 7.21 (ddd,  $J$  = 7.9, 2.5, 0.9 Hz, 1 H), 7.19–7.14 (m, 1 H), 7.11–7.07 (m, 2 H), 3.96 (s, 3 H,  $\text{OCH}_3$ ) ppm.

$^{13}\text{C}$  NMR (125 MHz,  $\text{CDCl}_3$ )  $\delta$  = 167.8, 165.0, 158.1, 156.4, 140.7, 137.5, 136.4, 133.4, 130.2, 129.9, 123.9, 122.1, 122.1, 121.4, 119.5, 117.5, 116.7, 115.1, 52.8 ( $\text{OCH}_3$ ) ppm.

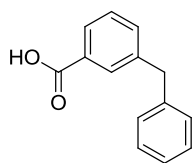
LC/MS:  $m/z$  = no ionization;  $t_R$  = 16.15 min; 95.1 % pure (UV).



**5-bromo-2-(3-phenoxybenzamido)benzoic acid<sup>5</sup> (17)** was prepared according to method C. For purification the remaining solid was washed with hot MeOH to provide the pure compound; yield: 52 %. Mp: 240–242 °C.  $^1\text{H}$  NMR (500 MHz,  $\text{DMSO}-d_6$ )  $\delta$  = 12.05 (br. s, 1 H, NH), 8.59 (d,  $J$  = 9.1 Hz, 1 H), 8.10 (d,  $J$  = 2.5 Hz, 1 H), 7.83 (dd,  $J$  = 9.1, 2.5 Hz, 1 H), 7.72–7.67 (m, 1 H), 7.63–7.57 (m, 1 H), 7.53–7.50 (m, 1 H), 7.47–7.40 (m, 2 H), 7.30–7.26 (m, 1 H), 7.24–7.17 (m, 1 H), 7.14–7.06 (m, 2 H) ppm.

$^{13}\text{C}$  NMR (125 MHz,  $\text{DMSO}-d_6$ )  $\delta$  = 168.6, 163.9, 157.3, 156.0, 140.0, 136.7, 136.2, 133.2, 130.8, 130.2, 130.1, 124.1, 122.2, 122.1, 121.6, 119.0, 116.9, 114.5 ppm.

LC/MS:  $m/z$  = 409 and 411 [ $\text{M} - \text{H}^+$ ];  $t_R$  = 13.90 min; 95.2 % pure (UV).

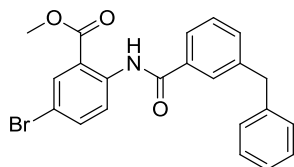


**3-benzylbenzoic acid (18d).** A mixture of methyl 3-(bromomethyl)benzoate (1 equiv), phenylboronic acid (1.5 equiv),  $\text{CsCO}_3$  (3 equiv) and tetrakis(triphenylphosphine)-palladium (0.01 equiv) in a degassed DME/water (1:1) solution was refluxed under a nitrogen atmosphere for 18 h. The reaction mixture was cooled to room temperature. The mixture was extracted with EtOAc. The combined organic layers were washed with 1 M HCl and dried over  $\text{MgSO}_4$ . The product was purified by CC ( $\text{CH}_2\text{Cl}_2$ ); yield: 81 %.  $^1\text{H}$  NMR (500 MHz, Acetone- $d_6$ )  $\delta$  = 7.93–7.92 (m, 1H), 7.89–7.87 (m, 1H), 7.52–7.50 (m, 1H), 7.44–7.41 (m, 1H), 7.31–7.26 (m, 4H), 7.22–7.17 (m, 1H), 4.07 (s, 2H,  $\text{CH}_2$ ) ppm.



$^{13}\text{C}$  NMR (125 MHz, Acetone- $d_6$ )  $\delta$  = 167.7, 143.0, 141.9, 134.3, 131.7, 130.9, 129.8, 129.5, 129.5, 128.3, 127.1, 42.1 ( $\text{CH}_2$ ) ppm.

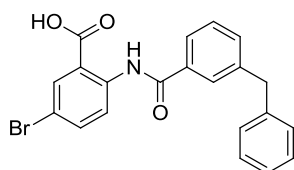
LC/MS:  $m/z$  = no ionization;  $t_R$  = 11.15 min; 98.4 % pure (UV).



**methyl 2-(3-benzylbenzamido)-5-bromobenzoate (18a)** was prepared according to method BII. For purification the solvent was evaporated and the remaining solid was suspended in MeOH. After filtration the precipitate was washed with MeOH to provide the pure compound; yield: 23 %.  $^1\text{H}$  NMR (500 MHz,  $\text{CDCl}_3$ )  $\delta$  = 11.94 (s, 1H), 8.87 (d,  $J$  = 9.0 Hz, 1H), 8.21 (d,  $J$  = 2.4 Hz, 1H), 7.93–7.89 (m, 1H), 7.89–7.82 (m, 1H), 7.69 (dd,  $J$  = 2.4, 9.0 Hz, 1H), 7.46–7.43 (m, 1H), 7.42–7.37 (m, 1H), 7.35–7.29 (m, 2H), 7.26–7.20 (m, 3H), 4.09 (s, 2H,  $\text{CH}_2$ ), 3.98 (s, 3H,  $\text{CH}_3$ ) ppm.

$^{13}\text{C}$  NMR (125 MHz,  $\text{CDCl}_3$ )  $\delta$  = 167.8, 165.8, 142.1, 140.9, 140.4, 137.5, 134.7, 133.4, 132.7, 129.0, 129.0, 128.6, 128.2, 126.3, 124.9, 122.1, 116.7, 114.9, 52.8 ( $\text{CH}_3$ ), 41.8 ( $\text{CH}_2$ ) ppm.

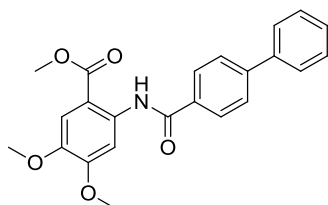
LC/MS:  $m/z$  = 424 and 426 [ $\text{M} + \text{H}^+$ ];  $t_R$  = 16.82 min; 99.5 % pure (UV).



**2-(3-benzylbenzamido)-5-bromobenzoic acid (18)** was prepared according to method C. Sufficient purity was achieved without further purification; yield: 98 %. Mp: 225–227 °C.  $^1\text{H}$  NMR (500 MHz,  $\text{DMSO}-d_6$ )  $\delta$  = 12.06 (s, 1H), 8.62 (d,  $J$  = 9.1 Hz, 1H), 8.10 (d,  $J$  = 2.2 Hz, 1H), 7.85–7.80 (m, 2H), 7.77–7.72 (m, 1H), 7.52–7.47 (m, 2H), 7.32–7.24 (m, 4H), 7.22–7.16 (m, 1H), 4.04 (s, 2H,  $\text{CH}_2$ ) ppm.

$^{13}\text{C}$  NMR (125 MHz, DMSO- $d_6$ )  $\delta$  = 168.8, 164.9, 142.4, 140.8, 140.3, 136.8, 134.5, 133.3, 132.8, 129.2, 128.8, 128.7, 127.6, 126.3, 124.7, 122.1, 118.9, 114.4, 41.0 ( $\text{CH}_2$ ) ppm.

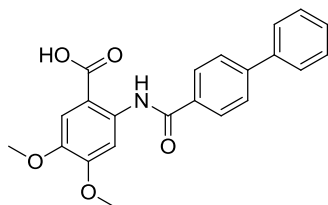
LC/MS:  $m/z$  = 410 and 412 [ $\text{M} + \text{H}^+$ ];  $t_R$  = 14.62 min; 100.0 % pure (UV).



**methyl 2-([1,1'-biphenyl]-4-ylcarboxamido)-4,5-dimethoxybenzoate (19a)** was prepared according to method BI. For purification the solvent was evaporated and the remaining solid was suspended in MeOH. After filtration the precipitate was washed with MeOH to provide the pure compound; yield: 40 %.  $^1\text{H}$  NMR (500 MHz,  $\text{CDCl}_3$ )  $\delta$  = 12.21 (br. s, 1 H, NH), 8.75 (s, 1 H), 8.15–8.12 (m, 2 H), 7.78–7.75 (m, 2 H), 7.68–7.65 (m, 2 H), 7.52 (s, 1 H), 7.51–7.47 (m, 2 H), 7.44–7.39 (m, 1 H), 4.05 (s, 3 H,  $\text{OCH}_3$ ), 3.97 (s, 3 H,  $\text{OCH}_3$ ), 3.93 (s, 3 H,  $\text{OCH}_3$ ) ppm.

$^{13}\text{C}$  NMR (125 MHz,  $\text{CDCl}_3$ )  $\delta$  = 168.8, 165.4, 154.1, 144.6, 144.0, 140.0, 138.1, 133.5, 128.9, 128.0, 127.8, 127.5, 127.2, 112.1, 106.8, 103.4, 56.2 ( $\text{OCH}_3$ ), 56.1 ( $\text{OCH}_3$ ), 52.3 ( $\text{OCH}_3$ ) ppm.

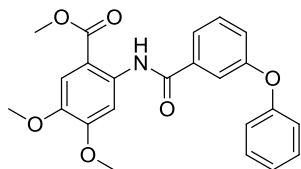
LC/MS:  $m/z$  = 392 [ $\text{M} + \text{H}^+$ ];  $t_R$  = 14.81 min; 98.4 % pure (UV).



**2-([1,1'-biphenyl]-4-ylcarboxamido)-4,5-dimethoxybenzoic acid (19)** was prepared according to method C. Sufficient purity was achieved without further purification; yield: 29 %. Mp: 185 °C (decomposition).  $^1\text{H}$  NMR (500 MHz, DMSO- $d_6$ )  $\delta$  = 14.78 (br. s, 1 H, NH), 8.54 (s, 1 H), 8.14–8.08 (m, 2 H), 7.78–7.73 (m, 2 H), 7.72–7.61 (m, 3 H), 7.56–7.33 (m, 3 H), 3.81 (s, 3 H,  $\text{OCH}_3$ ), 3.74 (s, 3 H,  $\text{OCH}_3$ ) ppm.

$^{13}\text{C}$  NMR (125 MHz,  $\text{DMSO-}d_6$ )  $\delta$  = 163.4, 150.5, 143.2, 142.9, 139.0, 135.7, 134.1, 129.0, 128.1, 127.8, 126.8, 126.8, 117.6, 117.4, 114.3, 102.6, 55.5 ( $\text{OCH}_3$ ), 55.4 ( $\text{OCH}_3$ ) ppm.

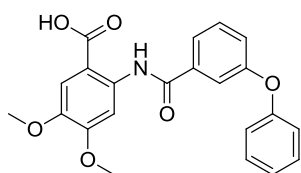
LC/MS:  $m/z$  = 378 [ $\text{M} + \text{H}^+$ ];  $t_R$  = 12.37 min; 95.6 % pure (UV).



**methyl 4,5-dimethoxy-2-(3-phenoxybenzamido)benzoate (20a)** was prepared according to method BI. For purification the solvent was evaporated and the remaining solid was suspended in MeOH. After filtration the precipitate was washed with MeOH to provide the pure compound; yield: 57 %.  $^1\text{H}$  NMR (500 MHz,  $\text{CDCl}_3$ )  $\delta$  = 12.12 (br. s, 1 H, NH), 8.67 (s, 1 H), 7.76–7.73 (m, 1 H), 7.69 (dd,  $J$  = 2.0, 2.0 Hz, 1 H), 7.51–7.47 (m, 2 H), 7.40–7.34 (m, 2 H), 7.21 (ddd,  $J$  = 8.2, 2.5, 0.9 Hz, 1 H), 7.17–7.12 (m, 1 H), 7.12–7.06 (m, 2 H), 4.01 (s, 3 H,  $\text{OCH}_3$ ), 3.93 (s, 3 H,  $\text{OCH}_3$ ), 3.91 (s, 3 H,  $\text{OCH}_3$ ) ppm.

$^{13}\text{C}$  NMR (125 MHz,  $\text{CDCl}_3$ )  $\delta$  = 168.6, 165.0, 158.1, 156.5, 154.0, 144.0, 137.9, 136.8, 130.1, 129.9, 123.8, 122.0, 121.3, 119.4, 117.4, 112.1, 106.8, 103.3, 56.1 ( $\text{OCH}_3$ ), 56.1 ( $\text{OCH}_3$ ), 52.2 ( $\text{OCH}_3$ ) ppm.

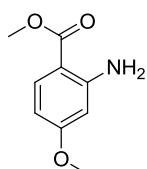
LC/MS:  $m/z$  = 408 [ $\text{M} + \text{H}^+$ ], 815 [ $2\text{M} + \text{H}^+$ ];  $t_R$  = 14.56 min; 95.5 % pure (UV).



**4,5-dimethoxy-2-(3-phenoxybenzamido)benzoic acid (20)** was prepared according to method C. Sufficient purity was achieved without further purification; yield: 98 %. Mp: 218–219 °C.  $^1\text{H}$  NMR (500 MHz,  $\text{DMSO-}d_6$ )  $\delta$  = 12.29 (br. s, 1 H, NH), 8.45 (s, 1 H), 7.70–7.66 (m, 1 H), 7.59 (dd,  $J$  = 7.9, 7.9 Hz, 1 H), 7.52–7.49 (m, 1 H), 7.49–7.41 (m, 3 H), 7.27 (ddd,  $J$  = 8.2, 2.5, 0.9 Hz, 1 H), 7.21 (tt,  $J$  = 7.5, 1.0 Hz, 1 H), 7.14–7.06 (m, 2 H), 3.84 (s, 3 H,  $\text{OCH}_3$ ), 3.78 (s, 3 H,  $\text{OCH}_3$ ) ppm.

$^{13}\text{C}$  NMR (125 MHz,  $\text{DMSO}-d_6$ )  $\delta$  = 169.8, 163.6, 157.4, 155.9, 153.3, 143.8, 136.7, 136.5, 130.8, 130.3, 124.1, 121.9, 121.3, 119.2, 116.7, 112.8, 107.8, 103.1, 55.6 ( $\text{OCH}_3$ ), 55.6 ( $\text{OCH}_3$ ) ppm.

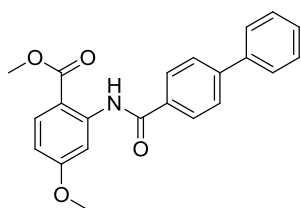
LC/MS:  $m/z$  = 394 [ $\text{M} + \text{H}^+$ ], 435 [ $\text{M} + \text{H}^+ \text{CH}_3\text{CN}$ ];  $t_R$  = 12.32 min; 96.9 % pure (UV).



**methyl 2-amino-4-methoxybenzoate (21b)** was prepared according to method A. The product was purified by CC (*n*-hexane/EtOAc 6:4); yield: 12 %.  $^1\text{H}$  NMR (500 MHz,  $\text{CDCl}_3$ )  $\delta$  = 7.79 (d,  $J$  = 8.8 Hz, 1 H), 6.24 (dd,  $J$  = 8.8, 2.2 Hz, 1 H), 6.11 (d,  $J$  = 2.2 Hz, 1 H), 5.80 (br. s, 2 H,  $\text{NH}_2$ ), 3.84 (s, 3 H,  $\text{OCH}_3$ ), 3.79 (s, 3 H,  $\text{OCH}_3$ ) ppm.

$^{13}\text{C}$  NMR (125 MHz,  $\text{CDCl}_3$ )  $\delta$  = 168.3, 164.2, 152.4, 133.0, 104.5, 104.4, 99.4, 55.1 ( $\text{OCH}_3$ ), 51.2 ( $\text{OCH}_3$ ) ppm.

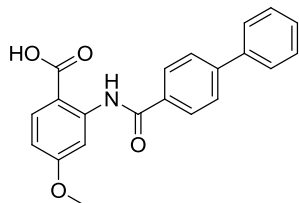
LC/MS:  $m/z$  = 182 [ $\text{M} + \text{H}^+$ ];  $t_R$  = 8.73 min; 100.0 % pure (UV).



**methyl 2-([1,1'-biphenyl]-4-ylcarboxamido)-4-methoxybenzoate (21a)** was prepared according to method BI. For purification the solvent was evaporated and the remaining solid was suspended in MeOH. After filtration the precipitate was washed with MeOH to provide the pure compound; yield: 26 %.  $^1\text{H}$  NMR (500 MHz,  $\text{CDCl}_3$ )  $\delta$  = 12.32 (br. s, 1 H, NH), 8.66 (d,  $J$  = 2.5 Hz, 1 H), 8.17–8.13 (m, 2 H), 8.02 (d,  $J$  = 8.8 Hz, 1 H), 7.78–7.75 (m, 2 H), 7.68–7.64 (m, 2 H), 7.51–7.47 (m, 2 H), 7.44–7.39 (m, 1 H), 6.67 (dd,  $J$  = 8.8, 2.5 Hz, 1 H), 3.96 (s, 3 H,  $\text{OCH}_3$ ), 3.95 (s, 3 H,  $\text{OCH}_3$ ) ppm.

$^{13}\text{C}$  NMR (125 MHz,  $\text{CDCl}_3$ )  $\delta$  = 169.0, 165.7, 164.7, 144.7, 144.1, 140.0, 133.5, 132.5, 128.9, 128.0, 127.9, 127.5, 127.2, 110.2, 107.7, 103.9, 55.6 ( $\text{OCH}_3$ ), 52.2 ( $\text{OCH}_3$ ) ppm.

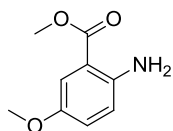
LC/MS:  $m/z = 362$   $[M + H^+]$ ,  $403$   $[M + H^+ CH_3CN]$ ,  $723$   $[2M + H^+]$ ;  $t_R = 15.61$  min; 99.6 % pure (UV).



**2-([1,1'-biphenyl]-4-ylcarboxamido)-4-methoxybenzoic acid (21)** was prepared according to method C. Sufficient purity was achieved without further purification; yield: 98 %. Mp: 248–249 °C.  $^1H$  NMR (500 MHz, DMSO- $d_6$ )  $\delta = 12.51$  (br. s, 1 H, NH), 8.44 (d,  $J = 2.5$  Hz, 1 H), 8.06–7.99 (m, 3 H), 7.92–7.85 (m, 2 H), 7.78–7.73 (m, 2 H), 7.55–7.48 (m, 2 H), 7.47–7.39 (m, 1 H), 6.77 (dd,  $J = 8.8, 2.5$  Hz, 1 H), 3.86 (s, 3 H, OCH<sub>3</sub>) ppm.

$^{13}C$  NMR (125 MHz, DMSO- $d_6$ )  $\delta = 170.1, 164.5, 163.8, 143.8, 143.3, 138.9, 133.2, 133.2, 129.1, 128.3, 127.7, 127.2, 127.0, 108.8, 108.5, 104.5, 55.6$  (OCH<sub>3</sub>) ppm.

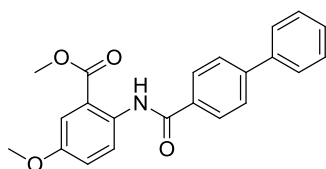
LC/MS:  $m/z = 348$   $[M + H^+]$ ,  $389$   $[M + H^+ CH_3CN]$ ,  $695$   $[2M + H^+]$ ;  $t_R = 13.50$  min; 100.0 % pure (UV).



**methyl 2-amino-5-methoxybenzoate (22b)** was prepared according to method A. Sufficient purity was achieved without further purification; yield: 62 %.  $^1H$  NMR (500 MHz, CDCl<sub>3</sub>)  $\delta = 7.36$  (d,  $J = 3.2$  Hz, 1 H), 6.96 (dd,  $J = 8.8, 3.2$  Hz, 1 H), 6.64 (d,  $J = 8.8$  Hz, 1 H), 5.43 (br. s, 2 H, NH<sub>2</sub>), 3.88 (s, 3 H, OCH<sub>3</sub>), 3.77 (s, 3 H, OCH<sub>3</sub>) ppm.

$^{13}C$  NMR (125 MHz, CDCl<sub>3</sub>)  $\delta = 168.3, 150.5, 145.1, 123.3, 118.2, 113.1, 110.7, 55.8$  (OCH<sub>3</sub>), 51.6 (OCH<sub>3</sub>) ppm.

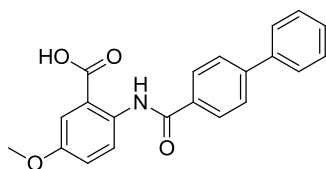
LC/MS:  $m/z = 182$   $[M + H^+]$ ,  $223$   $[M + H^+ CH_3CN]$ ;  $t_R = 5.88$  min; 95.2 % pure (UV).



**methyl 2-([1,1'-biphenyl]-4-ylcarboxamido)-5-methoxybenzoate (22a)** was prepared according to method BII. For purification the solvent was evaporated and the remaining solid was suspended in MeOH. After filtration the precipitate was washed with MeOH to provide the pure compound; yield: 82 %.  $^1\text{H}$  NMR (500 MHz,  $\text{CDCl}_3$ )  $\delta$  = 11.85 (br. s, 1 H, NH), 8.91 (d,  $J$  = 9.1 Hz, 1 H), 8.13–8.11 (m, 2 H), 7.77–7.74 (m, 2 H), 7.67–7.64 (m, 2 H), 7.59 (d,  $J$  = 3.2 Hz, 1 H), 7.50–7.47 (m, 2 H), 7.44–7.38 (m, 1 H), 7.21 (dd,  $J$  = 9.1, 3.2 Hz, 1 H), 3.99 (s, 3 H,  $\text{OCH}_3$ ), 3.86 (s, 3 H,  $\text{OCH}_3$ ) ppm.

$^{13}\text{C}$  NMR (125 MHz,  $\text{CDCl}_3$ )  $\delta$  = 168.8, 165.0, 154.5, 144.5, 140.1, 135.6, 133.7, 128.9, 128.0, 127.8, 127.4, 127.2, 122.0, 121.2, 116.1, 114.7, 55.6 ( $\text{OCH}_3$ ), 52.6 ( $\text{OCH}_3$ ) ppm.

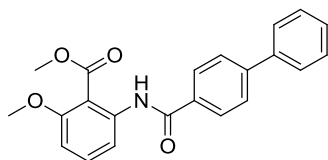
LC/MS:  $m/z$  = 362 [ $\text{M} + \text{H}^+$ ], 403 [ $\text{M} + \text{H}^+ \text{CH}_3\text{CN}$ ], 723 [ $2\text{M} + \text{H}^+$ ];  $t_R$  = 15.45 min; 98.1 % pure (UV).



**2-([1,1'-biphenyl]-4-ylcarboxamido)-5-methoxybenzoic acid (22)** was prepared according to method C. For purification the remaining solid was washed with MeOH and  $\text{CH}_2\text{Cl}_2$  to provide the pure compound; yield: 92 %. Mp: 236–239 °C.  $^1\text{H}$  NMR (500 MHz,  $\text{DMSO}-d_6$ )  $\delta$  = 11.90 (br. s, 1 H, NH), 8.61 (d,  $J$  = 9.1 Hz, 1 H), 8.04–8.00 (m, 2 H), 7.89–7.86 (m, 2 H), 7.77–7.73 (m, 2 H), 7.54 (d,  $J$  = 2.8 Hz, 1 H), 7.53–7.48 (m, 2 H), 7.45–7.39 (m, 1 H), 7.28 (dd,  $J$  = 9.1, 2.8 Hz, 1 H), 3.80 (s, 3 H,  $\text{OCH}_3$ ) ppm.

$^{13}\text{C}$  NMR (125 MHz,  $\text{DMSO}-d_6$ )  $\delta$  = 169.6, 163.9, 154.4, 143.5, 138.9, 134.5, 133.4, 129.1, 128.2, 127.6, 127.1, 126.9, 121.9, 120.3, 118.2, 115.0, 55.4 ( $\text{OCH}_3$ ) ppm.

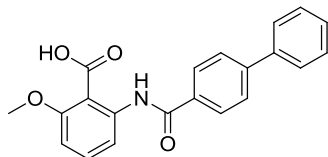
LC/MS:  $m/z$  = 348 [ $\text{M} + \text{H}^+$ ], 695 [ $2\text{M} + \text{H}^+$ ];  $t_R$  = 13.07 min; 96.8 % pure (UV).



**methyl 2-([1,1'-biphenyl]-4-ylcarboxamido)-6-methoxybenzoate (23a)** was prepared according to method BIII. For purification the solvent was evaporated and the remaining solid was suspended in MeOH. After filtration the precipitate was washed with MeOH to provide the pure compound; yield: 46 %.  $^1\text{H}$  NMR (500 MHz,  $\text{CDCl}_3$ )  $\delta$  = 10.78 (br. s, 1 H, NH), 8.31 (dd,  $J$  = 8.5, 0.9 Hz, 1 H), 8.07–8.04 (m, 2 H), 7.76–7.73 (m, 2 H), 7.67–7.64 (m, 2 H), 7.51–7.47 (m, 3 H), 7.44–7.39 (m, 1 H), 6.76 (dd,  $J$  = 8.5, 0.9 Hz, 1 H), 3.99 (s, 3 H,  $\text{OCH}_3$ ), 3.90 (s, 3 H,  $\text{OCH}_3$ ) ppm.

$^{13}\text{C}$  NMR (125 MHz,  $\text{CDCl}_3$ )  $\delta$  = 169.2, 165.1, 159.4, 144.7, 140.2, 140.0, 133.4, 133.4, 128.9, 128.0, 127.8, 127.4, 127.2, 113.8, 109.4, 107.2, 56.3 ( $\text{OCH}_3$ ), 52.6 ( $\text{OCH}_3$ ) ppm.

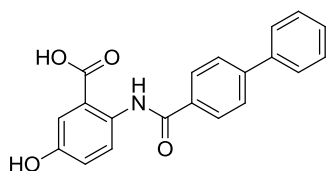
LC/MS:  $m/z$  = 362 [ $\text{M} + \text{H}^+$ ], 723 [ $2\text{M} + \text{H}^+$ ];  $t_{\text{R}}$  = 13.57 min; 96.5 % pure (UV).



**2-([1,1'-biphenyl]-4-ylcarboxamido)-6-methoxybenzoic acid (23)** was prepared according to method C. Sufficient purity was achieved without further purification; yield: 90 %. Mp: 158–162 °C.  $^1\text{H}$  NMR (500 MHz,  $\text{DMSO}-d_6$ )  $\delta$  = 10.44 (br. s, 1 H, NH), 8.02–7.99 (m, 2 H), 7.86–7.83 (m, 2 H), 7.77–7.75 (m, 2 H), 7.53–7.46 (m, 4 H), 7.45–7.41 (m, 1 H), 6.98 (dd,  $J$  = 7.9, 1.6 Hz, 1 H), 3.83 (s, 3 H,  $\text{OCH}_3$ ) ppm.

$^{13}\text{C}$  NMR (125 MHz,  $\text{DMSO}-d_6$ )  $\delta$  = 167.7, 164.7, 157.5, 143.4, 139.0, 137.2, 133.1, 131.3, 129.1, 128.2, 128.1, 126.9, 126.8, 116.8, 116.6, 108.6, 56.1 ( $\text{OCH}_3$ ) ppm.

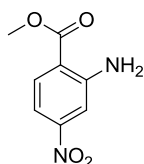
LC/MS:  $m/z$  = 348 [ $\text{M} + \text{H}^+$ ], 695 [ $2\text{M} + \text{H}^+$ ];  $t_{\text{R}}$  = 13.30 min; 99.2 % pure (UV).



**2-([1,1'-biphenyl]-4-ylcarboxamido)-5-hydroxybenzoic acid (24)** was prepared according to method E. The product was purified by CC (starting with *n*-hexane/EtOAc 1:1 to EtOAc + 3 % formic acid) followed by preparative TLC ( $\text{CH}_2\text{Cl}_2$  + 7 drops formic acid per 10 mL solvent); yield: 34 %. Mp: 193–196 °C.  $^1\text{H}$  NMR (500 MHz,  $\text{DMSO}-d_6$ )  $\delta$  = 11.88 (br. s, 1 H, NH), 9.64 (br. s, 1 H, ArOH), 8.51 (d,  $J$  = 8.8 Hz, 1 H), 8.03–8.00 (m, 2 H), 7.89–7.85 (m, 2 H), 7.78–7.74 (m, 2 H), 7.53–7.49 (m, 2 H), 7.46 (d,  $J$  = 2.8 Hz, 1 H), 7.45–7.38 (m, 1 H), 7.08 (dd,  $J$  = 8.8, 2.8 Hz, 1 H) ppm.

$^{13}\text{C}$  NMR (125 MHz,  $\text{DMSO}-d_6$ )  $\delta$  = 169.8, 163.7, 152.7, 143.3, 139.0, 133.6, 133.1, 129.1, 128.2, 127.6, 127.1, 126.9, 121.9, 121.1, 118.4, 116.8 ppm.

LC/MS:  $m/z$  = 334  $[\text{M} + \text{H}^+]$ , 667  $[2\text{M} + \text{H}^+]$ ;  $t_{\text{R}}$  = 11.31 min; 96.6 % pure (UV).

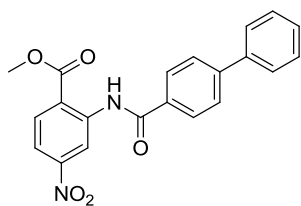


**methyl 2-amino-4-nitrobenzoate (25b)** was prepared according to method A. The product was purified by CC (*n*-hexane/EtOAc 6:4); yield: 37 %.  $^1\text{H}$  NMR (500 MHz,  $\text{CDCl}_3$ )  $\delta$  = 8.01 (d,  $J$  = 8.8 Hz, 1 H), 7.51 (d,  $J$  = 2.2 Hz, 1 H), 7.41 (dd,  $J$  = 8.8, 2.2 Hz, 1 H), 6.06 (br. s, 2 H,  $\text{NH}_2$ ), 3.93 (s, 3 H,  $\text{OCH}_3$ ) ppm.

$^{13}\text{C}$  NMR (125 MHz,  $\text{CDCl}_3$ )  $\delta$  = 167.3, 151.3, 150.7, 132.8, 114.9, 111.1, 110.1, 52.2 ( $\text{OCH}_3$ ) ppm.

LC/MS:  $m/z$  = no ionization;  $t_{\text{R}}$  = 10.08 min; 100.0 % pure (UV).

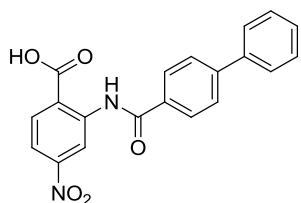




**methyl 2-([1,1'-biphenyl]-4-ylcarboxamido)-4-nitrobenzoate (25a)** was prepared according to method BI. For purification the solvent was evaporated and the remaining solid was suspended in MeOH. After filtration the precipitate was exhaustively washed with MeOH and CH<sub>2</sub>Cl<sub>2</sub> to provide the pure compound; yield: 15 %. <sup>1</sup>H NMR (500 MHz, CDCl<sub>3</sub>) δ = 12.17 (br. s, 1 H, NH), 9.89 (d, *J* = 2.2 Hz, 1 H), 8.28 (d, *J* = 8.8 Hz, 1 H), 8.21–8.10 (m, 2 H), 7.94 (dd, *J* = 8.8, 2.2 Hz, 1 H), 7.84–7.73 (m, 2 H), 7.72–7.61 (m, 2 H), 7.54–7.47 (m, 2 H), 7.47–7.39 (m, 1 H), 4.07 (s, 3 H, OCH<sub>3</sub>) ppm.

<sup>13</sup>C NMR (125 MHz, CDCl<sub>3</sub>) δ = 167.8, 165.6, 151.4, 145.3, 142.9, 139.8, 132.5, 132.1, 129.0, 128.2, 128.0, 127.6, 127.3, 119.3, 116.6, 115.5, 53.3 (OCH<sub>3</sub>) ppm.

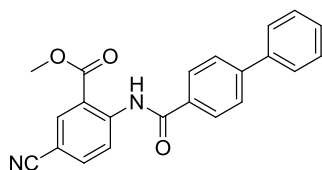
LC/MS: *m/z* = 377 [M + H<sup>+</sup>], 418 [M + H<sup>+</sup> CH<sub>3</sub>CN]; *t<sub>R</sub>* = 15.03 min; 97.6 % pure (UV).



**2-([1,1'-biphenyl]-4-ylcarboxamido)-4-nitrobenzoic acid (25)** was prepared according to method C. For purification the remaining solid was washed with MeOH and CH<sub>2</sub>Cl<sub>2</sub> to provide the pure compound; yield: 94 %. Mp: 280–283 °C. <sup>1</sup>H NMR (500 MHz, DMSO-*d*<sub>6</sub>) δ = 12.48 (br. s, 1 H, NH), 9.55 (d, *J* = 2.2 Hz, 1 H), 8.28 (d, *J* = 8.8 Hz, 1 H), 8.09–8.04 (m, 2 H), 8.01 (dd, *J* = 8.8, 2.2 Hz, 1 H), 7.95–7.90 (m, 2 H), 7.81–7.74 (m, 2 H), 7.56–7.49 (m, 2 H), 7.47–7.41 (m, 1 H) ppm.

<sup>13</sup>C NMR (125 MHz, DMSO-*d*<sub>6</sub>) δ = 168.6, 164.9, 150.2, 144.1, 141.5, 138.8, 132.8, 132.6, 129.1, 128.4, 127.9, 127.3, 127.0, 122.6, 117.2, 114.3 ppm.

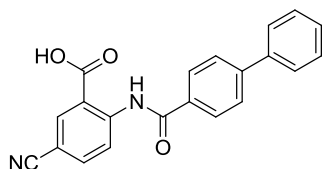
LC/MS: *m/z* = 363 [M + H<sup>+</sup>], 404 [M + H<sup>+</sup> CH<sub>3</sub>CN], 725 [2M + H<sup>+</sup>]; *t<sub>R</sub>* = 13.25 min; 100.0 % pure (UV).



**methyl 2-([1,1'-biphenyl]-4-ylcarboxamido)-5-cyanobenzoate (26a)** was prepared according to method BII. For purification the solvent was evaporated and the remaining solid was suspended in MeOH. After filtration the precipitate was washed with MeOH to provide the pure compound; yield: 43 %.  $^1\text{H}$  NMR (500 MHz,  $\text{CDCl}_3$ )  $\delta$  = 12.29 (br. s, 1 H, NH), 9.13 (d,  $J$  = 8.8 Hz, 1 H), 8.42 (d,  $J$  = 2.0 Hz, 1 H), 8.13–8.11 (m, 2 H), 7.84 (dd,  $J$  = 8.8, 2.0 Hz, 1 H), 7.79–7.76 (m, 2 H), 7.67–7.64 (m, 2 H), 7.51–7.48 (m, 2 H), 7.45–7.40 (m, 1 H), 4.04 (s, 3 H,  $\text{OCH}_3$ ) ppm.

$^{13}\text{C}$  NMR (125 MHz,  $\text{CDCl}_3$ )  $\delta$  = 167.6, 165.6, 145.4, 145.3, 139.7, 137.6, 135.4, 132.5, 129.0, 128.2, 128.0, 127.6, 127.2, 120.9, 118.0, 115.3, 105.9, 53.1 ( $\text{OCH}_3$ ) ppm.

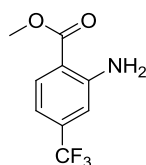
LC/MS:  $m/z$  = 357 [ $\text{M} + \text{H}^+$ ], 713 [ $2\text{M} + \text{H}^+$ ];  $t_{\text{R}}$  = 15.32 min; 97.2 % pure (UV).



**2-([1,1'-biphenyl]-4-ylcarboxamido)-5-cyanobenzoic acid<sup>5</sup> (26)** was prepared according to method C. Sufficient purity was achieved without further purification; yield: 80 %. Mp: 246–247 °C.  $^1\text{H}$  NMR (500 MHz,  $\text{DMSO}-d_6$ )  $\delta$  = 12.46 (br. s, 1 H, NH), 8.87 (d,  $J$  = 8.8 Hz, 1 H), 8.38 (d,  $J$  = 2.0 Hz, 1 H), 8.07 (dd,  $J$  = 8.8, 2.0 Hz, 1 H), 8.04–8.01 (m, 2 H), 7.90–7.87 (m, 2 H), 7.77–7.73 (m, 2 H), 7.53–7.48 (m, 2 H), 7.46–7.41 (m, 1 H) ppm.

$^{13}\text{C}$  NMR (125 MHz,  $\text{DMSO}-d_6$ )  $\delta$  = 168.6, 164.7, 144.6, 144.1, 138.7, 137.5, 135.4, 132.5, 129.1, 128.4, 127.9, 127.2, 127.0, 120.2, 118.1, 117.2, 105.0 ppm.

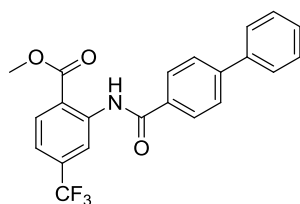
LC/MS:  $m/z$  = 343 [ $\text{M} + \text{H}^+$ ], 685 [ $2\text{M} + \text{H}^+$ ];  $t_{\text{R}}$  = 13.30 min; 97.5 % pure (UV).



**methyl 2-amino-4-(trifluoromethyl)benzoate (27b)** was prepared according to method A. The product was purified by CC (*n*-hexane/EtOAc 1:1); yield: 61 %.  $^1\text{H}$  NMR (500 MHz,  $\text{CDCl}_3$ )  $\delta$  = 7.96 (d,  $J$  = 8.2 Hz, 1 H), 6.93–6.89 (m, 1 H), 6.88–6.82 (m, 1 H), 5.92 (br. s, 2 H,  $\text{NH}_2$ ), 3.91 (s, 3 H,  $\text{OCH}_3$ ) ppm.

$^{13}\text{C}$  NMR (125 MHz,  $\text{CDCl}_3$ )  $\delta$  = 167.7, 150.2, 135.7 (q,  $J_{\text{CF}}$  = 32.1 Hz), 132.2, 120.3 (q,  $J_{\text{CF}}$  = 272.0 Hz), 113.4 (q,  $J_{\text{CF}}$  = 3.7 Hz), 113.0 (q,  $J_{\text{CF}}$  = 1.8 Hz), 112.3 (q,  $J_{\text{CF}}$  = 3.7 Hz), 51.9 ( $\text{OCH}_3$ ) ppm.

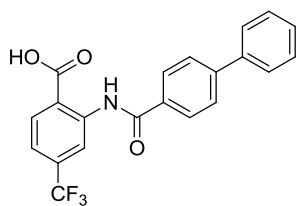
LC/MS:  $m/z$  = 261 [ $\text{M} + \text{H}^+$   $\text{CH}_3\text{CN}$ ];  $t_{\text{R}}$  = 12.01 min; 85.2 % pure (UV).



**methyl 2-([1,1'-biphenyl]-4-ylcarboxamido)-4-(trifluoromethyl)benzoate (27a)** was prepared according to method BII. For purification the solvent was evaporated and the remaining solid was suspended in MeOH. After filtration the precipitate was washed with MeOH to provide the pure compound; yield: 22 %.  $^1\text{H}$  NMR (500 MHz,  $\text{CDCl}_3$ )  $\delta$  = 12.16 (br. s, 1 H, NH), 9.36 (dd,  $J$  = 1.3, 0.6 Hz, 1 H), 8.22 (d,  $J$  = 8.2 Hz, 1 H), 8.15–8.12 (m, 2 H), 7.79–7.76 (m, 2 H), 7.68–7.64 (m, 2 H), 7.51–7.47 (m, 2 H), 7.46–7.40 (m, 1 H), 7.38 (ddd,  $J$  = 8.2, 1.3, 0.6 Hz, 1 H), 4.04 (s, 3 H,  $\text{OCH}_3$ ) ppm.

$^{13}\text{C}$  NMR (125 MHz,  $\text{CDCl}_3$ )  $\delta$  = 168.2, 165.6, 145.1, 142.3, 139.9, 136.1 (q,  $J_{\text{CF}}$  = 32.0 Hz), 132.9, 131.6, 129.0, 128.2, 127.9, 127.6, 127.2, 123.4 (q,  $J_{\text{CF}}$  = 273.1 Hz), 118.9 (q,  $J_{\text{CF}}$  = 3.7 Hz), 117.5 (q,  $J_{\text{CF}}$  = 4.2 Hz), 53.0 ( $\text{OCH}_3$ ) ppm.

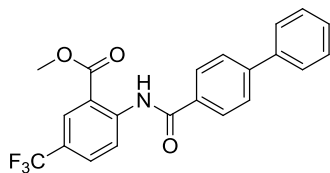
LC/MS:  $m/z$  = 400 [ $\text{M} + \text{H}^+$ ], 441 [ $\text{M} + \text{H}^+$   $\text{CH}_3\text{CN}$ ], 799 [ $2\text{M} + \text{H}^+$ ];  $t_{\text{R}}$  = 16.51 min; 100.0 % pure (UV).



**2-([1,1'-biphenyl]-4-ylcarboxamido)-4-(trifluoromethyl)benzoic acid (27)** was prepared according to method C. Sufficient purity was achieved without further purification; yield: 84 %. Mp: 245–246 °C.  $^1\text{H}$  NMR (500 MHz,  $\text{DMSO}-d_6$ )  $\delta$  = 12.35 (br. s, 1 H, NH), 9.10 (d,  $J$  = 1.6 Hz, 1 H), 8.26 (d,  $J$  = 8.2 Hz, 1 H), 8.08–8.04 (m, 2 H), 7.95–7.89 (m, 2 H), 7.81–7.75 (m, 2 H), 7.57 (dd,  $J$  = 8.2, 1.6 Hz, 1 H), 7.55–7.49 (m, 2 H), 7.47–7.41 (m, 1 H) ppm.

$^{13}\text{C}$  NMR (125 MHz,  $\text{DMSO}-d_6$ )  $\delta$  = 169.0, 164.8, 144.0, 141.4, 138.8, 133.4 (q,  $J_{\text{CF}}$  = 32.0 Hz), 132.7, 132.5, 129.1, 128.4, 127.8, 127.2, 127.0, 122.9 (q,  $J_{\text{CF}}$  = 273.1 Hz), 119.2 (q,  $J_{\text{CF}}$  = 3.7 Hz), 116.3 (q,  $J_{\text{CF}}$  = 3.7 Hz) ppm.

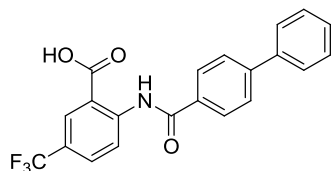
LC/MS:  $m/z$  = 386 [ $\text{M} + \text{H}^+$ ], 427 [ $\text{M} + \text{H}^+ \text{CH}_3\text{CN}$ ], 771 [ $2\text{M} + \text{H}^+$ ];  $t_{\text{R}}$  = 14.11 min; 100.0 % pure (UV).



**methyl 2-([1,1'-biphenyl]-4-ylcarboxamido)-5-(trifluoromethyl)benzoate (28a)** was prepared according to method BII. For purification the solvent was evaporated and the remaining solid was suspended in MeOH. After filtration the precipitate was washed with MeOH followed by CC (*n*-hexane/EtOAc 9:1) to provide the pure compound; yield: 42 %.  $^1\text{H}$  NMR (500 MHz,  $\text{CDCl}_3$ )  $\delta$  = 12.24 (br. s, 1 H, NH), 9.13 (d,  $J$  = 8.8 Hz, 1 H), 8.38 (d,  $J$  = 2.0 Hz, 1 H), 8.15–8.12 (m, 2 H), 7.85 (dd,  $J$  = 8.8, 2.0 Hz, 1 H), 7.79–7.76 (m, 2 H), 7.68–7.65 (m, 2 H), 7.52–7.48 (m, 2 H), 7.45–7.40 (m, 1 H), 4.04 (s, 3 H,  $\text{OCH}_3$ ) ppm.

$^{13}\text{C}$  NMR (125 MHz,  $\text{CDCl}_3$ )  $\delta$  = 168.2, 165.6, 145.2, 144.6, 139.8, 132.9, 131.4 (q,  $J_{\text{CF}}$  = 3.6 Hz), 129.0, 128.3 (q,  $J_{\text{CF}}$  = 3.6 Hz), 128.2, 128.0, 127.6, 127.2, 124.5 (q,  $J_{\text{CF}}$  = 33.9 Hz), 120.6, 122.6 (q,  $J_{\text{CF}}$  = 271.3 Hz), 114.9, 52.9 ( $\text{OCH}_3$ ) ppm.

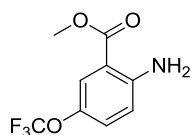
LC/MS:  $m/z = 400 [M + H^+]$ , 441  $[M + H^+ CH_3CN]$ , 799  $[2M + H^+]$ ;  $t_R = 16.70$  min; 95.1 % pure (UV).



**2-([1,1'-biphenyl]-4-ylcarboxamido)-5-(trifluoromethyl)benzoic acid (28)** was prepared according to method C. For purification the remaining solid was washed with MeOH and  $CH_2Cl_2$  to provide the pure compound; yield: 49 %. Mp: 265–266 °C.  $^1H$  NMR (500 MHz,  $DMSO-d_6$ )  $\delta = 12.41$  (br. s, 1 H, NH), 8.93 (d,  $J = 8.8$  Hz, 1 H), 8.28 (d,  $J = 2.0$  Hz, 1 H), 8.06–8.03 (m, 2 H), 8.01 (dd,  $J = 8.8, 2.0$  Hz, 1 H), 7.92–7.87 (m, 2 H), 7.78–7.73 (m, 2 H), 7.54–7.47 (m, 2 H), 7.46–7.40 (m, 1 H) ppm.

$^{13}C$  NMR (125 MHz,  $DMSO-d_6$ )  $\delta = 168.9, 164.7, 144.3, 144.0, 138.8, 132.7, 130.9$  (q,  $J_{CF} = 3.7$  Hz) 129.1, 128.4, 127.9 (q,  $J_{CF} = 3.7$  Hz), 127.8, 127.2, 127.0, 123.8 (q,  $J_{CF} = 271.3$  Hz), 122.8 (q,  $J_{CF} = 33.0$  Hz) 120.4, 116.8 ppm.

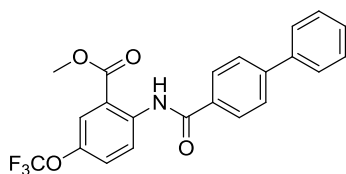
LC/MS:  $m/z = 386 [M + H^+]$ , 771  $[2M + H^+]$ ;  $t_R = 14.60$  min; 99.8 % pure (UV).



**methyl 2-amino-5-(trifluoromethoxy)benzoate (29b)** was prepared according to method A. The product was purified by CC (*n*-hexane/EtOAc 1:1); yield: 26 %.  $^1H$  NMR (500 MHz,  $CDCl_3$ )  $\delta = 7.77$ –7.68 (m, 1 H), 7.20–7.11 (m, 1 H), 6.65 (d,  $J = 9.5$  Hz, 1 H), 5.80 (br. s, 2 H,  $NH_2$ ), 3.89 (s, 3 H,  $OCH_3$ ) ppm.

$^{13}C$  NMR (125 MHz,  $CDCl_3$ )  $\delta = 167.6, 149.2, 138.8$  (q,  $J_{CF} = 1.8$  Hz), 127.9, 123.8, 120.7 (q,  $J_{CF} = 256.0$  Hz), 117.5, 110.5, 51.8 ( $OCH_3$ ) ppm.

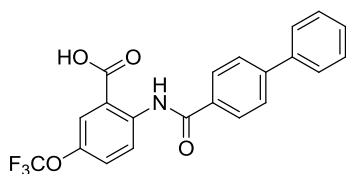
LC/MS:  $m/z = 236 [M + H^+]$ , 277  $[M + H^+ CH_3CN]$ ;  $t_R = 12.13$  min; 96.0 % pure (UV).



**methyl 2-([1,1'-biphenyl]-4-ylcarboxamido)-5-(trifluoromethoxy)benzoate (29a)** was prepared according to method BIII. For purification the solvent was evaporated and the remaining solid was suspended in MeOH. After filtration the precipitate was washed with MeOH to provide the pure compound; yield: 86 %.  $^1\text{H}$  NMR (500 MHz,  $\text{CDCl}_3$ )  $\delta$  = 12.06 (br. s, 1 H, NH), 9.05 (d,  $J$  = 9.1 Hz, 1 H), 8.16–8.09 (m, 2 H), 7.96 (d,  $J$  = 2.5 Hz, 1 H), 7.81–7.74 (m, 2 H), 7.68–7.64 (m, 2 H), 7.51–7.48 (m, 3 H), 7.44–7.40 (m, 1 H), 4.02 (s, 3 H,  $\text{OCH}_3$ ) ppm.

$^{13}\text{C}$  NMR (125 MHz,  $\text{CDCl}_3$ )  $\delta$  = 168.0, 165.5, 145.0, 143.4 (q,  $J_{\text{CF}}$  = 1.8 Hz), 140.7, 139.9, 133.1, 130.7, 129.0, 128.1, 127.9, 127.5, 127.2, 123.4, 122.0, 120.5 (q,  $J_{\text{CF}}$  = 257.5 Hz), 116.1, 52.9 ( $\text{OCH}_3$ ) ppm.

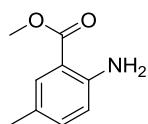
LC/MS:  $m/z$  = 416 [ $\text{M} + \text{H}^+$ ], 457 [ $\text{M} + \text{H}^+ \text{CH}_3\text{CN}$ ], 831 [ $2\text{M} + \text{H}^+$ ];  $t_{\text{R}}$  = 16.64 min; 100.0 % pure (UV).



**2-([1,1'-biphenyl]-4-ylcarboxamido)-5-(trifluoromethoxy)benzoic acid (29)** was prepared according to method C. Sufficient purity was achieved without further purification; yield: 98 %. Mp: 245–246 °C.  $^1\text{H}$  NMR (500 MHz,  $\text{DMSO}-d_6$ )  $\delta$  = 12.17 (br. s, 1 H, NH), 8.81 (d,  $J$  = 9.1 Hz, 1 H), 8.06–8.03 (m, 2 H), 7.92 (dd,  $J$  = 3.0, 0.8 Hz, 1 H), 7.91–7.88 (m, 2 H), 7.78–7.74 (m, 2 H), 7.74–7.68 (m, 1 H), 7.53–7.49 (m, 2 H), 7.46–7.41 (m, 1 H) ppm.

$^{13}\text{C}$  NMR (125 MHz,  $\text{DMSO}-d_6$ )  $\delta$  = 168.6, 164.5, 143.9, 142.7 (q,  $J_{\text{CF}}$  = 1.8 Hz), 140.1, 138.8, 132.9, 129.1, 128.3, 127.8, 127.2, 127.0, 127.0, 123.3, 121.9, 118.6, 120.0 (q,  $J_{\text{CF}}$  = 256.0 Hz) ppm.

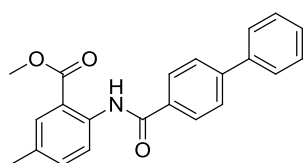
LC/MS:  $m/z$  = 402 [ $\text{M} + \text{H}^+$ ], 803 [ $2\text{M} + \text{H}^+$ ];  $t_{\text{R}}$  = 14.58 min; 100.0 % pure (UV).



**methyl 2-amino-5-methylbenzoate (30b)** was prepared according to method A. Sufficient purity was achieved without further purification; yield: 82 %.  $^1\text{H}$  NMR (500 MHz,  $\text{CDCl}_3$ )  $\delta$  = 7.67 (d,  $J$  = 2.2 Hz, 1 H), 7.10 (dd,  $J$  = 8.2, 2.2 Hz, 1 H), 6.60 (d,  $J$  = 8.2 Hz, 1 H), 5.55 (br. s, 2 H,  $\text{NH}_2$ ), 3.88 (s, 3 H,  $\text{OCH}_3$ ), 2.24 (s, 3 H,  $\text{CH}_3$ ) ppm.

$^{13}\text{C}$  NMR (125 MHz,  $\text{CDCl}_3$ )  $\delta$  = 168.6, 148.3, 135.2, 130.8, 125.4, 116.8, 110.7, 51.4 ( $\text{OCH}_3$ ), 20.2 ( $\text{CH}_3$ ) ppm.

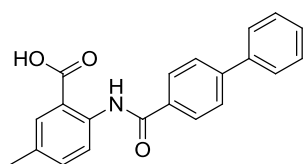
LC/MS:  $m/z$  = no ionization;  $t_R$  = 8.48 min; 98.0 % pure (UV).



**methyl 2-([1,1'-biphenyl]-4-ylcarboxamido)-5-methylbenzoate (30a)** was prepared according to method BII. For purification the solvent was evaporated and the remaining solid was suspended in MeOH. After filtration the precipitate was washed with MeOH to provide the pure compound; yield: 85 %.  $^1\text{H}$  NMR (500 MHz,  $\text{CDCl}_3$ )  $\delta$  = 12.00 (br. s, 1 H, NH), 8.86 (d,  $J$  = 8.8 Hz, 1 H), 8.15–8.12 (m, 2 H), 7.91 (d,  $J$  = 2.2 Hz, 1 H), 7.77–7.75 (m, 2 H), 7.68–7.65 (m, 2 H), 7.51–7.47 (m, 2 H), 7.44 (dd,  $J$  = 8.8, 2.2 Hz, 1 H), 7.43–7.39 (m, 1 H), 3.98 (s, 3 H,  $\text{OCH}_3$ ), 2.38 (s, 3 H,  $\text{CH}_3$ ) ppm.

$^{13}\text{C}$  NMR (125 MHz,  $\text{CDCl}_3$ )  $\delta$  = 169.1, 165.2, 144.5, 140.1, 139.5, 135.6, 133.7, 132.1, 131.0, 128.9, 128.0, 127.9, 127.4, 127.2, 120.4, 115.0, 52.4 ( $\text{OCH}_3$ ), 20.7 ( $\text{CH}_3$ ) ppm.

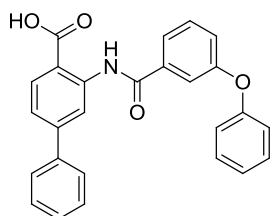
LC/MS:  $m/z$  = 346 [ $\text{M} + \text{H}^+$ ], 691 [ $2\text{M} + \text{H}^+$ ];  $t_R$  = 16.44 min; 99.1 % pure (UV).



**2-([1,1'-biphenyl]-4-ylcarboxamido)-5-methylbenzoic acid (30)** was prepared according to method C. Sufficient purity was achieved without further purification; yield: 95 %. Mp: 246–248 °C.  $^1\text{H}$  NMR (500 MHz,  $\text{DMSO-}d_6$ )  $\delta$  = 12.13 (br. s, 1 H, NH), 8.63 (d,  $J$  = 8.8 Hz, 1 H), 8.05–8.01 (m, 2 H), 7.90–7.86 (m, 3 H), 7.79–7.74 (m, 2 H), 7.53–7.47 (m, 3 H), 7.46–7.40 (m, 1 H), 2.33 (s, 3 H,  $\text{CH}_3$ ) ppm.

$^{13}\text{C}$  NMR (125 MHz,  $\text{DMSO-}d_6$ )  $\delta$  = 170.1, 164.1, 143.6, 138.9, 138.8, 134.8, 133.3, 132.1, 131.3, 129.1, 128.3, 127.6, 127.1, 126.9, 119.9, 116.4, 20.2 ( $\text{CH}_3$ ) ppm.

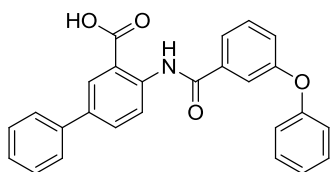
LC/MS:  $m/z$  = 332 [ $\text{M} + \text{H}^+$ ], 663 [ $2\text{M} + \text{H}^+$ ];  $t_{\text{R}}$  = 13.78 min; 100.0 % pure (UV).



**3-(3-phenoxybenzamido)-[1,1'-biphenyl]-4-carboxylic acid (31)** was prepared according to method D. The product was purified by CC (*n*-hexane/EtOAc 8:2); yield: 91 %. Mp: 189–190 °C.  $^1\text{H}$  NMR (500 MHz,  $\text{DMSO-}d_6$ )  $\delta$  = 12.26 (br. s, 1 H, NH), 9.02 (d,  $J$  = 1.9 Hz, 1 H), 8.12 (d,  $J$  = 8.2 Hz, 1 H), 7.74–7.71 (m, 3 H), 7.62 (d,  $J$  = 7.9, 7.9 Hz, 1 H), 7.55–7.50 (m, 4 H), 7.47–7.42 (m, 3 H), 7.29 (ddd,  $J$  = 8.2, 2.5, 0.9 Hz, 1 H), 7.21 (tt,  $J$  = 7.4, 1.1 Hz, 1 H), 7.14–7.08 (m, 2 H) ppm.

$^{13}\text{C}$  NMR (125 MHz,  $\text{DMSO-}d_6$ )  $\delta$  = 169.9, 164.1, 157.4, 155.9, 145.7, 141.4, 138.9, 136.4, 131.9, 130.8, 130.3, 129.2, 128.6, 126.9, 124.1, 122.1, 121.5, 121.3, 119.2, 117.9, 116.8, 115.4 ppm.

LC/MS:  $m/z$  = 410 [ $\text{M} + \text{H}^+$ ], 819 [ $2\text{M} + \text{H}^+$ ];  $t_{\text{R}}$  = 15.23 min; 99.1 % pure (UV).

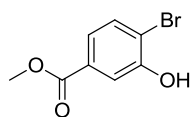




**4-(3-phenoxybenzamido)-[1,1'-biphenyl]-3-carboxylic acid (32)** was prepared according to method D. The product was purified by preparative TLC (*n*-hexane/EtOAc 1:1 + 7 drops formic acid per 10 mL solvent) and washed with CH<sub>2</sub>Cl<sub>2</sub>; yield: 42 %. Mp: 207–208 °C. <sup>1</sup>H NMR (500 MHz, DMSO-*d*<sub>6</sub>)  $\delta$  = 12.20 (br. s, 1 H, NH), 8.75 (d, *J* = 8.8 Hz, 1 H), 8.29 (d, *J* = 2.5 Hz, 1 H), 7.98 (dd, *J* = 8.8, 2.5 Hz, 1 H), 7.78–7.72 (m, 1 H), 7.71–7.66 (m, 2 H), 7.61 (dd, *J* = 7.9, 7.9 Hz, 1 H), 7.57–7.53 (m, 1 H), 7.53–7.42 (m, 4 H), 7.41–7.34 (m, 1 H), 7.32–7.25 (m, 1 H), 7.24–7.17 (m, 1 H), 7.16–7.04 (m, 2 H) ppm.

<sup>13</sup>C NMR (125 MHz, CDCl<sub>3</sub>)  $\delta$  = 169.9, 163.9, 157.3, 156.0, 140.1, 138.7, 136.4, 134.7, 132.3, 130.8, 130.3, 129.1, 128.9, 127.6, 126.4, 124.1, 122.1, 121.6, 120.6, 119.1, 117.3, 116.9 ppm.

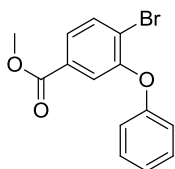
LC/MS: *m/z* = 410 [M + H<sup>+</sup>], 451 [M + H<sup>+</sup> CH<sub>3</sub>CN], 819 [2M + H<sup>+</sup>]; *t<sub>R</sub>* = 14.61 min; 100.0 % pure (UV).



**methyl 4-bromo-3-hydroxybenzoate (33f).** To 3-hydroxybenzoate (1 equiv) in acetic acid was added bromine (1 equiv) dropwise. The reaction mixture was stirred at room temperature for 18 h, water was added and the mixture was extracted with EtOAc. The combined organic layers were washed with brine and dried over MgSO<sub>4</sub>. The product was purified by CC (*n*-hexane/EtOAc 92.5:7.5) followed by crystallization from EtOAc/*n*-hexane (in fridge overnight); yield: 48 %. <sup>1</sup>H NMR (500 MHz, METHANOL-*d*<sub>4</sub>)  $\delta$  = 11.51 (br. s, 1 H, OH), 8.43 (d, *J* = 8.2 Hz, 1 H), 8.33 (d, *J* = 2.0 Hz, 1 H), 8.11 (dd, *J* = 8.2, 2.0 Hz, 1 H), 4.64 (s, 3 H, OCH<sub>3</sub>) ppm.

<sup>13</sup>C NMR (125 MHz, METHANOL-*d*<sub>4</sub>)  $\delta$  = 175.3, 163.9, 142.9, 139.7, 130.5, 126.0, 124.7, 61.9 (OCH<sub>3</sub>) ppm.

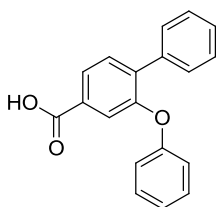
LC/MS: *m/z* = no ionization; *t<sub>R</sub>* = 9.28 min; 97.8 % pure (UV).



**methyl 4-bromo-3-phenoxybenzoate (33e).** A mixture of methyl 4-bromo-3-hydroxybenzoate (**33f**, 1 equiv), phenylboronic acid (2 equiv), copper acetate (1 equiv), triethylamine (5 equiv) and 3 Å molecular sieves in  $\text{CH}_2\text{Cl}_2$  was stirred at room temperature for 72 h under a  $\text{N}_2$  atmosphere. After filtration over celite the solvent was evaporated. Purification by CC (*n*-hexane/EtOAc 8:2) provided the pure compound; yield: 37 %.  $^1\text{H}$  NMR (500 MHz,  $\text{CDCl}_3$ )  $\delta$  = 7.72 (d,  $J$  = 8.2 Hz, 1 H), 7.68 (dd,  $J$  = 8.2, 1.9 Hz, 1 H), 7.59 (d,  $J$  = 1.9 Hz, 1 H), 7.39–7.36 (m, 2 H), 7.16 (tt,  $J$  = 7.4, 1.1 Hz, 1 H), 7.02–6.97 (m, 2 H), 3.87 (s, 3 H,  $\text{OCH}_3$ ) ppm.

$^{13}\text{C}$  NMR (125 MHz, Acetone- $d_6$ )  $\delta$  = 148.0, 138.6, 136.5, 116.2, 113.2, 112.1, 107.5, 106.2, 102.2, 102.0, 100.5, 33.8 ( $\text{OCH}_3$ ) ppm.

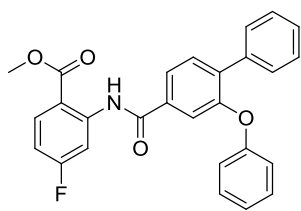
LC/MS:  $m/z$  = no ionization;  $t_R$  = 13.54 min; 97.5 % pure (UV).



**2-phenoxy-[1,1'-biphenyl]-4-carboxylic acid (33d)** was prepared according to method D. The product was purified by CC (*n*-hexane/EtOAc 7:3); yield: 66 %.  $^1\text{H}$  NMR (500 MHz,  $\text{CDCl}_3$ )  $\delta$  = 7.94 (dd,  $J$  = 7.9, 1.6 Hz, 1 H), 7.72 (d,  $J$  = 1.6 Hz, 1 H), 7.63–7.56 (m, 3 H), 7.43–7.39 (m, 2 H), 7.38–7.35 (m, 1 H), 7.34–7.29 (m, 2 H), 7.09 (tt,  $J$  = 7.4, 1.1 Hz, 1 H), 7.00–6.94 (m, 2 H) ppm.

$^{13}\text{C}$  NMR (125 MHz,  $\text{CDCl}_3$ )  $\delta$  = 171.1, 157.1, 153.9, 139.0, 136.7, 131.4, 129.8, 129.6, 129.2, 128.3, 128.0, 125.5, 123.3, 121.2, 118.5 ppm.

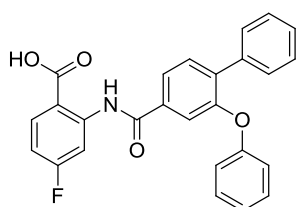
LC/MS:  $m/z$  = no ionization;  $t_R$  = 12.33 min; 97.6 % pure (UV).



**methyl 4-fluoro-2-(2-phenoxy-[1,1'-biphenyl]-4-ylcarboxamido)benzoate (33a)** was prepared according to method BIII. The product was purified by CC (*n*-hexane/EtOAc 9:1); yield: 65 %.  $^1\text{H}$  NMR (500 MHz,  $\text{CDCl}_3$ )  $\delta$  = 12.19 (br. s, 1 H, NH), 8.72 (dd,  $J$  = 12.1, 2.6 Hz, 1 H), 8.09 (dd,  $J$  = 9.0, 6.5 Hz, 1 H), 7.84 (dd,  $J$  = 8.0, 1.9 Hz, 1 H), 7.70 (d,  $J$  = 1.9 Hz, 1 H), 7.67–7.60 (m, 3 H), 7.44–7.32 (m, 5 H), 7.11–7.08 (m, 1 H), 7.06–7.01 (m, 2 H), 6.81 (ddd,  $J$  = 9.0, 7.5, 2.6 Hz, 1 H), 3.94 (s, 3 H,  $\text{OCH}_3$ ) ppm.

$^{13}\text{C}$  NMR (125 MHz,  $\text{CDCl}_3$ )  $\delta$  = 168.3, 166.4 (d,  $J_{\text{CF}}$  = 253.0 Hz), 164.9, 156.9, 154.5, 143.9 (d,  $J_{\text{CF}}$  = 13.7 Hz), 137.0, 136.8, 134.9, 133.2 (d,  $J_{\text{CF}}$  = 10.1 Hz), 131.7, 129.8, 129.2, 128.3, 127.9, 123.4, 122.0, 118.8, 118.8, 111.3 (d,  $J_{\text{CF}}$  = 2.7 Hz), 110.0 (d,  $J_{\text{CF}}$  = 22.0 Hz), 107.5 (d,  $J_{\text{CF}}$  = 28.4 Hz), 52.5 ( $\text{OCH}_3$ ) ppm.

LC/MS:  $m/z$  = 442 [ $\text{M} + \text{H}^+$ ], 483 [ $\text{M} + \text{H}^+ \text{CH}_3\text{CN}$ ], 883 [ $2\text{M} + \text{H}^+$ ];  $t_{\text{R}}$  = 17.02 min; 89.0 % pure (UV).

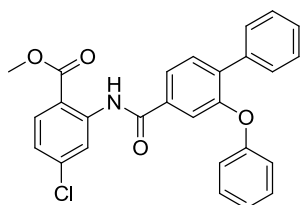


**4-fluoro-2-(2-phenoxy-[1,1'-biphenyl]-4-ylcarboxamido)benzoic acid (33)** was prepared according to method C. For purification the remaining solid was washed with MeOH to provide the pure compound; yield: 77 %. Mp: 223–227 °C.  $^1\text{H}$  NMR (500 MHz,  $\text{DMSO}-d_6$ )  $\delta$  = 12.45 (br. s, 1 H, NH), 8.50 (dd,  $J$  = 12.1, 2.6 Hz, 1 H), 8.14–8.09 (m, 1 H), 7.84–7.80 (m, 1 H), 7.73 (d,  $J$  = 8.2 Hz, 1 H), 7.62–7.59 (m, 2 H), 7.52 (d,  $J$  = 1.9 Hz, 1 H), 7.46–7.42 (m, 2 H), 7.41–7.34 (m, 3 H), 7.12 (tt,  $J$  = 7.3, 1.2 Hz, 1 H), 7.07–7.03 (m, 1 H), 7.03–6.99 (m, 2 H) ppm.

$^{13}\text{C}$  NMR (125 MHz,  $\text{DMSO}-d_6$ )  $\delta$  = 169.4, 165.0 (d,  $J$  = 249.0 Hz), 163.9, 156.5, 153.5, 143.1 (d,  $J$  = 12.8 Hz), 136.7, 136.1, 134.7, 134.0 (d,  $J_{\text{CF}}$  = 11.0 Hz), 131.9, 130.2, 129.0,

128.4, 128.0, 123.5, 122.3, 118.5, 118.2, 113.0 (d,  $J_{CF} = 2.8$  Hz), 110.1 (d,  $J_{CF} = 22.0$  Hz), 106.4 (d,  $J_{CF} = 27.0$  Hz) ppm.

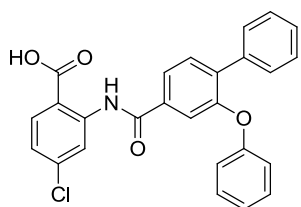
LC/MS:  $m/z = 428$  [ $M + H^+$ ], 469 [ $M + H^+ CH_3CN$ ], 855 [ $2M + H^+$ ];  $t_R = 15.13$  min; 97.2 % pure (UV).



**methyl 4-chloro-2-(2-phenoxy-[1,1'-biphenyl]-4-ylcarboxamido)benzoate (34a)** was prepared according to method BIII. The product was purified by CC (*n*-hexane/EtOAc 9:1); yield: 22 %.  $^1H$  NMR (500 MHz,  $CDCl_3$ )  $\delta = 12.08$  (br. s, 1 H, NH), 9.01 (d,  $J = 2.2$  Hz, 1 H), 8.00 (d,  $J = 8.5$  Hz, 1 H), 7.83 (dd,  $J = 7.9, 1.9$  Hz, 1 H), 7.68 (d,  $J = 1.9$  Hz, 1 H), 7.64–7.60 (m, 3 H), 7.44–7.40 (m, 2 H), 7.38–7.31 (m, 3 H), 7.11–7.07 (m, 2 H), 7.05–7.01 (m, 2 H), 3.95 (s, 3 H,  $OCH_3$ ) ppm.

$^{13}C$  NMR (125 MHz,  $CDCl_3$ )  $\delta = 168.4, 164.9, 156.9, 154.6, 142.6, 141.2, 137.0, 136.8, 134.9, 132.0, 131.7, 129.9, 129.2, 128.3, 127.9, 123.4, 123.0, 121.9, 120.3, 118.9, 118.7, 113.3, 52.6$  ( $OCH_3$ ) ppm.

LC/MS:  $m/z = 458$  and 460 [ $M + H^+$ ], 915 and 917 [ $2M + H^+$ ];  $t_R = 17.56$  min; 97.5 % pure (UV).



**4-chloro-2-(2-phenoxy-[1,1'-biphenyl]-4-ylcarboxamido)benzoic acid (34)** was prepared according to method C. For purification the remaining solid was washed with MeOH to provide the pure compound; yield: 92 %. Mp: 230–234 °C.  $^1H$  NMR (500 MHz,  $DMSO-d_6$ )  $\delta = 12.31$  (br. s, 1 H,  $OCH_3$ ), 8.75 (d,  $J = 2.2$  Hz, 1 H), 8.04 (d,  $J = 8.5$  Hz, 1 H), 7.82 (dd,  $J =$

7.9, 1.9 Hz, 1 H), 7.73 (d,  $J = 7.9$  Hz, 1 H), 7.63–7.59 (m, 2 H), 7.52 (d,  $J = 1.9$  Hz, 1 H), 7.46–7.42 (m, 2 H), 7.40–7.34 (m, 3 H), 7.27 (dd,  $J = 8.5, 2.2$  Hz, 1 H), 7.16–7.09 (m, 1 H), 7.03–6.99 (m, 2 H) ppm.

$^{13}\text{C}$  NMR (125 MHz, DMSO- $d_6$ )  $\delta = 169.3, 163.8, 156.5, 153.5, 141.9, 138.6, 136.7, 136.1, 134.7, 132.9, 131.9, 130.2, 129.0, 128.4, 128.0, 123.5, 123.0, 122.4, 119.3, 118.5, 118.2, 115.4$  ppm.

LC/MS:  $m/z = 444$  [ $\text{M} + \text{H}^+$ ], 485 [ $\text{M} + \text{H}^+ \text{CH}_3\text{CN}$ ], 887 [ $2\text{M} + \text{H}^+$ ];  $t_R = 15.37$  min; 97.3 % pure (UV).

## Computational chemistry

**Pharmacophore modelling and virtual screening.** The following compounds **I–VII** were retrieved from literature<sup>1,6–9</sup>:

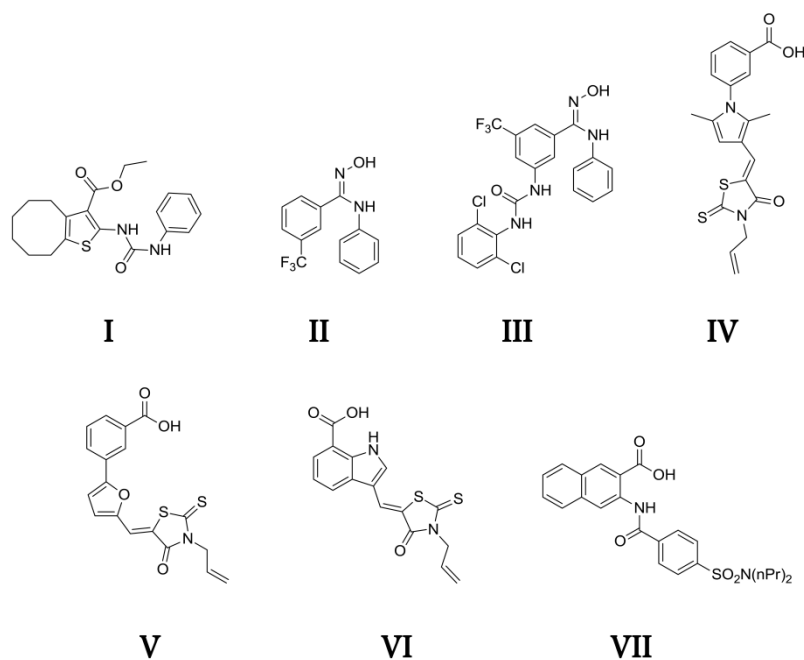


**Figure S1.** Compounds used for the flexible alignment.

**I:** Published by Arhin et al.<sup>6</sup> (“compound 1”) as inhibitor of *S. aureus* RNAP. It was shown that these compounds do not bind to the Rifamycin binding site, but the exact mode of action is not known.

**II** and **III**: Published by Artsimovitch et al.<sup>7</sup> (“CBR703 and CBR9379”) as inhibitors of *E. coli* RNAP. They bind to a surface exposed groove at the junction of the  $\beta'$ -bridge helix and the  $\beta$ -subunit.

**IV**, **V** and **VI**: Published by André et al.<sup>8</sup> (“SB8 and SB2”) and Villain-Guillot<sup>9</sup> (“compound 11b”) as inhibitors of *E. coli* RNAP. The mode of action of these compounds is the prevention of the protein-protein interaction between  $\sigma^{70}$  and the RNAP core enzyme.

**VII**: Published by Larsen et al.<sup>1</sup> (“compound 1”) as inhibitor of transcription/ translation in *S. aureus*. Resynthesis and testing in our *E. coli* RNAP *in vitro* inhibition assay revealed **VII** as a potent inhibitor of *E. coli* RNAP (IC<sub>50</sub> 42  $\mu$ M).

Compounds **I–VII** (Fig. S1) were aligned using the flexible alignment module of MOE (*Molecular Operating Environment*)<sup>10</sup> with the stochastic search option turned on. We modified the default flexible alignment settings; the Aromaticity and CO<sub>2</sub>-type centroid weights were set at 2 – strikingly these two chemical moieties are present in most of the initial seven template compounds. Weights on volume and acceptor/donor projection features were switched on. Further, we set the configuration limit to 100 and conjugate gradient minimization steps to 1000. The alignment with the best similarity score was retained and refined within MOE.

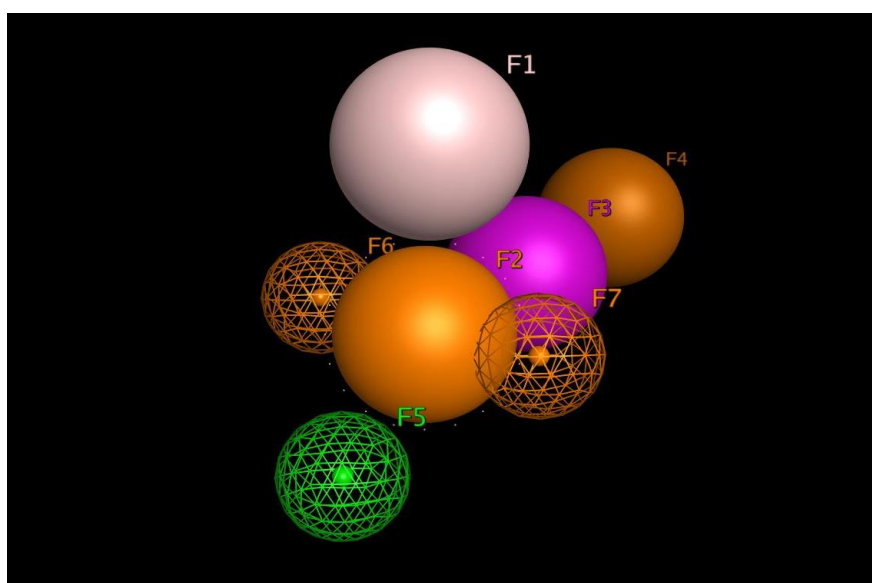


**Figure S2.** Final pharmacophore model used for virtual screening.

This alignment was used to identify common features within the seven superimposed ligands via the Pharmacophore Consensus utility (tolerance of 1.2 and threshold value of 50% (ligands that match one feature)). The resulting pharmacophore model (consisting of 9 features) was manually refined and reduced to 7 features with 6 needed partial matches. The final pharmacophore model (Fig. S2) consisted of following features (F1-F4 - feature radius of 1.5 Å, F5-F7 - feature radius of 1 Å):

Feature F1 (rose): O2|Ani|N[O,o]|(O(C=O)C (this includes CO<sub>2</sub>-like centroids (both acids and ester), anionic atoms as well as N.sp<sup>2</sup>-O moieties (i.e. oximes, nitro)

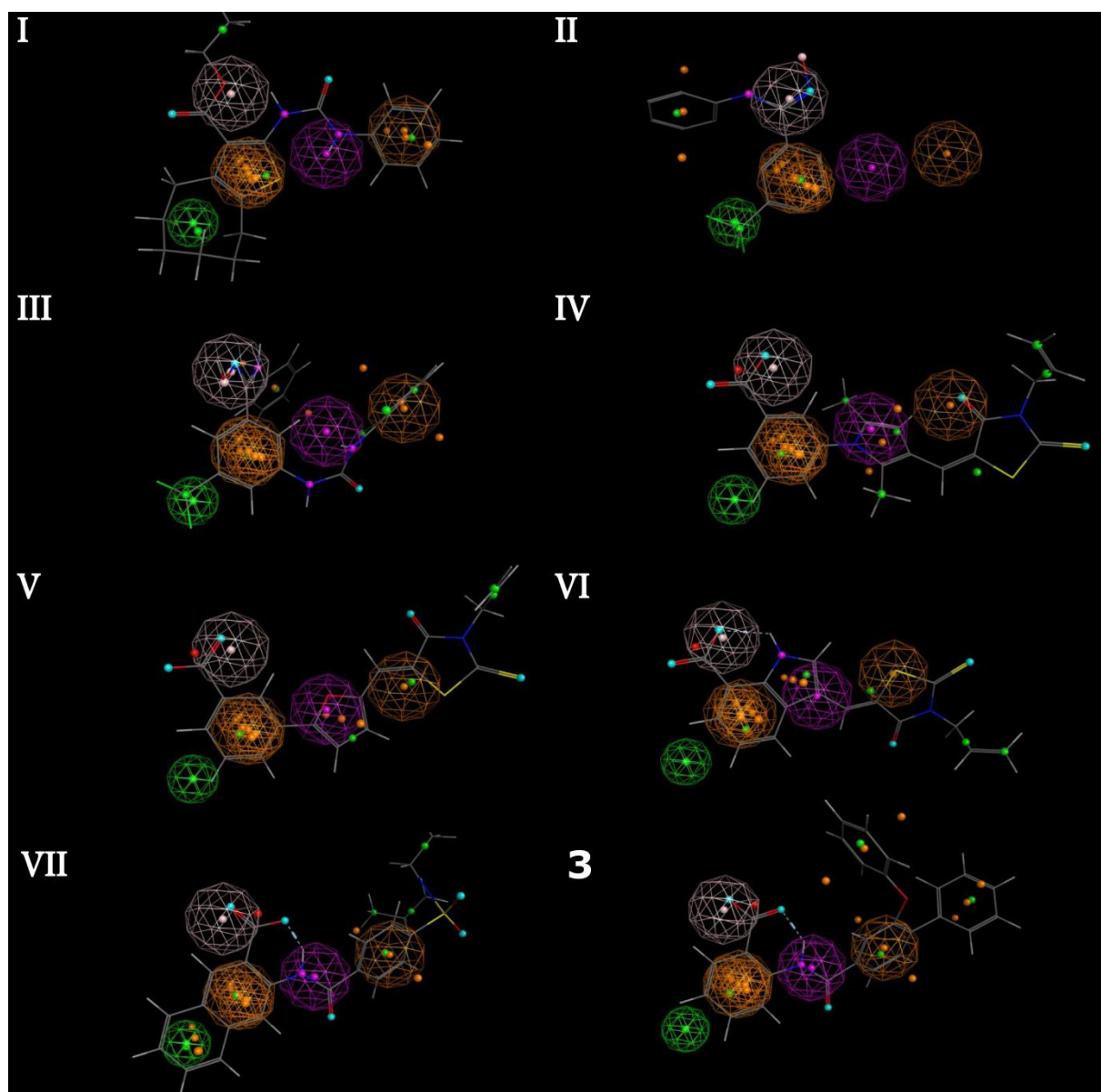
Feature F2 (orange): Aro (all aromatic systems)

Feature F3 (violet): HBD/HBA/Aro (this feature can be matched by either a hydrogen-bond donor or acceptor or by an aromatic system)

Feature F4: Aro/Hyd/pi (in this position aromatic, hydrophobic or planar-conjugated pi systems are requested)

Feature F5 (green): Hydrophobic

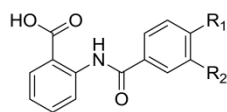
Features F6+F7 (hatched orange): Aromatic ring projections



**Figure S3.** Overlay of the resulting pharmacophore model with inhibitors I–VII and 3.

A virtual library was built including approximately 2000 synthetic *in-house* compounds that had been developed as aromatase, CYP17, CYP11B1, CYP11B2, thromboxane A2, 5 $\alpha$  reductase, 17 $\beta$  HSD1, 17 $\beta$  HSD2, FabH and PqsD inhibitors. For each compound a conformational search was performed using the default parameters of the conformational search module of MOE2010. Conformers were energy minimized using MMFF94xs forcefield and the Generalized Born implicit solvent model. The obtained multiple-conformer database was now used in the pharmacophore search.



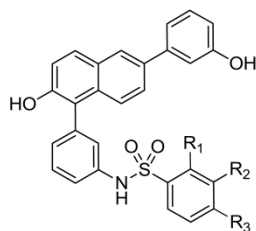
Class 1

Hit1 ( $R_1=\text{Ph}$ ,  $R_2=\text{H}$ )  
 Hit2 ( $R_1=\text{H}$ ,  $R_2=\text{OPh}$ )  
 Hit3 ( $R_1=\text{Ph}$ ,  $R_2=\text{OPh}$ )

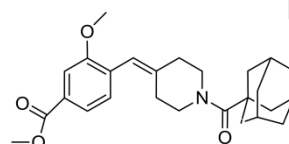
Class 3

not shown due  
to patent issues

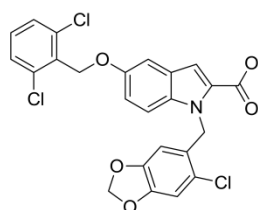
Hit7  
 Hit8  
 Hit9

Class 2

Hit4  
 ( $R_1=\text{NO}_2$ ,  $R_2=\text{H}$ ,  $R_3=\text{NO}_2$ )  
 Hit5  
 ( $R_1=\text{NO}_2$ ,  $R_2=\text{H}$ ,  $R_3=\text{H}$ )  
 Hit6  
 ( $R_1=\text{H}$ ,  $R_2=\text{NO}_2$ ,  $R_3=\text{H}$ )

Class 4

Hit10

Class 5

Hit11

**Figure S4.** Experimentally validated virtual hit compounds.

In total 64 hits were found matching at least the four core features and the two aromatic projections, while the presence of the accessory feature was not mandatory. All hit compounds were tested on inhibitory potency, for eleven of them (comprising five different structural classes) an inhibition >20% was measured at 200  $\mu\text{M}$  (Fig. S4).

Based on the activities of **1–4**, the seven-feature pharmacophore model (Fig. S2) was extended by two additional features (F8 and F9):

Features F8+F9 (hatched yellow): Aro/Hyd (feature radius of 1.5 Å)

Using this model (Fig. S5) in further screenings, a compound will be defined as a hit if, beside the 4 core features, at least one of the new accessory features is present.

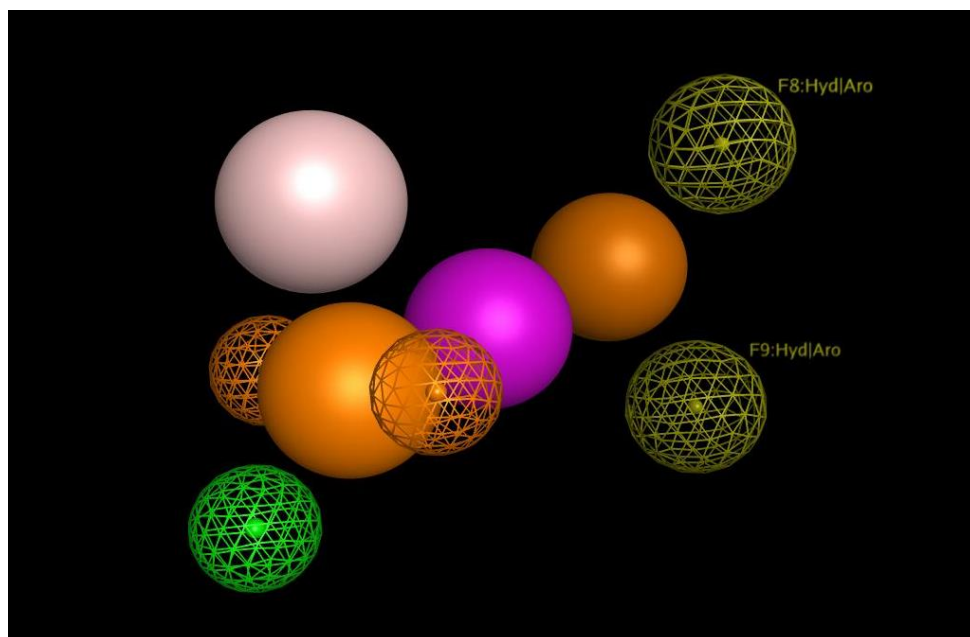


**Figure S5.** Extended pharmacophore model.

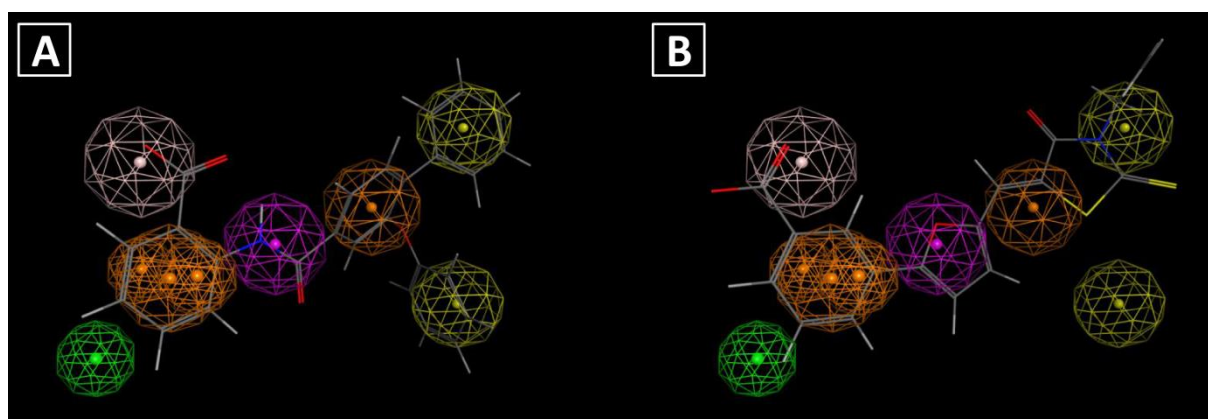


**Figure S6.** Overlay of the extended pharmacophore model with A) most potent hit compound 3 B) described inhibitor V

### Supplemental references

- (1) Larsen, S. D.; Hester, M. R.; Craig Ruble, J.; Kamilar, G. M.; Romero, D. L.; Wakefield, B.; Melchior, E. P.; Sweeney, M. T.; Marotti, K. R. Discovery and initial development of a novel class of antibacterials: Inhibitors of *Staphylococcus aureus* transcription/translation. *Bioorg. Med. Chem. Lett.* **2006**, *16*, 6173–6177.
- (2) Heikkilä, T.; Thirumalairajan, S.; Davies, M.; Parsons, M. R.; McConkey, A. G.; Fishwick, C. W. G.; Johnson, A. P. The first de novo designed inhibitors of *Plasmodium falciparum* dihydroorotate dehydrogenase. *Bioorg. Med. Chem. Lett.* **2006**, *16*, 88–92.

- (3) Nie, Z.; Perretta, C.; Lu, J.; Su, Y.; Margosiak, S.; Gajiwala, K. S.; Cortez, J.; Nikulin, V.; Yager, K. M.; Appelt, K.; Chu, S. Structure-based design, synthesis, and study of potent inhibitors of  $\beta$ -ketoacyl-acyl carrier protein synthase III as potential antimicrobial agents. *J. Med. Chem.* **2005**, *48*, 1596–1609.
- (4) Meyer, H. The linking of aromatic amino acids. *Liebigs Ann. Chem.* **1907**, *351*, 267–282.
- (5) Thorarensen, A.; Ruble, C. J.; Romero, D. L. Preparation of aminoarylbenzoic acid derivatives as antibacterial agents for use as disinfectants and therapeutic agents. *PCT Int. Appl.* (2004), WO 2004018414 A2 20040304. **2004**.
- (6) Arhin, F.; Bélanger, O.; Ciblat, S.; Dehbi, M.; Delorme, D.; Dietrich, E.; Dixit, D.; Lafontaine, Y.; Lehoux, D.; Liu, J.; McKay, G. A.; Moeck, G.; Reddy, R.; Rose, Y.; Srikumar, R.; Tanaka, K. S. E.; Williams, D. M.; Gros, P.; Pelletier, J.; Parr Jr, T. R.; Far, A. R. A new class of small molecule RNA polymerase inhibitors with activity against rifampicin-resistant *Staphylococcus aureus*. *Bioorgan. Med. Chem.* **2006**, *14*, 5812–5832.
- (7) Artsimovitch, I.; Chu, C.; Lynch, A. S.; Landick, R. A New class of bacterial RNA polymerase inhibitor affects nucleotide addition. *Science* **2003**, *302*, 650–654.
- (8) André, E.; Bastide, L.; Michaux-Charachon, S.; Gouby, A.; Villain-Guillot, P.; Latouche, J.; Bouchet, A.; Gualtieri, M.; Leonetti, J.-P. Novel synthetic molecules targeting the bacterial RNA polymerase assembly. *J. Antimicrob. Chemoth.* **2006**, *57*, 245–251.
- (9) Villain-Guillot, P.; Gualtieri, M.; Bastide, L.; Roquet, F. O.; Martinez, J.; Amblard, M.; Pugniere, M.; Leonetti, J.-P. Structure-activity relationships of phenyl-furanyl-rhodanines as inhibitors of RNA polymerase with antibacterial activity on biofilms. *J. Med. Chem.* **2007**, *50*, 4195–4204.
- (10) *Molecular Operating Environment*, 2010.10; Chemical Computing Group Inc., 1010 Sherbooke St. West, Suite #910, Montreal, QC, Canada, H3A 2R7, **2010**.

## 6.4 Supporting information to Publication IV

### Materials and methods

**Transcription assay.** Core and holo enzyme of RNA polymerase (*E. coli* origin) were purchased from Epicentre Biotechnologies (Madison, WI). *E. coli*  $\sigma^{70}$  factor was cloned and purified as described below. Final concentrations in a total volume of 30  $\mu$ l were one unit of RNA polymerase (0.7  $\mu$ g core or 0.5  $\mu$ g holo enzyme) which were used along with 0.53  $\mu$ M of [5,6- $^3$ H]-UTP, 400  $\mu$ M of ATP, CTP and GTP as well as 100  $\mu$ M of UTP, 20 units of RNase inhibitor (RiboLock, Fermentas), 10 mM DTT, 40 mM Tris-HCl (pH 7.5), 150 mM KCl, 10 mM MgCl<sub>2</sub> and 0.01 % Triton-X-100. Ten different DNA templates (properties and concentrations described below) were used. Prior to starting the experiment, the compounds were dissolved in DMSO (final concentration during experiments: 2 %). Dilution series of compounds were prepared using a liquid handling system (Janus, Perkin Elmer, Waltham, MA). The components described above (including the inhibitors) were preincubated in absence of NTPs and DNA for 10 min at 25 °C. Transcription reactions were started by the addition of a mixture containing DNA template and NTPs. When core enzyme was used (with or without  $\sigma^{70}$ ) the incubation was performed for 20 min at 37 °C, in case of holo enzyme the incubation time was only 10 min. For experiments with separate addition of  $\sigma^{70}$ , core enzyme was preincubated with  $\sigma^{70}$  or DMSO for 10 min at 25 °C to allow formation of the holo enzyme. The following steps were carried out as described above for the holo enzyme. The reaction was stopped by the addition of 10 % TCA, followed by a transfer of this mixture to a 96 well Multiscreen GFB plate (Millipore, Billerica, MA) and incubation for 45 min at 4 °C. The plate underwent several centrifugation and washing steps with 10 % TCA and 95 % ethanol to remove residual unincorporated  $^3$ H-UTP. After that the plate was dried (30 min, 50 °C) and 30  $\mu$ l of scintillation fluid (Optiphase Supermix, 1 Perkin Elmer) was added to each well. After 10 min the wells were assayed for presence of  $^3$ H-RNA by counting using a Wallac MicroBeta TriLux system (Perkin Elmer). To obtain inhibition values for each sample, their counts were related to DMSO controls.

**DNA templates.** Kool NC-45 template was purchased from Epicentre Biotechnologies. According to the supplier the sequence of this circular and single-stranded DNA is ctggaggagattttgtggtatcgattcgtctcttagaggaagcta which does not contain a hammerhead. Unsheared genomic calf thymus DNA and T-phage DNA were purchased from Sigma-Aldrich (St. Louis, MO). Poly(dA:dT) template was purchased from Invivogen (San Diego, CA). pcDNA3.1/V5-His-TOPO (pcDNA3.1) plasmid was used in religated form (purchased

from Invitrogen, Carlsbad, CA). pGEM beta-gal Control (pGEM) was purchased from Promega (Madison, WI). Both plasmids were amplified and purified using MaxiPrep kits according to the guidelines of the manufacturer (Sigma-Aldrich). To obtain genomic DNA from *E.coli*, DH5 $\alpha$  cells were incubated in TE buffer substituted with SDS and proteinase K followed by subsequent phenol and chloroform treatment (twice each). Nucleic acids obtained after ethanol precipitation were treated with RNase A and precipitated again with ammonium acetate and isopropanol resulting in pure genomic DNA. To obtain T7A1 PCR fragments, a two-step PCR was performed using Taq DNA polymerase (NEB, Ipswich, MA). Firstly, parts of the neomycin gene of pcDNA3.1 were amplified. The different 3' primers defined the length of the PCR product (oligo 3pp-1 for fragment "T7A1\_149": acccaagcggccggagaacctg; oligo 3pp-2 for fragment "T7A1\_437": ttctcggcaggagcaaggtag; oligo 3pp-3 for fragment "T7A1\_763": tgtcctgatagcggtag). The universal 5' oligo was flanked by the T7A1 promoter containing the -10 and -35 consensus sequences (oligo T7A1-5pr: gactcagtgatataaaaagagtattgacttaaagtctaactataggatacttacagccatcgagaggctgatcaagagacaggatgagg) resulting in PCR products all containing a 59 bp T7A1 promoter on their 5' ends. The exact sizes of the PCR products were 149 bp (MW: 97 kDa) for "T7A1\_149", 437 bp (MW: 284 kDa) for "T7A1\_437" and 763 bp (MW: 496 kDa) for "T7A1\_763". To obtain the „T7\_promoter template“ the same procedure as with "T7A1\_437" was followed with the difference that the T7A1 promoter sequence was substituted by the T7 promoter sequence. The PCR products were gel purified (kit from PEQLAB, Erlangen, Germany) and elongated in a second PCR using the same 3' oligos and a 5' oligo increasing the size by 13 bp (oligo T7A1-elong: cagaccatgatcagactcagtgtatc). These PCR products were directly purified (kit from Fermentas) and served as templates in transcription assays.

**RNA polymerase inhibitors.** Lipiarmycin was a generous gift from Novartis (Basel, Switzerland). Corallopyronin, Myxopyronin and Sorangicin were donated by Klaus Gerth (HZI, Braunschweig, Germany). The Rifamycins were purchased from Sigma-Aldrich. SB2 (Benzoic acid, 3-[5-[[4-oxo-3-(2-propen-1-yl)-2-thioxo-5-thiazolidinylidene]methyl]-2-furanyl]) was purchased from ChemDiv (San Diego, CA) and synthesized as described in literature (57). CBR703 (Benzenecarboximidamide, N-hydroxy-N'-phenyl-3-(trifluoromethyl)) was synthesized according to a published procedure (WO 01/51456A2).

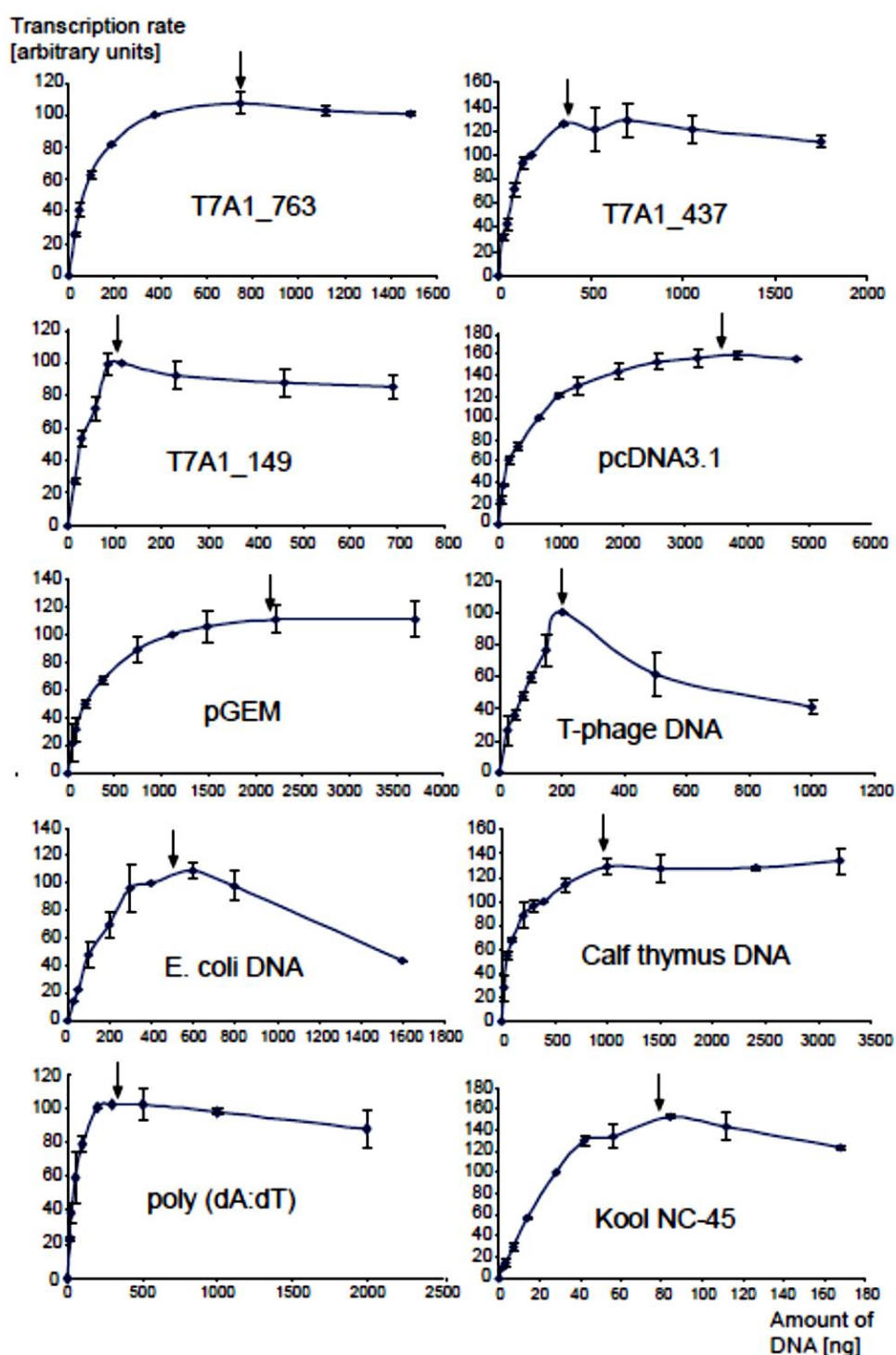
**Determination of IC<sub>50</sub> values.** Three different concentrations of a compound were chosen for the determination of an IC<sub>50</sub> value (two samples for each concentration). The calculation of the IC<sub>50</sub> value was performed by plotting the percent inhibition vs. the concentration of

inhibitor on a semi-log plot. From this the molar concentration causing 50 % inhibition was calculated. At least three independent determinations were performed for each compound.

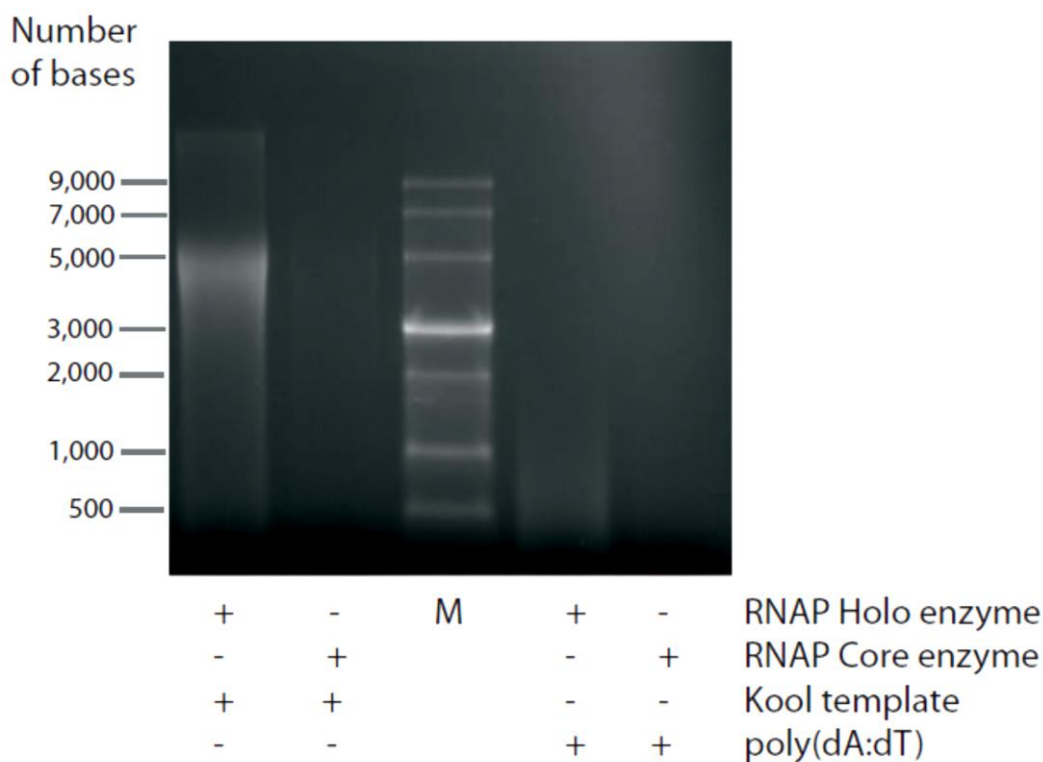
**Cloning and purification of Ec  $\sigma^{70}$ .** For cloning of *E. coli*  $\sigma^{70}$  factor into an expression vector, genomic DNA from DH5 $\alpha$  cells was used (purified as described above). To amplify  $\sigma^{70}$  sequence primers were used being flanked by the restriction site KpnI and a thrombin cutting site (oligo Ec-5-sigma: gagacggtaccctggtgccgcgcggcagcatggagcaaaacccgcagtcacag) or SacI (oligo Ec-3-sigma: gagaggagctcttaatcgccaggaagctacgcag). Amplification was performed using Phusion HF DNA polymerase (NEB, Ipswich, MA). The PCR product was cloned into pCR Blunt II TOPO vector by TOPO reaction (Invitrogen) followed by restriction digestion with KpnI and SacI to obtain  $\sigma^{70}$  sequence. In a next step the fragment was gel purified and ligated into the KpnI/SacI linearized final expression vector pET45b(+) (purchased from Merck, Darmstadt, Germany). The sequence of the final expression vector was verified by sequencing (performed by Seqlab, Goettingen, Germany). Recombinant *E. coli*  $\sigma^{70}$  factor was overexpressed in *E. coli* BL21 (DE3) in presence of 0.5 mM IPTG (Acros Organics, Geel, Belgium) for 16 h at 16 °C. After several sonication cycles the cell lysate was treated with DNase I (Roche, Basel, Switzerland). Inclusion bodies were collected by centrifugation and washed twice with lysis buffer (40 mM Tris-HCl, pH 7.5, 500 mM NaCl, 5 % Glycerol, 1 mM BME, 0.1 mM PMSF, 0.35 mg/ml lysozyme). Finally, the pellet was solubilized in denaturation buffer (40 mM Tris HCl, pH 7.9, 6 M guanidinium HCl, 10 % glycerol, 1 mM EDTA, 10 mM DTT) for 1 h under vigorous stirring. After centrifugation the supernatant was dialysed over night at 4°C against renaturation buffer (20 mM Tris HCl, pH 7.9 at 4 °C, 300 mM NaCl, 20 % glycerol, 1 mM BME). In a next step the fusion protein was purified by IMAC on an ÄKTA purifier (GE Healthcare) with a HisTrap FF column (GE Healthcare). Peak fractions were concentrated with VIVASPIN (MWCO 10 kDa, Sartorius Group, Goettingen, Germany) followed by a buffer exchange into storage buffer using PD-10 columns (GE Healthcare).

**Formaldehyde agarose gel electrophoresis.** To separate RNA transcripts a formaldehyde agarose (1 %) gel was prepared (containing MOPS buffer (40 mM MOPS, pH 7.0; 10 mM sodium acetate; 1 mM EDTA, pH 8.0) and 3.7 % formaldehyde). The RNA was dissolved in loading buffer (Roti-Load RNA) (Carl Roth, Karlsruhe, Germany) containing ethidium bromide for staining. On each of four sample lanes phenol-chloroform extracted and purified RNA from 8 transcription reactions was loaded next to a ssRNA ladder (New England Biolabs, Ipswich, MA).

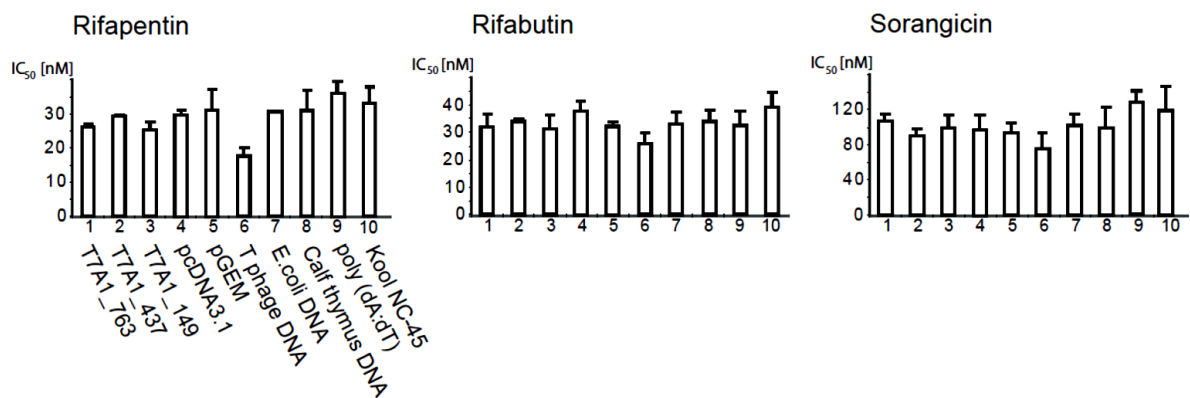
## Supplemental figures



**Supplementary Figure 1.** Optimization of DNA template concentration. Different concentrations of the ten different DNA templates were used in transcription assays (performed with RNAP holo enzyme) to determine the concentration leading to the best transcription rate. Arbitrary units are shown. Arrows indicate the optimal concentration of templates (see also Table 2). Standard deviations are indicated by error bars.

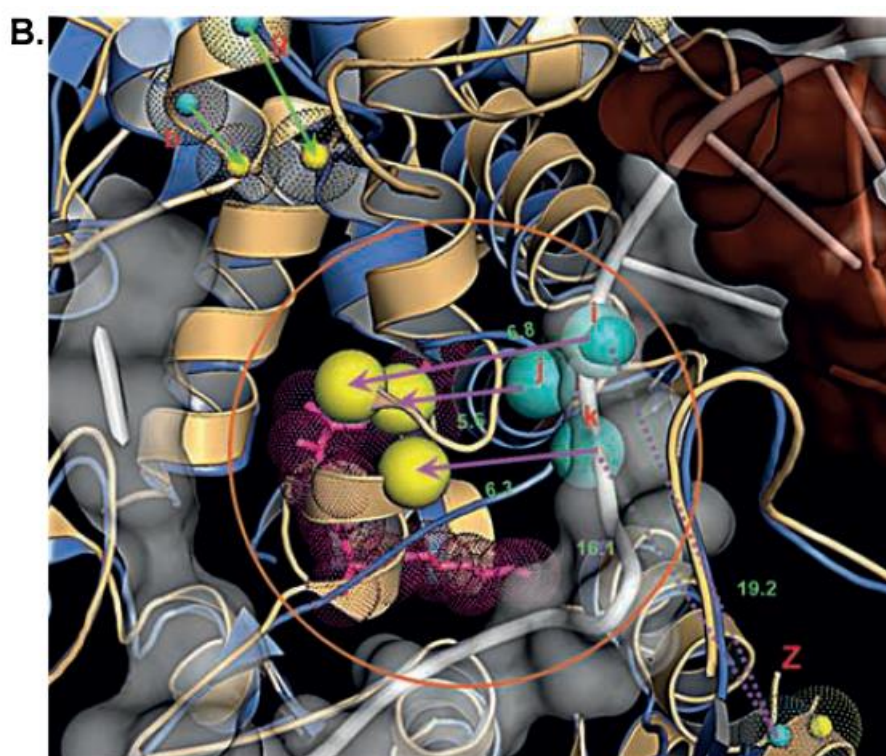
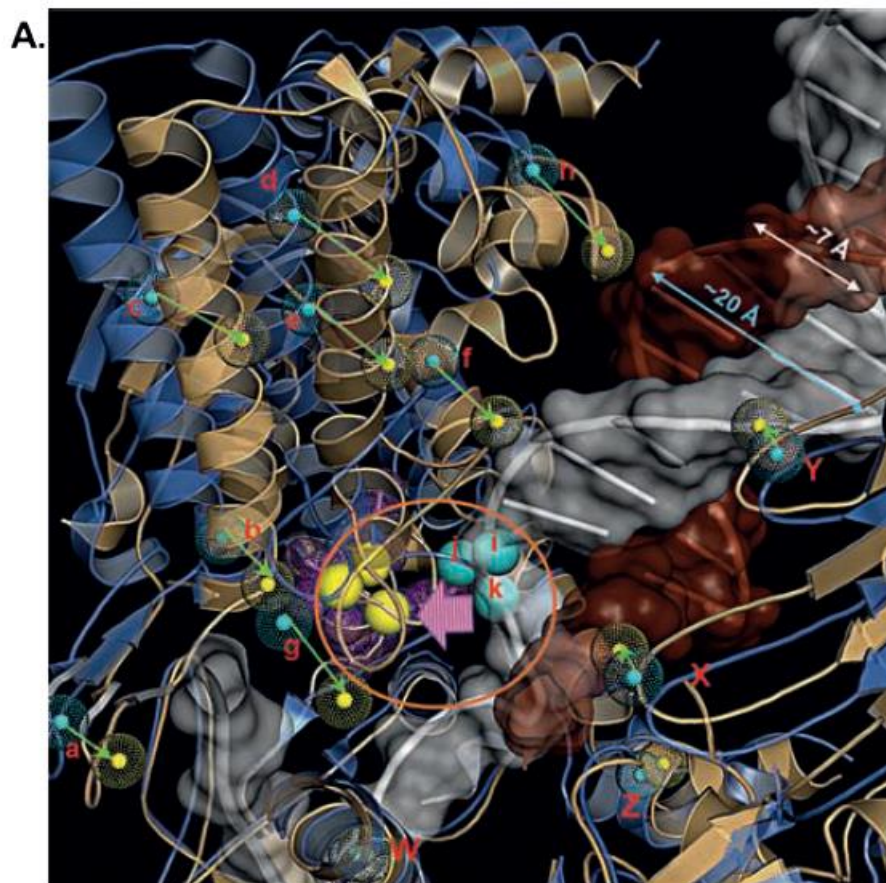


**Supplementary Figure 2.** RNAP holo enzyme leads to a more efficient transcription of Kool and poly(dA:dT) templates compared to core enzyme. Formaldehyde agarose gel electrophoresis was performed to visualize transcripts formed after using RNAP holo and core enzyme along with Kool and poly(dA:dT) templates. M, RNA ladder.



**Supplementary Figure 3.** Inhibition values of Rifapentin, Rifabutin and Sorangicin after usage of ten different DNA templates. IC<sub>50</sub> values are displayed. The template that has been used is shown under each bar of the Rifapentin figure along with corresponding numbers (1-10) which are also used in the figures of the other compounds. Standard deviations are indicated by error bars. sd, standard deviation.





**C.**

Fix AA	code	Flex AA	code	region	dFix-Flex (Å)		$\Delta_{\text{open-closed}}$
					open	closed	
E384 $\beta$ -lobe 2	W	R534	a	$\beta'$ -lid	21.5	17.5	4
		R550	c	coiled-coil	36.9	32.5	4.4
		G595	g	$\beta'$ -rudder	14.6	9.5	5.1
R168 $\beta$ -lobe 1	X	E122	h	coiled-coil	37.8	30.4	7.4
		D539	b		32.9	27.2	5.7
		R550	c		36.9	32.5	4.4
		R572	d		37.4	27.7	9.7
		R576	e		34.2	25.6	8.6
		R587	f	$\beta'$ -rudder	29	21.5	7.5
R189 $\beta$ -lobe 1	Y	R587	f	$\beta'$ -rudder	24.8	18.3	6.5
		E122	h		27.3	18.3	9
L1086 $\beta'$ -bridge helix	Z	R613	i	switch-2	19.2	26	-6.8
		F614	j		19.7	25.3	-5.6
		R615	k		16.1	22.4	-6.3

**Supplementary Figure 4.** Superimposition of the open holoenzyme (PDB-id 3dxj; blue; in complex with Myxopyronin) and the closed elongation complex core (2ppb; pale yellow) of *T. thermophilus* RNAP. The opening of the main channel is summarized by the distances between Fix and Flex AA (dFix-Flex) as well as by the differences between open and closed state ( $\Delta_{\text{open-closed}} = \text{dFix-Flex open} - \text{dFix-Flex closed}$ ). The distances between Z (Leu1086), placed centrally on the bridge helix, and the “switch-2” residues i-k decrease comparing an active and an inhibited holoenzyme RNAP complex (e.g.  $\text{dZ-k} = \text{dL1086-R615} = 22.4 - 16.1 \text{ Å}$ ). Non template (brown) and template strand (white; deeply buried in the catalytic center) of the dsDNA are rendered as cartoons and transparent surfaces. (A) Enlargement of the main channel of RNAP is shown by the outward shifted coiled-coil, lid and rudder loop regions of the opened holoenzyme. The cyan (open) and yellow (closed) dots and spheres indicate the C $\alpha$  atoms of four “fixed” (Fix AA; W-Z; C $\alpha$  RMSD <1.0 Å) and eleven “flexible” residues (Flex AA; a-k). The green arrows (length proportional to distance) schematize the atomic shift of Flex AA between the open and the closed RNAP. (B) Zoomed view of the “switch-2” region (orange circle). The Flex AA Arg613 (i), Phe614 (j), and Arg615 (k) are pushed centrally into the main channel in presence of Myxopyronin (purple dots). The magenta arrows (inverted compared to the green ones) highlight the narrowing of the access to the catalytic center. (C) Table illustrating the distances between Fix and Flex AA (dFix-Flex) in the open and closed RNAP states. AA, amino acids.

Compound	IC <sub>50</sub> Core enzyme	IC <sub>50</sub> Holo enzyme	Ratio Core:Holo
Rifampicin	15.7 (± 1.3) nM	27.4 (± 7.2) nM	0.57
Sorangicin	84.6 (± 2.7) nM	110.6 (± 12.1) nM	0.76
CBR703	6.5 (± 0.3) μM	13.2 (± 0.8) μM	0.49
Lipiarmycin	3.1 (± 0.7) μM	0.9 (± 0.2) μM	3.47

**Supplementary Table 1.** Comparison of RNAP holo and core enzyme inhibition by selected compounds. IC<sub>50</sub> values were determined for four compounds using either the RNAP core enzyme along with 350 ng of T7\_promoter template or the RNAP holo enzyme along with 350 ng of T7A1\_437 template. The core to holo IC<sub>50</sub> ratios are given to highlight the differences between the single compounds.

## 7 Acknowledgments

Herzlich bedanken möchte ich mich bei:

Prof. Dr. Rolf W. Hartmann für die Möglichkeit einer Promotion, das interessante Thema, die Betreuung, konstruktive Diskussionen und den Freiraum bei der wissenschaftlichen Umsetzung.

Prof. Dr. Alexandra K. Kiemer für die Begleitung der Promotion sowie die Übernahme des Zweitgutachtens.

Dr. Jörg Haupenthal für die Betreuung, Ratschläge, Diskussionen und seinen Optimismus.

Dr. Matthias Negri für die kreativen Lösungsansätze und zahlreiche Literaturhinweise.

Allen Mitgliedern der RNAP Gruppe für die gute Zusammenarbeit.

Stefan Hinsberger, Henning Sahner, Walid Elgaher und Johannes de Jong für die Synthese des Test- und Referenzverbindungen.

Katrin Schmitt für die einwandfreie Organisation.

Dr. Christina Zimmer für praktische Hinweise und die gemeinsame Betreuung des Biochemie-Praktikums.

Jeannine Jung für die Übernahme der Routinetestung und die gemeinsame Betreuung des Bioinformatik-Praktikums.

Lothar Jager für Hilfe bei technischen Problemen jeder Art und seine große Schraubenziehersammlung.

Nico Dankbar von Xantec Bioanalytics für die kompetente Unterstützung in allen SPR Fragen.

Den „guten Leuten“ aus Büro 1.31 und allen Mitgliedern der Arbeitskreise Hartmann, Titz und Ducho für die angenehme Arbeitsatmosphäre, Hilfsbereitschaft und Erheiterung, sowie unterhaltsame Mittagspausen in der Mensa oder beim Picknick auf der Wiese.

Meinen Wahlpflicht- und Vertiefungspraktikanten Fabian Panter, Elisabeth-Soizic Zanter und Tobias Geid für ihre Motivation, Fleiß und die schönen Ergebnisse.

Ines Joachim, Lilli Weidel, Michael Storz, Michael Zender, Christine Maurer, Juliette Emmerich, Stefan Hinsberger, Martina Fruth, Stefan Boettcher und Benjamin Kirsch für die tolle Zeit inner- und außerhalb der Arbeitszeiten. Vielen Dank für Eure Freundschaft!

Meiner Familie für bedingungslose Unterstützung und Liebe. Ihr seid die Besten ☺

## 8 Appendix

### 8.1 Curriculum vitae

#### **Kristina Hüsecken**

Birth: 14.05.1986 in Hagen

Citizenship: German

#### *Working Experience*

Jan. 2011–July 2014: **PhD student at Helmholtz-Institute for Pharmaceutical Research Saarland (HIPS), Saarbrücken**

May 2010–Dec. 2010: **Pharmacist in training at Hohwisch Apotheke, Bremen**

Oct. 2009–Apr. 2010: **Research assistant at The University of British Columbia, Vancouver, BC, Canada**

Sep.–Oct. 2007: **Research internship at Peninsula Medical School, Universities of Exeter and Plymouth, Exeter, England**

Aug. 2006: **Training at Production and Quality assurance of MEDICE Arzneimittel Pütter GmbH & Co KG, Iserlohn**

Mar. 2006: **Training at Brunnen Apotheke, Iserlohn**

July 2005: **Training at Rathaus-Apotheke, Hagen**

Feb. 2004: **Training at Quality control of MEDICE Arzneimittel Pütter GmbH & Co KG, Iserlohn**

#### *Education and Qualifications*

Dec. 2010: **Approbation as Pharmacist, Saarbrücken**

Sep. 2010: **Diplom in Pharmacy, Saarland University, Saarbrücken**

Oct. 2005–Sep. 2009: **Pharmacy studies, Saarland University, Saarbrücken**

June 2005: **High School Graduation, Gymnasium Hohenlimburg, Hagen**

Oct. 2002: **Training in chemistry at Ruhr-Universität Bochum, Bochum**

#### *Awards and Honors*

- Oct. 2009: Rewarded as a top three pharmacy student, Saarland University, Saarbrücken
- Since 2004: Numerous awards in gymnastics, trampolin, and track and field

#### *Memberships*

- Deutsche Pharmazeutische Gesellschaft (DPhG)

## 8.2 Publications

1. Hüsecken, K. (2010) Investigating the Role of the Src Homology 3 Domain in the Interaction between Protein Arginine N-Methyltransferase 2 and Histone H4. Diplomarbeit. The University of British Columbia, Vancouver, BC, Kanada und Universität des Saarlandes, Saarbrücken
2. Pak, M.L., Lakowski, T.M., Thomas, D., Vhuiyan, M.I., Hüsecken, K., and Frankel, A. (2011) A Protein Arginine N-Methyltransferase 1 (PRMT1) and 2 Heteromeric Interaction Increases PRMT1 Enzymatic Activity. *Biochemistry* **50** (38), 8226-8240.
3. Haupenthal, J., Hüsecken, K., Negri, M., Maurer, C.K., and Hartmann, R.W. (2012) Influence of DNA template choice on transcription and inhibition of Escherichia coli RNA polymerase. *Antimicrob. Agents Chemother.* **56** (8), 4536-4539.
4. Bielecki, P., Lukat, P., Hüsecken, K., Dötsch, A., Steinmetz, H., Hartmann, R.W., Müller, R., and Häussler, S. (2012) Mutation in elongation factor G confers resistance to the antibiotic argyrin in the opportunistic pathogen Pseudomonas aeruginosa. *Chembiochem.* **13** (16), 2339-2345.
5. Hüsecken, K., Negri, M., Fruth, M., Boettcher, S., Hartmann, R.W., and Haupenthal, J. (2013) Peptide-based investigation of the Escherichia coli RNA polymerase  $\sigma^{70}$ :core interface as target site. *ACS Chem. Biol.* **8** (4), 758-766.
6. Hinsberger, S., Hüsecken, K., Groh, M., Negri, M., Haupenthal, J., and Hartmann, R.W. (2013) Discovery of Novel Bacterial RNA Polymerase Inhibitors: Pharmacophore based Virtual Screening and Hit Optimization. *J. Med. Chem.* **56** (21), 8332-8338.
7. Hüsecken, K., Hinsberger, S., Haupenthal, J., and Hartmann, R.W. (2014) Surface plasmon resonance – more than a screening technology: Insights in the binding mode of  $\sigma^{70}$ :core RNAP inhibitors. *Future Med. Chem.* Accepted.

### 8.3 Oral presentations

1. Hüsecken, K. Identification of a hot spot in *E. coli* RNA polymerase using a peptide approach. *6<sup>th</sup> Summer School "Medicinal Chemistry"*. Sept. 2012. Regensburg, Germany.

### 8.4 Poster presentations

1. Hüsecken, K., Haupenthal, J., Negri, M., and Hartmann, R.W. Identification of a hot spot in *E. coli* RNA polymerase using a peptide approach. *6<sup>th</sup> Summer School "Medicinal Chemistry"*. Sept. 2012. Regensburg, Germany.
2. Hüsecken, K., Haupenthal, J., Negri, M., Fruth, M., Boettcher, S., Empting, M., Kamal, A., and Hartmann, R.W. Peptide-based investigation of the *Escherichia coli* RNA polymerase  $\sigma^{70}$ :core interface as target site. *3<sup>rd</sup> International HIPS Symposium*. July 2013. Saarbrücken, Germany.
3. Hüsecken, K., Negri, M., Fruth, M., Boettcher, S., Hartmann, R.W., and Haupenthal, J. Peptide-based investigation of the *Escherichia coli* RNA polymerase  $\sigma^{70}$ :core interface as target site. *DPhG Annual Meeting 2013 "Drug Discovery inspired by Nature"*. October 2013. Freiburg, Germany.